Physics Lib NEW SERVICE TO READERS — SEE SECTION FOLLOWING TABLE OF CONTENTS
FEB 9 - 1932

VOLUME 39 SECOND SERIES NUMBER 1

Copy 2

THE PHYSICAL REVIEW

A JOURNAL OF EXPERIMENTAL AND THEORETICAL PHYSICS

CONDUCTED BY

THE AMERICAN PHYSICAL SOCIETY

BOARD OF EDITORS

Managing Editor, JOHN T. TATE, University of Minnesota, Minneapolis
Assistant Editor, J. W. BUCHTA, University of Minnesota, Minneapolis
K. F. HERZFELD, A. W. HULL, F. W. LOOMIS, A. J. DEMPSTER, DAVID M. DENNISON, J. C. SLATER, R. C. GIBBS, E. O. LAWRENCE, J. H. VAN VLECK

JANUARY 15, 1932

Variation in the Effective Lattice Constant of Crystals with Wave-Lengths — J. M. Cork 1
Theory of Complex Spectra. Part I. Energy Levels — M. H. Johnson, Jr. 17
Beryllium Molecule — W. H. Furry and J. H. Hartley, Jr. 39
Thermionic Radiation and Space Charge — M. H. Fraser 53
Study of a Neon Discharge by Use of Collectors — Clifton G. Found and Irving Langmuir 57
Dissociation of Nitrogen and Carbon Monoxide by Electron Impact — John T. Tate and W. Wallace Logsdon 65
Efficiencies of Ionization and Ionization Potentials of Various Gases under Electron Impact — John T. Tate and P. T. Smith 73
Zeeman Effect and A-Type and Spin Doubling in the CaH Bands — William W. Watson 85
Polarization of Mercury Resonance Radiation — L. Larrick and M. F. Hasler 97
Polarization of Resonance Radiation and Hyperfine Structure: The Caesium Resonance Lines — A. Ellett and Lewis Larrick 106
Relative Efficiency of Some of the Mercury Arc Lines in Exciting the Raman Spectrum of Benzol — Sister Marina Wheeler 109
On the Origin of the Solar System — Reid Grant 111
Possibilities in Relativistic Thermodynamics for Irreversible Processes without Relaxation of Free Energy — Richard C. Tolman 119
Ferromagnetic Symposium and Conference at the Summer Meeting of the American Physical Society at Schenectady, September 12, 1931
On the Interpretation of Some Ferromagnetic Phenomena — Frances Bitter 127
Some New Experimental Methods in Ferromagnetism — S. L. Quimby 135
Barkhausen Effect: Orientation of Magnetization in Elementary Domains — Richard M. Bozorth 139
Further Experiments on the Propagation of Large Barkhausen Discontinuities — K. J. Sixtus and L. Tonks 147
Effect of Impurities on Ferromagnetism — T. D. Yensen 155
Hydrogenated Iron — P. P. Cioffi 161
Magnetization and Thermal E. M. F's — S. R. Williams 165
Magnetostriction and Magnetoresistance — L. W. McKeehan 171
On the Verification of the Theory of Magnetization of Single Crystals — Frances Bitter 175
Discussion of Papers by Messrs. Bozorth and Sixtus 183
Discussion of Papers by Messrs. Yensen and Cioffi 185
Discussion of Paper by Williams 187
Letters to the Editor
Absorption of γ-Rays — Arthur Haslett 189
Superconductivity with Respect to Alternating Currents — F. B. Silsbee, R. B. Scott, J. W. Cook and F. G. Brickwedde 192
Spectrum of Carbon Dioxide. II. Electron Levels — H. D. Smyth 193
Some Studies of Negative Point Discharges at Low Pressures — Willi M. Cohn 195
High-Speed Protons — M. A. Tuve, L. R. Hafstad, O. Dahl 197
On the Classification of Certain Lines of Rubium — Walter Albertson 199
Molecular Beams of Salt Vapors — W. E. Ramsperger and W. F. Hersey 201
Book Reviews 207
Current Literature of Physics

PUBLISHED BY THE AMERICAN PHYSICAL SOCIETY

THE AMERICAN PHYSICAL SOCIETY

OFFICERS OF THE SOCIETY

President:	W. F. G. Swann	Bartol Research Foundation, Philadelphia, Pa.
Vice-President:	Paul D. Foote	The Gulf Companies, Pittsburgh, Pa.
Secretary:	W. L. Severinghaus	Columbia University, New York City
Treasurer:	G. B. Pegram	Columbia University, New York City
Editor:	John T. Tate	University of Minnesota, Minneapolis, Minn.
Local Secretary for the Pacific Coast:	L. B. Loeb	University of California, Berkeley, Calif.

THE PHYSICAL REVIEW

Published by the American Physical Society. Executive office: University of Minnesota, Minneapolis, Minn. Two volumes annually, twelve issues per volume.

First series. From July 1, 1893, to January 1, 1913, the Review was conducted by Edward L. Nichols, Ernest Merritt and Frederick Bedell, with the financial support of Cornell University. The first four volumes were issued annually; subsequent volumes, semi-annually; thirty-five volumes in all.

Second series. On January 1, 1913, the Review was transferred to the American Physical Society as announced on the first page of the new series which was then begun. Since then it has been conducted by a Board of Editors elected by the Society. Semi-annual volumes begin in January and July. Since July 1, 1929, the Review has been issued twice a month.

Contributors are referred to page 2 of the advertisements for further information.

Annual subscription, throughout the Postal Union, $12.00 in advance.

General index, 1893-1920, $4.00 in advance.

Back Volumes, $9.00 per volume; Back Numbers, $1.50 per copy for issues prior to July 1, 1929 (Vols. 1-33), $.75 per copy for issues subsequent thereto. Postage is free if remittance accompanies order; otherwise postage is extra. No bound volumes can be supplied. The Review offers to purchase a limited number of First Series, Vol. 1, No. 1 (at $2.00 each); Second Series, Vol. 7, No. 1, January 1916; Vol. 7, No. 2, February 1916; Vol. 7, No. 4, April 1916; and Vol. 7, No. 5, May 1916 (at $2.00 each).

Advertisements. Rates will be supplied by the Editor on request. Copy for each number must be received at Minneapolis two weeks prior to the dates of issue; old copy is used until new copy is received. Send electrotypes direct to the printers, George Banta Publishing Co., Menasha, Wis.

Discount of ten percent is allowed to members of the American Physical Society on purchase of back numbers.

Changes of Address and Complaints of failure to receive the Review, in the case of members of the Physical Society, should be addressed to the Treasurer; in the case of other subscribers, to the Editor. New copies can be sent free in response to complaints of non-delivery only if notice of non-delivery is received within three months of date of issue.

Editorial Correspondence should be addressed to the Physical Review, University of Minnesota, Minneapolis, Minn.

Entered at the post office at Menasha, Wis., as second class matter.
Acceptance for mailing at special rate of postage provided for in section 1103, Act of October 3, 1917, authorized September 6, 1926.

Second Series *January 15, 1932* *Vol. 39, No. 2*

THE
PHYSICAL REVIEW

VARIATION IN THE EFFECTIVE LATTICE CONSTANT OF CRYSTALS WITH WAVE-LENGTHS

By J. M. Cork
University of Michigan

(Received October 30, 1931)

Abstract

This investigation is carried out to determine to what extent x-ray wave-lengths determined by a calcite crystal are consistent over a considerable wave-length range where the refractive index is known to vary. To this end the reflection angles for particular emission wave-lengths up to 5.5A are observed using a quartz crystal. These angles are combined with corresponding values obtained with calcite. The values for $\log (\lambda \text{ (calcite)}/2 \sin\theta \text{ (quartz)})$ when plotted with wave-length, assuming $(1-\mu)/\sin^2\theta$ constant for quartz, result in a curve showing the variation due to calcite. A discontinuity exists at the wave-length of the K absorption edge for calcium. The nature of the curve is in agreement with a similar one obtained by Larsen from measurements of the index of refraction. The discontinuity is in the sense to be expected from the dispersion theories of Kallmann and Mark and Kronig. Assuming quartz as ideal in the range one to five Angstroms, measurements with a calcite crystal are not inconsistent by as much as one third of one tenth of a percent.

IN THE absolute determination of x-ray wave-lengths by ruled gratings, values are obtained somewhat different from those reported by using the crystal method. Different observers,[1] however, using the grating method and employing different wave-lengths do not agree upon the magnitude of the discrepancy. It is of importance therefore to inquire regarding the certainty of the crystal measurements throughout the wave-length range granting them correct at a certain short wave-length. The values for characteristic wave-lengths up through five Angstrom units generally accepted as best values have been obtained almost entirely by the use of calcite crystals.

In this wave-length range comes the K absorption edge of calcium at 3.0643A. Due to the abrupt change in refractive index in the crystal in the neighborhood of this wave-length as well as a systematic variation with increasing wave-length, results reported without a corresponding correction in wave-length might be expected to be somewhat in error. The refractive indices of quartz and calcite have now been thoroughly investigated by Larsen.[2] Unfortunately the results of Larsen were not available to the writer until after the completion of the present investigation.

[1] See Bearden, Phys. Rev. **37**, 1210 (1931).
[2] Larsen, Dissertation, Upsala Universitets, 1929.

In the present investigation the over all wave-length values of various characteristic radiations are observed without regard to the absolute value of the refractive index. Precision angular determinations were made for certain characteristic emission lines with a quartz crystal. These angles were compared with the corresponding ones for the same wave-lengths with a calcite crystal. Quartz, consisting of light atoms, has no characteristic absorption frequency in the wave-length range investigated. Now by forming the ratios of the sines for the corresponding pairs of angles any irregularity observed is attributed entirely to the calcite. The dispersion curve obtained by Larsen for quartz shows only a slight deviation from a constant, from one to five Angstroms.

A somewhat similar comparison was carried out by Siegbahn and Hjalmer[3] for calcite and gypsum crystals. Both of these substances however contain calcium in about the same proportion. The sulphur K absorption edge at 5.009A should produce an important effect. In their investigation a striking effect was observed at the calcium edge as well as at that of sulphur.

A Siegbahn vacuum spectrometer was employed in the investigation. At each characteristic wave-length several plates were taken for some of which the plate holder was shifted 180° to account for any eccentricity of the conical axis. The quartz crystal used, exposed a very perfect prism face and gave excellent reflections.

Results

To show the comparative values for the two crystals, the logarithms of the ratio $[\lambda(\text{calcite})/2d \sin\theta\ (\text{quartz})]$ are tabulated at each wave-length in Table I. The λ (calcite) (recorded value) has in every case been found by multiplying the observed 2 sin θ (calcite) by a value of d (calcite) assumed

Table I.

Wave-length λ	X-ray Line	$\log \frac{\lambda(\text{Calcite})}{2\sin\theta\ (\text{quartz})}$
1.473A	W L α_1	0.62803
2.284	Cr K α_1	0.62794
2.743	Ti K α_1	0.62792
2.995	Sn L γ_1	0.62785
3.378	Sn L β_1	0.62791
3.730	Cd L β_1	0.62789
3.948	Cd L α_1	0.62791
4.145	Ag K α_1	0.62791
4.588	Rh L α_1	0.62788
5.394	Mo L α_1	0.62785

constant (3.02910A at 20°C.) with no correction for refraction in the crystal. Now if there were no variation in the effective lattice constant for either crystal, this ratio would, of course, be the constant value of d(quartz).

The observed values for the logarithms of the ratio are plotted in Fig. 1 as a function of wave-length. The overall error in angular measurements were probably not over five seconds of arc and in Fig. 1 a vertical displacement of

[3] Siegbahn and Hjalmar, Nature **115**, 85 (1925).

one division at the left end (i.e., small wave-lengths) corresponds to an angular displacement of ten seconds while at the right end one division represents about thirty seconds of arc.

The curve differs definitely from a horizontal straight line. There is, moreover, a discontinuity at the K absorption wave-length of calcium. This is revealed particularly by the value of the ratio obtained for the γ_1, line of tin. To make sure that the position of this point off a smooth curve was not an experimental error, about thirty plates for it and adjacent wave-lengths were taken. The nature of the discontinuity is in agreement with that observed by Siegbahn and Hjalmar at the sulphur K edge.

Discussion

Because of the refraction in the crystal a correction need be applied to the Bragg law so that

$$n\lambda = 2D \sin\theta \left(1 - \frac{1-\mu}{\sin^2\theta}\right) \tag{1}$$

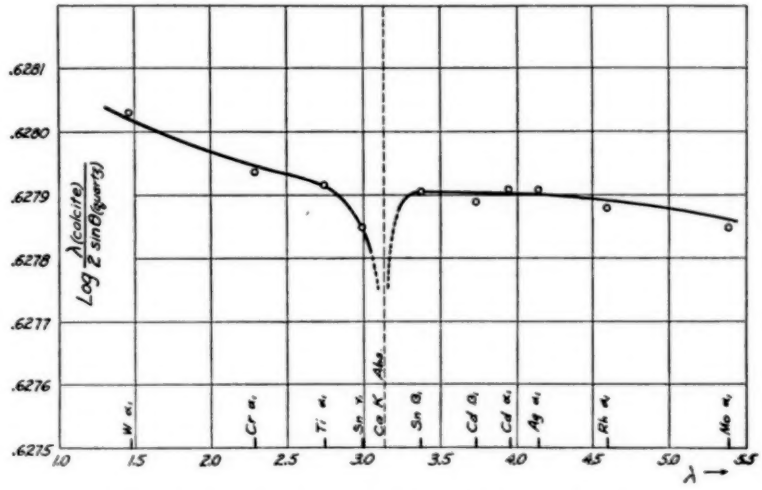

Fig. 1. Variation in angular ratios with wave-length.

where λ is the true wave-length, D the true lattice constant, θ the observed reflection angle and the parenthesis, containing μ the index of the refraction, is a multiplying factor whose value is variable and always slightly less than unity.

The usual expression for $1-\mu$, deduced from classical polarization theory gives

$$1 - \mu = \frac{e^2}{2\pi m} \sum^{N} \frac{n_e}{\nu_x^2 - \nu_e^2} \tag{2}$$

where ν_x and ν_e are the frequencies of the x-ray beam and bound electron respectively and N is the total number of mobile electrons per unit-volume summed in groups of n_e having the common frequency ν_e. Thus for the $2K$ electrons ν_e is the K absorption frequency.

Now it is apparent that if this expression were valid then the discontinuity at a wave-length just shorter than that of the absorption edge should be opposite in sense to that experimentally observed in Fig. 1. That is, for ν_x just greater than ν_e, $(1-\mu)$ abruptly increases and the parenthesis in Eq. (1) decreases. This applied to the numerator of the ratio in Fig. 1 would exaggerate the discontinuity rather than remove it as should be the case.

More satisfactory expressions to represent the variation of refractive index with wave-length change have been developed by Kallman[4] and Mark and by Kronig.[5] The latter development based upon an atomic scattering formula of Hartree[6] and Waller yields the following, where the symbols have the same significance as in Eq. (1).

$$1-\mu=\frac{c}{2\pi^2\nu_x^2}\left[\frac{1}{\nu_e^2}-\frac{1}{\nu_x^2}\log\frac{\nu_e^2}{\nu_x^2-\nu_e^2}\right]. \tag{3}$$

For the two K electrons this would yield a discontinuity in the sense of the observed values for ν_x greater than ν_e.

The expression of Kallman and Mark obtained by considering the damping factors neglected in Eq. (1) gives

$$1-\mu=\frac{e^2}{2\pi mc^2}\sum^{N}\frac{n_e}{\nu_x^2}\left[1+\frac{\nu_e^2}{\nu_x^2}\log\frac{\nu_e^2-\nu_x^2}{\nu_e^2}\right]. \tag{4}$$

For values of ν_x slightly less than ν_e this yields a result of the nature of the dotted portion of the curve in Fig. 1. No experimental points were obtained in this region.

From the values obtained for the refractive index at each wave-length Larsen constructed a $(\Delta\lambda)$ correction curve to be applied to measurements with a calcite crystal. This curve agrees qualitatively with Fig. 1 as regards the dissymmetry in the neighborhood of the calcium absorption edge. The The total deviations are however less than would be expected from the results of the present investigation.

In conclusion, if quartz be assumed an ideal crystal, over the wave-length range one to five Angstrom units, then measurements with a calcite crystal (except perhaps extremely near the wave-length of the calcium K edge) are consistent to better than one third of one tenth of one percent. While this effect is small compared with the differences observed by experimenters using the gratings method at different wave-lengths, it may in certain cases play a small part.

[4] Kallman and Mark, Ann. d. Physik **82,** 585 (1927).
[5] R. de L. Kronig, Phys. Zeits. **30,** 521 (1929).
[6] Waller and Hartree, Proc. Roy. Soc. **A124,** 119 (1929).

THE THEORY OF COMPLEX SPECTRA. PART I. ENERGY LEVELS

By M. H. Johnson, Jr.
Harvard University

(Received November 17, 1931)

Abstract

A general method of finding the wave function for LS coupling which is similar to that of Gray and Wills is described. The successive transformations which carry the angular momentum matrices, S^2, L^2 and J^2 to a diagonal form, are determined by writing down these matrices in terms of the unperturbed wave functions and solving the resulting linear equations for the transformation coefficients. This yields the wave functions appropriate for LS coupling. The method is applied to give the wave functions for all the states of LS coupling with the smallest value of $|M_J|$ in the following electronic configurations: p^2, d^2, p^3, p^2s and p^3s. The matrix of the spin-orbit interaction is calculated with these wave functions and is factored according to J values because J^2 is an integral of the motion. By adding the electrostatic energies as computed by Slater's method to the diagonal elements (the electrostatic energy is known to be a diagonal matrix in LS coupling), the complete energy matrix is obtained. Setting the determinant of the matrix equal to zero, the secular equation for each J value is found for the above electronic configurations. These equations determine the position of the energy levels in intermediate coupling provided that second order perturbations may be neglected and provided magnetic effects other than the spin-orbit interaction do not contribute appreciably to the Hamiltonian.

Introduction

In A previous paper[1] the calculation of the matrix elements of the spin-orbit interaction in LS coupling has been made for any two-electron configuration from the commutation relations which angular momentum vectors satisfy in matrix mechanics. This makes it possible to obtain in a simple manner the secular equations for any two-electron configuration. Although the method can probably be employed for more complex configurations, there are difficulties connected with the necessary extension. Furthermore, if the precise form of the magnetic interaction terms in the Hamiltonian is not correct, other calculations which it may not be possible to carry out by this method, must be made. For these reasons it is profitable to consider a quite different approach to the whole problem.

It was remarked in the above mentioned paper that difficulties with the unperturbed wave functions used by Slater[2] arose because these functions were not written for definite values of the total angular momentum, J^2. In this paper we propose to find the transformation to functions which make J^2 a diagonal matrix. Now such a transformation is by no means uniquely determined and, in fact, wave functions correct for any coupling scheme in an isolated atomic system have this property. For in any such coupling scheme

[1] M. H. Johnson, Jr. Phys. Rev. **38,** 1628 (1931).
[2] J. C. Slater, Phys. Rev. **34,** 1293 (1929).

J^2 is always an integral of the motion so that the proper wave functions must be written for definite values of J^2. For several reasons it is preferable to find the wave functions for LS coupling rather than those for jj coupling (say). In the first place we know that in LS coupling the electrostatic energy is a diagonal matrix. We can then avail ourselves of the calculation of electrostatic energies by Slater's method in the cases where such calculations have been made. By his method we can always obtain the electrostatic energies if there are no two multiplets of the same kind in the group of states considered. In any other coupling scheme we should have to compute the whole matrix of the electrostatic energy, a task which it is profitable to avoid if possible. In the second place it is often very easy in LS coupling to find the matrices of other quantities such as the electric moment, the energy in a magnetic field etc., directly from matrix relations. This may obviate the necessity of using the wave functions, which are rather awkward sums of determinants, in finding such matrices.

From our present point of view the situation is greatly simplified by the existence of spatial degeneracy and the fact that Slater's functions are written for definite values of J_z. J_z is an integral of the motion so that in the transformations we contemplate it is a diagonal invariant. It is therefore only necessary in making these transformations to use linear combinations of functions with the same value of M_J. Because of the spatial degeneracy we know that all the states of distinct energy will be represented among the functions for the smallest value of $|M_J|$. Hence for the energy level problem it is only necessary to consider functions for the smallest value of $|M_J|$. This will still be true no matter how the Hamiltonian is modified (for an isolated atom) for no internal interaction can affect the spatial degeneracy or the fact that J_z is an integral of motion. Then if the actual Hamiltonian differs from the one which we shall employ, the transformations we determine can still be used to advantage.

The Method of Finding Wave Functions for LS Coupling

Our method of obtaining the wave functions for LS coupling is perfectly straight-forward. We compute the matrices of L^2, S^2 and J^2 with the unperturbed functions and then find the transformations to make these matrices diagonal. We know that the wave functions for LS coupling must be written for definite values of L^2, S^2, J^2, and J_z so that this is an obvious procedure. The matrix components in which we are interested may be calculated from the following formulas which can be obtained by an application of the equations that Condon[3] has given for matrix elements calculated with Slater's

[3] E. U. Condon, Phys. Rev. **36**, 1121 (1930). The notation used here is very similar to Condon's. The single electron wave functions are written as $u_\alpha(1)$. The 1 stands for all the coordinates (including spin) of electron 1 and the subscript α stands for the set of single electron quantum numbers n_α l_α $m_{l\alpha}$ and $m_{s\alpha}$. The antisymmetric wave functions are

$$\psi_A = (N!)^{-1/2} \quad \Sigma(-1)^P P u_\alpha(1) u_\beta(2) \cdots u_\xi(N)$$

where the sum is extended over all the permutations, P. Matrix components are written in the Dirac notation

wave functions. Rather than use J^2, we use $\boldsymbol{L}.\boldsymbol{S}$ which must also be diagonal if L^2, S^2 and J^2 are diagonal.

$$(A \mid L^2 \mid A') = 4\{(\alpha \mid l_x \mid \alpha')(\beta \mid l_x \mid \beta') - (\alpha \mid l_x \mid \beta')(\beta \mid l_x \mid \alpha')\} \text{ if } A' \text{ differs from } A \text{ in } \alpha \text{ and } \beta$$

$$(A \mid L^2 \mid A) = M_L{}^2 + \sum_{\alpha}\{l_\alpha(l_\alpha+1) - m_{l\alpha}{}^2\} - \sum_{\substack{\text{all pairs}\\ \alpha,\beta}}\{l_\alpha(l_\alpha+1) - m_{l\alpha}(m_{l\alpha}\pm 1)\}(n_\alpha l_\alpha m_{l\alpha} \pm 1 m_{s\alpha} \mid 1 \mid n_\beta l_\beta m_{l\beta} m_{s\beta})$$

$$(A \mid L^2 \mid A') = 0 \text{ otherwise}$$

$$(A \mid S^2 \mid A') = 4\{(\alpha \mid s_x \mid \alpha')(\beta \mid s_x \mid \beta') - (\alpha \mid s_x \mid \beta')(\beta \mid s_x \mid \alpha')\} \text{ if } A' \text{ differs from } A \text{ in } \alpha \text{ and } \beta$$

$$(A \mid S^2 \mid A) = M_S{}^2 + \tfrac{1}{2}N - N' \text{ where } N = \text{number of electrons}$$

N' = number of pairs α, β with the same n, l, and m_l

$$(A \mid S^2 \mid A') = 0 \text{ otherwise}$$

$$(A \mid \boldsymbol{L}\cdot\boldsymbol{S} \mid A') = 2\{(\alpha \mid l_x \mid \alpha')(\beta \mid s_x \mid \beta') + (\beta \mid l_x \mid \beta')(\alpha \mid s_x \mid \alpha') - (\alpha \mid l_x \mid \beta')(\beta \mid s_x \mid \alpha') - (\beta \mid l_x \mid \alpha')(\alpha \mid s_x \mid \beta')\} \text{ if } A' \text{ differs from } A \text{ in } \alpha \text{ and } \beta.$$

$$(A \mid \boldsymbol{L}\cdot\boldsymbol{S} \mid A') = 2\left\{\sum_{\alpha''}(\alpha \mid \overset{**}{l_x} \mid \alpha'')(\alpha'' \mid s_x \mid \alpha') - \sum_{\beta}(\beta \mid l_x \mid \alpha')(\alpha \mid s_x \mid \beta)\right\} \text{ if } A' \text{ differs from } A \text{ in } \alpha$$

$$(A \mid \boldsymbol{L}\cdot\boldsymbol{S} \mid A) = M_L M_S$$

$$(A \mid \boldsymbol{L}\cdot\boldsymbol{S} \mid A') = 0 \text{ otherwise.}$$

In these formulas

$$(\alpha \mid l_x \mid \beta) = \tfrac{1}{2}\{l_\alpha(l_\alpha+1) - m_{l\alpha}(m_{l\alpha}\pm 1)\}^{1/2}(n_\alpha l_\alpha m_{l\alpha} \pm 1 m_{s\alpha} \mid 1 \mid n_\beta l_\beta m_{l\beta} m_{s\beta})$$

$$(\alpha \mid s_x \mid \beta) = \tfrac{1}{2}(n_\alpha l_\alpha m_{l\alpha} m_{s\alpha} \pm 1 \mid 1 \mid n_\beta l_\beta m_{l\beta} m_{s\beta})$$

$$(A \mid H \mid A') = \int \bar{\psi}_A H \psi_{A'}$$

where the integration implies a summation over the spin coordinates. The abbreviation

$$(\alpha \mid f \mid \beta) = \int \bar{u}_\alpha(k) f(k) u_\beta(k)$$

which is consistent with the above notation, is also introduced. Thus, for example, formula (b) on page 1129 of Condon's paper is, in this notation

$$(A \mid F \mid A') = (\alpha \mid f \mid \alpha')$$

if A' differs from A only in the individual set of quantum numbers α.

** In carrying out this summation it must be remembered that the exclusion principle operates to eliminate the terms for which α'' is equal to any of the other quantum numbers $\beta \cdots \xi$.

$$M_L = \sum_\alpha m_{l\alpha}$$
$$M_S = \sum_\alpha m_{s\alpha}.$$

All the diagonal elements of the unit matrix are unity and all the nondiagonal elements are zero. The signs must always be so chosen that $M_J = M_J'$. We see that L^2 and S^2 have no components between states of different M_L and M_S values as is required by the fact that both these matrices commute with L_z and S_z. Although the furmulas appear formidable, they are actually very easy to use when one has become familiar with the notation.

The required transformations are easy to obtain because the matrices L^2, S^2 and $\boldsymbol{L.S}$ commute with one another. The matrix $\boldsymbol{S}^2$ is usually the simplest so that we first find the transformation, $\boldsymbol{R}$, which carries it to a diagonal form.[4]

$$RS^2R^{-1} = (S^2)'$$
$$RL^2R^{-1} = (L^2)'$$
$$R(\boldsymbol{L}\cdot\boldsymbol{S})R^{-1} = (\boldsymbol{L}\cdot\boldsymbol{S})'$$

where $(S^2)'$ is diagonal and commutes with $(L^2)'$ and $(\boldsymbol{L.S})'$. The last two matrices can therefore have components only between the degenerate states of $(S^2)'$. Thus $\boldsymbol{R}$ tends to simplify the matrices L^2 and $\boldsymbol{L.S}$. Let T carry $(L^2)'$ to a diagonal form, leaving $(S^2)'$ invariant.

$$T(L^2)'T^{-1} = (L^2)''$$
$$T(S^2)'T^{-1} = (S^2)'' = (S^2)'$$
$$T(\boldsymbol{L}\cdot\boldsymbol{S})'T^{-1} = (\boldsymbol{L}\cdot\boldsymbol{S})''$$

where $(L^2)''$ is diagonal. Now $(\boldsymbol{L.S})''$ can only have components between states which are degenerate in both $(L^2)''$ and $(S^2)''$, and so is further simplified. As L^2 and S^2 had no components between states of different M_L and M_S values, the transformations R and T have no components between states of different M_L and different M_S. Hence $L_z'' = L_z$ and $S_z'' = S_z$. The transformation TR carries us to a representation in which L^2, S^2, L_z and S_z are diagonal matrices. Finally let U carry $(\boldsymbol{L.S})''$ to a diagonal form, leaving $(L^2)''$ and $(S^2)''$ invariant.

$$U(\boldsymbol{L}\cdot\boldsymbol{S})''U^{-1} = (\boldsymbol{L}\cdot\boldsymbol{S})'''$$
$$U(L^2)''U^{-1} = (L^2)''' = (L^2)''$$
$$U(S^2)''U^{-1} = (S^2)''' = (S^2)'$$

Where $(\boldsymbol{L.S})'''$ is diagonal. This transformation involves together the states of a single multiplet. After it the wave functions will be correct for LS coup-

[4] R is determined in the manner in which any principle axis transformation is found. The determinant of the matrix S^2 is set equal to zero in order to obtain its characteristic values. (It is not actually necessary to do this as the characteristic values of S^2 are known from the commutation rules which the components of $\boldsymbol{S}$ obey.) The set of homogeneous linear equations $RS^2 = (S^2)'R$ together with the normalization condition determine the transformation coefficients.

ling as we still then have secured that L^2, S^2, J^2 and J_z be diagonal matrices. We can combine the three transformations into a single one, UTR, which will enable us to pass directly from the unperturbed functions to the functions correct for LS coupling. It is apparent one advantage of treating L^2, S^2 and $\boldsymbol{L.S}$ separately, instead of attempting to make J^2 diagonal directly, is that we factor the transformation into relatively simple parts.

The spin-orbit interaction is

$$H_2 = \sum_k f(r_k) \boldsymbol{l}_k \cdot \mathbf{s}_k .$$

Its matrix components in the initial representation are easily found from the formulas Condon[3] has given. They are

$$(A \mid H_2 \mid A') = \tfrac{1}{2}(n_\alpha l_\alpha \mid f \mid n_\alpha' l_\alpha')\left[l_\alpha(l_\alpha+1) - m_{l\alpha}(m_{l\alpha} \pm 1)\right]^{1/2}$$
$$(m_{l\alpha} \pm 1 m_{s\alpha} \pm 1 \mid 1 \mid m_{l\alpha'} m_{s\alpha'}) \text{ if } A' \text{ differs from } A \text{ in } \alpha$$

$$(A \mid H_2 \mid A) = \sum_\alpha (n_\alpha l_\alpha \mid f \mid n_\alpha l_\alpha) m_{l\alpha} m_{s\alpha}$$

$$(A \mid H_2 \mid A') = 0 \text{ otherwise}$$

where $(n_\alpha l_\alpha \mid f \mid n_{\alpha'} l_{\alpha'}) = \int R_{n_\alpha l_\alpha}(r) f(r) R_{n_{\alpha'} l_{\alpha'}}(r) dr .$

Then the matrix of the spin-orbit interaction in LS coupling is given by

$$H_2''' = (UTR) H_2 (UTR)^{-1}.$$

H_2''' should be factored according to J values since J^2 is an integral of the motion and is diagonal in this representation. We observe that the energy matrix will always factor according to J values after the transformation UTR though the form of the interaction terms be quite different than the above. For no matter what the internal interactions in the atom may be, J^2 will always be an integral of the motion.

As we remarked before, we can obtain the whole energy matrix by adding the electrostatic energies to the diagonal elements of H_2'''. It is easily shown that the diagonal element of the whole energy matrix are the energies of the states of the atom if LS coupling is physically realized (that is if L^2 and S^2 are also integrals of the motion). The secular equations in any case are found in the usual way by setting the determinant of the energy matrix equal to zero. As the matrix is factored according to J values, we obtain a separate algebraic equation for each J value which is of the same order as the number of states with this J value.

The procedure we have followed is closely related to the method used by Gray and Wills[5] to find the wave functions for LS coupling. If we examine the meaning underlying their manipulation with the operators $L_x \pm iL_y$ and $S_x \pm iS_y$, we see that they determine linear combinations of the unperturbed wave functions which make L^2, S^2, L_z and S_z diagonal (strong field functions). Thus the result of their first process is just the transformation TR with the

[5] Gray and Wills, Phys. Rev. **38**, 248 (1931).

difference that they determine all the strong field functions whereas we determine only those for the smallest value of $|M_J|$. Similarly their second process with the operators $J_x \pm iJ_y$ gives the transformation U, again for all the wave functions. Our method is essentially the same as theirs, the only difference being in the manner in which the transformations are determined. The possible advantages of the present method are in the first place the compactness furnished by the matrix notation and in the second place the fact that it is only necessary to use the wave functions for the smallest value of $|M_J|$.

To illustrate our procedure in detail the complete calculation is given below for the configuration p^2. Only the results, that is the transformation UTR, the energy matrix in LS coupling and the secular equations are given for the configurations d^2, p^3, p^2s and p^3s.

Applications

The configuration p^2

From Slater's notation[6] the wave functions for the smallest value of $|M_J|$, $M_J = 0$, are

	P^2		M_L	M_S
I	(0 ½)	(−1½)	−1	1
II	(1 ½)	(−1 −½)	0	0
III	(0 ½)	(0 −½)	0	0
IV	(−1½)	(1 −½)	0	0
V	(1 −½)	(0 −½)	1	−1

The angular momentum matrices determined by our formulas are

$L^2 =$

	I	II	III	IV	V
I	2		0		0
II		2	2	0	
III	0	2	4	2	0
IV		0	2	2	
V	0		0		2

$L \cdot S =$

−1	$\sqrt{½}$	0	$-\sqrt{½}$	0
$\sqrt{½}$				$\sqrt{½}$
0		0		0
$-\sqrt{½}$				$-\sqrt{½}$
0	$\sqrt{½}$	0	$-\sqrt{½}$	−1

$S^2 =$

2		0		0
	1	0	−1	
0	0	0	0	0
	−1	0	1	
0		0		2

The transformation R is very easy to obtain and is

$R =$

1		0		0	
	$\sqrt{½}$	0	$\sqrt{½}$		
0	0	1	0	0	$= R^{-1}$***
	$\sqrt{½}$	0	$-\sqrt{½}$		
0		0		1	

[6] Reference 2. In each bracket is placed the set of quantum numbers α for one of the electrons. The quantum numbers $n_\alpha, l_\alpha, n_\beta, l_\beta \cdots n_\xi, l_\xi$ are omitted from the brackets as these quantum numbers do not change in the set of wave functions for one electronic configuration.

*** The reciprocals of any of our transformations are easily obtained because of their unitary character. Thus $R^{-1} = R^*$. As all our transformations are real, it is only necessary to interchange the rows and columns of a transformation matrix to obtain its reciprocal.

$$(S^2)' = \begin{array}{|c|ccc|c|}\hline 2 & & 0 & & 0 \\ \hline & 0 & 0 & 0 & \\ 0 & 0 & 0 & 0 & 0 \\ & 0 & 0 & 2 & \\ \hline 0 & & 0 & & 2 \\ \hline \end{array} \qquad (L^2)' = \begin{array}{|c|ccc|c|}\hline 2 & & 0 & & 0 \\ \hline & 2 & 2\sqrt{2} & 0 & \\ 0 & 2\sqrt{2} & 4 & 0 & 0 \\ & 0 & 0 & 2 & \\ \hline 0 & & 0 & & 2 \\ \hline \end{array} \qquad (L\cdot S)' = \begin{array}{|c|ccc|c|}\hline -1 & 0 & 0 & 1 & 0 \\ \hline 0 & & & & 0 \\ 0 & & 0 & & 0 \\ 1 & & & & 1 \\ \hline 0 & 0 & 0 & 1 & -1 \\ \hline \end{array}$$

We observe that in fact $(L^2)'$ and $(\boldsymbol{L}.\boldsymbol{S})'$ have components only between the degenerate states of $(S^2)'$. The transformation T is equally simple.

$$T = \begin{array}{|c|ccc|c|}\hline 1 & & 0 & & 0 \\ \hline & \sqrt{1/3} & \sqrt{2/3} & 0 & \\ 0 & \sqrt{2/3} & -\sqrt{1/3} & 0 & 0 \\ & 0 & 0 & 1 & \\ \hline 0 & & 0 & & 1 \\ \hline \end{array} = T^{-1}$$

$$(S^2)'' = (S^2)' \qquad (L^2)'' = \begin{array}{|c|ccc|c|}\hline 2 & & 0 & & 0 \\ \hline & 6 & 0 & 0 & \\ 0 & 0 & 0 & 0 & 0 \\ & 0 & 0 & 2 & \\ \hline 0 & & 0 & & 2 \\ \hline \end{array} \qquad (L\cdot S)'' = (L\cdot S)'$$

The invariance of $(\boldsymbol{L}.\boldsymbol{S})'$ to T is peculiar to this case and does not represent the general situation. The product TR

$$TR = \begin{array}{|c|ccc|c|}\hline 1 & & 0 & & 0 \\ \hline & \sqrt{1/6} & \sqrt{2/3} & \sqrt{1/6} & \\ 0 & \sqrt{1/3} & -\sqrt{1/3} & \sqrt{1/3} & 0 \\ & \sqrt{1/2} & 0 & -\sqrt{1/2} & \\ \hline 0 & & 0 & & 1 \\ \hline \end{array}$$

is the transformation from the initial to the strong field functions. Finally for U we have

$$U = \begin{array}{|cccc|c|}\hline \sqrt{1/6} & 0 & 0 & 2\sqrt{1/6} & \sqrt{1/6} \\ \hline 0 & 1 & 0 & 0 & 0 \\ 0 & 0 & 1 & 0 & 0 \\ \sqrt{1/2} & 0 & 0 & 0 & -\sqrt{1/2} \\ \hline \sqrt{1/3} & 0 & 0 & -\sqrt{1/3} & \sqrt{1/3} \\ \hline \end{array}$$

$$(S^2)''' = (S^2)' \qquad (L^2)''' = L^2)'' \qquad (L\cdot S)''' = \begin{array}{|c|ccc|c|}\hline 1 & & 0 & & 0 \\ \hline & 0 & 0 & 0 & \\ 0 & 0 & 0 & 0 & 0 \\ & 0 & 0 & -1 & \\ \hline 0 & & 0 & & -2 \\ \hline \end{array}$$

The transformation to LS coupling is then

$$UTR = \begin{array}{c|ccccc} & \text{I} & \text{II} & \text{III} & \text{IV} & \text{V} \\ \hline {}^3P_2 & \sqrt{1/6} & \sqrt{1/3} & 0 & -\sqrt{1/3} & \sqrt{1/6} \\ {}^1D_2 & 0 & \sqrt{1/6} & \sqrt{2/3} & \sqrt{1/6} & 0 \\ {}^1S_0 & 0 & \sqrt{1/3} & -\sqrt{1/3} & \sqrt{1/3} & 0 \\ {}^3P_1 & \sqrt{1/2} & 0 & 0 & 0 & -\sqrt{1/2} \\ {}^3P_0 & \sqrt{1/3} & -\sqrt{1/6} & 0 & \sqrt{1/6} & \sqrt{1/3} \end{array}$$

$$(S^2)''' = \begin{array}{|c|ccc|c|} \hline 1\cdot2 & & 0 & & 0 \\ \hline & 0 & 0 & 0 & \\ 0 & 0 & 0 & 0 & 0 \\ & 0 & 0 & 1\cdot2 & \\ \hline 0 & & 0 & & 1\cdot2 \\ \hline \end{array} \qquad (L^2)''' = \begin{array}{|c|ccc|c|} \hline 1\cdot2 & & 0 & & 0 \\ \hline & 2\cdot3 & 0 & 0 & \\ 0 & 0 & 0 & 0 & 0 \\ & 0 & 0 & 1\cdot2 & \\ \hline 0 & & 0 & & 1\cdot2 \\ \hline \end{array} \qquad (J^2)''' = \begin{array}{|c|ccc|c|} \hline 2\cdot3 & & 0 & & 0 \\ \hline & 2\cdot3 & 0 & 0 & \\ 0 & 0 & 0 & 0 & 0 \\ & 0 & 0 & 1\cdot2 & \\ \hline 0 & & 0 & & 0 \\ \hline \end{array}$$

The connection between the Roman numerals and the ordinary multiplet notation as shown by the labelling of UTR, is evident when we remember that the characteristic values of the angular momenta are of the form $1(1+1)$. These characteristic values are the basis of the usual multiplet notation.

The matrix of H_2 calculated with the initial wave functions,* is

$$H_2 = \begin{array}{|ccccc|} \hline -a/2 & 0 & a\sqrt{1/2} & -a\sqrt{1/2} & 0 \\ \hline 0 & a & 0 & 0 & 0 \\ a\sqrt{1/2} & 0 & 0 & 0 & a\sqrt{1/2} \\ -a\sqrt{1/2} & 0 & 0 & -a & a\sqrt{1/2} \\ \hline 0 & 0 & a\sqrt{1/2} & -a\sqrt{1/2} & -a/2 \\ \hline \end{array}$$

Applying UTR, we obtain for the spin-orbit interaction in LS coupling

$$H_2''' = \begin{array}{c|ccccc} & {}^3P_2 & {}^1D_2 & {}^1S_0 & {}^3P_1 & {}^3P_0 \\ \hline {}^3P_2 & a/2 & a\sqrt{1/2} & 0 & 0 & 0 \\ {}^1D_2 & a\sqrt{1/2} & 0 & 0 & 0 & 0 \\ {}^1S_0 & 0 & 0 & 0 & 0 & -a\sqrt{2} \\ {}^3P_1 & 0 & 0 & 0 & -a/2 & 0 \\ {}^3P_0 & 0 & 0 & -a\sqrt{2} & 0 & -a \end{array}$$

This is in agreement with the result previously found for this configuration.[1] As the secular equations, determined from the above matrix, have already been given, we will not write them down again.

* In this matrix and following matrices of the spin-orbit interaction, a is an abbreviation for $(n1\,|f|\,n1)$.

The configuration d^2

The wave functions for $M_J = 0$ are

	d^2	M_L	M_S
I	$(2\,-1/2)\ (-1\,-1/2)$	1	-1
II	$(1\,-1/2)\ (0\,-1/2)$	1	-1
III	$(2\,1/2)\ (-2\,-1/2)$	0	0
IV	$(1\,1/2)\ (-1\,-1/2)$	0	0
V	$(0\,1/2)\ (0\,-1/2)$	0	0
VI	$(2\,-1/2)\ (-2\,1/2)$	0	0
VII	$(1\,-1/2)\ (-1\,1/2)$	0	0
VIII	$(1\,1/2)\ (-2\,1/2)$	-1	1
IX	$(-1\,1/2)\ (0\,1/2)$	-1	1

The transformation into LS coupling is

UTR=	I	II	III	IV	V	VI	VII	VIII	IX
$^3F_4$	$3\sqrt{7}/10$	$\sqrt{3}/35$	$\sqrt{7}/35$	$2\sqrt{7}/35$	0	$\sqrt{7}/35$	$2\sqrt{7}/35$	$3\sqrt{7}/10$	$-\sqrt{3}/35$
$^3P_2$	$\sqrt{1}/5$	$-\sqrt{1}/10$	$2\sqrt{1}/5$	$-\sqrt{1}/5$	0	$2\sqrt{1}/5$	$-\sqrt{1}/5$	$\sqrt{1}/5$	$\sqrt{1}/10$
$^3F_3$	$\sqrt{3}/10$	$\sqrt{1}/5$	0	0	0	0	0	$-\sqrt{3}/10$	$\sqrt{1}/5$
$^3P_1$	$\sqrt{1}/5$	$-\sqrt{3}/10$	0	0	0	0	0	$-\sqrt{1}/5$	$-\sqrt{7}/10$
$^1S_0$	0	0	$\sqrt{1}/5$	$-\sqrt{1}/5$	$\sqrt{1}/5$	$-\sqrt{1}/5$	$\sqrt{1}/5$	0	0
$^1D_2$	0	0	$-\sqrt{7}/7$	$-\sqrt{1}/14$	$\sqrt{7}/7$	$\sqrt{7}/7$	$\sqrt{1}/14$	0	0
$^1G_4$	0	0	$\sqrt{1}/10$	$4\sqrt{1}/10$	$3\sqrt{7}/35$	$-\sqrt{1}/10$	$-4\sqrt{1}/10$	0	0
$^3P_0$	$\sqrt{7}/15$	$-\sqrt{1}/5$	$-2\sqrt{1}/30$	$\sqrt{1}/30$	0	$-2\sqrt{1}/30$	$\sqrt{1}/30$	$\sqrt{7}/15$	$\sqrt{1}/5$
$^3F_2$	$\sqrt{7}/35$	$2\sqrt{1}/35$	$-\sqrt{1}/70$	$-2\sqrt{7}/70$	0	$-\sqrt{7}/70$	$-2\sqrt{1}/14$	$\sqrt{7}/35$	$-2\sqrt{1}/35$

If we transform the matrix of the spin-orbit interaction into LS coupling, we obtain a result which has already been given.[1] For this reason we do not write down the matrix of the spin-orbit interaction and the secular equations.

The configuration p^3

The wave functions for $M_J = \frac{1}{2}$ are

	P^3	M_L	M_S
I	$(1\,-1/2)\ (0\,1/2)\ (0\,-1/2)$	1	-1/2
II	$(1\,-1/2)\ (1\,1/2)\ (-1\,-1/2)$	1	-1/2
III	$(1\,1/2)\ (0\,1/2)\ (-1\,-1/2)$	0	1/2
IV	$(1\,1/2)\ (0\,-1/2)\ (-1\,1/2)$	0	1/2
V	$(1\,-1/2)\ (0\,1/2)\ (-1\,1/2)$	0	1/2

The transformation into LS coupling is

$$\text{UTR} = \begin{array}{c|ccccc} & \text{I} & \text{II} & \text{III} & \text{IV} & \text{V} \\ \hline {}^3D_{5/2} & \sqrt{1/5} & \sqrt{1/5} & \sqrt{1/10} & -2\sqrt{1/10} & \sqrt{1/10} \\ {}^2P_{3/2} & \sqrt{1/2} & -\sqrt{1/2} & \sqrt{1/3} & 0 & -\sqrt{1/3} \\ {}^2P_{1/2} & \sqrt{1/3} & -\sqrt{1/3} & -\sqrt{1/6} & 0 & \sqrt{1/2} \\ {}^4S_{3/2} & 0 & 0 & \sqrt{1/3} & \sqrt{1/3} & \sqrt{1/3} \\ {}^2D_{3/2} & \sqrt{3/10} & \sqrt{3/10} & \sqrt{1/15} & 2\sqrt{1/15} & -\sqrt{1/15} \end{array}$$

The matrix of the spin-orbit interaction in LS coupling is

$J = 5/2$

	${}^2D_{5/2}$
${}^2D_{5/2}$	0

$J = 3/2$

	${}^2P_{3/2}$	${}^4S_{3/2}$	${}^2D_{3/2}$
${}^2P_{3/2}$	0	a	$-a/2\sqrt{5}$
${}^4S_{3/2}$	a	0	0
${}^2D_{3/2}$	$a/2\sqrt{5}$	0	0

$J = 1/2$

	${}^2P_{1/2}$
${}^2P_{1/2}$	0

The electrostatic energies calculated by Slater's method when referred to the ${}^2D$ multiplet are[2]

$$\begin{aligned} {}^2D&: \quad 0 \\ {}^2P&: \quad 6/25F^2 = 2X \\ {}^4S&: \quad -9/25F^2 = -3X. \end{aligned}$$

Taking ${}^2D_{5/2}$ as the reference level the secular equations are

$$\begin{aligned} J = 5/2 \quad & -W = 0 \\ J = 3/2 \quad & -W^3 - W^2X + W(9a^2/4 + 6X^2) + 15/4Xa^2 = 0 \\ J = \tfrac{1}{2} \quad & -W + 2X = 0. \end{aligned}$$

The secular equations are in agreement with those obtained by Inglis[7] for this configuration.

The configuration p^2s

The wave functions for $M_J = \frac{1}{2}$ are

[7] D. R. Inglis, Phys. Rev. **38**, 862 (1931). This calculation also confirms the results obtained by D. R. Inglis and M. H. Johnson, Jr. (Phys. Rev. **38**, 1642 (1931)) who found the matrix of the spin-orbit interaction in LS coupling for this configuration by working backwards from the secular equations.

	P^2	S	M_L	M_S
I	(1 -½) (0 ½)	(0 -½)	1	-½
II	(1 ½) (0 -½)	(0 -½)	1	-½
III	(1 -½) (0 -½)	(0 ½)	1	-½
IV	(1 ½) (-1 ½)	(0 -½)	0	½
V	(1 ½) (-1 -½)	(0 ½)	0	½
VI	(0 ½) (0 -½)	(0 ½)	0	½
VII	(-1 ½) (1 -½)	(0 ½)	0	½
VIII	(0 ½) (-1 ½)	(0 ½)	-1	3/2

The transformation into LS coupling is

$$UTR = \begin{array}{c|cccccccc} & \text{I} & \text{II} & \text{III} & \text{IV} & \text{V} & \text{VII} & \text{VI} & \text{VIII} \\ \hline {}^2P_{3/2} & \frac{1}{3}\sqrt{\frac{1}{2}} & \frac{1}{3}\sqrt{\frac{1}{2}} & -\frac{1}{3}\sqrt{2} & \frac{2}{3} & -\frac{1}{3} & 0 & \frac{1}{3} & 0 \\ {}^4P_{3/2} & \sqrt{\frac{1}{10}} & \sqrt{\frac{1}{10}} & \sqrt{\frac{1}{10}} & \sqrt{\frac{1}{15}} & \sqrt{\frac{1}{15}} & 0 & -\sqrt{\frac{1}{15}} & \sqrt{\frac{1}{10}} \\ {}^2D_{5/2} & \sqrt{\frac{1}{15}} & -\sqrt{\frac{1}{15}} & 0 & 0 & -\sqrt{\frac{1}{10}} & -\sqrt{\frac{2}{15}} & -\sqrt{\frac{1}{10}} & 0 \\ \hline {}^2S_{1/2} & 0 & 0 & 0 & 0 & \sqrt{\frac{1}{3}} & -\sqrt{\frac{1}{3}} & \sqrt{\frac{1}{3}} & 0 \\ {}^4P_{1/2} & \frac{2}{3}\sqrt{\frac{1}{15}} & \frac{2}{3}\sqrt{\frac{1}{15}} & \frac{2}{3}\sqrt{\frac{1}{15}} & -\frac{1}{3}\sqrt{\frac{1}{15}} & -\frac{1}{3}\sqrt{\frac{1}{15}} & 0 & \frac{1}{3}\sqrt{\frac{1}{15}} & -\sqrt{\frac{2}{15}} \\ {}^2P_{1/2} & \frac{1}{3} & \frac{1}{3} & -\frac{2}{3} & -\frac{1}{3}\sqrt{2} & \frac{1}{3}\sqrt{\frac{1}{2}} & 0 & -\frac{1}{3}\sqrt{\frac{1}{2}} & 0 \\ {}^2D_{3/2} & -\sqrt{\frac{1}{10}} & \sqrt{\frac{1}{10}} & 0 & 0 & -\sqrt{\frac{1}{15}} & -2\sqrt{\frac{1}{15}} & -\sqrt{\frac{1}{15}} & 0 \\ \hline {}^4P_{1/2} & \frac{1}{3}\sqrt{\frac{1}{2}} & \frac{1}{3}\sqrt{\frac{1}{2}} & \frac{1}{3}\sqrt{\frac{1}{2}} & -\frac{1}{3} & -\frac{1}{3} & 0 & \frac{1}{3} & \sqrt{\frac{1}{2}} \end{array}$$

The matrix of the spin-orbit interaction transformed into LS coupling is

$J = 5/2$

	${}^2D_{5/2}$	${}^4P_{5/2}$
${}^2D_{5/2}$	0	$-a\sqrt{\frac{1}{2}}$
${}^4P_{5/2}$	$-a\sqrt{\frac{1}{2}}$	$a/2$

$J = 3/2$

	${}^2D_{3/2}$	${}^4P_{3/2}$	${}^2P_{3/2}$
${}^2D_{3/2}$	0	$a\frac{1}{2}\sqrt{\frac{1}{3}}$	$a\frac{2}{3}\sqrt{\frac{1}{3}}$
${}^4P_{3/2}$	$a\frac{1}{2}\sqrt{\frac{1}{3}}$	$-a/3$	$a\frac{1}{6}\sqrt{5}$
${}^2P_{3/2}$	$a\frac{2}{3}\sqrt{\frac{1}{3}}$	$a\frac{1}{6}\sqrt{5}$	$a/3$

$J = 1/2$

	${}^4P_{1/2}$	${}^2P_{1/2}$	${}^2S_{1/2}$
${}^4P_{1/2}$	$-5a/6$	$a\frac{1}{3}\sqrt{\frac{1}{2}}$	$-2a\sqrt{\frac{1}{3}}$
${}^2P_{1/2}$	$a\frac{1}{3}\sqrt{\frac{1}{2}}$	$-2a/3$	$a\sqrt{\frac{2}{3}}$
${}^2S_{1/2}$	$-2a\sqrt{\frac{1}{3}}$	$a\sqrt{\frac{2}{3}}$	0

The electrostatic energies calculated by Slater's method, are[8]

$$^2D: 2F^0(Ps) + F^0(P^2) + 1/25E^2 - \tfrac{1}{3}G^1$$
$$^4P: 2F^0(Ps) + F^0(P^2) - 5/25F^2 - \tfrac{2}{3}G^1$$
$$^2P: 2F^0(Ps) + F^0(P^2) - 5/25F^2 + \tfrac{1}{3}G^1$$
$$^2S: 2F^0(Ps) + F^0(P^2) + 10/25F^2 - \tfrac{1}{3}G^1.$$

[8] E. U. Condon and G. H. Shortley, Phys. Rev. **37**, 1025 (1931).

It is convenient to use the midpoint between the $^2D_{5/2}$ and the $^4P_{5/2}$ levels as a reference point from which to measure energies. The electrostatic energies become

$$\begin{aligned} {}^2D: &\quad 3/25F^2 + \tfrac{1}{6}G^1 = \alpha \\ {}^4P: - &\quad 3/25F^2 - \tfrac{1}{6}G^1 = -\alpha \\ {}^2P: - &\quad 3/25F^2 + \tfrac{5}{6}G^1 = \beta \\ {}^2S: &\quad 12/25F^2 + \tfrac{1}{6}G^1 = \gamma. \end{aligned}$$

The secular equations are

$$\begin{aligned} J = 5/2 \quad & W^2 - (\alpha - a/4)^2 - a^2/2 = 0 \\ J = 3/2 \quad & -W^3 + W^2(\beta - \tfrac{3}{4}a) + W\{\alpha^2 + a/6(2\alpha + 5\beta) + (\tfrac{3}{4}a)^2\} \\ & - \alpha^2\beta - 1/12a\alpha(\alpha + 4\beta) + 1/16a^2(4\alpha + \beta) + (\tfrac{3}{4}a)^3 = 0 \\ J = \tfrac{1}{2} \quad & -W^3 + W^2\{-\alpha + \beta + \gamma - 9/4a\} - W\{-\alpha(\beta + \gamma) + \beta\gamma \\ & + a/6(7\alpha - 12\gamma - 8\beta) - (3a/4)^2\} - \alpha\beta\gamma \\ & + a/12(11\alpha\gamma + 3\alpha\beta - 13\beta\gamma) + a^2/16(7\alpha - 17\beta + 15\gamma) + 3(3a/4)^3 = 0. \end{aligned}$$

The configuration p^3s

The wave functions for $M_J = 0$ are

	P^3			S	M_L	M_S
I	(1 -½)	(0½)	(0 -½)	(0 -½)	1	-1
II	(1 -½)	(1½)	(-1 -½)	(0 -½)	1	-1
III	(1½)	(0½)	(-1 -½)	(0 -½)	0	0
IV	(1½)	(0 -½)	(-1½)	(0 -½)	0	0
V	(1 -½)	(0½)	(-1½)	(0 -½)	0	0
VI	(1 -½)	(0 -½)	(-1½)	(0½)	0	0
VII	(1 -½)	(0½)	(-1 -½)	(0½)	0	0
VIII	(1½)	(0 -½)	(-1 -½)	(0½)	0	0
IX	(-1½)	(0 -½)	(0½)	(0½)	-1	1
X	(-1½)	(-1 -½)	(1½)	(0½)	-1	1

The transformation into LS coupling is

UTR =

	I	II	III	IV	V	VI	VII	VIII	IX	X
$^3D_3$	$\sqrt{1/10}$	$\sqrt{1/10}$	$\frac{1}{2}\sqrt{1/5}$	$-\sqrt{1/5}$	$\frac{1}{2}\sqrt{1/5}$	$-\frac{1}{2}\sqrt{1/5}$	$\sqrt{1/5}$	$-\frac{1}{2}\sqrt{1/5}$	$\sqrt{1/10}$	$\sqrt{1/10}$
$^3P_2$	$\frac{1}{2}\sqrt{1/3}$	$-\frac{1}{2}\sqrt{1/3}$	$\sqrt{1/6}$	0	$-\sqrt{1/6}$	$-\sqrt{1/6}$	0	$\sqrt{1/6}$	$-\frac{1}{2}\sqrt{1/3}$	$\frac{1}{2}\sqrt{1/3}$
$^1P_1$	0	0	½	0	-½	½	0	-½	0	0
$^5S_2$	0	0	$\sqrt{1/6}$	$\sqrt{1/6}$	$\sqrt{1/6}$	$\sqrt{1/6}$	$\sqrt{1/6}$	$\sqrt{1/6}$	0	0
$^1D_2$	0	0	$\frac{1}{2}\sqrt{1/3}$	$-\sqrt{1/3}$	$\frac{1}{2}\sqrt{1/3}$	$\frac{1}{2}\sqrt{1/3}$	$-\sqrt{1/3}$	$\frac{1}{2}\sqrt{1/3}$	0	0
$^3P_1$	½	-½	0	0	0	0	0	0	½	-½
$^3S_1$	0	0	$\sqrt{1/6}$	$\sqrt{1/6}$	$\sqrt{1/6}$	$-\sqrt{1/6}$	$-\sqrt{1/6}$	$-\sqrt{1/6}$	0	0
$^3D_2$	½	½	0	0	0	0	0	0	-½	-½
$^3D_1$	$\frac{1}{2}\sqrt{1/5}$	$\frac{1}{2}\sqrt{1/5}$	$-\frac{1}{2}\sqrt{1/5}$	$\sqrt{1/15}$	$-\frac{1}{2}\sqrt{1/5}$	$\frac{1}{2}\sqrt{1/5}$	$-\sqrt{1/15}$	$\frac{1}{2}\sqrt{1/5}$	$\frac{1}{2}\sqrt{1/5}$	$\frac{1}{2}\sqrt{1/5}$
$^3P_0$	$\sqrt{1/6}$	$-\sqrt{1/6}$	$-\frac{1}{2}\sqrt{1/3}$	0	$\frac{1}{2}\sqrt{1/3}$	$\frac{1}{2}\sqrt{1/3}$	0	$-\frac{1}{2}\sqrt{1/3}$	$-\sqrt{1/6}$	$\sqrt{1/6}$

The matrix of the spin-orbit interaction in LS coupling is

$J = 3$

	$^3D_3$
$^3D_3$	0

$J = 2$

	$^3P_2$	$^5S_2$	$^1D_2$	$^3D_2$
$^3P_2$	0	a	$a\sqrt{1/2}$	$-a/2\sqrt{3}$
$^5S_2$	a	0	0	0
$^1D_2$	$a\sqrt{1/2}$	0	0	0
$^3D_2$	$-a/2\sqrt{3}$	0	0	0

$J = 1$

	$^1P_1$	$^3P_1$	$^3S_1$	$^3D_1$
$^1P_1$	0	0	$a\sqrt{1/3}$	$-a\sqrt{1/6}$
$^3P_1$	0	0	$a\sqrt{1/3}$	$-a/2\sqrt{5/3}$
$^3S_1$	$a\sqrt{1/3}$	$a\sqrt{1/3}$	0	0
$^3D_1$	$-a\sqrt{1/6}$	$-a/2\sqrt{5/3}$	0	0

$J = 0$

	$^3P_0$
$^3P_0$	0

The electrostatic energies calculated by Slater's method are, when referred to the ^3D multiplet,

$$
\begin{aligned}
^3D&: \quad 0 \\
^1D&: \quad \tfrac{2}{3}G^1 &&= \alpha \\
^3P&: \quad 6/25F^2 &&= \beta \\
^1P&: \quad 6/25F^2 + \tfrac{2}{3}G^1 &&= \gamma \\
^5S&: -9/25F^2 - \tfrac{1}{3}G^1 &&= \delta \\
^3S&: -9/25F^2 + G^1 &&= \mu .
\end{aligned}
$$

We find the following secular equations with the $^3D_3$ as the reference level.

$$
\begin{aligned}
J = 3 \quad & -W = 0 \\
J = 2 \quad & W^4 - W^3(\alpha + \beta + \delta) + W^2\{\alpha(\beta + \delta) + \beta\delta - 9/4a^2\} \\
& - W\{\alpha\beta\delta - a^2/4(7\alpha + 5\delta)\} - \tfrac{3}{4}\alpha\delta a^2 = 0 \\
J = 1 \quad & W^4 - W^3(\beta + \gamma + \mu) + W^2\{\beta(\gamma + \mu) + \gamma\mu - 9/4a^2\} \\
& - W\{\beta\gamma\mu - a^2/4(6\beta + 3\gamma + 5\mu)\} - 5/12a^2\mu(2\beta + \gamma) = 0 \\
J = 0 \quad & -W + \beta = 0.
\end{aligned}
$$

In conclusion it is the writer's pleasant duty to acknowledge his indebtedness to the counsel of Professor J. C. Slater under whose direction this work was done, to the discussions and criticisms of Professor E. C. Kemble and Dr. L. A. Young, and finally to Harvard University for the award of a Whiting Fellowship which made the completion of this work possible.

THE BERYLLIUM MOLECULE

By W. H. Furry and J. H. Bartlett, Jr.
University of Illinois

(Received November 29, 1931)

Abstract

The interaction of a normal Be atom with one which has an electronic configuration $2s2p$ has been studied by means of the Heitler-London method. Of the eight possible molecular states, two are calculated to be stable, namely $^1\Sigma A^N$ and $^1\Pi A^N$, and the $^1\Sigma$ state is the lower of the two. An attempt to obtain agreement with experiment in the case where a normal Li atom interacts with one in the $2p^2P$ state has not been successful, at least for the resulting II states.

ONE cannot regard the problem of chemical valence as solved until the approximate validity of a few simple rules of wide applicability has been established by methods based on the quantum mechanics. Even for a diatomic molecule, where one must study the motion of a system of several elections in a field of two centers, no very powerful methods have as yet been developed, so that the degree of success to date is hardly commensurate with the effort expended.

One of the simplest cases, that of the interaction of two normal hydrogen atoms, has been studied by Heitler and London,[1] Sugiura,[2] Wang,[3] and Hylleraas.[4] For the heat of dissociation, Sugiura obtained 3.0 volts and Wang 3.6 volts, as compared with the experimental value of 4.4 volts. The preliminary work of Hylleraas still showed a discrepancy of 0.5 volt, and there appeared to be no convenient way to diminish this. However, Hylleraas was able to give an estimate of upper and lower limits to the heat of dissociation value. If one starts with an unperturbed system of two electrons moving independently of each other in a field of two centers, and introduces the electrostatic interaction between the two electrons as a perturbation, then it is possible to calculate the electronic energy as a function of the distance (leaving aside the $2/R$ term). The exact values for $R=0$ and $R=\infty$, respectively, are -5.8072 and -2.000. The values calculated with the above method are -5.6817 and -1.3932. The values found from the variation method are -5.6953 and -2.000. The assumption is made that the ratio of exact energy to the approximate value is a monotonic function of R. Accordingly, if we multiply values from the "separation" method by $5.8072/5.6817$, we shall find an upper limit for the electronic energy, and if we multiply values from the variation method by $5.8072/5.6953$, then we shall obtain a lower limit. The heat of dissociation then comes out to be $D=(4.37\pm0.12)$ volts. This renders the assumption of monotone character plausible, but does not, of course, prove it.

[1] W. Heitler u. F. London, Zeits. f. Physik **44,** 455 (1927).
[2] Y. Sugiura, Zeits. f. Physik **45,** 484 (1927).
[3] S. C. Wang, Phys. Rev. **31,** 579 (1928).
[4] E. Hylleraas, Zeits. f. Physik **71,** 739 (1931).

The status of the matter at present, then, is that there still remains at least 0.5 volt discrepancy between experimental and theoretical value. This agreement is not good, and apparently the only way to improve it is to employ a method similar to that used by Hylleraas[5] for helium, where the wave function contains as one of its arguments the distance between the two electrons.

Kemble and Zener,[6] and Zener and Guillemin[7] have attempted to calculate the heats of dissociation for some of the two-quantum states of the hydrogen molecule, and were unable to get good quantitative results. The first two writers considered only the Π states, assuming that most of the other states would be repulsive in character. This work thus gives us only limited information concerning the relative positions of the resulting energy levels. In the later paper,[7] it was shown how the earlier calculations of Sugiura could be simplified, but the quantitative results were not in good agreement with experiment. Hylleraas,[4] with the two-center wave functions as the unperturbed ones, has been able to improve on these results considerably. He obtains as heats of dissociation of the $p^1\Pi$, $p^3\Pi$ and $p^1\Sigma$ states the values 2.197 volts, 2.655 volts, and 3.185 volts, respectively, as against the experimental values 2.27, 2.84 and 3.37. The method breaks down for the $s\Sigma$ states, which probably need special consideration.

The present work was practically completed before the results of Hylleraas became known, and was based on the idea that though good quantitative agreement was not to be expected from the Heitler-London method, still the method should be capable of giving correctly the relative positions of the molecular energy levels. For small separations, however, one cannot hope for good results. If one wishes accuracy, then the procedure of Hylleraas should be adopted.

Since the atomic wave functions of Zener[8] gave good quantitative results[9] for Li_2, they will be used in the following calculations. When there are but two electrons on each atom, one can calculate rather readily the relative positions of the resulting energy levels. The mutual influence of the K-shells may be neglected, as Delbrück has shown[10] and so it is possible to ascertain whether or not beryllium molecules are stable. We have already shown[9] that two normal beryllium atoms repel each other, and shall now find out what happens when a normal beryllium atom interacts with one in the first excited state $(2s2p)$.

Interaction of a Normal Be Atom with an Excited Be Atom

Notation. For the most part, the notation will be that previously used.[8] However, to secure greater generality, some modifications must be made.[11] The wave function of electron 1 referred to nucleus a may now be written

[5] E. A. Hylleraas, Zeits. f. Physik **54,** 347 (1929).
[6] E. C. Kemble and C. Zener, Phys. Rev. **33,** 512 (1929).
[7] C. Zener and V. Guillemin, Phys. Rev. **34,** 999 (1929).
[8] C. Zener, Phys. Rev. **36,** 51 (1930).
[9] J. H. Bartlett, Jr. and W. H. Furry, Phys. Rev. **38,** 1615 (1931).
[10] M. Delbrück, Ann. d. Physik **5,** 36 (1930).
[11] J. H. Bartlett, Jr., Phys. Rev. **37,** 507 (1931). The signs of i_5, i_6, and i_7 should be reversed. This means that on p. 530 the rôles of $^1\Pi$ and $^3\Pi$ will be interchanged.

$a_{\alpha n_1}(1)$ or $a_{\beta n_1}(1)$ where α and β denote the spin orientation and n_1 the orbital orientation.

Let

$$J(n_1n_2;\ n_3n_4) = \int H' a_{n_1}{}^*(1) a_{n_2}(1) b_{n_3}{}^*(2) b_{n_4}(2) dv$$

$$J'(n_1n_2;\ n_3n_4) = \int H' a_{n_1}{}^*(1) b_{n_2}(1) a_{n_3}(2) b_{n_4}{}^*(2) dv$$

$$J_a''(n_1n_2;\ n_3n_4) = \int H' a_{n_1}{}^*(1) a_{n_2}(1) a_{n_3}{}^*(2) b_{n_4}(2) dv$$

$$J_b''(n_1n_2;\ n_3n_4) = \int H' b_{n_1}{}^*(1) b_{n_2}(1) b_{n_3}{}^*(2) a_{n_4}(2) dv$$

$$S_{n_1n_2}^{1/2} = \int a_{n_1}{}^*(1) b_{n_2}(1) dv_1$$

$$S_{n_1n_2,n_3n_4} = S_{n_1n_2}^{1/2} S_{n_3n_4}^{1/2}.$$

The H' is to operate on the unstarred functions, and since the form of H' depends on the functions on which it operates, it follows that the order of the arguments in these integrals may not in general be changed without altering the values of the integral. For example,

$$J_a''(n_1n_2;\ n_3n_4) \neq J_a''(n_1n_2;\ n_4n_3).$$

The same is true for the S integrals, i.e., $S_{n_1n_2}{}^{1/2} \neq S_{n_2n_1}{}^{1/2}$, in general.

Instead of n_1n_2 etc., it proves convenient to use the letters s and p, where p takes on the value 0 or 1, according to the value of the magnetic quantum number. With this notation, one finds $S_{s0}{}^{1/2} = -S_{0s}{}^{1/2}$, illustrating the rule above. A further relation is that $J_a'' = (-)^m J_b''$, if m denotes the number of zeros occurring among the arguments n_1, n_2, n_3, n_4.

As before, small letters j, j', and j'' will refer to the contribution from the $(2/r)$ part of H' to the total integral.

If we define

$$I_a(n_1n_2) = \int a_{n_1}{}^* a_{n_2}(2/b) dv$$

$$I_b(n_1n_2) = \int b_{n_1}{}^* b_{n_2}(2/a) dv$$

$$I_a'(n_1n_2) = \int a_{n_1}{}^* b_{n_2}(2/b) dv$$

$$I_b'(n_1n_2) = \int a_{n_1}{}^* b_{n_2}(2/a) dv$$

then

$$J(n_1n_2;\ n_3n_4) = (2/R)\delta_{n_1n_2}\delta_{n_3n_4} + j(n_1n_2;\ n_3n_4) - \delta_{n_1n_2} I_b(n_3n_4) - I_a(n_1n_2)\delta_{n_3n_4}$$

$$J'(n_1n_2;\ n_3n_4) = (2/R)S_{n_1n_2,n_3n_4} + j'(n_1n_2;\ n_3n_4) - S^{1/2}_{n_1n_2}I_a'(n_3n_4) - I_b'(n_1n_2)S^{1/2}_{n_3n_4}$$

$$J_a''(n_1n_2;\ n_3n_4) = (2/R)\delta_{n_1n_2}S^{1/2}_{n_3n_4} + j_a''(n_1n_2;\ n_3n_4) - \delta_{n_1n_2}I_b'(n_3n_4) - I_a(n_1n_2)S^{1/2}_{n_3n_4}.$$

In particular,

$$I_a(s0) = -I_b(s0)$$
$$I_a'(s0) = -I_b'(0s)$$
$$I_a'(0s) = -I_b'(s0)$$
$$I_a'(00) = I_b'(00).$$

Calculation of the energies. As unperturbed wave functions, we take

$$\Psi_1 = (1/24)^{1/2}\sum_P(-)^{\sigma_P}P\{a_{\alpha p}(1)a_{\beta s}(2)b_{\alpha s}(3)b_{\beta s}(4)\}$$
$$\Psi_2 = (1/24)^{1/2}\sum_P(-)^{\sigma_P}P\{a_{\alpha s}(1)a_{\beta p}(2)b_{\alpha s}(3)b_{\beta s}(4)\}$$
$$\Psi_3 = (1/24)^{1/2}\sum_P(-)^{\sigma_P}P\{a_{\alpha s}(1)a_{\beta s}(2)b_{\alpha p}(3)b_{\beta s}(4)\}$$
$$\Psi_4 = (1/24)^{1/2}\sum_P(-)^{\sigma_P}P\{a_{\alpha s}(1)a_{\beta s}(2)b_{\alpha s}(3)b_{\beta p}(4)\}.$$

Here P denotes a permutation of the numbers (1234), and σ_P its order.

There will result, from the combination $(2s)^2$ and $2s2p$, states of Σ and Π types, of singlet or triplet character, and either symmetrical or antisymmetrical in the nuclei (S^N or A^N). That is, eight states are possible.

Forming linear combinations of the above functions, we obtain

$$u_1 = \Psi_1 + \Psi_2 + \Psi_3 + \Psi_4 \quad (S^E\,S^N)$$
$$u_2 = \Psi_1 - \Psi_2 + \Psi_3 - \Psi_4 \quad (A^E\,S^N)$$
$$u_3 = \Psi_1 + \Psi_2 - \Psi_3 - \Psi_4 \quad (S^E\,A^N)$$
$$u_4 = \Psi_1 - \Psi_2 - \Psi_3 + \Psi_4 \quad (A^E\,A^N).$$

The symmetry types are indicated, S^E denoting a singlet, and A^E a triplet.

The energy is

$$E = \frac{\int u^*Hu\,dv}{\int u^*u\,dv}$$

where

$$H = -\sum_{i=1}^{4}\Delta_i + (8/R) - \sum_{i=1}^{4}\left(\frac{4}{a_i} + \frac{4}{b_i}\right) + \sum_{i<j}2/r_{ij}.$$

It is seen that H is symmetrical in the nuclei and in the electrons. Now let

$$H_{ij} = \int \Psi_i^* H \Psi_j dv$$

$$N_{ij} = \int \Psi_i^* \Psi_j dv.$$

The functions Ψ_1, Ψ_2, Ψ_3, and Ψ_4 are connected with each other by the transpositions $(\alpha\beta)$ and (ab).

$$(\alpha\beta)\Psi_1 = \Psi_2 \qquad (ab)\Psi_1 = \Psi_3 \qquad (\alpha\beta)(ab)\Psi_1 = \Psi_4$$

Accordingly

$$H_{11} = H_{22} = H_{33} = H_{44}$$
$$H_{12} = H_{21} = H_{34} = H_{43}$$
$$H_{13} = H_{31} = H_{24} = H_{42}$$
$$H_{14} = H_{41} = H_{23} = H_{32}.$$

Similar relations hold for the N_{ij}'s.

As before H may be broken up into two parts, an unperturbed operator H_0 and a perturbing term H', the actual form of the H' depending upon the function upon which it operates. The unperturbed energy will depend only upon the symmetry in the electrons, so that for S^E, $H_0 u = E_a u$, and for A^E, $H_0 u = E_b u$, where $E_a - E_b$ equals the energy difference between the two levels ^1P and ^3P in the beryllium atom.

The energies are then:

$$E_1 = E_a + (H_{11}' + H_{12}' + H_{13}' + H_{14}')/(N_{11} + N_{12} + N_{13} + N_{14})$$
$$E_2 = E_b + (H_{11}' - H_{12}' + H_{13}' - H_{14}')/(N_{11} - N_{12} + N_{13} - N_{14})$$
$$E_3 = E_a + (H_{11}' + H_{12}' - H_{13}' - H_{14}')/(N_{11} + N_{12} - N_{13} - N_{14})$$
$$E_4 = E_b + (H_{11}' - H_{12}' - H_{13}' + H_{14}')/(N_{11} - N_{12} - N_{13} + N_{14}).$$

We may write

$$H_{ij} = \int \sum_P (-)^{\sigma_P} [P a_{\alpha n_1}(1) a_{\beta n_2}(2) b_{\alpha n_3}(3) b_{\beta n_4}(4)]^* H \cdot [a_{\alpha n_1'}(1) a_{\beta n_2'}(2) b_{\alpha n_3'}(3) b_{\beta n_4}(4)] dv$$

and

$$H = H_0 + H'(14) + H'(24) + H'(13) + H'(23)$$

where

$$H'(kl) = (2/R) - (2/b_k) - (2/a_l) + (2/r_{kl})$$
$$H_{ij}'(13) = (\delta_{n_2 n_2'}\delta_{n_4 n_4'} - S_{n_2' n_4, n_3 n_4'})\{J(n_1 n_1'; n_3 n_3') - J'(n_1 n_3'; n_1' n_3)\}$$
$$H_{ij}'(24) = (\delta_{n_1 n_1'}\delta_{n_3 n_3'} - S_{n_1' n_3, n_1 n_3'})\{J(n_2 n_2'; n_4 n_4') - J'(n_2 n_4'; n_2' n_4)\}$$
$$H_{ij}'(14) = \delta_{n_2 n_2'}\delta_{n_3 n_3'} J(n_1 n_1'; n_4 n_4') - \delta_{n_2 n_2'} S_{n_1 n_3'}^{1/2} J_b''(n_4 n_4'; n_3 n_1') - \delta_{n_3 n_3'} S_{n_2' n_4}^{1/2} J_a''(n_1 n_1'; n_2 n_4') + S_{n_2' n_4, n_1 n_3'} J'(n_2 n_4'; n_1' n_3)$$
$$H_{ij}'(23) = \delta_{n_1 n_1'}\delta_{n_4 n_4'} J(n_2 n_2'; n_3 n_3') - \delta_{n_1 n_1'} S_{n_2 n_4'}^{1/2} J_b''(n_3 n_3'; n_4 n_2') - \delta_{n_4 n_4'} S_{n_1' n_3}^{1/2} J_a''(n_2 n_2'; n_1 n_3') + S_{n_1' n_3, n_2 n_4'} J'(n_1 n_3'; n_2' n_4).$$

Let us calculate H'_{11}, H'_{21}, H'_{31}, and H'_{41}. For all these quantities $(n_1'n_2'n_3'n_4') = (psss)$.

For

$$H'_{11},\ (n_1n_2n_3n_4) = (psss)$$
$$H'_{21},\ (n_1n_2n_3n_4) = (spss)$$
$$H'_{31},\ (n_1n_2n_3n_4) = (ssps)$$
$$H'_{41},\ (n_1n_2n_3n_4) = (sssp)$$

$$H_{11}'(13) = (1 - S_{ss})\{J(pp; ss) - J'(ps; ps)\}$$
$$H_{21}'(13) = \quad - S_{ss,ps}\{J(sp; ss) - J'(ss; ps)\}$$
$$H_{31}'(13) = (1 - S_{ss})\{J(sp; ps) - J'(ss; pp)\}$$
$$H_{41}'(13) = \quad S_{sp,ss}\{J(sp; ss) - J'(ss; ps)\}$$
$$H_{11}'(24) = (1 - S_{ps})\{J(ss; ss) - J'(ss; ss)\}$$
$$H_{21}'(24) = \quad - S_{ps,ss}\{J(ps; ss) - J'(ps; ss)\}$$
$$H_{31}'(24) = \quad - S_{pp,ss}\{J(ss; ss) - J'(ss; ss)\}$$
$$H_{41}'(24) = \quad - S_{ps,ss}\{J(ss; ps) - J'(ss; sp)\}$$

$$H_{11}'(14) = J(pp; ss) - S_{ps}^{1/2}J_b''(ss; sp) - S_{ss}^{1/2}J_a''(pp; ss) + S_{ss,ps}J'(ss; ps)$$
$$H_{21}'(14) = \quad - S_{ss}^{1/2}J_a''(sp; ps) + S_{ss}J'(ps; ps)$$
$$H_{31}'(14) = \quad - S_{ss}^{1/2}J_b''(ss; pp) \quad + S_{ss}J'(ss; pp)$$
$$H_{41}'(14) = J(sp; ps) - S_{ss}^{1/2}J_b''(ps; sp) - S_{sp}^{1/2}J_a''(sp; ss) + S_{sp,ss}J'(ss; ps)$$
$$H_{11}'(23) = J(ss; ss) - S_{ss}^{1/2}J_b''(ss; ss) - S_{ps}^{1/2}J_a''(ss; ps) + S_{ps,ss}J'(ps; ss)$$
$$H_{21}'(23) = \quad - S_{ps}^{1/2}J_a''(ps; ss) + S_{ps,ps}J'(ss; ss)$$
$$H_{31}'(23) = \quad - S_{pp}^{1/2}J_a''(ss; ss) + S_{pp,ss}J'(ss; ss)$$
$$H_{41}'(23) = \quad + S_{ps,ss}J'(ss; sp).$$

For the terms in the denominators we have

$$N_{ij} = \int \sum_P (-)^{\sigma_P}[Pa_{\alpha n_1}(1)a_{\beta n_2}(2)b_{\alpha n_3}(3)b_{\beta n_4}(4)]^* \cdot a_{\alpha n_1'}(1)a_{\beta n_2'}(2)b_{\alpha n_3'}(3)b_{\beta n_4'}(4)dv$$
$$= (\delta_{n_1n_1'}\delta_{n_2n_2'} - S_{n_1n_3',n_1'n_3})(\delta_{n_2n_2'}\delta_{n_4n_4'} - S_{n_2n_4',n_2'n_4})$$
$$N_{11} = (1 - S_{ps})(1 - S_{ss})$$
$$N_{21} = S_{ss,ps} \cdot S_{ss,ps} = S_{ps} \cdot S_{ss}$$
$$N_{31} = - S_{ss,pp}(1 - S_{ss})$$
$$N_{41} = S_{ss,ps} \cdot S_{ss,sp}.$$

Three typical integrals will now be evaluated, and the others just tabulated.

$$\text{I.} \qquad j(s0;\, s0) = c^2c_2{}^2 \int (2/r)a_1{}^2b_2{}^2 \cos\theta_{a_1} \cos\theta_{b_2} e^{-\kappa(a_1+b_2)} dv_1 dv_2.$$

If $(2/r)$ is expanded in terms of b_1, b_2, and $P_n(\cos\gamma)$, then one can integrate over dv_2, obtaining

$$j(s0;\, s0) = (8\pi c^2c_2{}^2/3\kappa^4) \int a^2 \cos\theta_a \cos\theta_b \{\gamma_6(\kappa b)/(\kappa b)^2 + (\kappa b)\Gamma_3(\kappa b)\} \cdot e^{-\kappa a} dv.$$

This may be divided into two parts; one is conveniently integrated in the (a, b) coördinate system, while the (λ, μ) system is more suitable for the other. No difficulty is encountered, for the integrands do not give infinite contributions at any points of the regions involved. The result is:

$$\begin{aligned} j(s0;\, s0) = {} & (1/72)(\alpha/2)^3\kappa\{80[-240/\alpha^6 + 2A_5 + A_2] - 15(2A_0 + 14A_2/3) \\ & + 15(\alpha/2)(2A_3 + 2A_1) - (15/2)(\alpha/2)^2[-8A_2/5 + (\tfrac{2}{3})(A_4 - A_0)] \\ & - (9/4)(\alpha/2)^3[-12A_3/5 + (\tfrac{2}{3})(A_5 + A_1)] \\ & - (\tfrac{3}{8})(\alpha/2)^4[2A_6/3 - 14A_4/5 + 34A_2/21 - 2A_0/5]\}_{(1,\alpha)} \end{aligned}$$

$$\text{II.} \qquad j'(ss;\, s0) = c^3c_2 \int (2/r)a_1b_1a_2b_2 \cos\theta_{b_2} e^{-(\kappa/2)(a_1+a_2+b_1+b_2)} dv_{12}.$$

For the j' and j'' integrals, we make use of the Neumann expansion. The calculation was facilitated by grouping certain terms together. New symbols were introduced, definited as given below.

$$\begin{aligned} v_0(m, n, \alpha) &= \int_1^\infty \int_1^\infty Q_0\left(\frac{\lambda_2}{\lambda_1}\right) \lambda_1{}^m\lambda_2{}^n e^{-(\alpha/2)(\lambda_1+\lambda_2)} d\lambda_1 d\lambda_2 \\ &= s_0(m, n, \alpha) + s_0(n, m, \alpha) \\ v_1(m, n, \alpha) &= \int_1^\infty \int_1^\infty Q_1\left(\frac{\lambda_2}{\lambda_1}\right) P_1\left(\frac{\lambda_1}{\lambda_2}\right) \lambda_1{}^m\lambda_2{}^n e^{-(\alpha/2)(\lambda_1+\lambda_2)} d\lambda_1 d\lambda_2 \\ &= s_1(m, n+1, \alpha) + s_1(n, m+1, \alpha) \\ v_2(m, n, \alpha) &= \int_1^\infty \int_1^\infty Q_2\left(\frac{\lambda_2}{\lambda_1}\right) P_2\left(\frac{\lambda_1}{\lambda_2}\right) \lambda_1{}^m\lambda_2{}^n e^{-(\alpha/2)(\lambda_1+\lambda_2)} d\lambda_1 d\lambda_2 \\ &= (3/2)s_2(m, n+2) - (\tfrac{1}{2})s_2(m, n) + (3/2)s_2(n, m+2) - (\tfrac{1}{2})s_2(n, m) \\ w_1(m, n, \alpha) &= \int_1^\infty \int_1^\infty \frac{dQ_1}{d\lambda}\left(\frac{\lambda_2}{\lambda_1}\right) (\lambda_1{}^2 - 1)(\lambda_2{}^2 - 1)\lambda_1{}^m\lambda_2{}^n e^{-(\alpha/2)(\lambda_1+\lambda_2)} d\lambda_1\lambda_2 d \end{aligned}$$

$$= s_1(m+1, n+2) + s_1(n+1, m+2) - s_1(m+1, n)$$
$$- s_1(n+1, m) - s_0(m, n+2) - s_0(n, m+2) + s_0(m, n)$$
$$+ s_0(n, m)$$

$$w_2(m, n, \alpha) = \int_1^\infty \int_1^\infty \frac{dQ_2}{d\lambda}\binom{\lambda_2}{\lambda_1} \frac{dP_2}{d\lambda}\binom{\lambda_1}{\lambda_2}$$
$$(\lambda_1^2 - 1)(\lambda_2^2 - 1)\lambda_1^m \lambda_2^n e^{-(\alpha/2)(\lambda_1+\lambda_2)} d\lambda_1 d\lambda_2$$
$$= 6\{s_2(m+1, n+3) + s_2(n+1, m+3) - s_2(m+1, n+1)$$
$$- s_2(n+1, m+1) - s_1(m, n+3) - s_1(n, m+3) + s_1(m, n+1)$$
$$+ s_1(n, m+1)\}$$

$$\{\mathrm{I}, n\}_0 = v_0(4, n) - (\tfrac{2}{3})v_0(2, n) + (\tfrac{1}{5})v_0(0, n)$$
$$\{\mathrm{II}, m, n\}_0 = v_0(m, n) - (\tfrac{1}{5})v_0(m-2, n)$$
$$\{\mathrm{III}, n\}_0 = (\tfrac{1}{3})v_0(4, n) - (6/5)v_0(2, n) + (\tfrac{1}{3})v_0(0, n)$$
$$\{\mathrm{I}, n\}_1 = v_1(4, n) - (8/5)v_1(2, n) + (3/5)v_1(0, n)$$
$$\{\mathrm{II}, n\}_1 = w_1(3, n) - (\tfrac{1}{5})w_1(1, n)$$
$$\{\mathrm{I}, n\}_2 = (\tfrac{1}{3})v_2(2, n) - (1/7)v_2(0, n)$$
$$\{\mathrm{II}, m, n\}_2 = v_2(m, n) + (1/7)v_2(m-2, n)$$
$$\{\mathrm{III}, n\}_2 = (\tfrac{1}{3})v_2(4, n) - (2/7)v_2(2, n) + (\tfrac{1}{3})v_2(0, n)$$
$$\{\mathrm{IV}, n\}_2 = (\tfrac{1}{3})w_2(2, n) - (1/7)w_2(0, n)$$
$$C_n(\alpha) = (3/2)B_{n+2}(\alpha) - (\tfrac{1}{2})B_n(\alpha).$$

With these symbols it becomes easy to write the resulting expressions for the integrals in question. For $\tau = 0$.

$$j'(ss; s0)^{(0)} = (2\pi)^2 c^3 c_2 \int (2/r)(\lambda_1^2 - \mu_1^2)(\lambda_2 + \mu_2)(\lambda_2\mu_2 - 1)(R/2)^{10}$$
$$e^{-\alpha(\lambda_1+\lambda_2)/2}(\lambda_1^2 - \mu_1^2)(\lambda_2^2 - \mu_2^2) d\lambda_1 d\lambda_2 d\mu_1 d\mu_2$$
$$= -\kappa(3^{1/2}/432)(\alpha/2)^9[\{\mathrm{I}, 3\}_0 - (\tfrac{1}{5})\{\mathrm{I}, 1\}_0]$$

For $\tau = 2$,

$$j'(ss; s0)^{(2)} = -\kappa(3^{1/2}/540)(\alpha/2)^9[\{\mathrm{I}, 3\}_2 + (\tfrac{1}{7})\{\mathrm{I}, 1\}_2]$$

III. $$j_a''(s0; ss) = c^3 c_2 \int (2/r) a_1^2 e^{-\kappa a_1} \cos\theta_{a_1} e^{-\kappa(a_2+b_2)/2} a_2 b_2 dv$$

$$j_a''(s0; ss)^{(0)} = \kappa(3^{1/2}/576)(\alpha/2)^9[B_1\{\mathrm{I}, 4\}_0 + (B_2 + B_0)\{\mathrm{I}, 3\}_0$$
$$+ (B_1 - B_3)\{\mathrm{I}, 2\}_0 - (B_4 + B_2)\{\mathrm{I}, 1\}_0 - B_3\{\mathrm{I}, 0\}_0]$$

$$j_a''(s0; ss)^{(1)} = 0$$

$$j_a''(s0; ss)^{(2)} = -\kappa(3^{1/2}/144)(\alpha/2)^9[C_1\{\mathrm{I}, 4\}_2 + (C_2 + C_0)\{\mathrm{I}, 3\}_2$$
$$+ (C_1 - C_3)\{\mathrm{I}, 2\}_2 - (C_4 + C_2)\{\mathrm{I}, 1\}_2 - C_3\{\mathrm{I}, 0\}_2].$$

The j'' integrals could be calculated directly without recourse to the Neumann expansion, but the formulation is much more awkward and does not enable one to obtain the result with reasonable speed. Both methods were used for j'' $(ss; ss)$, giving results almost exactly the same, which indicated that the expansion converges rapidly. For the other integrals of this type a method due to Dr. A. S. Coolidge could be applied; it was used to calculate the values at $\alpha=3$ of those j'' integrals not having 1 as an argument, and a check was obtained in every case. This method consists of expanding functions referred to one atom in spherical harmonics of the other atom.[12]

The list of j, j', and j'' integrals follows.

$$p = 0:$$

$$j(ss; ss) = j$$

$$j(ss; s0) = -I_a(s0) + \kappa(3^{1/2}/288)(\alpha/2)^4[24\{5A_2/3 + A_0/3\} + 18(\alpha/2)\{4A_3/3 - 8A_1/15\} + 6(\alpha/2)^2\{A_4 - 2A_2/3 + A_0/5\} + (\alpha/2)^3\{2A_5/3 - 4A_3/15 + 2A_1/35\}]_{(1,\alpha)}$$

$$j(ss; 00) = (2i_3/3) + (i_0/3) = (k/192)\text{II}c$$

$$j(s0; s0) = \text{expression already given.}$$

$$j'(ss; ss) = k$$

$$j'(ss; s0)^{(0)} = \text{expression already given}$$

$$j'(ss; s0)^{(2)} = \text{expression already given}$$

$$j'(ss; 00)^{(0)} = (\kappa/96)(\alpha/2)^9[(\tfrac{1}{3})\{\text{I}, 4\}_0 - (6/5)\{\text{I}, 2\}_0 + (\tfrac{1}{3})\{\text{I}, 0\}_0]$$

$$j'(ss; 00)^{(2)} = -(\kappa/60)(\alpha/2)^9[(\tfrac{1}{3})\{\text{III}, 2\}_2 - (1/7)\{\text{III}, 0\}_2]$$

$$j'(s0; s0)^{(0)} = +(\kappa/216)(\alpha/2)^9[\{\text{II}, 3, 3\}_0 - (\tfrac{1}{5})\{\text{II}, 3, 1\}_0]$$

$$j'(s0; s0)^{(1)} = (\kappa/288)(\alpha/2)^9[\{\text{I}, 4\}_1 - (8/5)\{\text{I}, 2\}_1 + (3/5)\{\text{I}, 0\}_1]$$

$$j'(s0; s0)^{(2)} = (\kappa/1080)(\alpha/2)^9[\{\text{II}, 3, 3\}_2 + (1/7)\{\text{II}, 3, 1\}_2]$$

$$j''(ss; ss) = j''$$

$$j_a''(ss; s0)^{(0)} = -\kappa(3^{1/2}/864)(\alpha/2)^9[B_0\{\text{II}, 3, 4\}_0 + 2B_1\{\text{II}, 3, 3\}_0 - 2B_3\{\text{II}, 3, 1\}_0 - B_4\{\text{II}, 3, 0\}_0]$$

$$j_a''(ss; s0)^{(1)} = \kappa(3^{1/2}/576)(\alpha/2)^9[B_1\{\text{I}, 4\}_1 + 2B_2\{\text{I}, 3\}_1 - 2B_4\{\text{I}, 1\}_1 - B_5\{\text{I}, 0\}_1]$$

$$j_a''(ss; s0)^{(2)} = \kappa(3^{1/2}/864)(\alpha/2)^9[C_0\{\text{II}, 3, 4\}_2 + 2C_1\{\text{II}, 3, 3\}_2 - 2C_3\{\text{II}, 3, 1\}_2 - C_4\{\text{II}, 3, 0\}_2]$$

$$j''(ss; 00)^{(0)} = (\kappa/192)(\alpha/2)^9[B_0\{\text{III}, 4\}_0 + 2B_1\{\text{III}, 3\}_0 - 2B_3\{\text{III}, 1\}_0 - B_4\{\text{III}, 0\}_0]$$

[12] We appreciate greatly the courtesy of Dr. Coolidge (Harvard University) in making us acquainted with his expansion method before publication.

$$j''(ss;\,00)^{(2)} = (\kappa/96)(\alpha/2)^9[C_0\{\mathrm{III},4\}_2 + 2C_1\{\mathrm{III},3\}_2 - 2C_3\{\mathrm{III},1\}_2 - C_4\{\mathrm{III},0\}_2]$$

$$j_a''(ss;\,0s)^{(0)} = -\,j_a''(ss;\,s0)^{(0)} \qquad j''(s0;\,0s)^{(0)} = -\,j''(s0;\,s0)^{(0)}$$

$$j_a''(ss;\,0s)^{(1)} = j_a''(ss;\,s0)^{(1)} \qquad j''(s0;\,0s)^{(1)} = j''(s0;\,s0)^{(1)}$$

$$j_a''(ss;\,0s)^{(2)} = -\,j_a''(ss;\,s0)^{(2)} \qquad j''(s0;\,0s)^{(2)} = -\,j''(s0;\,s0)^{(2)}$$

$$j''(s0;\,s0)^{(0)} = -\,(\kappa/288)(\alpha/2)^9[B_1\{\mathrm{II},3,4\}_0 + (B_2+B_0)\{\mathrm{II},3,3\}_0 + (B_1-B_3)\{\mathrm{II},3,2\}_0 - (B_4+B_2)\{\mathrm{II},3,1\}_0 - B_3\{\mathrm{II},3,0\}_0]$$

$$j''(s0;\,s0)^{(1)} = (\kappa/192)(\alpha/2)^9[B_2\{\mathrm{I},4\}_1 + (B_3+B_1)\{\mathrm{I},3\}_1 + (B_2-B_4)\{\mathrm{I},2\}_1 - (B_5+B_3)\{\mathrm{I},1\}_1 - B_4\{\mathrm{I},0\}_1]$$

$$j''(s0;\,s0)^{(2)} = (\kappa/288)(\alpha/2)^9[C_1\{\mathrm{II},3,4\}_2 + (C_2+C_0)\{\mathrm{II},3,3\}_2 + (C_1-C_3)\{\mathrm{II},3,2\}_2 - (C_4+C_2)\{\mathrm{II},3,1\}_2 - C_3\{\mathrm{II},3,0\}_2]$$

$$j_a''(s0;\,ss)^{(0)} = \text{expression already given.}$$

$$j_a''(s0;\,ss)^{(2)} = \text{expression already given.}$$

$$j''(00;\,ss)^{(0)} = (\kappa/192)(\alpha/2)^9[B_2\{\mathrm{I},4\}_0 + 2B_1\{\mathrm{I},3\}_0 + (B_0-B_4)\{\mathrm{I},2\}_0 - 2B_3\{\mathrm{I},1\}_0 - B_2\{\mathrm{I},0\}_0]$$

$$j''(00;\,ss)^{(2)} = -\,(\kappa/48)(\alpha/2)^9[C_2\{\mathrm{I},4\}_2 + 2C_1\{\mathrm{I},3\}_2 + (C_0-C_4)\{\mathrm{I},2\}_2 - 2C_3\{\mathrm{I},1\}_2 - C_2\{\mathrm{I},0\}_2]$$

$$p = 1;$$

$$j(ss;\,11) = (2i_1/3) + (i_3/3) = (\kappa/384)Ic$$

$$j(s1;\,s1) = (\kappa/1152)[(160/\alpha)\{(120/\alpha^2) + \alpha^4(A_2-A_5)\} - 320(\alpha/2)^3\cdot(A_0-A_2) - 120(\alpha/2)^4(4A_3-4A_1) - 60(\alpha/2)^5\cdot\{(4/3)(A_4-A_2) + (4/15)(A_2-A_0)\} - 18(\alpha/2)^6\cdot\{(4/3)(A_5-A_3) - (4/15)(A_3-A_1)\} - 3(\alpha/2)^7\cdot\{(4/3)(A_5-A_4) - (8/15)(A_4-A_2) + (4/35)(A_2-A_0)\}]_{(1,\alpha)}$$

$$j'(ss;\,11)^{(0)} = (\kappa/288)(\alpha/2)^9[\{\mathrm{I},4\}_0 - (6/5)\{\mathrm{I},2\}_0 + (\tfrac{1}{5})\{\mathrm{I},0\}_0]$$

$$j'(ss;\,11)^{(2)} = (\kappa/360)(\alpha/2)^9[\{\mathrm{I},4\}_2 - (6/7)\{\mathrm{I},2\}_2 - (1/7)\{\mathrm{I},0\}_2]$$

$$j'(s1;\,s1)^{(1)} = -\,(\kappa/576)(\alpha/2)^9[\{\mathrm{II},3\}_1 - (\tfrac{1}{5})\{\mathrm{II},1\}_1]$$

$$j'(s1;\,s1)^{(2)} = -\,(\kappa/960)(\alpha/2)^9[(\tfrac{1}{3})\{\mathrm{IV},2\}_2 - (1/7)\{\mathrm{IV},0\}_2]$$

$$j''(ss;\,11)^{(0)} = (\kappa/576)(\alpha/2)^9[B_0(\{\mathrm{II},4,4\}_0 - \{\mathrm{II},2,4\}_0) + 2B_1(\{\mathrm{II},4,3\}_0 - \{\mathrm{II},2,3\}_0) - 2B_3(\{\mathrm{II},4,1\}_0 - \{\mathrm{II},2,1\}_0) - B_4(\{\mathrm{II},4,0\}_0 - \{\mathrm{II},2,0\}_0)]$$

$$j''(ss;\,11)^{(2)} = -(\kappa/576)(\alpha/2)^9[C_0(\{\mathrm{II},4,4\}_2 - \{\mathrm{II},2,4\}_2) + 2C_1(\{\mathrm{II},4,3\}_2 - \{\mathrm{II},2,3\}_2) - 2C_3(\{\mathrm{II},4,1\}_2 - \{\mathrm{II},2,1\}_2) - C_4(\{\mathrm{II},4,0\}_2 - \{\mathrm{II},2,0\}_2)]$$

$$j''(1s;\,s1)^{(1)} = -(\kappa/768)(\alpha/2)^9[(B_0 - B_2)\{\mathrm{II},3\}_1 + (B_1 - B_3)\{\mathrm{II},2\}_1 - (B_2 - B_4)\{\mathrm{II},1\}_1 - (B_3 - B_5)\{\mathrm{II},0\}_1]$$

$$j''(1s;\,s1)^{(2)} = -(\kappa/768)(\alpha/2)^9[(B_1 - B_3)\{\mathrm{IV},3\}_2 + (B_2 - B_4)\{\mathrm{IV},2\}_2 - (B_3 - B_5)\{\mathrm{IV},1\}_2 - (B_4 - B_6)\{\mathrm{IV},0\}_2]$$

$$j''(s1;\,1s)^{(1)} = j''(1s;\,s1)^{(1)} \quad j''(s1;\,1s)^{(2)} = -j''(1s;\,s1)^{(2)}$$

$$j''(11;\,ss)^{(0)} = (\kappa/384)(\alpha/2)^9[(B_0 - B_2)(\{\mathrm{I},4\}_0 - \{\mathrm{I},2\}_0) - (B_2 - B_4)(\{\mathrm{I},2\}_0 - \{\mathrm{I},0\}_0)]$$

$$j''(11;\,ss)^{(2)} = -(\kappa/96)(\alpha/2)^9[(C_0 - C_2)(\{\mathrm{I},4\}_2 - \{\mathrm{I},2\}_2) - (C_2 - C_4)(\{\mathrm{I},2\}_2 - \{\mathrm{I},0\}_2)].$$

In calculating the $s_\tau(m,n,\alpha)$ use was made of the following formulas in addition to those previously given.[11]

$$s_\tau(m,\,n+1,\,\alpha) = (2/\alpha)(n+1)s_\tau(m,\,n,\,\alpha) + f_\tau(m,\,\alpha/2)A_0(1,\,\alpha/2) - \sigma_\tau(m+n+1,\,0,\,\alpha)$$

$$s_2(m,\,n,\,\alpha) = (3/2)s_1(m+1,\,n,\,\alpha) - (\tfrac{1}{2})s_0(m,\,n,\,\alpha).$$

The following tables contain such necessary s_τ as have not been published previously. We then proceed to tabulate the resulting values of the integrals.

TABLE I. $s_0(m,\,n,\,\alpha)$.

α	$\alpha=3$	4	5	6	7	8	9	10
$s_0(0,1,\alpha)$	0.0^2952	0.0^22161	0.0^3547	0.0^31481	0.0^4420	0.0^41234	0.0^53718	0.0^51145
$s_0(0,3,\alpha)$	0.01775	0.0^2345	0.0^3793	0.0^32019	0.0^4547	0.0^41555	0.0^5457	0.0^51375
$s_0(0,5,\alpha)$	0.0449	0.0^2672	0.0^31310	0.0^3303	0.0^4764	0.0^4207	0.0^5582	0.0^51715
$s_0(0,6,\alpha)$	0.0832	0.01042	0.0^21800	0.0^3389	0.0^4937	0.0^4246	0.0^5670	0.0^51952
$s_0(1,0,\alpha)$	0.012998	0.0^22801	0.0^36833	0.0^31801	0.0^45004	0.0^41445	0.0^5430	0.0^51307
$s_0(1,1,\alpha)$	0.01708	0.0^33458	0.0^38105	0.0^32081	0.0^45666	0.0^41611	0.0^5474	0.0^51427
$s_0(1,2,\alpha)$	0.02381	0.0^24431	0.0^3986	0.0^32447	0.0^4651	0.0^41818	0.0^5527	0.0^51570
$s_0(1,3,\alpha)$	0.0358	0.0^25953	0.0^21239	0.0^32947	0.0^4760	0.0^42078	0.0^5593	0.0^51743
$s_0(1,4,\alpha)$	0.0590	0.0^2848	0.0^21619	0.0^33647	0.0^4907	0.0^42413	0.0^5675	0.0^51954
$s_0(1,5,\alpha)$	0.1082	0.01301	0.0^2222	0.0^4467	0.0^31111	0.0^42856	0.0^5780	0.0^5222
$s_0(1,6,\alpha)$	0.225	0.0218	0.0^3322	0.0^4625	0.0^31401	0.0^4346	0.0^5918	0.0^5255
$s_0(2,1,\alpha)$	0.03442	0.0^26019	0.0^21281	0.0^33073	0.0^4796	0.0^42176	0.0^56201	0.0^51823
$s_0(2,3,\alpha)$	0.0816	0.01126	0.0^22078	0.0^34548	0.0^31103	0.0^42881	0.0^5793	0.0^52266
$s_0(2,5,\alpha)$	0.295	0.0279	0.0^2408	0.0^4770	0.0^31688	0.0^4411	0.0^51074	0.0^5295
$s_0(2,6,\alpha)$	0.673	0.0504	0.0^2627	0.0^31074	0.0^32200	0.0^4510	0.0^51287	0.0^5345
$s_0(3,0,\alpha)$	0.05535	0.0^2883	0.0^31764	0.0^44039	0.0^31011	0.0^42687	0.0^5749	0.0^52164
$s_0(3,1,\alpha)$	0.07936	0.01158	0.0^22188	0.0^44825	0.0^31176	0.0^43062	0.0^5840	0.0^52398
$s_0(3,2,\alpha)$	0.1237	0.01603	0.0^22815	0.0^35913	0.0^31395	0.0^43542	0.0^5954	0.0^52684
$s_0(3,3,\alpha)$	0.2136	0.02370	0.0^33786	0.0^3749	0.0^31693	0.0^44173	0.0^51098	0.0^53036
$s_0(3,4,\alpha)$	0.4150	0.03801	0.0^35381	0.0^3985	0.0^32115	0.0^45024	0.0^51287	0.0^5349
$s_0(3,5,\alpha)$	0.916	0.0669	0.0^3817	0.0^31365	0.0^32740	0.0^46205	0.0^51538	0.0^5406
$s_0(3,6,\alpha)$	2.300	0.1305	0.01336	0.0^31983	0.0^3370	0.0^4791	0.0^51881	0.0^5483
$s_0(4,1,\alpha)$	0.2122	0.02502	0.0^24089	0.0^38137	0.0^31835	0.0^44516	0.0^51184	0.0^53257
$s_0(4,3,\alpha)$	0.6422	0.0559	0.0^37562	0.0^31330	0.0^32747	0.0^4635	0.0^51589	0.0^5421
$s_0(4,5,\alpha)$	3.218	0.1782	0.01798	0.0^32602	0.0^3470	0.0^4987	0.0^52304	0.0^5580
$s_0(4,6,\alpha)$	8.77	0.373	0.03121	0.0^33398	0.0^3657	0.0^41293	0.0^52886	0.0^5702

TABLE II. s_1 (m, n, α).

α	$\alpha=3$	4	5	6	7	8	9	10
$s_1(0,0,\alpha)$	$0.0^{2}1936$	$0.0^{3}513$	$0.0^{3}1445$	$0.0^{4}4240$	$0.0^{4}1283$	$0.0^{5}3963$	$0.0^{5}1248$	$0.0^{5}3990$
$s_1(0,1,\alpha)$	$0.0^{2}2339$	$0.0^{3}597$	$0.0^{3}1641$	$0.0^{4}4730$	$0.0^{4}1412$	$0.0^{5}4319$	$0.0^{5}1349$	$0.0^{4}4279$
$s_1(0,2,\alpha)$	$0.0^{2}2930$	$0.0^{3}711$	$0.0^{3}1895$	$0.0^{4}5337$	$0.0^{4}1569$	$0.0^{5}4743$	$0.0^{5}1468$	$0.0^{4}4625$
$s_1(0,3,\alpha)$	$0.0^{2}3849$	$0.0^{3}874$	$0.0^{2}2233$	$0.0^{4}6122$	$0.0^{4}1766$	$0.0^{5}5258$	$0.0^{5}1609$	$0.0^{4}5028$
$s_1(0,4,\alpha)$	$0.0^{2}5385$	$0.0^{3}1117$	$0.0^{2}2705$	$0.0^{4}7151$	$0.0^{4}2015$	$0.0^{5}5891$	$0.0^{5}1778$	$0.0^{4}5495$
$s_1(0,5,\alpha)$	$0.0^{2}819$	$0.0^{3}1503$	$0.0^{3}3387$	$0.0^{4}854$	$0.0^{4}2336$	$0.0^{5}6685$	$0.0^{5}1985$	$0.0^{4}6068$
$s_1(0,6,\alpha)$	0.01392	$0.0^{2}2167$	$0.0^{4}4433$	$0.0^{3}1050$	$0.0^{4}2768$	$0.0^{5}7704$	$0.0^{5}2245$	$0.0^{4}658$
$s_1(1,1,\alpha)$	$0.0^{2}3695$	$0.0^{3}868$	$0.0^{2}2253$	$0.0^{4}623$	$0.0^{4}1805$	$0.0^{5}539$	$0.0^{5}1650$	$0.0^{5}5152$
$s_1(1,3,\alpha)$	$0.0^{2}669$	$0.0^{3}1353$	$0.0^{3}3201$	$0.0^{4}833$	$0.0^{4}2314$	$0.0^{5}670$	$0.0^{5}1998$	$0.0^{4}612$
$s_1(1,5,\alpha)$	0.01640	$0.0^{2}2560$	$0.0^{3}5155$	$0.0^{3}1218$	$0.0^{4}3169$	$0.0^{5}876$	$0.0^{5}2520$	$0.0^{4}753$
$s_1(2,0,\alpha)$	$0.0^{2}4964$	$0.0^{3}1106$	$0.0^{2}2772$	$0.0^{4}747$	$0.0^{4}2121$	$0.0^{5}6233$	$0.0^{5}1883$	$0.0^{5}582$
$s_1(2,1,\alpha)$	$0.0^{2}6451$	$0.0^{3}1352$	$0.0^{3}3259$	$0.0^{4}856$	$0.0^{4}2384$	$0.0^{5}691$	$0.0^{5}2063$	$0.0^{4}632$
$s_1(2,2,\alpha)$	$0.0^{2}888$	$0.0^{3}1712$	$0.0^{3}3926$	$0.0^{4}999$	$0.0^{4}2717$	$0.0^{5}774$	$0.0^{5}2281$	$0.0^{4}691$
$s_1(2,3,\alpha)$	0.01314	$0.0^{2}2271$	$0.0^{4}4878$	$0.0^{3}1190$	$0.0^{4}3145$	$0.0^{5}877$	$0.0^{5}2545$	$0.0^{4}762$
$s_1(2,4,\alpha)$	0.02135	$0.0^{3}3194$	$0.0^{3}6300$	$0.0^{3}1457$	$0.0^{4}3715$	$0.0^{4}1010$	$0.0^{5}2874$	$0.0^{5}850$
$s_1(2,5,\alpha)$	0.03872	$0.0^{2}4832$	$0.0^{3}853$	$0.0^{3}1844$	$0.0^{4}4490$	$0.0^{4}1184$	$0.0^{5}3290$	$0.0^{5}956$
$s_1(2,6,\alpha)$	0.07952	$0.0^{2}7991$	$0.0^{2}1228$	$0.0^{3}2431$	$0.0^{4}5592$	$0.0^{4}1418$	$0.0^{5}3828$	$0.0^{5}1093$
$s_1(3,1,\alpha)$	0.01262	$0.0^{2}2289$	$0.0^{3}5025$	$0.0^{3}1235$	$0.0^{4}3276$	$0.0^{5}915$	$0.0^{5}2652$	$0.0^{5}793$
$s_1(3,3,\alpha)$	0.02920	$0.0^{2}4176$	$0.0^{3}799$	$0.0^{3}1793$	$0.0^{4}4465$	$0.0^{4}1192$	$0.0^{5}3341$	$0.0^{5}975$
$s_1(3,5,\alpha)$	0.1027	0.01005	$0.0^{3}1530$	$0.0^{2}2964$	$0.0^{4}668$	$0.0^{4}1668$	$0.0^{4}4443$	$0.0^{5}1251$
$s_1(4,0,\alpha)$	0.01995	$0.0^{3}3298$	$0.0^{3}6792$	$0.0^{3}1596$	$0.0^{4}4087$	$0.0^{4}1111$	$0.0^{5}3159$	$0.0^{5}928$
$s_1(4,1,\alpha)$	0.02836	$0.0^{2}4290$	$0.0^{3}836$	$0.0^{3}1892$	$0.0^{4}4717$	$0.0^{4}1258$	$0.0^{5}3524$	$0.0^{5}1023$
$s_1(4,2,\alpha)$	0.04380	$0.0^{2}5880$	$0.0^{3}1065$	$0.0^{2}2299$	$0.0^{4}5550$	$0.0^{4}1445$	$0.0^{5}3975$	$0.0^{5}1138$
$s_1(4,3,\alpha)$	0.0748	$0.0^{2}860$	$0.0^{3}1419$	$0.0^{2}2883$	$0.0^{4}667$	$0.0^{4}1688$	$0.0^{4}4543$	$0.0^{5}1279$
$s_1(4,4,\alpha)$	0.1439	0.01364	$0.0^{2}1997$	$0.0^{3}3755$	$0.0^{4}826$	$0.0^{4}2013$	$0.0^{5}528$	$0.0^{5}1458$
$s_1(4,5,\alpha)$	0.3143	0.02376	$0.0^{3}3000$	$0.0^{3}5125$	$0.0^{3}1056$	$0.0^{4}2464$	$0.0^{5}625$	$0.0^{5}1685$
$s_1(4,6,\alpha)$	0.7803	0.04595	$0.0^{2}4821$	$0.0^{3}7393$	$0.0^{3}1406$	$0.0^{4}3102$	$0.0^{4}757$	$0.0^{5}1985$
$s_1(5,0,\alpha)$	0.0501	$0.0^{3}676$	$0.0^{3}1208$	$0.0^{2}2574$	$0.0^{4}6140$	$0.0^{4}1583$	$0.0^{4}4316$	$0.0^{5}1226$
$s_1(5,1,\alpha)$	0.0744	$0.0^{3}908$	$0.0^{3}1524$	$0.0^{3}3111$	$0.0^{4}7200$	$0.0^{4}1814$	$0.0^{4}4861$	$0.0^{5}1363$
$s_1(5,2,\alpha)$	0.1215	0.01299	$0.0^{2}2004$	$0.0^{3}3872$	$0.0^{4}8621$	$0.0^{4}2114$	$0.0^{5}5548$	$0.0^{5}1529$
$s_1(5,3,\alpha)$	0.2224	0.02002	$0.0^{2}2775$	$0.0^{4}4998$	$0.0^{3}1061$	$0.0^{4}2514$	$0.0^{4}643$	$0.0^{5}1741$
$s_1(5,4,\alpha)$	0.463	0.03381	$0.0^{2}4090$	$0.0^{3}674$	$0.0^{3}1348$	$0.0^{4}3061$	$0.0^{4}759$	$0.0^{5}2009$
$s_1(5,5,\alpha)$	1.101	0.0633	$0.0^{3}644$	$0.0^{3}960$	$0.0^{3}1781$	$0.0^{4}3839$	$0.0^{4}917$	$0.0^{5}2360$
$s_1(5,6,\alpha)$	2.984	0.1322	0.01099	$0.0^{3}1453$	$0.0^{3}2463$	$0.0^{4}4982$	$0.0^{4}1136$	$0.0^{5}2830$

TABLE III. $B_n(\alpha/2)$ *and* $C_n(\alpha/2)$.

α	$\alpha=3$	4	5	6	7	8	9	10
$B_0(\alpha/2)$	2.8390	3.6269	4.8402	6.6786	9.4531	13.645	20.001	29.681
$B_1(\alpha/2)$	−1.2439	−1.9488	−2.9698	−4.4858	−6.7694	−10.243	−15.561	−23.748
$B_2(\alpha/2)$	1.1806	1.6781	2.4644	3.6882	5.5849	8.524	13.085	20.182
$B_3(\alpha/2)$	−0.7754	−1.2451	−1.9485	−3.0238	−4.6832	−7.262	−11.283	−17.575
$B_4(\alpha/2)$	0.7713	1.1368	1.7226	2.6470	4.1009	6.384	9.972	15.621
$B_5(\alpha/2)$	−0.5656	−0.9203	−1.4606	−2.3003	−3.6118	−5.675	−8.926	−14.063
$B_6(\alpha/2)$	0.5766	0.8659	1.3348	2.0781	3.2614	5.132	8.100	12.805
$C_0(\alpha/2)$	0.3513	0.7037	1.2765	2.1930	3.6508	5.963	9.627	15.432
$C_1(\alpha/2)$	−0.5412	−0.8933	−1.4379	−2.2928	−3.6401	−5.771	−9.144	−14.489
$C_2(\alpha/2)$	0.5666	0.8662	1.3517	2.1264	3.3589	5.314	8.415	13.341
$C_3(\alpha/2)$	−0.4607	−0.7579	−1.2166	−1.9386	−3.0761	−4.882	−7.747	−12.307
$C_4(\alpha/2)$	0.4792	0.7305	1.1409	1.7937	2.8417	4.506	7.164	11.397

TABLE IV. j, j', *and* j'' *integrals for* Σ *states.*

α	$\alpha=3$	4	5	6	7	8	9	10
$j(ss;ss)/\kappa$	0.3367	0.3177	0.2969	0.2746	0.2527	0.2316	0.2121	0.1948
$j(ss;s0)/\kappa$	−0.0560	−0.0660	−0.0705	−0.0710	−0.0676	−0.0622	−0.0559	−0.0494
$j(s0;s0)/\kappa$	0.0386	0.0179	$0.0^{4}4$	−0.0117	−0.0189	−0.0218	−0.0219	−0.0204
$j(ss;00)/\kappa$	0.3458	0.3312	0.3140	0.2942	0.2734	0.2542	0.2302	0.2110
$j'(ss;ss)/\kappa$	0.2856	0.2379	0.1888	0.1432	0.1022	0.0714	0.0477	0.0302
$j'(ss;s0)^0/\kappa$	−0.1368	−0.1492	−0.1423	−0.1234	−0.0985	−0.0734	−0.0516	−0.0346
$j'(ss;s0)^1/\kappa$	$-0.0^{2}7$	$-0.0^{2}14$	$-0.0^{2}23$	$-0.0^{2}25$	$-0.0^{2}25$	$-0.0^{2}23$	$-0.0^{2}18$	$-0.0^{2}14$
$j'(ss;00)^0/\kappa$	0.1304	0.0361	−0.0287	−0.0608	−0.0693	−0.0629	−0.0502	−0.0369
$j'(ss;00)^2/\kappa$	$-0.0^{2}24$	$-0.0^{2}41$	$0.0^{2}54$	$-0.0^{2}50$	$-0.0^{2}49$	$-0.0^{2}42$	$-0.0^{2}33$	$-0.0^{2}25$
$j'(s0;s0)^0/\kappa$	0.0681	0.0964	0.1107	0.1097	0.0970	0.0779	0.0582	0.0410
$j'(s0;s0)^1/\kappa$	0.0479	0.0343	0.0225	0.0139	$0.0^{2}83$	$0.0^{2}47$	$0.0^{2}26$	$0.0^{2}14$
$j'(s0;s0)^2/\kappa$	$0.0^{2}14$	$0.0^{2}29$	$0.0^{2}41$	$0.0^{2}43$	$0.0^{2}42$	$0.0^{2}39$	$0.0^{2}32$	$0.0^{2}24$
$j''(ss;ss)/\kappa$	0.3155	0.2834	0.2482	0.2124	0.1762	0.1426	0.1132	0.0876
$j_a''(s;s0)^0/\kappa$	−0.1508	−0.1771	−0.1860	−0.1816	−0.1667	−0.1466	−0.1257	−0.1038
$j_a''(ss;s0)^1/\kappa$	−0.0248	−0.0280	−0.0273	−0.0245	−0.0214	−0.0178	−0.0149	−0.0119
$j_a''(ss;s0)^2/\kappa$	$-0.0^{2}1$	$+0.0^{2}12$	$-0.0^{2}21$	$+0.0^{2}14$	$+0.0^{2}9$	$+0.0^{2}7$	$+0.0^{2}7$	$+0.0^{2}18$
$j''(ss;00)^0/\kappa$	0.1459	0.0464	−0.0334	−0.0855	−0.1130	−0.1224	−0.1176	−0.1069
$j''(ss;00)^2/\kappa$	$0.0^{2}18$	$0.0^{2}70$	$-0.0^{2}56$	$-0.0^{2}1$	$0.0^{2}33$	$0.0^{2}17$	$-0.0^{2}17$	$0.0^{2}24$
$j''(s0;s0)^0/\kappa$	−0.0171	−0.0245	−0.0296	−0.0318	−0.0320	−0.0285	−0.0222	−0.0181
$j''(s0;s0)^1/\kappa$	0.0529	0.0411	0.0288	0.0195	0.0135	$0.0^{2}91$	$0.0^{2}70$	$0.0^{2}53$
$j''(s0;s0)^2/\kappa$	$-0.0^{2}33$	$-0.0^{2}98$	$-0.0^{2}55$	−0.0119	−0.0104	$-0.0^{2}86$	$-0.0^{2}65$	$-0.0^{2}68$
$j_a''(s0;ss)^0/\kappa$	0.0264	0.0308	0.0308	0.0290	0.0283	0.0222	0.0182	0.0161
$j_a''(s0;ss)^2/\kappa$	$0.0^{2}17$	$0.0^{2}40$	$0.0^{2}48$	$0.0^{2}48$	$0.0^{2}69$	$0.0^{2}62$	$0.0^{2}41$	$0.0^{2}14$
$j''(00;ss)^0/\kappa$	0.3189	0.2882	0.2541	0.2176	0.1777	0.1480	0.1178	0.0900
$j''(00;ss)^2/\kappa$	$-0.0^{2}17$	$-0.0^{2}30$	$-0.0^{2}11$	$+0.0^{2}3$	$-0.0^{2}21$	$-0.0^{2}13$	$+0.0^{2}8$	$+0.0^{2}43$

TABLE V. *j, j′, and j″ integrals for* Π *states.*

α	$\alpha=3$	4	5	6	7	8	9	10
$j(ss;11)/\kappa$	0.3313	0.3107	0.2878	0.2643	0.2424	0.2216	0.2028	0.1862
$j(s1;S1)/\kappa$	0.0651	0.0558	0.0464	0.0377	0.0300	0.0237	0.0187	0.0146
$j_\sigma'(ss;11)^0/\kappa$	0.2539	0.1961	0.1420	0.0983	0.0644	0.0407	0.0243	0.0145
$j_\sigma'(ss;11)^2/\kappa$	0.0^211	0.0^216	0.0^219	0.0^215	0.0^213	0.0^29	0.0^26	0.0^24
$j_\sigma'(s1;\cdot1)^1/\kappa$	0.0583	0.0456	0.0330	0.0232	0.0152	0.0^294	0.0^257	0.0^234
$j'(s1;\cdot1)^2/\kappa$	0.0^28	0.0^28	0.0^27	0.0^27	0.0^25	0.0^23	0.0^22	0.0^22
$j_{\sigma\sigma}''(ss;11)^0/\kappa$	0.2814	0.2350	0.1885	0.1480	0.1115	0.0840	0.0620	0.0450
$j''(ss;11)^2/\kappa$	-0.0^210	-0.0^239	$+0.0^227$	-0.0^23	-0.0^224	-0.0^220	$+0.0^27$	-0.0^229
$j_{\sigma\sigma}''(s1;s1)^1/\kappa$	0.0651	0.0556	0.0452	0.0367	0.0283	0.0210	0.0156	0.0116
$j_{\sigma\sigma}''(s1;s1)^2/\kappa$	-0.0^224	-0.0^217	-0.0^244	-0.0^230	-0.0^236	-0.0^230	-0.0^223	-0.0^225
$j_{\sigma\sigma}''(i1;ss)^0/\kappa$	0.3136	0.2816	0.2446	0.2088	0.1723	0.1402	0.1118	0.0872
$j''(11;ss)^2/\kappa$	0.0^39	0.0^212	0.0^39	0.0^24	-0.0^23	-0.0^25	-0.0^211	-0.0^218

The integrals $I_a(ss)$, $I_a(00)$, $I_a(11)$, $I_a'(ss)$, $S_{ss}^{1/2}$, $S_{00}^{1/2}$, and $S_{11}^{1/2}$ either have already been given or are readily obtainable from previous work.[11] No new procedure is involved in getting the formulations for the others integrals of this type, and we simply list the expressions. Numerical values are then tabulated.

$$I_a(ss) = \mathrm{I}. \quad I_a(00) = (\kappa/192)IIa. \quad I_a(11) = (\kappa/384)Ia$$

$$I_a(s0) = \kappa(3^{1/2}/36)\alpha^4\{120/\alpha^6 - A_5(1,\alpha) + A_2(1,\alpha)\}$$

$$I_a'(ss) = I'$$

$$I_a'(s0) = -\kappa(3^{1/2}/576)\alpha^4\{A_2(1,\alpha/2) + A_0(1,\alpha/2)\}$$

$$I_a'(0s) = \kappa(3^{1/2}/192)\alpha^4\{A_2(1,\alpha/2) - (\tfrac{1}{3})A_0(1,\alpha/2)\}$$

$$I_a'(00) = (\kappa/64)\alpha^4\{(\tfrac{1}{3})A_3(1,\alpha/2) - A_1(1,\alpha/2)\}$$

$$I_a'(11) = (\kappa/192)\alpha^4\{A_3(1,\alpha/2) - A_1(1,\alpha/2)\}$$

$$S_{ss}^{1/2} = S^{1/2}$$

$$S_{s0}^{1/2} = -(3^{1/2}/36)(\alpha/2)^5\{A_3(1,\alpha/2) - (\tfrac{1}{5})A_1(1,\alpha/2)\}$$

TABLE VI. *I and I′ integrals.*

α	$\alpha=3$	4	5	6	7	8	9	10
$I_a(ss)/\kappa$	0.4468	0.4022	0.3564	0.3138	0.2772	0.2463	0.2206	0.1995
$I_a(s0)/\kappa$	0.1761	0.1692	0.1487	0.1247	0.1024	0.0835	0.0684	0.0565
$I_a(00)/\kappa$	0.5367	0.4928	0.4357	0.3782	0.3276	0.2846	0.2500	0.2218
$I_a(11)/\kappa$	0.4010	0.3568	0.3162	0.2813	0.2521	0.2268	0.2057	0.1878
$I_a'(ss)/\kappa$	0.4324	0.3835	0.3289	0.2738	0.2221	0.1761	0.1368	0.1045
$I_a'(s0)/\kappa$	−0.1530	−0.1823	−0.1925	−0.1869	−0.1704	−0.1480	−0.1239	−0.1005
$I_a'(0s)/\kappa$	0.3140	0.3386	0.3308	0.3018	0.2619	0.2185	0.1772	0.1394
$I_a'(00)/\kappa$	0.1534	0.0225	−0.0702	−0.1245	−0.1478	−0.1496	−0.1382	−0.1202
$I_a'(11)/\kappa$	0.3626	0.2932	0.2291	0.1744	0.1297	0.0946	0.0680	0.0483

TABLE VII. $S^{1/2}$ *and* S *integrals.*

α	$\alpha=3$	4	5	6	7	8	9	10
$S_{ss}^{1/2}$	0.8897	0.8149	0.7291	0.6373	0.5448	0.4562	0.3748	0.3024
S_{ss}	0.7916	0.6641	0.5316	0.4061	0.2968	0.2081	0.1405	0.0914
$S_{s0}^{1/2}$	−0.3865	−0.4636	−0.5036	−0.5088	−0.4859	−0.4441	−0.3911	−0.3339
S_{s0}	0.1494	0.2149	0.2536	0.2589	0.2361	0.1972	0.1530	0.1115
$S_{00}^{1/2}$	0.4825	0.2256	0.0^251	−0.1597	−0.2649	−0.3187	−0.3326	−0.3190
S_{00}	0.2328	0.0509	0.0^23	0.0256	0.0702	0.1016	0.1106	0.1017
$S_{11}^{1/2}$	0.8089	0.6947	0.5778	0.4679	0.3702	0.2871	0.2185	0.1641
S_{11}	0.6542	0.4826	0.3339	0.2189	0.1370	0.0824	0.0477	0.0269

TABKE VIII. *J, J', and J'' integrals for* Σ *states.*

α	$\alpha=3$	4	5	6	7	8	9	10
$J(ss;ss)/\kappa$	0.1098	0.0133	−0.0159	−0.0197	−0.0160	−0.0110	−0.0069	−0.0042
$J(00;ss)/\kappa$	0.0290	−0.0638	−0.0781	−0.0645	−0.0457	−0.0267	−0.0182	−0.0103
$J(0s;ss)/\kappa$	−0.1201	−0.1032	−0.0782	−0.0537	−0.0348	−0.0213	−0.0125	−0.0071
$J(s0;0s)/\kappa$	0.0386	0.0179	0.0004	−0.0117	−0.0189	−0.0218	−0.0219	−0.0204
$J'(ss;ss)/\kappa$	0.0439	−0.0550	−0.0782	−0.0704	−0.0550	−0.0373	−0.0236	−0.0147
$J'(ss;0s)/\kappa$	−0.0798	−0.1142	−0.1153	−0.0976	−0.0740	−0.0515	−0.0339	−0.0209
$J'(ss;s0)/\kappa$	−0.0635	−0.0131	0.0145	0.0244	0.0241	0.0193	0.0139	0.0091
$J'(ss;00)/\kappa$	0.0691	0.0191	0.0169	0.0233	0.0239	0.0208	0.0161	0.0109
$J'(0s;0s)/\kappa$	0.0365	−0.0004	−0.0249	−0.0345	−0.0331	−0.0269	−0.0198	−0.0130
$J''(ss;ss)/\kappa$	0.0787	−0.0204	−0.0489	−0.0490	−0.0413	−0.0318	−0.0230	−0.0167
$J_a''(ss;s0)/\kappa$	0.0533	0.0894	0.0935	0.0872	0.0706	0.0532	0.0367	0.0253
$J_a''(ss;0s)/\kappa$	0.0581	0.0109	−0.0098	−0.0213	−0.0219	−0.0183	−0.0132	−0.0102
$J_a''(0s;0s)/\kappa$	−0.1286	−0.1031	−0.0728	−0.0457	−0.0206	−0.0097	−0.0033	+0.0004
$J_a''(ss;00)/\kappa$	0.1004	0.0530	0.0314	0.0358	0.0358	0.0277	0.0184	0.0155
$J_a''(s0;0s)/\kappa$	0.1006	0.0852	0.0686	0.0392	0.0209	0.0091	0.0051	−0.0007
$J_a''(s0;0s)/\kappa$	0.0052	−0.0030	−0.0110	−0.0002	0.0061	0.0091	0.0089	0.0113
$J_a''(00;ss)/\kappa$	0.0004	−0.0924	−0.1020	−0.0845	−0.0692	−0.0451	−0.0286	−0.0168

TABLE IX. *J, J', and J'' integrals for* Π *states.*

α	$\alpha=3$	4	5	6	7	8	9	10
$J(1s;ss)/\kappa$	0.1502	0.0517	0.0152	0.0025	−0.0012	−0.0015	−0.0013	−0.0011
$J(s1;s1)/\kappa$	0.0651	0.0558	0.0464	0.0377	0.0300	0.0237	0.0187	0.0146
$J'(ss;1s)/\kappa$	0.0624	−0.0245	−0.0446	−0.0400	−0.0296	−0.0193	−0.0123	−0.0069
$J'(s1;S1)/\kappa$	0.0591	0.0464	0.0337	0.0239	0.0157	0.0097	0.0059	0.0036
$J''(ss;1s)/\kappa$	0.0957	0.0058	−0.0127	−0.0175	−0.0174	−0.0115	−0.0049	−0.0061
$J''(1s;s1)/\kappa$	0.0627	0.0539	0.0408	0.0337	0.0247	0.0180	0.0133	0.0091
$J''(s1;1s)/\kappa$	0.0675	0.0573	0.0496	0.0397	0.0319	0.0240	0.0179	0.0141
$J''(1s;ss)/\kappa$	0.1184	0.0160	−0.0222	−0.0315	−0.0317	−0.0258	−0.0199	−0.0154

TABLE X. H_{i1}' *for* Σ *states.*

α	$\alpha=3$	4	5	6	7	8		10
H_{11}'/κ	0.1155	0.0719	0.0421	0.0363	0.0384	0.0361	0.0223	0.0163
H_{21}'/κ	0.1575	0.0780	0.0215	−0.0136	−0.0237	−0.0185	−0.0117	−0.0077
H_{31}'/κ	−0.0884	−0.0490	−0.0219	−0.0296	−0.0399	−0.0429	−0.0399	−0.0350
H_{41}'/κ	−0.1720	−0.1009	−0.0484	−0.0157	−0.0067	−0.0102	−0.0148	−0.0155

TABLE XI. H_{i1}' *for* Π *states.*

α	$\alpha=3$	4	5	6	7	8	9	10
H_{11}'/κ	0.1696	0.1387	0.1048	0.0721	0.0497	0.0312	0.0184	0.0106
H_{21}'/κ	−0.0132	−0.0159	−0.0183	−0.0156	−0.0127	−0.0089	−0.0059	−0.0040
H_{31}'/κ	−0.1147	−0.0496	−0.0028	+0.0278	+0.0389	+0.0361	+0.0284	+0.0222
H_{41}'/κ	0.0093	0.0119	0.0167	0.0162	0.0165	0.0155	0.0137	0.0118

TABLE XII. N_{i1} *for* Σ *states.*

α	$\alpha=3$	4	5	6	7	8	9	10
N_{11}	0.1773	0.2637	0.3497	0.4401	0.5370	0.6356	0.7281	0.8073
N_{21}	0.1183	0.1427	0.1348	0.1052	0.0702	0.0411	0.0215	0.0102
N_{31}	−0.0895	−0.0617	−0.0017	+0.0604	+0.1015	+0.1151	+0.1072	+0.0877
N_{41}	−0.1183	−0.1427	−0.1348	−0.1052	−0.0702	−0.0411	−0.0215	− .0102

TABLE XIII. N_{i1} *for* Π *states.*

α	$\alpha=3$	4	5	6	7	8	9	10
N_{11}	0.2084	0.3359	0.4684	0.5938	0.7032	0.7918	0.8595	0.9086
N_{21}	0.0000	—	—	—	—	—	—	—
N_{31}	−0.1500	−0.1902	−0.1973	−0.1771	−0.1418	−0.1037	−0.0704	−0.0451
N_{41}	0.0000	—	—	—	—	—	—	—

TABLE XIV. *Energies.*

α	$\alpha=3$	4	5	6	7	8	9	10
$(1/\kappa)$ $(^1\Sigma S^N-E_a)$	0.1435	(0.0100)	−0.0193	−0.0452	−0.0500	(−0.0520)	−0.0528	−0.0468
$(1/\kappa)$ $(^3\Sigma S^N-E_b)$	0.4738	0.2267	0.1353	0.0719	0.0453	0.0292	0.0106	0.0050
$(1/\kappa)$ $(^1\Sigma A^N-E_a)$	1.0596	0.4908	0.2156	0.1152	0.1064	(0.1020)	0.0984	0.0799
$(1/\kappa)$ $(^3\Sigma A^N-E_b)$	−4.1589	−1.4500	−0.0721	+0.3768	+0.3229	+0.1992	+0.1023	+0.0622
$(1/\kappa)$ $(^1\Pi S^N-E_a)$	0.8733	0.5841	0.3703	0.2412	0.1646	0.1074	0.0692	0.0470
$(1/\kappa)$ $(^3\Pi S^N-E_b)$	1.0068	0.6390	0.3821	0.2383	0.1511	0.0882	0.0494	0.0290
$(1/\kappa)$ $(^1\Pi A^N-E_a)$	0.7305	0.3051	0.1091	0.0162	−0.0218	−0.0327	−0.0318	−0.0287
$(1/\kappa)$ $(^3\Pi A^N-E_b)$	0.8560	0.4108	0.2142	0.0987	0.0473	0.0218	(0.0136)	(0.0060)

DISCUSSION

The potential energy curves indicate that a stable beryllium molecule may be formed when a normal beryllium atom interacts with one in the $2s2p\ ^1P$ state. There result two attractive states, $^1\Pi$ and $^1\Sigma$, of which the $^1\Sigma$ is the lower. This confirms the rule[11] that those states tend to lie lowest which have the smallest value of $\Sigma_i m_l(i)$, where $m_l(i)$ denotes the component of orbital angular momentum of the ith electron in the direction of the internuclear axis.

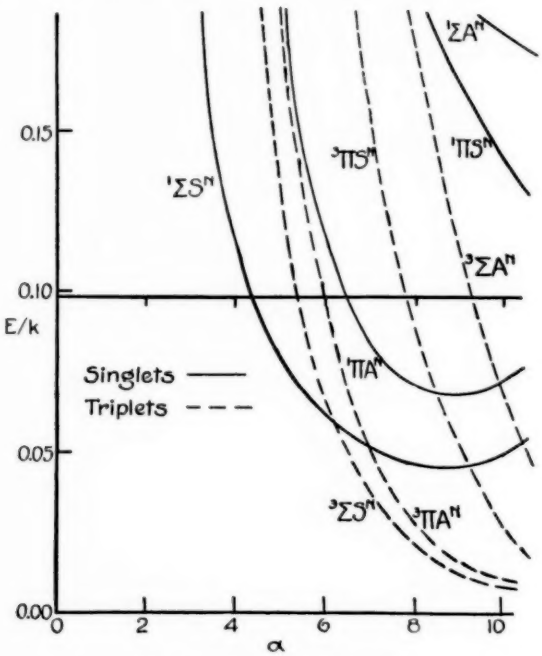

Fig. 1. Energy curves for Be_2.

For small values of the internuclear distance, the $^3\Sigma A^N$ curve, which indicates a repulsive state for large separations, behaves erratically. This probably means that the Heitler-London method is not applicable in this region.

An investigation has been made of the interaction of a normal lithium atom with one in the $2p\ ^2P$ state. The integrals $J(pp,ss)$, $J'(pp,ss)$, $J(ps,ps)$, and $J'(ps,ps)$ occur in the energy expressions. It has not been possible to attain good agreement with experiment,[13] the most glaring discrepancy being

[13] F. W. Loomis and R. E. Nusbaum, Phys. Rev. **38**, 1447 (1931).

for the $^1\Pi S^N$ state, which according to the calculations is repulsive, and according to experiment is attractive. We would accordingly not regard the results obtained for the $^1\Pi$ state in Be_2 as conclusive, but those for the $^1\Sigma$ state are probably more correct. The anomaly in Li_2 is being studied more closely, and it may be necessary to apply other methods to obtain agreement.

As has been seen, the energy expressions for Be_2 involve many terms, since the interaction process is quite complicated. If an attempt were to be made to extend the calculations to B_2, the degree of complication would increase to such an extent that it is quite doubtful whether or not the results would have much meaning. From the results obtained in this and previous articles, it seems reasonable to suppose that in order to have the most stable B_2 molecule, one of the atoms should have the electron configuration $2s2p^2$.

In conclusion, it appears that the general many-electron problem for homonuclear molecules is still far from solution, and that much more powerful methods than that of Heitler and London must be developed before progress can be made. For heteronuclear molecules. the situation is even less satisfactory.

Correction:—The Σ states in this article have been assigned the wrong symmetry in the nuclei. This error arises essentially because the wave function $a_p + b_p$ is of the character S^N for Π states, but A^N for Σ states.

For $p = 0$,

$$\int (a_p + b_p)(a_s + b_s)dv = S_{ps}^{1/2} + S_{sp}^{1/2} = 0.$$

The convention followed is that the directions $\Theta_a = 0$ and $\Theta_b = 0$ are to be the same, and not opposite to each other. This correction also applies to the Π states of a previous paper[11] by of the writers.

THERMIONIC EMISSION AND SPACE CHARGE

By N. H. Frank
Massachusetts Institute of Technology

(Received November 14, 1931)

Abstract

The theory of thermionic currents for a plane parallel electrode arrangement including space charge effects is developed by using Fermi-Dirac statistics and by taking into account the wave-mechanical nature of the electron. The use of the Wentzel-Kramers-Brillouin approximate solution of the Schrödinger equation leads to results quite analogous to those of the classical calculations. The current-voltage characteristic is but slightly different but the expressions for potential distribution (and hence space charge, field, energy density, etc.) are appreciably modified by wave mechanics.

THE theory of thermionic currents when space charge effects are considered has been handled classically for the case of plane parallel electrodes by Epstein, Fry, Langmuir and Gans.[1] These authors have derived expressions for the voltage-current characteristics and for the potential distribution between electrodes. Applications of these theories can be made to special cases only with the help of numerical tables since the integrals occurring must be evaluated numerically or graphically. It is the purpose of this paper to investigate the modifications in the above theories which result from the use of quantum rather than classical mechanics.

We shall make the assumption that the area of the electrodes is large enough so that we may treat the problem as one-dimensional, and we shall think of the cathode surface as characterized by a sharp jump in potential. This is of course only an approximation to the actual state of affairs as the potential must change continuously from inside the metal to the space outside. Inside the hot cathode the number of electrons per unit volume whose energies lie between E and $E+dE$ ($E=mv_0^2/2$, where v_0 is the conponent of velocity normal to the emitting surface) give rise to an incident current.[2]

$$di = \frac{4\pi mekT}{h^3} \log (1 + Ae^{-E/kT})dE \tag{1}$$

where A is determined by

$$2mkT \log A = h^2\left(\frac{3n}{8\pi}\right)^{2/3} = \frac{h^2}{\lambda^2}. \tag{2}$$

Eq. (1) is derived on the assumption of a Fermi distribution of electrons inside the metal. The constants have the usual meaning, n is the number of free electrons per unit volume and λ a de Broglie wave-length.

[1] P. Epstein, Verh. d. Deutschen, Phys. Ges. **21,** 85 (1919); T. C. Fry, Phys. Rev. **17,** 441 (1921); I. Langmuir, Phys. Rev. **21,** 419 (1923); R. Gans, Ann. d. Physik **69,** 385 (1922).

[2] See e.g., A. Sommerfeld, Zeits. f. Physik **47,** 28 (1928).

The electrons escaping from the metal into the region between cathode and anode give rise to a current and space charge which depend on the applied potential difference and on the separation between anode and cathode. If we denote by $D(E)$ the probability that an electron of energy E (in the sense of Eq. (1)) inside the cathode escape from the metal (the so-called transmission coefficient) and by ψ_D the wave function of a transmitted electron from an incident electron beam ψ_i which is normalized to unit current, the total current may be written

$$i = \frac{4\pi mekT}{h^3} \int_0^\infty D(E) \log (1 + Ae^{-E/kT}) dE \tag{2}$$

and the potential in the region between cathode and anode $o < x < l$ is determined by Poisson's equation

$$\frac{d^2\phi}{dx^2} = -4\pi\rho = -\frac{16\pi^2 emkT}{h^3} \int_0^\infty \bar{\psi}_D \psi_D \log (1 + Ae^{-E/kT}) dE \tag{3}$$

where ψ_D is of course, a function of ϕ. Eqs. (2) and (3) together with the boundary conditions completely determine the current-voltage characteristic and the potential distribution between the electrodes. From the latter one may obtain expressions for the space charge, energy density, and field distributions by differentiation.

We shall employ approximate expressions for ψ_D and $D(E)$ as obtained by the use of the Wentzel-Kramers-Brillouin approximation to the solution of the Schrödinger equation. All the necessary formulae have been given by the author and L. A. Young.[3] Even with the help of these approximations it is not possible to obtain explicit expressions for $D(E)$ and ψ_D which are valid for all values of x and E when $\phi(x)$ is arbitrary, but we must break up the integrations in (2) and (3) into various ranges and use appropriate expressions for $D(E)$ and ψ_D in these ranges.

The problem divides itself into three subdivisions depending on the manner in which the potential varies from cathode to anode. Since according to Eq. (3) $d^2\phi/dx^2$ is always positive, we have the following possibilities:

Case I. ϕ increases monotonically from cathode to anode.
Case II. ϕ decreases monotonically from cathode to anode.
Case III. ϕ possesses one and only one minimum between cathode and anode.

We shall consider the three cases separately.

Case I. Accelerating field; no potential minimum

We shall restrict our discussion to such potential differences which, although large enough to prevent the formation of a potential minimum, are not so large that "field" currents become appreciable. Hence in this case we need consider only those electrons whose energies lie above a certain value W_a, since the transmission coefficient for the others is practically nil and their contribution to the space charge is completely negligible, except possibly for a region of atomic dimensions near the cathode.

In this case we write Eq. (2) as

$$i = \frac{4\pi emkT}{h^3} \int_{W_a}^{\infty} D(E) \log (1 + Ae^{-E/kT}) dE. \tag{4}$$

Fig. 1 shows a diagram of the barrier at the cathode surface, and the general shape of the potential energy curve. W_i is defined by

$$W_i = kT \log A .$$

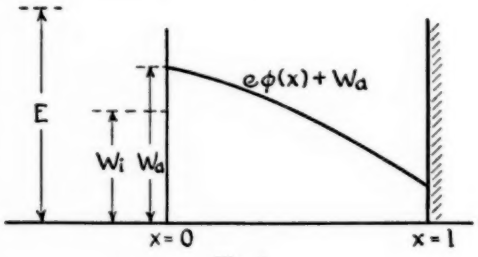

Fig. 1

For potential curves of the type shown in Fig. 1, it has been shown[3] that the transmission coefficient is very nearly

$$D(E) = \frac{4E^{1/2}(E - W_a)^{1/2}}{[E^{1/2} + (E - W_a)^{1/2}]^2 + \dfrac{h^2e^2(d\phi/dx)^2_{x=0}}{128\pi^2 m(E - W_a)^2}} .$$

Without appreciable error we may neglect the last term in the denominator and write

$$D(E) = \frac{4E^{1/2}(E - W_a)^{1/2}}{[E^{1/2} + (E - W_a)^{1/2}]^2} . \tag{5}$$

This expression is valid for $E > W_a$ and we shall introduce a slight error by using it for energies down to $E = W_a$. For zero field at the surface (5) is exact for $E \geqq W_a$ and in practice goes very nearly to zero as $E \to W_a$. The error so introduced will tend to make our results somewhat too small.

If now in Eq. (4) we change the variable to

$$y = \frac{E - W_a}{kT}$$

and write

$$\chi = W_a - W_i > 0 \tag{5a}$$

$$\beta = \frac{W_a}{kT}$$

there follows:

$$i = \frac{4\pi me(kT)^2}{h^3} \int_0^{\infty} D(y + \beta) \log (1 + e^{-\chi/kT} \cdot e^{-y}) dy$$

[3] N. H. Frank and L. A. Young, Phys. Rev. **38,** 80 (1931).

Expanding the logarithm, we obtain

$$i = \frac{4\pi me(kT)^2}{h^3} e^{-x/kT} \int_0^\infty D(y+\beta)e^{-y}dy \tag{6}$$

or

$$\left.\begin{aligned} i = i_{sat} &= \frac{4\pi me(kT)^2}{h^3} e^{-x/kT}\bar{D}(\beta) \\ \text{with} \\ D(\beta) &= \int_0^\infty D(y+\beta)e^{-y}dy = 4\int_0^\infty \frac{(y+\beta)^{1/2}y^{1/2}e^{-y}dy}{[y^{1/2}+(y+\beta)^{1/2}]^2} \end{aligned}\right\} \tag{7}$$

This is essentially the result obtained by Nordheim[4] and Sommerfeld[2] for saturation current. For all temperatures occurring in practice $\beta = W_a/kT$ is large compared to unity, so that we can evaluate $\bar{D}(\beta)$ by expanding $D(\beta+y)$ in powers of y/β. This expansion is, of course, not valid over the whole range of integration but the presence of the exponential nullifies any errors which might arise from large values of y.

The result of this integration gives:

$$\bar{D}(\beta) = \frac{2\pi^{1/2}}{\beta^{1/2}} - \frac{8}{\beta} + \frac{15\pi^{1/2}}{2\beta^{3/2}} - \cdots$$

or

$$\bar{D}\left(\frac{W_a}{kT}\right) = \frac{2\pi^{1/2}(kT)^{1/2}}{W_a{}^{1/2}} - \frac{8kT}{W_a} + \frac{15\pi^{1/2}(kT)^{3/2}}{W_a{}^{3/2}} - \cdots . \tag{8}$$

Numerically, for tungsten at about 2800°K, $W_a = 10$ volts; $kT \leqq 0.2$ volt, so that

$$\beta = \frac{W_a}{kT} \leqq 50$$

with this value of β

$$\bar{D}(\beta) = 0.40.$$

This result was found by Nordheim, who later retracted it in the light of calculations made with an image field.[5] It seems to the author that the latter question is open to objection and that the first results, essentially those obtained here, are more nearly correct. It must be further pointed out that the value of $\bar{D}$ here calculated is probably too small as the potential energy probably reaches the value W_a a short distance (order of atomic dimensions) from the cathode surface and then drops as we come into the metal. The effect of this is to reduce the value of β in Eq. (5) so that the value $\bar{D} = 0.50$ which is demanded by experiment seems entirely reasonable. The lowering of the work function due to the applied field (Schottky correction) is neglected in this treatment.

[4] L. Nordheim, Zeits. f. Physik **46**, 833 (1928).
[5] L. Nordheim, Proc. Roy. Soc. **A121**, 626 (1928).

To find the potential distribution for this case we employ Eq. (3) in which we replace the lower limit of the integral by W_a without appreciable error. For ψ_D we use the W–K–B approximation[3] (normalized to unit current),

$$\psi_D = \left(\frac{m}{2}\right)^{1/4}\left(\frac{8\pi^2 m}{h^2}\right)^{1/4} \frac{c \exp\left(i\int_0^x y^{1/2}dx\right)}{y^{1/4}}; \quad y = \frac{8\pi^2 m}{h^2}[E - W_a - e\phi]$$

whence

$$\psi_D\bar{\psi}_D = \left(\frac{m}{2}\right)^{1/2} \frac{c\bar{c}}{(E - W_a - e\phi)^{1/2}} = \left(\frac{m}{2}\right)^{1/2} \frac{D(E)}{(E - W_a - e\phi)^{1/2}} \tag{9}$$

Eq. (3) becomes

$$\frac{d^2\phi}{dx^2} = -\frac{16\pi^2 mekT}{h^3}\left(\frac{m}{2}\right)^{1/2} \int_{W_a}^{\infty} \frac{D(E)\log(1 + Ae^{-E/kT})dE}{(E - W_a - e\phi)^{1/2}} \tag{10}$$

with the notation

$$u = -\frac{e\phi}{kT}, \quad y = \frac{E - W_a}{kT} \quad (e \text{ negative})$$

and

$$g^2 = \frac{32\pi^2 m^2 e^2}{h^3}\left(\frac{2kT}{m}\right)^{1/2} e^{-\chi/kT} \tag{10'}$$

Eq. (10) goes over into

$$\frac{d^2u}{dx^2} = \frac{g^2}{4}\int_0^{\infty} \frac{D(y + \beta)}{(y + u)^{1/2}} e^{-y}dy. \tag{11}$$

One integration yields

$$\left(\frac{du}{dx}\right)^2 = g^2[p(u, \beta) - p(0, \beta) + c_1] \tag{12}$$

where we have placed

$$p(u, \beta) = \int_0^{\infty} D(y + \beta)(y + u)^{1/2}e^{-y}dy. \tag{13}$$

The constant c_1 depends on the field at the cathode by virtue of the relation

$$\left(\frac{du}{dx}\right)^2_{x=0} = g^2c_1$$

and hence is always positive.

Another integration of (12) gives

$$gx = \int_0^u \frac{dz}{(p(z, \beta) - p(0, \beta) + c_1)^{1/2}}. \tag{14}$$

Here we have chosen the second integration constant so that $u=0$ when $x=0$. To determine c_1, we place $x=l$ in Eq. (14) and find ($u=u_1$ at the anode)

$$gl = \int_0^{u_1} \frac{dz}{(p(z,\beta) - p(0,\beta) + c_1)^{1/2}} \tag{15}$$

which is a transcendental equation determining c_1. Inserting this value of c_1 into Eq. (14), we have found the potential u as a function of x. The condition that case I exist, expressed in terms of the potential difference between anode and cathode and of their separation, is obviously from (15)

$$gl \leqq \int_0^{u_1} \frac{dz}{(p(z,\beta) - p(0,\beta))^{1/2}} \tag{15'}$$

since $c_1 \geqq 0$.

The results so far obtained are very similar to those obtained classically. In fact, if we place $D(E)=1$ and introduce i_s instead of g^2 with the help of Eq. (7), the resulting equations are identical with the classical expressions. This is not surprising in view of the fact that for $0<x<l$ the electron density is so low that the Fermi-Dirac and Maxwell-Boltzmann statistics become indistinguishable.

Case II. Retarding field; no potential minimum

For this case the transmission coefficient is practically zero for all electrons in the cathode with energies less than $W_a+e\phi_1$ where ϕ_1 is the negative potential difference between anode and cathode. The expression for the current is according to Eq. (2);

$$i = \frac{4\pi mekT}{h^3} \int_{W_a+e\phi_1}^{\infty} D(E) \log (1 + Ae^{-E/kT}) dE.$$

Changing the integration variable to $y=[(E-W_a-e\phi_1)/kT]$ and expanding the logarithm as before, one obtains

$$i = \frac{4\pi me(kT)^2}{h^3} e^{-\chi/kT} \cdot e^{-e\phi_1/kT} \int_0^{\infty} D\left(y + \beta + \frac{e\phi_1}{kT}\right) e^{-y} dy \tag{16}$$

and placing $u_1 = -e\phi_1/kT$ there follows with the help of Eq. (7)

$$i = i_s e^{u_1} \frac{\overline{D}(\beta - u_1)}{\overline{D}(\beta)} \tag{17}$$

which is the equation of the characteristic for this case. $\overline{D}$ and β are defined as before. To evaluate $\overline{D}(\beta-u_1)$, we can write

$$D(y + \beta - u_1) = 1 - \frac{1}{\beta^2}[(y + \beta - u_1)^{1/2} - (y - u_1)^{1/2}]^4$$

which is equivalent to Eq. (5).

If we now remember that $\beta \gg 1$ and $-u_1 \gg 1$, the latter is necessary if the conditions of case II are fulfilled,* we may write, with

$$\gamma = -\frac{u_1}{\beta}$$

$$D(y+\beta-u_1) \leqq 1 - \left[(1+\gamma)^{1/2} - \gamma^{1/2}\right]^4 \left(1 - \frac{y}{2\beta(\gamma(1+\gamma))^{1/2}}\right)^4$$

whence there follows

$$\bar{D}(\beta - u_1) \leqq 1 - \left\{(1+\gamma)^{1/2} - \gamma^{1/2}\right\}^4 \left(1 - \frac{2}{\beta(\gamma(\gamma+1))^{1/2}}\right). \tag{18}$$

This expression is very much more nearly equal to unity than that for $\overline{D}(\beta)$ since it represents the effect of the transmission coefficient on the current which is due to electrons whose energies E lie far above W_a. ($E > W_a + e\phi_1$). For these electrons the transmission coefficient differs but little from unity. To obtain a rough idea of the magnitude of $\overline{D}\ (\beta - u_1)$ let us consider a retarding voltage of about 10 volts. Then

$$-u_1 \leqq \beta \leqq 50; \gamma = 1$$

so that

$$\bar{D} \leqq 1 - 0.03 = 0.97.$$

In finding the potential distribution between the electrodes for this case, we must remember that all electrons whose energies in the cathode lie above W_a contribute to the space charge. We must divide the energy range into two parts:

(a) $$E > W_a + e\phi_1$$

(b) $$W_a + e\phi < E < W_a + e\phi_1.$$

For (a), we have as before (Eq. 9)

$$\left.\begin{aligned} \psi_D\bar{\psi}_D &= \left(\frac{m}{2}\right)^{1/2} \frac{D(E)}{(E - W_a - e\phi)^{1/2}} \\ \text{and for (b) we use}^5 \quad \psi_D\bar{\psi}_D &= \left(\frac{m}{2}\right)^{1/2} \frac{4E^{1/2}(E - W_a)^{1/2}}{(2E - W_a)(E - W_a - e\phi)^{1/2}} \end{aligned}\right\} \tag{19}$$

Poisson's equation takes the form

* It is tacitly assumed that the separation of the electrodes is of the order of magnitude of one centimeter.

[5] This expression is obtained from Eq. (30), p. 85, Phys. Rev. **38**, (1931). Eq. (30) should read

$$\psi\bar{\psi} = \frac{4(y_0/y)^{1/2}}{p\left\{1 + \frac{1}{p^2}\left(\frac{\alpha^2}{16y_0^2} + y_0\right)\right\}}$$

and the term in α^2 is neglected compared to y_0

$$\frac{d^2\phi}{dx^2} = -\frac{16\pi^2 emkT}{h^3}\left(\frac{m}{2}\right)^{1/2}\left[4\int_{W_a+e\phi}^{W_a+e\phi_1}\frac{(E-W_a)^{1/2}E^{1/2}\log(1+Ae^{-E/kT})}{(2E-W_a)(E-W_a-e\phi)^{1/2}}dE + \int_{W_a+e\phi_1}^{\infty}\frac{D(E)\log(1+Ae^{-E/kT})}{(E-W_a-e\phi)^{1/2}}dE\right]. \tag{20}$$

The use of $W_a+e\phi$ as the lower limit of the first integral is necessary as no electrons whose energy in the cathode is less than $W_a+e\phi$ contribute to the density of charge at the position x where $E=W_a+e\phi(x)$. Changing the integration variable to $y=(E-W_a-e\phi)/kT$ and setting $u=-e\phi/kT$ (20) can be written after the logarithm has been expanded

$$\frac{d^2u}{dx^2} = \frac{g^2e^u}{4}\left[\int_0^{u-u_1}\frac{4(y-u)^{1/2}(y+\beta-u)^{1/2}e^{-v}dy}{y^{1/2}(2y+\beta-2u)} + \int_{u-u_1}^{\infty}\frac{D(y+\beta-u)e^{-v}dy}{y^{1/2}}\right] \tag{21}$$

where g^2 is defined by Eq. (10′). If we define

$$r(u-u_1) = \tfrac{1}{2}\left[\int_0^{u-u_1}\frac{4(y-u)^{1/2}(y+\beta-u)^{1/2}e^{-v}dy}{(2y+\beta-2u)y^{1/2}} + \int_{u-u_1}^{\infty}\frac{D(y+\beta-u)e^{-v}dy}{y^{1/2}}\right] \tag{21′}$$

one integration of Eq. (21) yields

$$\left(\frac{du}{dx}\right)^2 = g^2e^{u_1}\left[\int_0^{u-u_1}e^z r(z)dz + c_2\right]. \tag{22}$$

The constant c_2 is always positive since

$$\left(\frac{du}{dx}\right)^2_{x=l} = g^2e^{u_1}c_2.$$

Another integration leads to the equation for the potential distribution

$$e^{u_1/2}g(l-x) = \int_0^{u-u_1}\frac{ds}{(\rho(s)+c_2)^{1/2}} \tag{23}$$

where we have placed

$$\rho(s) = \int_0^s e^z r(z)dz. \tag{23′}$$

For $x=0$, Eq. (23) gives

$$e^{u_1/2}gl = \int_0^{-u_1}\frac{dz}{(\rho(z)+c_2)} \tag{24}$$

as the transcendental equation determining c_2. Since $c_2 \geqq 0$. Case II occurs when

$$gl \leqq e^{-u_1/2} \int_0^{-u_1} \frac{dz}{(\rho(z))^{1/2}} .$$

Case III. A potential minimum exists

Let us suppose that the minimum occurs at $x = x_m$, so that

$$\frac{du}{dx} < 0 \text{ for } 0 < x < x_m; \quad \frac{du}{dx} > 0 \text{ for } x_m < x < l.$$

(a) For the region $x_m < x < l$, we have the same relations as in case I except that now only those electrons with energies greater than $W_a + e\phi_m$ (rather than W_a) must be considered. Thus we obtain in place of Eq. (11)

$$\frac{d^2u}{dx^2} = \frac{g^2}{4} \int_{-u_m}^{\infty} \frac{D(y + \beta)e^{-y}dy}{(y + u)^{1/2}} \tag{25}$$

where

$$u_m = -\frac{e\phi_m}{kT} .$$

Changing the integration variable to $s = y + u_m$ and integrating (25) once with respect to u, there follows

$$\left(\frac{du}{dx}\right)^2 = g^2 e^{u_m} \left[\int_0^{\infty} D(s + \beta - u_m)(s + u - u_m)^{1/2} e^{-s} ds + c' \right] \tag{26}$$

where c' must be determined so that $du/dx = 0$ when $x = x_m$ (i.e., $u = u_m$). Thus we write

$$\left(\frac{du}{dx}\right)^2 = g^2 e^{u_m} [p(u - u_m, \beta - u_m) - p(0, \beta - u_m)] \tag{26a}$$

where the function $p(s, z)$ is defined by Eq. (13). Another integration yields

$$ge^{u_m/2}(x - x_m) = \int_0^{u - u_m} \frac{dz}{(p(z, \beta - u_m) - p(0, \beta - u_m))^{1/2}} . \tag{27}$$

Here the integration constant has been so determined that $u = u_m$ when $x = l$, we have

$$ge^{u_m/2}(l - x_m) = \int_0^{u - u_m} \frac{dz}{(p(z, \beta - u_m) - p(0, \beta - u_m))^{1/2}} \tag{28}$$

(b) For the region $0 < x < x_m$ we proceed analogously to case II, with the only difference that we replace l by x_m and u_1 by u_m. Hence we write

$$e^{u_m/2} g(x_m - x) = \int_0^{u - u_m} \frac{dz}{(\rho(z))^{1/2}} \tag{29}$$

where $\rho(z)$ is defined by (23′). For $x = 0$, there follows

$$e^{u_m/2} g x_m = \int_0^{-u_m} \frac{dz}{(\rho(z))^{1/2}} . \tag{30}$$

The sum of Eqs. (28) and (30) yields

$$gl = e^{-u_m/2}\left[\int_0^{u_1-u_m} \frac{dz}{[(p(z,\beta-u_m)-p(0,\beta-u_m)]^{1/2}} + \int^{-u_m} \frac{dz}{(p(z))^{1/2}}\right]. \tag{31}$$

These last two equations determine the position and magnitude of the potential minimum.

For the current we have in complete analogy to Eq. (4)

$$i = \frac{4\pi mekT}{h^3}\int_{W_a+e\phi_m}^{\infty} D(E)\log(1+Ae^{-E/kT})dE \tag{32}$$

whence there follows exactly as in case I

$$i = i_s e^{u_m}\frac{\bar{D}(\beta-u_m)}{\bar{D}(\beta)} \tag{33}$$

which is the equation of the characteristic for this case.

Summary and Conclusions

The theory of thermionic currents between plane parallel electrodes has been developed from the Fermi statistics and by taking into account the wave-mechanical nature of the electrons. The results are entirely analogous to those obtained classically. We must distinguish among three cases:

I. Accelerating field; no potential minimum.

II. Retarding field; no potential minimum.

III. The case of the existence of a potential minimum.

The current-voltage characteristics are:

I. $\quad i = i_s$

II. $\quad i = i_s e^{u_1}\dfrac{\bar{D}(\beta-u_1)}{\bar{D}(\beta)}$

III. $\quad i = i_s e^{u_m}\dfrac{\bar{D}(\beta-u_m)}{\bar{D}(\beta)}$.

If all the $\bar{D}$'s are set equal to unity, we have the classical equations except for the fact that u_m (the minimum value of the potential) is determined by a different equation (Eq. (31)).

Expressions for the potential as function of position between the electrodes have been derived which are quite analogous to the classical functions. For application of these equations it is necessary (just as in the classical case) to perform numerical or graphical integrations. A typical wave-mechanical difference occurs in the case of the expressions for charge density due to those electrons which emerge from the cathode but are turned around between cathode and anode. The density is calculated classically by dividing the cur-

rent due to these electrons by their velocity and multiplying by 2 (once going out and once returning). Quantum-mechanically, we must not form $\psi\bar{\psi}$ from the expressions for two travelling waves, but must find a ψ-function which represents a standing wave in the region considered and then form $\psi\bar{\psi}$. In so doing, interference effects which are totally foreign to classical calculations appear and modify the expression to be used for this density.

It is furthermore not necessary to carry out the numerical evaluation of the functions which determine the potential distributions in order to see the general difference between our results and the classical results. In every case the density of charge is less in our theory than in the corresponding classical case. Thus the potential distribution curves, although of the same general type as those obtained classically, will have decidedly smaller curvatures. Physically, this is easily understandable since the largest contribution to the classical density came from those electrons which, according to our theory, cannot get out of the metal because of the transmission coefficient $D(E)$.

We have neglected the dependence of the work function on the field and as we have not extended the theory to include strong fields this neglect is not serious. The omission of secondary reflection from the anode is perhaps more serious. Recently, R. S. Bartlett and A. T. Waterman[6] have published a series of papers in which they discuss the equilibrium distribution of electrons in the neighborhood of the surface of a metal and have drawn conclusions therefrom for the case of accelerating and retarding fields. The author does not consider such extension of their results entirely justified. The objections which they raise to the use of Poisson's equation because of the granular nature of the electron gas seem to the author to be largely nullified by the fact that the wave mechanical expression for density is a continuous function of the coordinates. An approximation in the theory here developed is the use of the equilibrium distribution function instead of a modified distribution which exists in the case of steady state flow of current. It can be easily shown that errors so introduced are entirely negligible.

[6] R. S. Bartlett, Phys. Rev. **37**, 959 (1931); A. T. Waterman, ibid. **38**, 1497 (1931).

STUDY OF A NEON DISCHARGE BY USE OF COLLECTORS

By Clifton G. Found and Irving Langmuir
Research Laboratory, General Electric Company, Schenectady, N. Y.

(Received November 19, 1931)

Abstract

Experiments are described from which it is concluded that electrons are emitted from a negatively charged collector in the positive column of a neon discharge. The influences of conditions in the plasma and conditions in the sheath are separated and their influence on the formation of a cold cathode discharge considered. Measurements of currents to a negatively charged collector in un-ionized neon beyond the end of the positive column, with variation of position of the collector, discharge current, and external conditions, support the theory that resonance radiation travels in straight lines over large distances beyond the end of the positive column. The absorption of this radiation and collisions of the second kind result in the formation of metastable atoms, which diffuse into contact with the walls or with metallic electrodes and there liberate electrons.

Introduction

A NUMBER of observers have found that currents to negatively charged electrodes in the positive column of a neon discharge exceed those predicted from the collector theory of Langmuir and Mott-Smith.[1] Measurements of Uyterhoeven[2] show that the observed current to a collector, in neon, at 150 volts negative to the surrounding space, is twice that calculated from the collector voltage and observed sheath thickness. The large observed current can be accounted for on the basis of a secondary electron emission from the collector. More recent results of Uyterhoeven and Harrington[3] show that at low pressures of neon from 15–50 percent of the current to a negatively charged collector is due to secondary electron emission, the greater part of which is caused by uncharged particles which are probably metastable atoms. Oliphant[4] accounts for the high secondary electron emission by neutral particles, which he obtained with a discharge in helium, as being due to metastable atoms striking the electrode and thereby releasing electrons.

Results of investigations with discharges in neon at 1 to 2 mm pressure indicate that electron currents of considerable magnitude leave a negatively charged electrode not only when the electrode is in the main discharge,[5] but also when the electrode is located in un-ionized neon at a distance as great as 30 cm from the end of the positive column. The present paper gives the experimental evidence for the conclusion that these currents are actually electron

[1] Langmuir and Mott Smith, G. E. Rev. **27,** 449, 538, 616, 762, 810 (1924).
[2] Uyterhoeven, Proc. Nat. Acad. Sci. **13,** 32 (1929).
[3] Uyterhoeven and Harrington, Phys. Rev. **36,** 709 (1930).
[4] Oliphant, Proc. Roy. Soc. May, (1929).
[5] Langmuir and Found, Phys. Rev. **36,** 604 (1930).

currents and also gives results which indicate that the secondary electrons originate from bombardment by metastable atoms.

Electrode in Positive Column

Studies with the rectifier type of hot cathode neon tube which has been described by Found and Forney[6] showed that a cold cathode discharge between the anodes occurs when the voltage between the anodes is much lower in neon than for similar tubes filled with mercury. In order to investigate the processes involved in the break-down between the anodes, a d.c. discharge was passed through neon at 2 mm pressure between the hot cathode located at one end of the cylindrical tube of 2.5 cm diameter and 45 cm long, and one of the anodes. The anodes were iron cups 1.3 cm in diameter and 1.3 cm deep

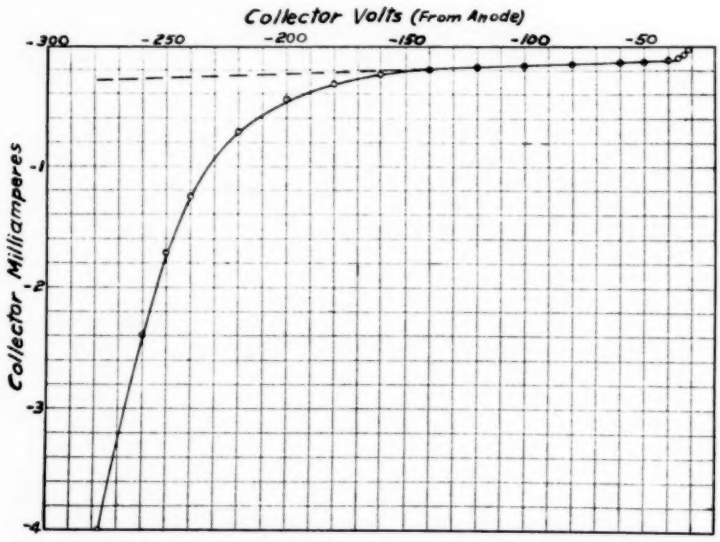

Fig. 1. Neon tube #381. Discharge current = 3.0 amps. Tube volts = 69. Neon pressure = 2 mm. Second anode as collector.

and were placed in side arms which extended at right angles to the main tube at the end opposite the cathode. The fronts of the anodes were 2.8 cm from the center of the main discharge. The second anode was used as a collector and the current to it measured as its potential was made increasingly negative with respect to the anode carrying the main discharge. The volt-ampere characteristics, given in Fig. 1, show that the current is not independent of the collector voltage, as predicted from the theory of sheaths, but increases as the potential of the electrode is made increasingly negative.

At voltages more negative than about -180 volts, the rate of increase of the negative current[7] is much more rapid, approximating an exponential

[6] Found and Forney, Trans. A.I.E.E. **47**, 751 (1928).

[7] A negative current is defined as one in the direction of electrons leaving an electrode and positive current, one in the direction of electrons to an electrode.

increase. In the voltage range, where the current increases rapidly, if the main cathode is disconnected, a cold cathode discharge is maintained between the collector and the anode. In order to maintain such a discharge, there must be an electron emission from the collector. That such an electron emission does exist is shown by the fact that when negative voltage on a collector within the positive column reaches the value at which the current increases rapidly, a dark space, resembling a Faraday dark space, is formed in the positive column on the anode side of the electrode.

Effect of Electrons Injected into the Positive Column

In order to connect the formation of a dark space with the emission of electrons, it is necessary to describe a phenomenon observed by the writers several years ago while measuring the potential distribution in a glow discharge.

The tube in which the observations were made was a cylindrical glass tube 6.5 cm in diameter. At each end of the tube was placed a flat disk-shaped aluminum electrode which filled the cross section of the tube. The distance between the electrodes was about 40 cm. The tube contained nitrogen at a pressure of 0.34 mm in which a d.c. discharge of 5 m.a. current passed between the electrodes. The cathode dark space of about 0.6 cm thickness was followed by the blueish cathode glow which extended about 1 cm. Beyond the cathode glow was the Faraday dark space for a distance of 13 cm. The remainder of the tube was filled with the reddish positive column which was striated, the distance between striations being about 3 cm. The voltage drop across the tube was about 750 volts, approximately half of which was cathode drop. A V-shaped tungsten filament of 1 cm length and 0.17 mm diameter was placed within the positive column about 5 cm from its cathode end (i.e., between the second and third striation).

When the filament is heated to a temperature at which it emits electrons, if the potential of the filament is negative to the space surrounding it, electrons are injected into the discharge with a velocity corresponding to the difference of potential between the filament and the space. The number of electrons injected can be controlled by the filament temperature and their velocity by the voltage on the filament. It was found that when electrons with a velocity greater than that corresponding to about 100 volts were injected into the positive column of the nitrogen discharge, a dark space, similar to the Faraday dark space, was observed on the anode side of the point where the electrons were injected. No change could be seen in the discharge on the cathode side of the filament. When the filament was connected directly to the main cathode, that is, the electron velocity corresponded to about 400 volts, it was found that an injected electron current of only 20 microamperes, or 0.4 percent of the discharge current, caused the formation of a dark space, extending from the filament a distance of 8 cm toward the anode. The length of the newly formed dark space increased almost linearly with the number of injected electrons, approaching a limiting length equal to the Faraday dark space between the cathode glow and the positive column. The value of the

injected electron, current, at which the limiting length of dark space was reached, was lower the higher the velocity of the injected electrons. For example, with 400 volt electrons the limit was reached with 20 micro amperes of injected current, while with 100 volt electrons it required about 400 microamperes.

The formation of the dark space, produced in the present experiment with neon, took place when the collector was about 150 volts negative to the space and increased in length as the collector voltage was increased. The close analogy between the two cases indicates that electrons of high velocity were being injected into the neon discharge when the collector was at high negative voltages.

Ionization by Collision

When electrons are emitted from an electrode into a gas the current from the electrode increases as the applied potential is increased. Dr. K. B. Blodgett[8] has made observations on the increase of current in argon and finds when the electronic mean free path is small compared to the sheath thickness, that the current increases according to the relation

$$i = i_0 2^n$$

where i_0 is the electron emission from the cathode and n the number of ionizing collisions within the sheath. When the sheath is thin compared to the mean free path the maximum increase of current with voltage corresponds to an arithmetic progression.

The current from a collector in a neon discharge increases with voltage in a manner similar to that observed by Dr. Blodgett for argon. When the collecting electrode is in a region of low ionization, as is the case when the second anode was used as collector for curve of Fig. 1, the collector current increases exponentially with increase in voltage. This is shown in Fig. 3 in which the logarithm of the difference between the observed current of Fig. 1 and the positive ion current expected from space charge considerations is plotted against the voltage. The equation of this curve is

$$i = 0.94 \times 2^{(V-21)/21} \times 10^{-6} \text{ amps.}$$

which, from analogy with Dr. Blodgett's results, corresponds to an electron emission from the collector of 0.94 microamperes.

Moreover, when the collector is in a region of intense ionization (i.e., when the sheath thickness is thin) the rate of increase of current decreases with increasingly negative voltages, approaching a limiting value as shown in the curve of Fig. 2, which is for a tungsten disk in the positive column of a discharge of 2 amps. in neon at 0.7 mm pressure.

Analysis of Current-Voltage Curve

The shape of the volt ampere characteristic of a collecting electrode depends greatly on the intensity of the discharge and also on the pressure of

[8] K. B. Blodgett, Proc. Nat. Acad. Sci. **15**, 233 (1929).

neon. The electron emission from the collector is due to conditions in the plasma and the increase of current is governed by the conditions in the sheath.

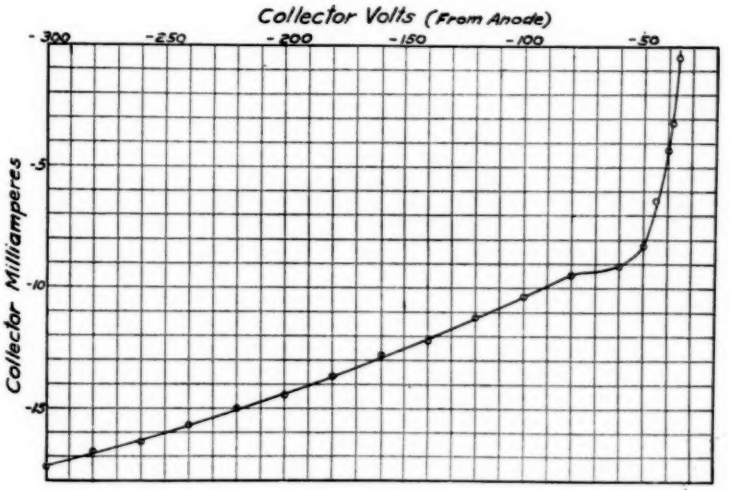

Fig. 2. Neon tube No. 19800. Discharge current = 2.0 amps. Neon pressure = 0.7 mm. Collector is tungsten disk in positive column.

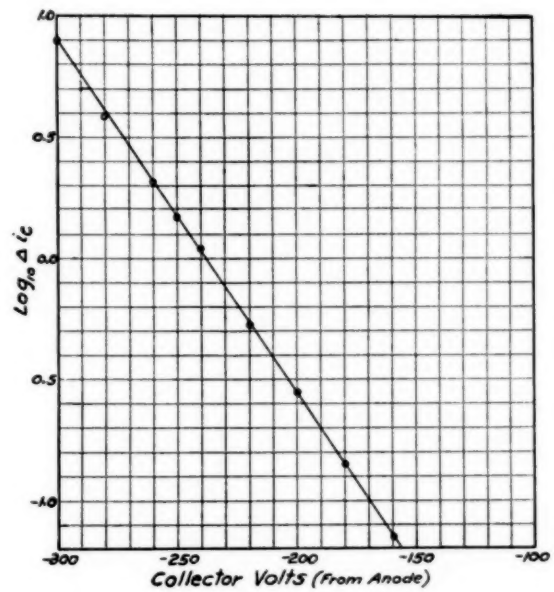

Fig. 3. Increase of negative collector current with voltage. Plotted from Fig. 1.

This is demonstrated in the curves of Fig. 4, which give the volt-ampere characteristics of a plane collector of 1.2 cm diameter at the center of a 5 cm

diameter tube in which is a neon discharge of 2 amperes. Although at low voltages the collector current increases with pressure up to about 1 mm, and then decreases again at higher pressures, the rate of increase of current at higher voltages continues to increase as the pressure is increased. At low pressures the m.f.p. of the electrons is so high that ionization by collision cannot take place within the sheath. Since at high pressures the thickness of the sheath increases due to the decrease in collector current, and the m.f.p. of the electron is less, ionization by collision within the sheath causes the collector current to increase rapidly.

The following experiment shows that the shape of the current voltage curve at low negative voltages is determined by conditions in the plasma, and at high voltages by conditions in the sheath. The collecting electrode was

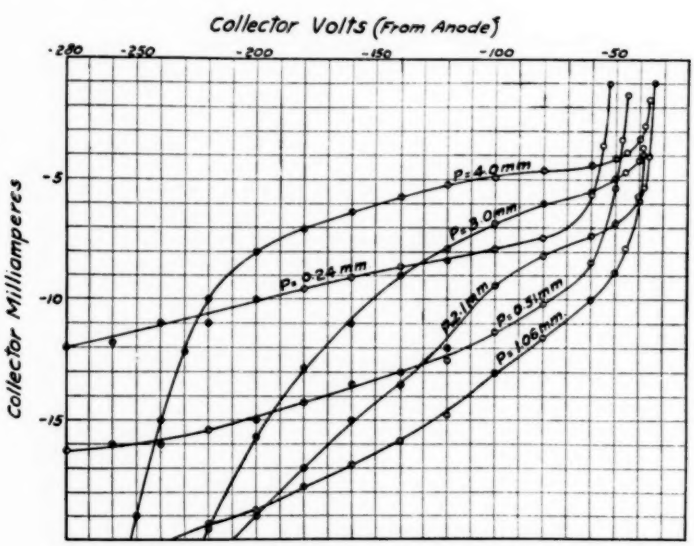

Fig. 4. Collector characteristics as function of pressure. Neon tube No. 19800. Discharge current 2.0 amps. Collector is tungsten disk in positive column.

placed in a side arm at a distance of about 2.5 cm from the edge of the main discharge of 2.0 amps. in neon at 2 mm pressure. Curve *ABC* of Fig. 5 gives the current-voltage curve for the collector. The side arm was then covered by a cloth which was cooled by means of liquid air, and a second voltage curve *ABD* was obtained. The curve remained unaltered at low voltages (*AB*), showing that this portion of the curve was controlled by conditions in the plasma, which were not altered by cooling the region around the collecting electrode. Since a similar current increase at the higher voltages can be obtained by increasing the pressure of neon 50 percent, as shown by the curve *EFD* for 3 mm pressure, we account for the rapid rise of current in this range of voltages by the increased density of gas in the region of the sheath, which permits more efficient ionization by collision and hence a faster increase in collector current with voltage.

Effect of Negative Currents on Formation of an Arc

The results just described are important in the design of full wave rectifiers in which there are two anodes and a cathode. In this type of tube, the maximum voltage at which the tube can operate is determined by the voltage at which a cold electrode discharge takes place between the two anodes.

Whether or not a cold cathode discharge will take place is determined not by the current to the negative electrode, but by the rate of increase of the current with voltage. This is illustrated in the curves of Fig. 4 which give the current as a function of negative voltage on a collector in a neon discharge.

Although the currents at 1.06 mm pressure are many times greater than those at 4.0 mm pressure, the curve at the former pressure is concave upwards

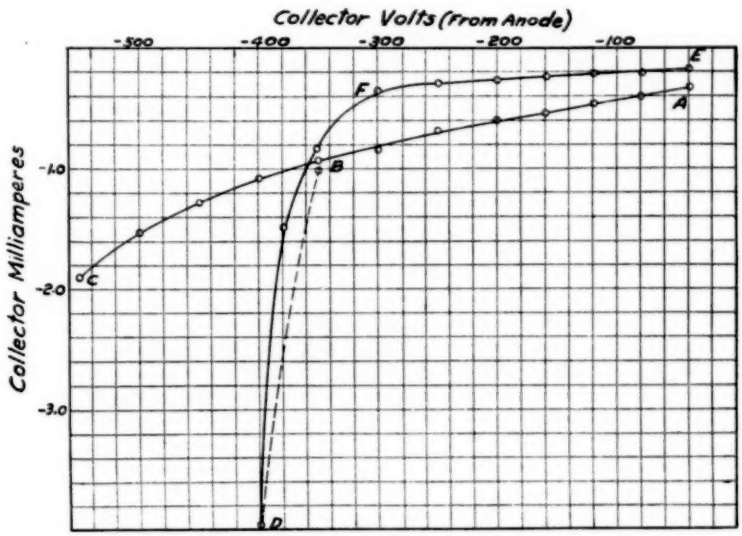

Fig. 5. Effect of pressure change on collector characteristics. Discharge current = 2.0 amps.

over the total voltage range, while the curve at 4.0 mm pressure is concave downward, showing a very sharp rise of current with voltage at about -200 volts, where the tendency to form a self-sustaining discharge is quite evident. When the anode is in a region of low ionization during the negative half cycle, the positive ion sheath about it is large permitting multiple ionizing collisions and thus favorable conditions are produced for the initiation of a discharge between the anodes, as illustrated by the curve for 4.0 mm pressure. On the other hand, when the anode is in a region of such dense ionization that the sheath thickness is of the order of an electronic m.f.p., a secondary electron can produce only one electron within the sheath, and although the positive ion currents to the anode may be high during the negative half cycle, no discharge will take place between the anodes as no cascading process of ionization can occur.

Thus in a discharge tube containing a multiplicity of anodes, there is less tendency for an arc to form between the anodes when they are so placed that

the electrodes, when negative, are in a region of intense ionization. However, in such position a great deal of bombardment is caused, and, consequently, a loss of electrode material by sputtering.

Studies of Secondary Electron Emission

The above experiments indicate that a negatively charged collector in the positive column of a neon discharge emits electrons, and it has been shown that these secondary electrons cause ionization by collision at relatively large negative voltages. In order to avoid the complications produced by ionization by collision, the following experiments to determine the source of secondary emission were performed with low negative voltages at which ionization by collision was negligible.

Variation of Currents with Distance of Electrode from Discharge

In order to study the variation of the currents to a negatively charged collector as a function of the concentration of ions, a tube of 2.5 cm diameter was used in which the collecting electrode could be moved along the tube

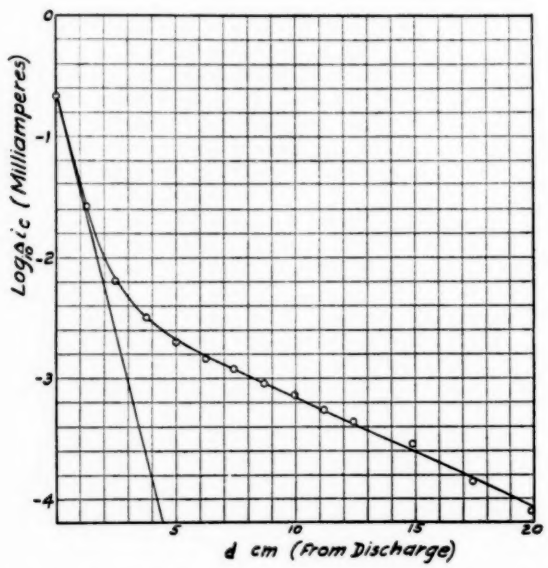

Fig. 6. Variation of negative collector current with distance from end of positive column. Discharge current = 0.05 amps. Neon pressure = 1 mm.

from a position in the discharge to a distance of several cm beyond the anode end of the positive column. The curve in Fig. 6 is a plot of the log of the current in m.a. to a collector at a potential 75 volts negative to the anode, as a function of the distance between the electrode and the anode end of the positive column. As the electrode is moved back from the discharge, the collector current decreases exponentially at first, but at distances greater than 5 cm from the discharge, the current decreases less rapidly. At short distances from the discharge where the collector current decreases exponentially, the same

processes are involved in the production of current as are responsible for the current when the collector is in the main discharge. For, whether the current is due to reception of positive ions, secondary electron emission by metastable or excited atoms, or photoelectrons produced by resonance radiation (of short free path) from the positive column, it will fall off exponentially according to the laws of diffusion. While most of the resonance radiation has a short free path, and will follow the laws of diffusion, there is, as will be pointed out in a later section, a small fraction which is not so strongly absorbed and, therefore, will decrease according to some other law. The theory of diffusion down a long cylinder has been worked out by Schottky.[9] Assuming that all diffusing particles are destroyed when they reach the walls, the number of particles which diffuse per second across a cross section of the tube at a distance Z from the origin as derived on the basis of Schottky's theory by Langmuir and Compton[10] is

$$i = 3.26 D n_0 a e^{-(2.405 Z/a)}$$

where n_0 is the number of particles per cm^3 at the origin; D, the diffusion coefficient; and, a, the radius of the tube. From the equation given above, it is seen that the exponential term alone determines the rate of decrease of intensity of the diffusing substance along the tube, and, since the attenuation constant, $2.405\ Z/a$ involves only the tube dimensions and is independent of the absolute value of the diffusion coefficient, the rate of decrease is the same for all substances which are destroyed when they reach the walls. Thus, due to diffusion, the collector current will be reduced to 1/10th value when the collector is moved away from the plasma a distance equal to the radius of the tube. The solid straight line in Fig. 6 represents such a decrease for this tube, and it is evident that the large currents at distances greater than 5 cm cannot be accounted for by diffusion from the discharge.

Currents not Caused by Diffusion

Experimental proof, that the large currents at great distances from the discharge are not due to diffusion, is supplied by the following experiment. In the tube used, the main discharge current of about 1 amp. took place in neon at about 1 mm pressure between a hot cathode and anode. One collector b, is placed in the main tube 15 cm beyond the anode end of the discharge; a second collector, d, of the same area as b is placed in a side tube which is attached to the main tube at a point about 5 cm from the anode end of the discharge. The position of d in the side tube is such that it is the same distance from the discharge as b. Since the mean free path of electrons, positive ions, atoms and most of the resonance radiation is small compared to the dimensions of the tube, diffusion should be the same in the side tube as in the main tube. However, with the collector 75 volts negative to the anode, the current to d in the side tube is less than 1/1000th of that to b in the main tube. Thus the larger collector currents to b cannot be due to diffusion of ions, metastable

[9] Schottky, Phys. Zeits. **25**, 635 (1924).
[10] Langmuir and Compton, Rev. Mod. Phys. **3**, 212 (1931).

atoms or resonance radiation, but are caused by something, having a long free path, and which, therefore cannot diffuse around the corner into the side tube.

That these large currents to *b* are observed only when light from the discharge can reach the neighborhood of this collector is indicated by a second experiment arranged as follows. At a distance of about 6 cm from the end of the neon positive column, the main tube, which had a diameter of 2.5 cm, was expanded into a bulb of 8 cm diameter, and beyond the bulb the tube diameter was again 2.5 cm. At a distance of 5 cm beyond the bulb, a collector of 1.9 cm diameter was placed in the axis of the tube. The side of the collector away from the discharge was backed with mica so that only the collector surface was facing the discharge. In the center of the bulb was a nickel disk of 3.75 cm diameter, which could be rotated about an axis perpendicular to the axis of the main tube. The disk was so mounted that when it was at right angles to the axis of the tube, it shadowed the collector completely from the main discharge. Since the shutter area was less than 1/4 the cross section of the bulb, it is apparent that the orientation of the shutter could have little or no effect on diffusion from the discharge to the collector. With the collector 75 volts negative to the anode, it was found that when the collector was shadowed from the discharge by the shutter (the shutter at right angles to the axis of the tube) the collector current was reduced to an extremely small value compared to that observed when the shutter was parallel to the axis and the collector could "see" the discharge. Also, as the angle of the shutter was changed, the effect varied as the direct rays from the positive column were intercepted by the shutter. Since positive ions, metastable atoms and electrons all have a short m.f.p., one is forced to conclude from the above observations that the secondary electron currents from a collector facing the discharge, but situated at a distance of several cm from it, are caused by some kind of radiation which originates in the discharge and which can travel long distances without change of direction.

Variation of Collector Currents with Discharge Currents

The variation of negative collector currents with change of discharge current is shown in Fig. 7, from which it is seen that when the collector is at the edge of the discharge, the current to it increases almost linearly with the discharge current. When the collector is at a distance of 7.5 cm from the plasma, the current to it increases to a maximum value at a discharge current of 0.5 amps. With still higher discharge currents the collector current decreases, approaching a constant value when the discharge reaches 1 amp. Since the results of the previous section show that diffusion from the plasma can contribute less than 1 percent of the current observed when the collector is at a distance of 7.5 cm, it is obvious from the curves of Fig. 7 that the negative currents to a collector in un-ionized neon several cm from the plasma do not originate from the same source as the negative currents due to diffusion of particles from the plasma. The shape of the curve of Fig. 7 for 7.5 cm is very similar to the curve of Fig. 8, which gives the variation with discharge current of the concentration of metastable atoms in the positive column of a

neon discharge as measured by Kopferman and Ladenburg[11] by anomalous dispersion. This similarity suggests that the currents at large distances beyond the plasma are due to metastable neon atoms, or that their production is

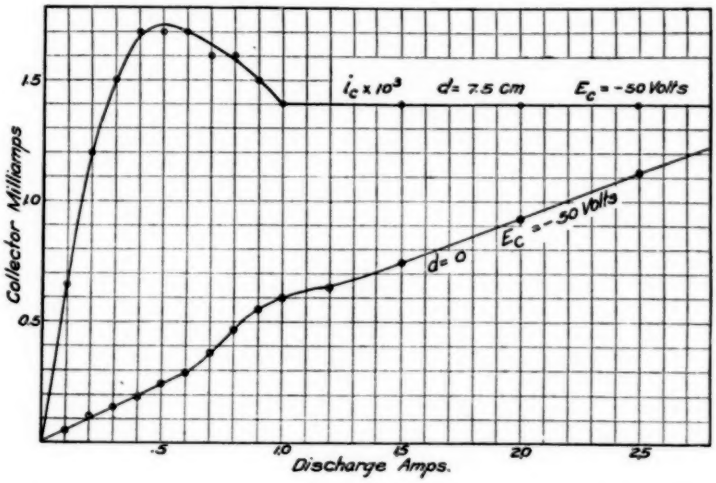

Fig. 7. Variation of negative collector current with discharge current. Neon pressure = 1 mm.

governed by the same conditions which govern the production of metastable atoms in the positive column. Moreover, in the present results, as well as in

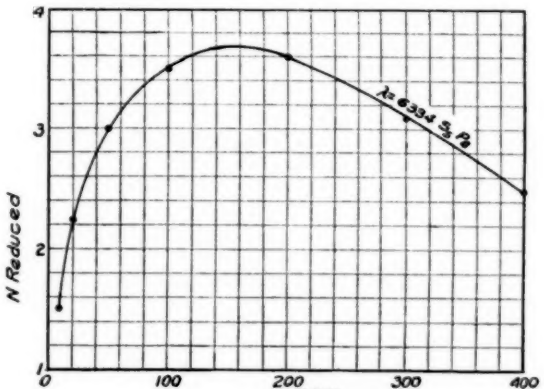

Fig. 8. Concentration of metastable atoms as function of discharge current (Kopferman and Ladenburg).

those of Kopferman and Ladenburg, the position of the maximum shifts to lower discharge current densities as the gas pressure and the tube diameter are increased.

[11] Kopferman and Ladenburg, Zeits. f. Physik **48,** 26 (1928); Zeits. f. physik Chem. Haber Band 375, 1928.

Discussion of Possible Sources of Secondary Electrons from a Collector in Un-ionized Neon

We have seen that the currents to a negatively charged collector at relatively long distances from the plasma are much greater than can be accounted for by diffusion of positive ions from the plasma. Also, these currents cannot be due to secondary emission by metastable atoms from the discharge as the number diffusing down the tube would fall off according to Schottky's diffusion law since they have a short m.f.p. and are destroyed when they come in contact with the walls. Since these collector currents appear to be so closely connected with the concentration of metastable atoms in the discharge, it may prove helpful to consider the processes responsible for the formation of these metastable atoms.

A normal neon atom is excited to resonance when an electron with a velocity corresponding to 16.6 volts collides with it. Because of the very short m.f.p., or high absorption coefficient of resonance radiation in normal gas,[12] this radiation is absorbed and re-emitted millions of times before it reaches the walls, and as practically all of the time is spent in the excited state, a collision of the second kind is almost certain to take place which will result in a transition from the resonance to an adjacent metastable level. This is more probable since the energy involved in such a transition corresponds to only 0.05 volts. Thus, if the metastable atoms in the plasma and the collector currents at large distances from the plasma have a common origin, we must look for the origin in the resonance radiation from the main discharge. If the m.f.p. of the resonance radiation is as short as given by classical theory, it cannot travel great distances, and since it is absorbed by the walls it will have the same attenuation constant as electrons, positive ions and metastable atoms. However, although little is known of the properties of the neon resonance lines (about 740A) it is safe to assume from experiments with mercury of R. W. Wood[13] that the emission line is much broader than the absorption line. The absorption coefficient mentioned above applies only to the center of the resonance line, and the radiation from the edges of the broadened resonance line will have a much lower coefficient and will be able to travel large distances. When this broadened resonance radiation, which travels down the tube, is finally absorbed, most of it will be re-emitted as a narrow line which is strongly absorbed. Consequently, such a process consists in the transformation of radiation having a long free path to radiation which has a short free path or high absorption coefficient. Due to the fact that the re-emitted radia-

[12] According to classical theory (R. Ladenburg, Ber. d. D. Phys. Gesell. **16**, 770, 1914) the absorption coefficient of a gas for resonance radiation is given by

$$\alpha_0 = \frac{Ne^2}{\nu_0 mv}$$

where N is the number of atoms in the normal state, ν_0 the frequency of the resonance radiation, v the average velocity of the gas atoms, e the charge and m the mass of an electron. Substituting the numerical values for neon resonance, we find $\alpha_0 = 1.55 \times 10^5$ or the m.f.p. for resonance radiation in neon at 1 mm pressure equals 6.45×10^{-6} cm.

[13] R. W. Wood, Phil. Mag. **44**, 1111 (1922).

tion has a high absorption coefficient, only that radiation re-emitted very close to the electrode will be incident on it. Also, as described above, the production of metastable atoms from the re-emitted, strongly absorbed resonance radiation, by collisions of the second kind, will be high. The metastable atoms, so formed, will strike the electrodes and glass walls of the vessel, and, as shown by Oliphant and Uyterhoeven, will cause a secondary electron emission from the electrode which would account for the large currents observed when the collector is at great distances from the positive column. The mathematical derivation of this theory, which will be presented in detail in a subsequent paper, leads to the following expression for the energy, E, absorbed per unit volume per second at a distance x from the source of resonance radiation.

$$E = 5.9 \times 10^{-7} \nu_0 I_\nu \frac{r^2}{x^3} \left(\frac{T}{M \ln (\alpha_0 x)} \right)^{1/2}$$

where α_0 is the absorption coefficient of the resonance radiation of frequency ν_0; I_ν is the density of resonance radiation per unit volume per unit frequency at end of positive column, M the molecular weight, and T the temperature of the gas, and r the radius of the tube.

Since $\alpha_0 x$ is an extremely large number, the expression under the square root sign varies only slightly with change in x. It is seen that the energy absorbed, and hence the number of metastable atoms formed, decreases inversely as the third power of the distance from the positive column. Experimental results are in good agreement with this relation.

Of course, the electron current from the collector could be attributed directly to photoelectron emission by the broadened resonance line. While such photoelectrons are undoubtedly emitted, experiments which will now be described indicate that the chief cause of the currents at large distances is the formation of metastable atoms by the resonance radiation rather than the resonance radiation itself.

Positive Currents to a Collector

When a collecting electrode, 10 cm or more from the end of the positive column, is made positive, it is found that there is a current in the direction of electrons to the electrode (positive current) of the same order of magnitude as the negative current. The fact that these positive currents vary with the discharge current in exactly the same way as the negative currents indicates that both originate from a common cause. It is very improbable that photoelectric currents of any measurable magnitude come from the glass. It seems more plausible to assume a secondary emission from the walls because of bombardment by metastable atoms which establishes a definite concentration of electrons in the space between the collector and the discharge and thereby gives it a definite conductivity.

Effect of Radiation from an External Neon Light

Penning[14] has shown that the addition of a slight trace of gas, such as ar-

[14] Penning, Zeits. f. Physik 45, 335 (1928).

gon, which has an ionization potential less than the energy of the metastable state of neon, lowers the arcing voltage of neon. This he attributes to ionization of the added gas by the metastable atoms of neon. Furthermore, he has demonstrated[15] that the arcing voltage of such a tube containing a trace of argon is increased when subjected to radiation from an external neon tube. This increase is accounted for by the destruction of neon metastable atoms by the radiation, and hence a decrease in the amount of ionization of the argon. Penning's curves show that these changes in break-down voltage occur only in the pressure range in which the break-down voltage for pure neon increases with increase of pressure, that is, in the range where the break-down is determined by the energy which an electron gains between collisions with gas atoms. Under these conditions, the presence of positive ions causes a redistribution of the electric field between the electrodes, which increases the voltage gradient at the cathode, thus permitting an electron to gain sufficient energy between collisions to ionize, although the voltage impressed between the electrodes is lower than for break-down in pure neon. In other words, the presence of positive ions is equivalent to a reduction of distance between the electrodes. At low pressures where the break-down voltage increases with decrease of pressure, the electrons gain sufficient energy between collisions to ionize, but ionization is limited by the frequency of collision of the electrons with gas atoms. Consequently, the presence of positive ions will have practically no effect on the starting voltage, as is shown by Penning's curves at these pressures.

Since the function of the positive ions is to change the field distribution, it is evident that a slight change in the positive ion concentration will result in a comparatively large change in break-down voltage. Such an amplified action is necessary to account for the large increase in starting voltage when the tube is irradiated by outside neon light.

The strong lines in the visible radiation of neon arise from transitions between ten closely grouped levels of the neon atom and four lower levels, two of which are resonance levels and two metastable levels. If metastable neon atoms are exposed to radiation from a second neon tube, some will be raised to one of the ten higher levels, from which they cannot return directly to the normal state, but must return first to one of the four intermediate levels unless they absorb radiation of a second frequency which will raise them to a still higher level, from which it may be possible to return directly to the normal state. However, the probability of such a double absorption is extremely small and very few metastable atoms will be destroyed by this process. Most of the metastable atoms which have been raised, by absorption of radiation, to a higher level will return to a metastable level but some will go to a resonance level, from which they will return to normal with emission of resonance radiation. This does not indicate that atoms returning to normal in this manner cause an appreciable decrease in the concentration of metastable atoms, for, as pointed out above, the resonance radiation is strongly absorbed and by collisions of the second kind, metastable atoms are again formed. From these

[15] Penning, Zeits. f. Physik **57**, 723 (1929).

considerations it is quite evident that radiation from a second neon light cannot ordinarily be very effective in destroying metastable atoms.

In view of Pennings' results, volt-ampere characteristics of a collector were taken when radiation from an external neon light fell on the un-ionized neon between the positive column and a collector placed 25 cm from the discharge. Such characteristics are given in Fig. 9 and show that although the collector currents at low voltages are only slightly decreased by the irradiation, at higher negative voltages, where the electric field is important, the decrease in current with radiation is much larger.

Moreover, not only the negative currents, but also the positive currents are decreased, proving that both are due to, or at least influenced by, the concentration of metastable neon atoms. By confining the external radiation

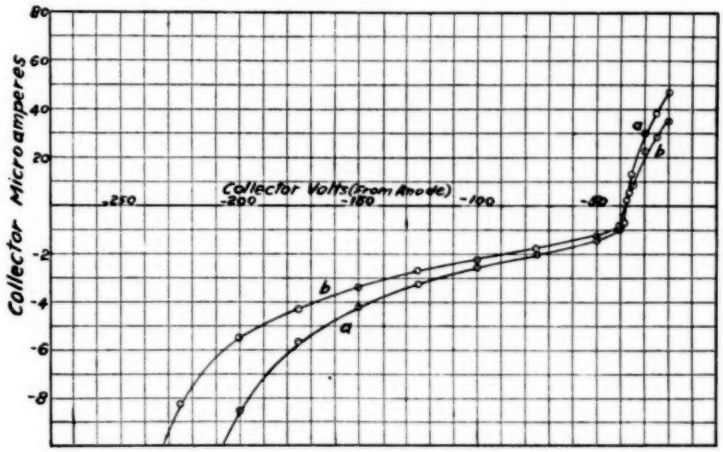

Fig. 9. Effect of radiation from external neon lamp operating at 3 amp. on collector currents. Tube #20091, diameter = 5 cm. Discharge current = 0.5 amp. Neon pressure = 1.75 mm. Collector 25 cm from end of positive column (a) without and (b) with external radiation.

to small regions of the space between the collector and the discharge, it was shown that the decrease in collector current took place when the irradiated region was close to the collector. Thus, the collector currents are caused chiefly by metastable atoms, formed close to collector, which reach it through diffusion.

No decrease in collector current was observed when the source of external radiation was other than a neon tube. Irradiation by helium, mercury and argon discharges, as well as by an incandescent lamp caused no change in collector current.

Effect of Orientation of Collector

The conclusions reached above as to the origin of the collector currents are confirmed by the results of measurements in which the collectors were two disks of exactly the same size, placed with their planes perpendicular to the axis of the tube in a 2.5 cm diameter discharge tube at a distance of 10 cm

from the positive column. One of the disks, *b*, was covered with mica on the side facing the source of resonance radiation so that the exposed surface could receive no direct radiation. The second disk, *d*, was covered with mica on the opposite side. From the curves of Fig. 10 it is seen that although *b* could receive no direct radiation from the discharge, its currents were of the same order of magnitude as those to *d*. If radiation is the cause of secondary electron currents, one would expect the current from *d*, which is exposed to all the radiations reaching that cross section of the tube to be much greater than

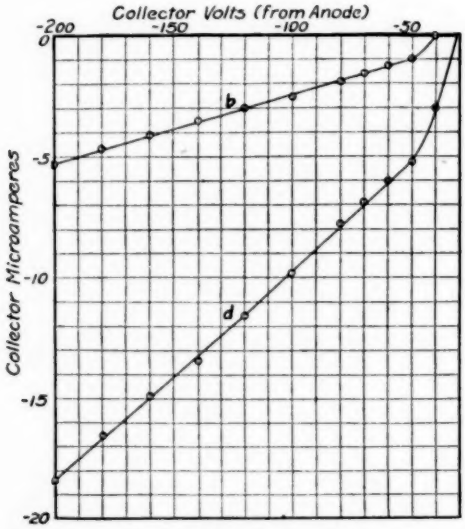

Fig. 10. Collector currents to electrode facing toward and away from discharge. Tube #23459, diameter 5 cm. Discharge current = 1.0 amps. Neon pressure = 0.37 mm. Collectors 10 cm from end of positive column. *d* faces discharge, *b* away from discharge.

the currents from *b* which is exposed to only that radiation absorbed, and subsequently reemitted in the region immediately back of the collectors. On the other hand, on the assumption that the secondary emission is due to metastable atoms formed by the resonance radiation, the currents from both electrodes would be proportional, not to the resonance radiation reaching them, but to the resonance radiation absorbed close to them, which would not differ greatly for the two cases.

Preparation of Tubes and Purity of Neon

The tubes used were baked out at high temperature and all metal parts were thoroughly degassed both by high frequency and discharge bombardment. The tubes were also operated for long periods of time with a discharge at low pressure. This was found a very effective method of freeing the glass walls and metal parts of gases which might be left after the heat treatment. Moreover, the high amperage discharges, which were used, clean up impurities very rapidly. After the above treatment, neon was admitted into the tube. Before being admitted to the tube, the neon was purified by means of a mag-

nesium arc and after admission was purified by running a discharge at high current for several hours.

C. Kenty[16] has attributed results with similar apparatus to a photoelectric effect of the resonance radiation and ionization of traces of impurities by metastable neon atoms. However, we believe that the results reported in this paper are characteristic of pure neon. We are led to this belief by the change in volt-ampere characteristics of a collector in un-ionized neon, when a minute amount (0.10 percent) of an impurity, such as argon, is added. When the collector is negative, the addition of argon causes very little change either in the shape of the curve or the order of magnitude of the currents. However, in the range of voltage where the current passes from negative to positive, the transition is very much steeper for the admixture and on the positive side the rate of current increase is from ten to one hundred times that for pure neon. If the original characteristics are due to impurities, an increase of impurity might be expected to change the magnitude of the effect, but the change in form of the volt-ampere characteristics indicates that the addition of argon brings in a new phenomenon. Moreover, when the admixed argon is absorbed in charcoal immersed in liquid air, the volt-ampere characteristic obtained is the same as before the argon was admitted. A more complete account of the effect of addition of gases will be reserved for a future publication.

Summary

From the experimental evidence described, we have been led to the conclusion that the resonance radiation from a neon arc can travel distances as great as 20 to 30 cm through un-ionized neon. The absorption of this radiation by the normal neon atoms results in the formation of excited neon atoms, which, by subsequent collisions of the second kind, arrive in the metastable state. The metastable atoms thus produced diffuse to the walls and metal electrodes and there liberate secondary electrons from both types of surfaces.

The writers are pleased to have this opportunity to express their appreciation for the assistance of Dr. P. Lowe in making many of the measurements.

THE DISSOCIATION OF NITROGEN AND CARBON MONOXIDE BY ELECTRON IMPACT

By John T. Tate and W. Wallace Lozier*
University of Minnesota
(Received December 1, 1931)

Abstract

The energies of the dissociation products of N_2 and CO formed by electron impact have been studied. The kinetic energy distributions of C^+ ions from CO and N^+ ions from N_2 have been measured and for both gases the most probable kinetic energy of the ions is about 3 volts. The variation with electron energy of the probability of production of N^+ ions from N_2 and C^+ ions from CO (the ions having specified energies) has been studied. The minimum electron energies necessary to produce C^+ and N^+ ions of specified energy have been determined and they satisfy the requirements of the principle of conservation of energy. From these measurements heats of dissociation as follows have been determined:

Process	Heat of dissociation (volts)
$N_2 \rightarrow N+N$	8.4 ± 0.5
$N_2^+ \rightarrow N^+ + N$	$\geqq 7.1 \pm 0.5$
$CO \rightarrow C+O$	9.3 ± 0.5
$CO^+ \rightarrow C^+ + O$	$\geqq 6.4 \pm 0.5$

The following are probably the dissociation processes detected in the experiments:

Process	Energy of ions (volts)	Energy of impacting electron (volts)
$N_2 \rightarrow N^+ + N + e$	2 to 7	27 to 37
$N_2 \rightarrow N^+ + N^* + e$	1 to 2	35 to 37
$N_2 \rightarrow N^+ + N^+ + 2e$	4 to 8	46 to 54

Negative ions (O^-) were observed and are believed to result from the following processes:

Process	Energy of O^- ions (volts)	Energy of impacting electron (volts)
$CO + e \rightarrow C + O^-$	0 to 1	10 to 14
$CO \rightarrow C^+ + O^-$	0 to 2	22 to 26

Introduction

COLLISIONS between electrons and molecules of a gas produce a number of fascinating phenomena. The results of such collisions are far more complicated than those involved in impact between electrons and atoms, for although the direct action of the projectile electron is doubtless upon the electrons of the molecule just as in atomic impact, the subsequent events are much more varied. Provided the pressure is sufficiently low an atom, once excited by impact, has little choice but to lose the energy of excitation by radiation. An excited molecule, on the other hand, may radiate or it may dissociate in a variety of ways. An interesting feature of the dissociating process is that in general the constituents fly apart with considerable velocity.[1] This results from the fact that the electron's action on the molecule is

* National Research Fellow.

[1] E. U. Condon, Phys. Rev. **35**, 658 (1930) abstract; W. Bleakney and J. T. Tate, Phys. Rev. **35**, 658 (1930) abstract; W. Bleakney, Phys. Rev. **35**, 1180 (1930).

completed before the constituent atoms have changed much in position (Franck-Condon principle). Thus when dissociation takes place the act of the projectile electron is so to modify the electron configuration of the molecules that the resultant force between atoms is repulsive while the atoms are still close together. The consequent effect of this is that the atoms fly apart and in doing so attain considerable kinetic energy.

A year ago one of us[2] described a method and apparatus[3] which are suitable for a study of these kinetic energies. The method was applied to the study of the dissociation of hydrogen by electron impact. In the case of hydrogen the forces between atoms for various electron configurations have been calculated by quantum mechanical methods so that a comparison with the experimental results was possible. The theoretical predictions were satisfactorily verified.

Unfortunately, for no gas other than hydrogen are the interatomic forces satisfactorily amenable to computation. On the other hand it seems desirable to extend the experimental study to other gases, for, as will be pointed out in this paper, such studies give some information about molecular binding forces and, in some instances at least, a quantitative measure of the heats of dissociation. We present here the results for nitrogen and carbon monoxide.

Relation Between Energy of Dissociating Products and that of Primary Electrons

If the energy communicated to the molecule by the electron impact is V_i and if $U_2 - U_1$ is the change in potential energy of the constituent parts of the molecule before and after dissociation, it is readily seen that the energy which appears as kinetic energy of the products of dissociation is

$$V_i - (U_2 - U_1).$$

If the masses of the products of dissociation are equal, as in the case of H_2 or N_2 the kinetic energy of each atom after dissociation will be

$$\tfrac{1}{2}[V_i - (U_2 - U_1)].$$

In general, however, if the masses of the products are not equal the kinetic energy will be divided in the inverse ratio of the masses. Thus, if the masses are m_1 and m_2 the kinetic energy of constituent 1 is

$$\frac{m_2}{m_1 + m_2}[V_i - (U_2 - U_1)].$$

Experimentally we can measure the minimum energy the electrons need to have (V_i) to produce a dissociating product which has the measured energy, V_F. It is evident that the relation between V_F and V_i should be a

[2] W. Wallace Lozier, Phys. Rev. **36,** 1285 (1930).

[3] Acknowledgment should be made that the apparatus used in this work was similar to one which had been devised in this laboratory by Mr. T. J. Jones for an unpublished study of the thermal velocities of atomic mercury ions.

linear one, that the slope should be $m_2/(m_1+m_2)$ and that the intercept on the V_i axis is the value of U_2-U_1. The measurements of V_i and V_F may therefore be checked for linearity and for slope and the value of U_2-U_1 be determined by projecting the straight line to the V_i axis.

The quantity U_2-U_1 is of interest because it contains among other things the heat of dissociation of the normal molecule. If the values of the other things entering into U_2-U_1 are known the heat of dissociation may be calculated.

Apparatus

Some initial studies were made on nitrogen with the apparatus described in the earlier work.[2] These were reported at the Chicago meeting of the American Physical Society.[4] Later the apparatus was extensively remodeled and nitrogen restudied. The results here given were obtained with the new form of apparatus.

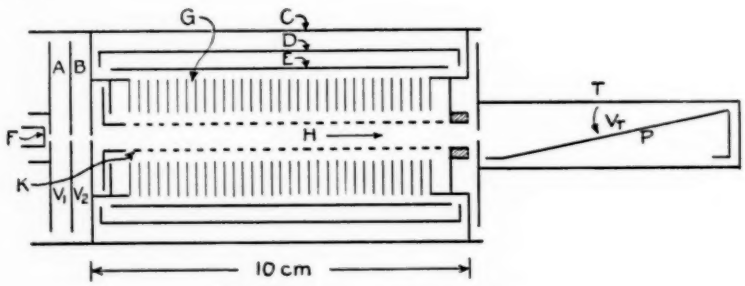

Fig. 1. Diagram of apparatus.

The new form of apparatus is shown in Fig. 1. The metal parts were of copper and were mainly cylindrical in form. The electrons from the filament F were accelerated through the first three holes, passed down the axis of the apparatus and finally entered the electron trap where they were directed by a potential V_T of 190 volts to the collecting plate P. A magnetic field H supplied by a solenoid external to the tube, constrained the electrons to move along the axis of the tube. Surrounding the electron beam was a cylindrical gauze K. Around this was the direction-defining system consisting of a number of thin, cylindrical disks G supported on three slotted bars (not shown). The electrometer collecting cylinder E of diameter 3.5 cm surrounded the disks, and around this were the electrometer guard cylinder D, from which E was supported, and finally the shield C.

The electrons, in traversing their path, ionize the gas and these ions pass through the gauze K. Of these a small portion—those having their direction of motion almost perpendicular to the electron beam—pass through the defining system G and travel toward the cylinder E. A radial electric field was applied between G and E for the purpose of measuring the kinetic energy of the ions. In the study of carbon monoxide, negative ions appeared in numbers great enough to interfere with the study of the energy of the positive ions.

[4] W. Wallace Lozier, Phys. Rev. **37**, 191 (1931) abstract.

Hence, the gauze K was added in order that an electric field might be applied (between G and K) to separate the negative from the positive ions.

The procedure for accelerating the electrons was that used by Smith[5] in a study of ultra-ionization potentials. The source of electrons was a strip of tungsten 1.5 cm long and 1 mm wide stretched across a hole a little less than 1 mm in diameter. In the region A a constant potential of 3.0 volts was applied to accelerate the electrons, while the variable accelerating potential was applied in the region B. With this arrangement the space charge around the filament and the magnitude of the electron current remain independent of the variable accelerating potential across B. The replacement of the slotted cylinder of the earlier apparatus[2] by the system of circular disks increased the intensities about five-fold without any loss in defining power. Finally, the new form of guard ring and the external shielding made the apparatus more free from external disturbances.

The nitrogen was generated by the action of bromine water on ammonia and the carbon monoxide by dropping formic acid into concentrated sulphuric acid. The respective gases were allowed to remain for several hours in contact with a liquid oxygen trap. The gas under study was admitted to the tube through a capillary leak, while the pumps ran continuously. The pressure in the experimental tube ranged from 10^{-5} to 10^{-4} mm Hg.

The ion currents were measured on a Compton electrometer of sensitivity 2300 mm per volt shunted by a high resistance and connected between D and E. Electron currents from 0.5 to 4.0 microamperes were used in the experiments. All the data on each figure have been reduced to the same pressure and electron current.

The initial-velocity correction for the electron current was determined in the studies of nitrogen by comparison with the first mercury ionization potential. In the study of carbon monoxide it was determined with respect to the ionization potential for the formation of CO^+ and hence depends on the correct value of this ionization potential. For reasons to be stated later this was taken to be 14.1 volts.

In the earlier paper[2] it was shown how the magnetic field caused the measured kinetic energy of the ions to be smaller than the true value. For ions as heavy as those of nitrogen and carbon monoxide, and with the smaller radius of the new apparatus, this effect is so small as to be comparable with the normal experimental uncertainties. For nitrogen the magnetic field used was 150 gauss, while that for carbon monoxide was 300 gauss.

Procedure

In the case of each gas, measurements were directed toward the determination of the following: (1) The distribution of kinetic energy among the ions produced by electrons having a specified velocity; (2) The minimum electron energies necessary to produce an ion of specified energy; (3) The relative efficiencies of production of ions having a specified energy as a function of the velocity of the incident electrons.

[5] P. T. Smith, Phys. Rev. **37**, 808 (1931).

Energy distribution function of the ions

The energy distribution function of the ions was measured by the method described in the work on hydrogen.[2] For a given electron velocity various retarding potentials were applied between G and E. The change produced in the positive ion current reaching E by varying the retarding potential by a small amount ΔV, was taken to be proportional to the slope of the ion-current vs. retarding-potential curve, i.e., to the ordinate of the energy distribution curve. The minimum electron energies necessary to produce ions of specified energies were measured, as before, by applying a definite retarding potential between G and E and varying the accelerating potential of the electrons.

Efficiencies of production of ions having specified energies

An energy distribution function gives the relative probabilities of the production of ions of different energies for a fixed electron velocity. However, if one fixes his attention on one specified energy of the distribution and plots the corresponding energy distribution ordinate as a function of the electron velocity, there is obtained a curve which shows the manner in which the probability of production of an ion of a specified velocity varies with electron velocities larger than the necessary minimum. As seen from the above discussion this variation of probability could be obtained directly from the energy distribution data for the ions. However, it was determined directly from experiment by measuring the energy distribution ordinate for one specified energy as a function of the incident electron velocity. It is well to point out that all measurements concerning the energy distributions refer to the number of ions contained in a small differential range of energies in the neighborhood of the specified energy.

NITROGEN

Results

In Fig. 2 are shown experimental readings from which the minimum electron energies necessary to produce N^+ ions of specified energy were found. These ions result from dissociation of N_2^+ into $N^+ + N$; the ions were identified as N^+ ions by Vaughan[6] who used the mass spectrograph designed by Bleakney.[7] These readings were taken on the electrometer by the rate-of-charge method. The results are plotted, energies of ions against the minimum electron energies, in Fig. 3 along with another set of determinations taken by the steady deflection method for measuring the positive ion current. In this work the initial velocity correction was determined by using the known ionization potential of mercury. The intercept of Fig. 3 which equals $U_2 - U_1$ has a mean value of 22.9 ± 0.5 volts.

If the curves of Fig. 2 are carried to higher potentials, sharp upward changes of slope occur which are taken to indicate the setting in of new modes of

[6] A. L. Vaughan, Phys. Rev. **38**, 1687 (1931).
[7] W. Bleakney, Phys. Rev. **35**, 139 (1930).

dissociation. Fig. 4 shows the relation between the energies of the ions from these dissociation processes and the minimum electron energy necessary to produce them. The results are not very satisfactory, for it is difficult to locate accurately the position of the breaks on the electron velocity scale. Also the

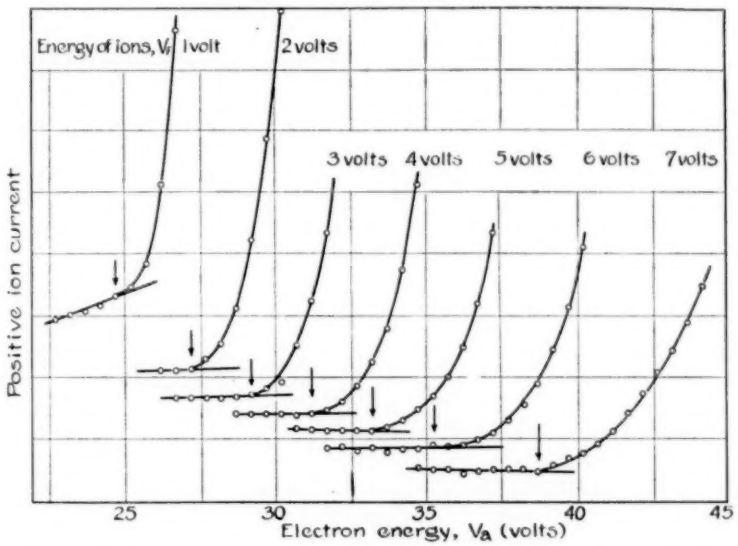

Fig. 2. Curves used to determine the minimum electron energies necessary to produce N^+ ions of different energies.

reproducibility of results was not very gratifying. But the fact that the points seem to group about two straight lines has an interesting interpretation, and furnishes corroboration for some independent work of Vaughan. The intercepts of these groups were taken as 33 ± 1 and 38 ± 2 volts.

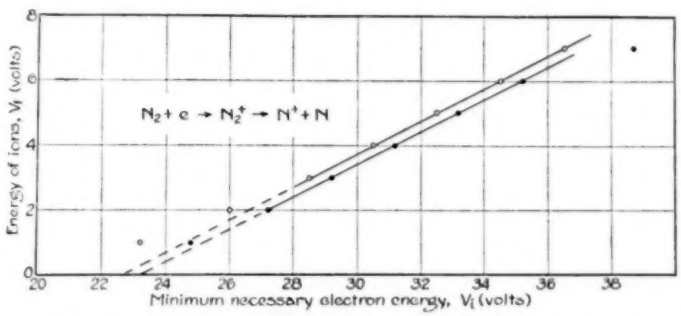

Fig. 3. Results of Fig. 2 (and another determination) plotted to show the energy of N^+ ions V_F as a function of the minimum electron energies V_i necessary to produce them; the slope of the lines has the theoretical value 1/2.

The energy distribution of the ions for various electron energies is shown in the curves of Fig. 5. The common distinctive characteristics of the curves taken at 75 and 85 volts are real and appeared on all curves taken at these potentials. Below 1 volt the N_2^+ ions having the low velocities of temperature agitation begin to mask the curves for the N^+ ions.

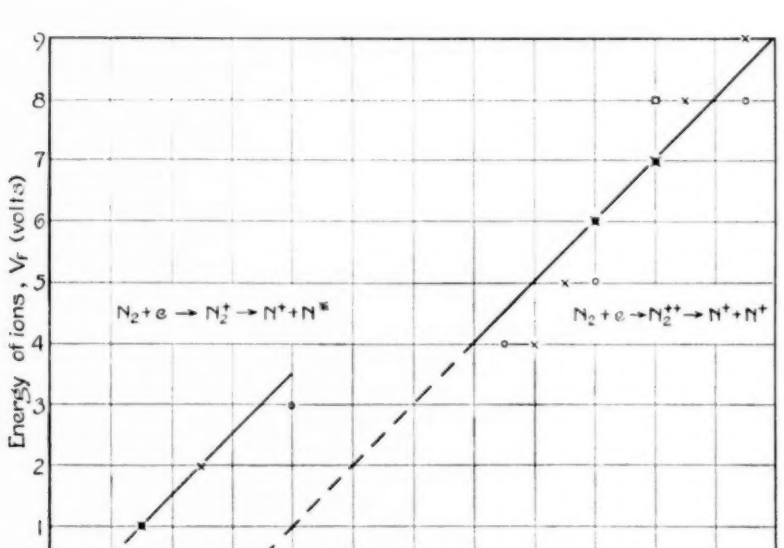
Energy of ions, V_F (volts)
Minimum necessary electron energy, V_i (volts)
$N_2+e \rightarrow N_2^+ \rightarrow N^+ + N^*$
$N_2+e \rightarrow N_2^{++} \rightarrow N^+ + N^+$

Fig. 4. Energies of N^+ ions plotted against some higher ionization potentials; the slopes are drawn with the theoretical value 1/2.

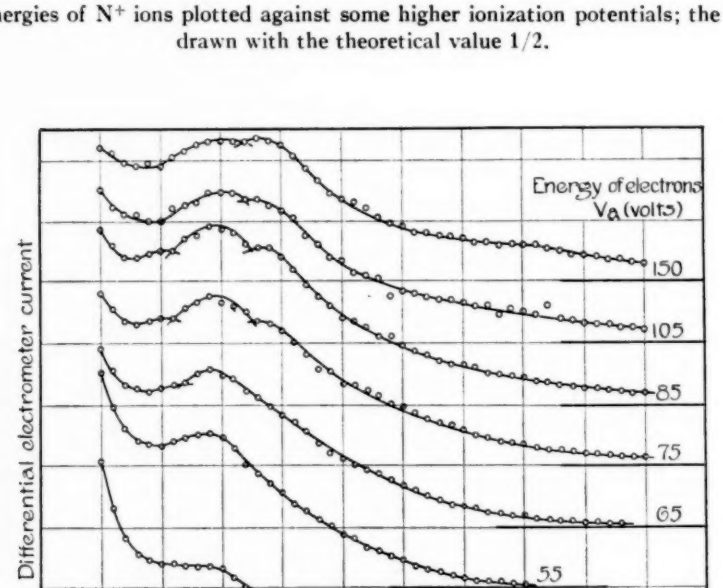

Fig. 5. Energy distribution curves of N^+ ions for various electron energies V_a. The differentiating potential was 0.24 volt.

In Fig. 6 are shown the efficiency curves for the production of ions of various specified energies. An ordinate on one of these curves is proportional to the number of ions lying in a small energy interval (0.24 volt) at the energy given for the curve and shows how this varies with electron voltage.

Some negative ions were present but they were so few in number that it was uncertain whether they were due to nitrogen or to impurities (such as H_2O).

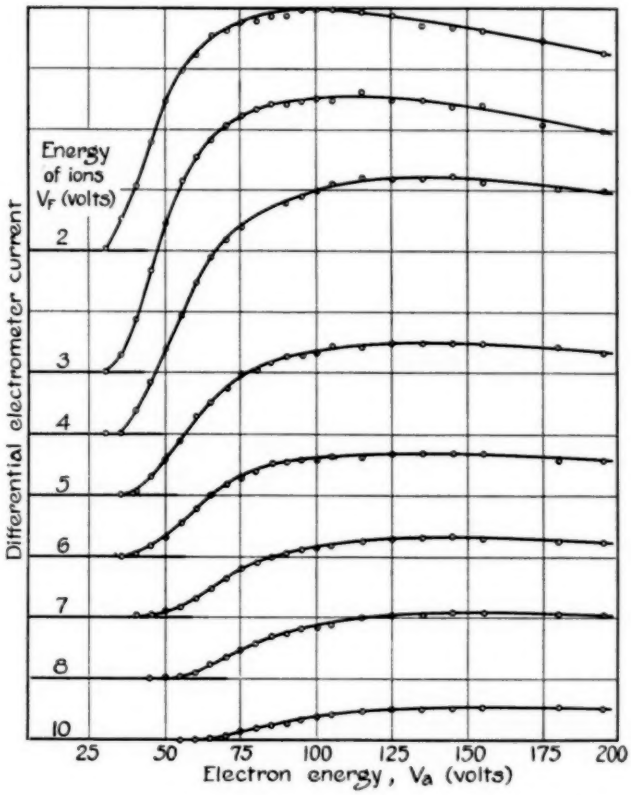

Fig. 6. Curves showing the variation with electron energy V_a of the probability of production of an N^+ ion of specified energy.

In the results reported at the Chicago meeting, the statement was made that above 60 volts electron velocity the N^+ ions exceeded in numbers the N_2^+ ions.[8] This statement has been found to be untrue. The magnetic field is theoretically capable of preventing the collection of ions of nitrogen possessing thermal velocities. But when the pressure was greater than 10^{-4} mm Hg it was found that N_2^+ ions were able to reach the collector even though the magnetic field was 300 gauss. However, with pressures below 10^{-5} mm Hg, the N_2^+ ions were not collected. It is not possible to measure

[8] Unfortunately this statement has been quoted by Kallman and Rosen, Phys. Zeits. **32**, 534 (1931).

relative numbers of the molecular and atomic ions with this apparatus. This has been done by Vaughan.[6]

Discussion of results

In Fig. 3 the two sets of data give an intercept differing by only 0.7 volts. The mean, 22.9 volts, has been given an experimental uncertainty of 0.5 volt. This, as has been pointed out, equals U_2-U_1, the increase in potential energy of the molecule, measured before impact and after dissociation. This process undoubtedly represents the dissociation of N_2^+ into N^++N. Hence U_2-U_1 can be evaluated in two ways. It equals, on the one hand, the heat of dissociation D_m of normal N_2 plus the ionization potential I_A of the nitrogen atom. On the other hand it is not greater than and probably is nearly equal to the sum of the ionization potential I_m for the formation of stable N_2^+ and the heat of dissociation D_I of N_2^+ into N^++N.

Thus $U_2-U_1=22.9\pm0.5$ volts $=D_m+I_A\leqq I_m+D_I$. From spectroscopy[9] I_A is known to be 14.5 volts; thus $D_m=8.4\pm0.5$ volts. Earlier values obtained from vibrational level extrapolations were as much as 3 volts higher, but these have been revised downward. The latest value given by Birge[10] is 9.1 volts.

Turner and Samson[11] have combined measurements on the excitation potential of the negative bands of N_2^+ with spectroscopic data to obtain a value for I_m+D_I of 22.9 volts, with which our value is in agreement. The analysis made by them is probably correct giving $I_m=15.8$ volts and $D_I=7.1$ volts.[12] Recent work of Vaughan[6] supports this value of 15.8 for I_m.

The range of energies in Fig. 3 for which the observations fall on a straight line appears to extend from about 2 to 7 volts. This probably is related to the shape of the potential energy curve in the Franck-Condon region—the region defined by the range of nuclear separations associated with the normal molecule in its lowest vibration state. This range for the nitrogen molecule covers about 0.1A, which is approximately one-fifth the extent of that for H_2. Invoking the Franck-Condon principle we would expect the potential energy curve to cross the boundaries of the Franck-Condon region approximately 16 and 4 volts above the asymptotic value of 22.9.[13] Considering the narrowness of the region and the range of energies, 16 to 4 volts, traversed by the curve therein, this probably implies, as pointed out by Smyth,[14] that the curve does not have a negative slope at all points; but rather, it may have a minimum at a nuclear separation much greater than that for the normal molecule. In Fig. 4 are observed two groups of ion-energies and

[9] H. N. Russell, Astrophys. J. **70,** 16 (1929).

[10] R. T. Birge, Faraday Society, Molecular Spectra and Molecular Structure, p. 713 (1929).

[11] L. A. Turner and E. W. Samson, Phys. Rev. **34,** 747 (1929).

[12] Later Birge mentioned some objections to the values of Turner and Samson. R. T. Birge, Phys. Rev. **34,** 1062 (1929).

[13] Vaughan (reference 6) finds that N^+ ions appear at 24.5 ± 9.1 volts. We were not able to determine accurately the potential at which N^+ ions first appeared.

[14] H. D. Smyth, Rev. Mod. Phys. **3,** 372 (1931).

minimum necessary electron energies. The lower group with an intercept value of $U_2 - U_1 = 33 \pm 1$ volts probably represents dissociation of N_2^+ into $N^+ + N^*$, where the energy of excitation of the N atom is 10 ± 1 volts. According to Compton and Boyce[15] there are two groups of metastable levels for the nitrogen atom at 2.37 and 3.56 volts. These lie so close to the energy of normal N that we would not be able to distinguish dissociation to these levels from that to $N^+ + N$ (22.9 volts). However at 10.3[15] volts a group of quartet *P* levels appears. This excitation energy agrees very closely with the postulated excitation energy of the process given above. The range of energies of the ions formed is very narrow 1 to 2 volts which would indicate that to bring the normal atom and the 10 volt excited atom to within about 1.0A of each other does not require an energy expenditure of more than about 4 volts. This would indicate that the potential energy curve is quite flat.

When the energy of the impacting electron is great enough to remove an electron from each nitrogen atom any dissociation into $N^+ + N^+$ should be detected because of the registration of both products of dissociation on the electrical apparatus. This is in all probability the process represented by the higher velocity group of Fig. 4. The value of $U_2 - U_1$ for this process should be $22.9 + 14.5 = 37.14$ volts which agrees with the experimental value of the intercept, 38 ± 2 volts. The range of energies of the ions extends from about 4 to 8 volts. As a first approximation the potential energy curve might be represented by the Coulomb repulsion curve e^2/r. If one draws this curve, he finds it crosses the Franck-Condon region 12 volts above the asymptotic energy. This would yield N^+ ions of 6 volts energy. It is interesting to note that this is approximately the center of the observed range.

Finally, Vaughan,[6] in his study of nitrogen, found two upward breaks in the efficiency curve for N^+ ions. These occurred at 40 ± 1 and 47 ± 1 volts electron energy. From our discussion above we would suspect the two potential energy curves last discussed to cross the Franck-Condon region 35 to 37 volts and 46 to 54 volts above the normal molecular state. The figures given by Vaughan are close to these two regions.

The energy distributions in Fig. 5 present nothing essentially new except the peculiar structure of the curves for electron velocities of 65 and 85 volts. Three distinct groups of ions appear to be present which probably result from the three processes of dissociation discussed above. The lower energy group at about 2 volts would be correlated with the dissociation products $N^+ + N^*$, the next group at 3 volts with $N^+ + N$, and the last at 4 volts with $N^+ + N^+$. The trailing out of the curves of Fig. 5 to higher energies is probably to be correlated with the multitude of dissociation products possible at higher electron velocities.

The efficiency curves of Fig. 6 bear a general resemblance to those for the probability of ionization of various atomic gases by electron impact, although our curves do not decrease so rapidly at higher voltages. As yet no satisfactory theoretical interpretation has been given to these curves.

[15] K. T. Compton and J. C. Boyce, Phys. Rev. **33**, 145 (1929).

Carbon Monoxide

Both positive and negative ions are formed by electron impact in carbon monoxide. In order to be able to study satisfactorily the processes of their formation the gauze K, Fig. 1, was introduced. By applying to K a suitable potential the passage of either positive or negative ions through the slit system could be prevented.

Positive ions of carbon monoxide. Results

In Fig. 7 are plotted experimental curves from which the minimum electron energies necessary to produce positive ions of specified energy were

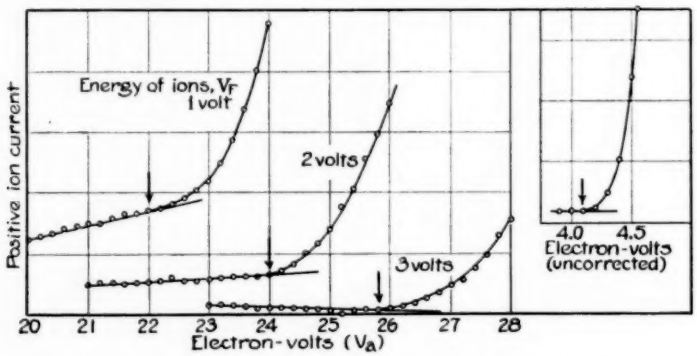

Fig. 7. Curves used to determine the minimum electron energies necessary to produce C^+ ions of different energies.

determined. These ions were identified by Vaughan[6] as C^+ and most likely result from dissociation of CO^+ into $C^+ + O$. In the inset are shown the readings used in determining the electron voltage correction where the ionization current is due to CO^+.

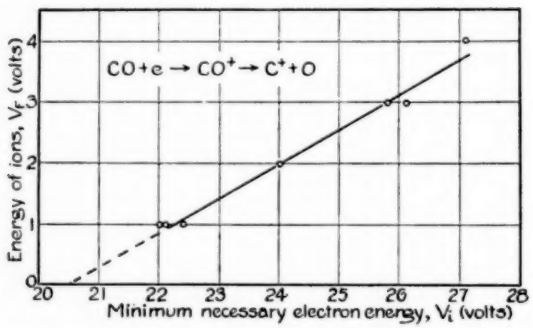

Fig. 8. Energies of C^+ ions plotted against the minimum electron energies necessary to produce them; the slope is drawn with the theoretical value 4/7.

Fig. 8 is a plot of the relation between the energy of the C^+ ions and the minimum energy of the electrons necessary to produce them. The solid line is drawn with the slope 4/7 which is the value appropriate to the C^+ ions from CO. The intercept on the axis of abscissas is taken as 20.5 ± 0.5 volts.

In Fig. 9 are shown the energy distribution curves for the positive ions. The differentiating potential is 0.30 volts. The curves showing the efficiencies of formation of ions of various specified energies as a function of electron velocities are shown in Fig. 10.

Discussion of results

As already noted the value of $U_2 - U_1$ taken from Fig. 8 is 20.5 volts. This value rests upon the assumption that the ionization potential of CO^+ is 14.1

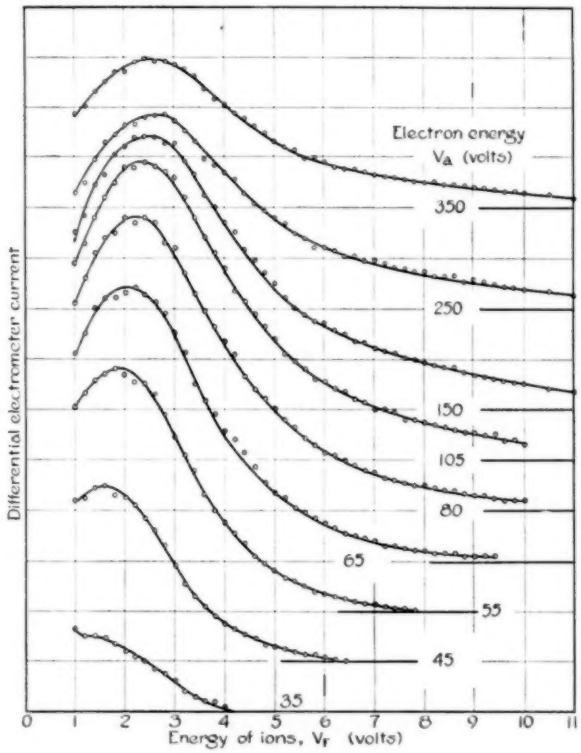

Fig. 9. Energy distribution curves of C^+ ions for various electron energies V_a; the differentiating potential was 0.30 volt.

volts. This is usually taken to be 14.2 volts but recent work of Vaughan[6] indicates that it should be lower than this, probably 13.9 ± 0.2 volts. The mean of these, 14.1 volts, certainly is not far wrong. Regardless, however, of the correct value for I_m (the ionization potential of the CO molecule) it is clear that in Fig. 8 we have measured correctly the difference between $U_2 - U_1$ and I_m and found it to be 6.4 volts. From the relation $U_2 - U_1 \leqq I_m + D_I$ it follows that the heat of dissociation of the CO^+ ion is not less than 6.4 volts. The value given by Birge and Sponer[9] is 9.8 volts which they obtained by a rather uncertain extrapolation of vibration levels. If we assume that $U_2 - U_1$ is 20.5 volts and that the ionization potential of the carbon atom is 11.2 volts we obtain from the relation $U_2 - U_1 = I_A + D_m$ a value of 9.3 ± 0.5 volts for the heat of dissociation of the CO molecule. This is again much

lower than the value 10.3 volts given by Birge.[16] If his calculation is revised by introducing a more recent value of the heat of dissociation of O_2, the heat of dissociation of CO comes out to be 8.9 volts, a value which is in fair agreement with our own.

The energy distribution curves of Fig. 9 are without any peculiar structure in agreement with the observation that no higher ionization potentials (as in Fig. 4 for N_2) were observed. The narrowness of the distribution is in agreement with the narrow range of the straight line of Fig. 8, namely ener-

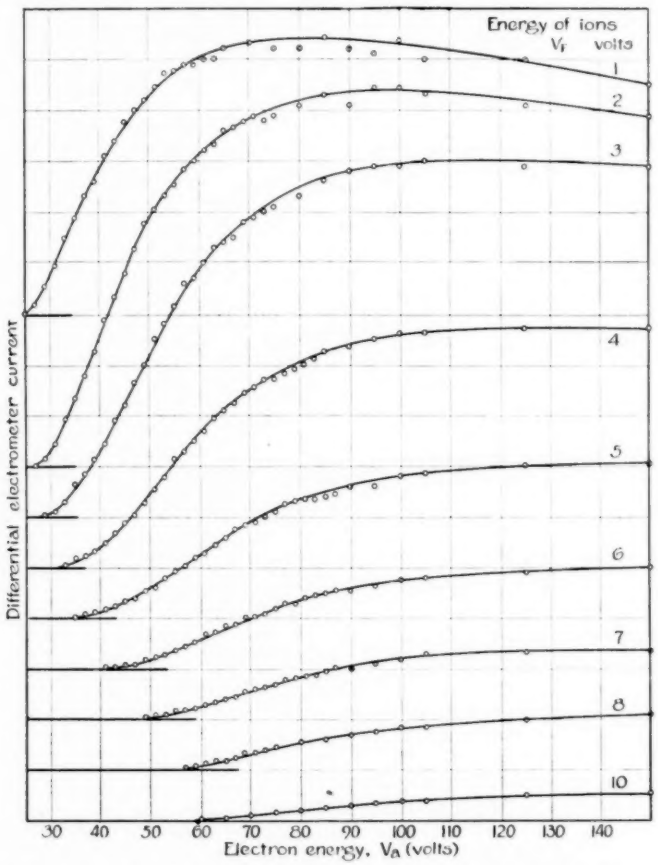

Fig. 10. Curves showing the variation with electron energy V_a, of the probability of production of a C^+ ion of a specified energy.

gies from 1 to 4 volts. This probably can be correlated with the narrow Franck-Condon region (less than 0.1A). Here again it is impossible to state whether the slope of the potential energy curve is everywhere negative or whether the curve has a minimum to the right of the Franck-Condon region. The efficiency curves of Fig. 10 are very similar to those of Fig. 6.

Negative ions in carbon monoxide. Results

When an electric field was placed between K and G (Fig. 1), sufficient to keep positive ions from being collected, a negative current was registered on

[16] R. T. Birge, Phys. Rev. **28**, 277 (1926).

the electrometer. This negative current as a function of the electron energy is shown in Fig. 11. The trailing off on the low velocity side is probably due to negative ions from water vapor.[17] An attempt was made to measure the kinetic energies of the two groups of ions. The electron velocity of maximum

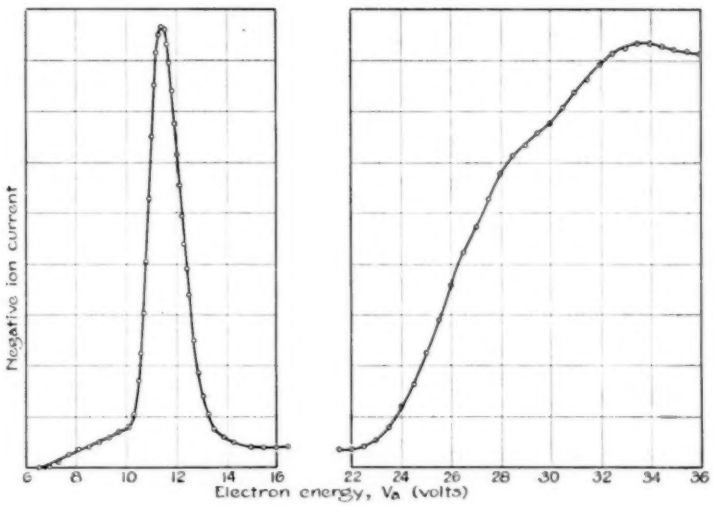

Fig. 11. Curves showing observed O^- current as a function of electron energy V_a.

efficiency in producing the low velocity group was 11.4 ± 0.3 volts. At this velocity the most probable energy possessed by the ions was about 0.4 volt and the maximum energy they had was about 0.9 volt. The negative ions of

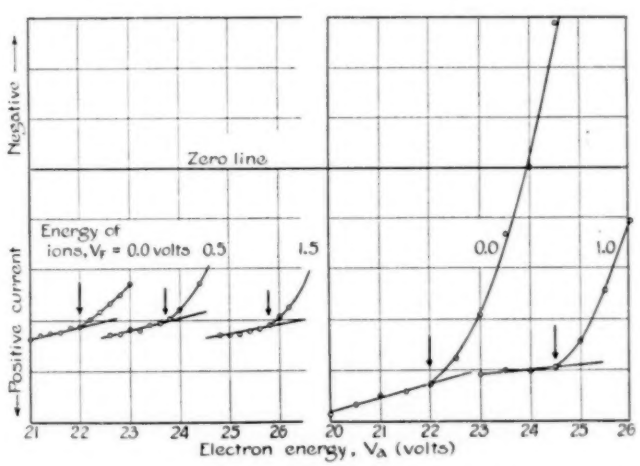

Fig. 12. Curves used in determining the minimum electron energies necessary to produce O^- ions of various energies. The current below the line is positive and is discussed in the text.

the second group, appearing at 22 volts electron energy were found to possess kinetic energy and we succeeded in getting values for the minimum electron velocities necessary to produce negative ions of specified energies. These readings are shown in Fig. 12. The currents were small and were measured

by the rate-of-deflection method. There is a background to the current which is due partly to the leak of the electrometer system and partly to another cause, mentioned later. The results of Fig. 12 are shown plotted in Fig. 13. The straight line has an intercept of 22.2 ± 0.5 volts.

Discussion of results

These negative ions were also observed by Vaughan[6] and definitely identified as O^-. The narrow group of Fig. 11 can very likely be considered as similar to those H^- ions found by one of us in some earlier work[17] and later observed by Smyth and Mueller.[18] The process of formation is probably represented by $CO+e \rightarrow CO^- \rightarrow C+O^-$. If this be correct, at the voltage of maximum efficiency (11.4 ± 0.3) the O^- ion has a maximum energy of 0.9 volt and thus the C atom and the O^- ion would possess a total kinetic enrgy of $7/3 \times 0.9 = 2.1$ volts. This would mean that the energy of the dissociated system $C+O^-$ lies 9.3 ± 0.3 volts above normal CO and 0.5 volt below $C+O$

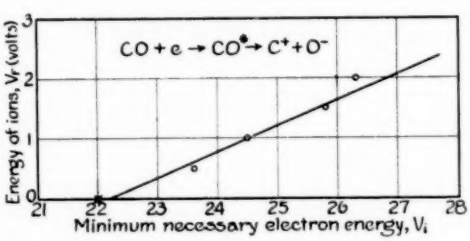

Fig. 13. Energies of O^- ions plotted against the minimum electron energy necessary to produce them; the slope has been given the theoretical value 3/7.

(9.8 volts). This allows only 0.5 volt for the electron affinity of O if the C atom and the O^- ion are unexcited. Trustworthy values are not known for the affinity of O for an electron. Senftleben[19] gives a value of 8.9 volts and Grimm[20] gives 6 volts. When one considers the processes involved in getting these values, their reliability becomes very questionable. If one takes tne iso-electronic sequence of F I and Ne II and plots the square root of the ionization potential against the atomic numbr and extrapolates this to atomic number 8, he obtains an oxygen electron affinity of 3.2 volts. The reliability of this, too, is questionable.[21] It is entirely possible, of course, that one or both of the products of dissociation are excited. In that case the electron affinity would be 0.5 volt plus whatever the excitation energy turned out to be. The C atom has a ^1D level 1.3 volts above the ground state and another, the ^1S, lying 2.7 volts above normal C.[22]

[17] W. Wallace Lozier, Phys. Rev. **36,** 1417 (1930).

[18] D. W. Mueller and H. D. Smyth, Paper 11, Program of Schenectady Meeting of American Physical Society, September 11, 1931.

[19] H. G. Grimm, Zeits. f. Elektrochem. **31,** 474 (1925).

[20] H. Senftleben, Zeits. f. Physik **37,** 539 (1926).

[21] This method gives chlorine an electron affinity of 5.4 volts to compare with 5.0 and 4.8 volts quoted by Foote and Mohler, Origin of Spectra, p. 179.,

[22] Paschen u. Krueger, Ann. d. Physik **7,** 1 (1930).

The narrow range of electron velocities involved in this group certainly leads one to suspect a capture of an electron by the neutral molecule. For if the impacting electron strikes the molecule, and loses all its energy, it is at rest with respect to the molecule and conditions are favorable for the capture of the impacting electron. Another fact which points to the correctness of this explanation is the observation that no positive ions were formed below 14.0 volts. Therefore, the charge on the O^- ions necessarily comes from some source external to the original molecule.

The O^- ions appearing at 22 volts possess considerably more kinetic energy than the group just discussed. The dissociation products are probably C^+ and O^-. The peculiar shape of the efficiency curve in the neighborhood of 30 volts is real—this has been checked by Vaughan and probably is indicative of another process, perhaps dissociation products of different degrees of excitation. The straight line in Fig. 13 has been drawn with the proper slope for O^- ions (3/7) and fits the experimental points fairly well. If the dissociation products are unexcited C^+ and O^-, we would expect a value of $U_2 - U_1$ less than that for $C^+ + O$ by the electron affinity of oxygen. It comes out 1.7 volts higher, a fact which indicates that the products of the dissociation must be excited. If we take the value of 3.2 volts for the electron affinity of O we would have excitation energy of amount 4.8 volts. The ground state of C^+ consists of a close doublet. The next known level of C^+ according to Grotrian[23] lies 9.2 volts above this. Thus, we have no knowledge of how to account for the energy of excitation of the products.

It is well to point out, that all current below the zero line in Fig. 12 is a positive current. One can see from the arrangement of the electric fields that these positive ions must have been formed in the region exterior to the defining system *G*. This effect has earlier been observed by Liska at the University of Minnesota and is under investigation now.

In conclusion we acknowledge our gratitude to Professor R. S. Mulliken, Professor A. G. Shenstone, Dr. P. T. Smith and Dr. J. E. Boyce for their helpful discussions and kindness in locating for us spectroscopic data. Also we are indebted to the Graduate School of the University of Minnesota for financial assistance during a part of this work.

[23] W. Grotrian, Handbuch d. Astrophysik, Band III, Zweite halfte, p. 574.

THE EFFICIENCIES OF IONIZATION AND IONIZATION POTENTIALS OF VARIOUS GASES UNDER ELECTRON IMPACT

By John T. Tate and P. T. Smith
Department of Physics, University of Minnesota

(Received December 1, 1931)

Abstract

The efficiencies of ionization of N_2, CO, O_2, NO, H_2 and C_2H_2 by electron impact have been measured. The curves are similar to those of He, Ne, A and Hg vapor. The ionization potentials of the molecules were found to be: N_2, 15.7; CO, 14.1; O_2, 12.5 and 16.1; NO, 9.5; H_2, 15.6; and C_2H_2, 11.6. The probable error in each case is about a tenth of a volt. Negative ions were formed by electron impact in NO, CO, O_2 and C_2H_2. None were observed in H_2 or N_2.

AN ELECTRON having sufficient energy may, at impact with an atom or molecule, cause one or more electrons to be ejected. This ionization process is of prime importance in the study of all electrical discharges in gases. The present paper is a continuation of a systematic study begun some time ago in this laboratory of the probabilities of ionization, by electron impact, of various atoms and molecules.

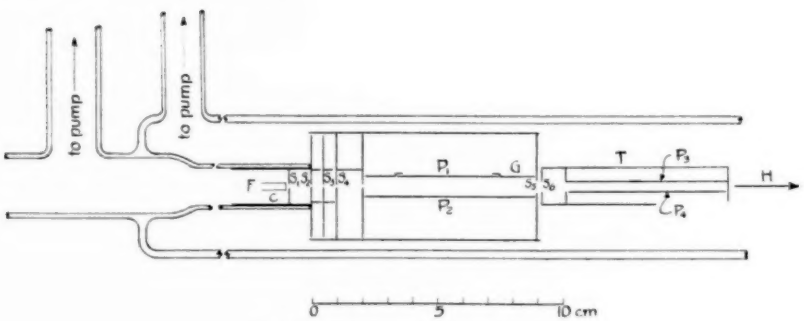

Fig. 1. Diagram of apparatus.

The results for helium, neon, argon and mercury vapor have already been reported.[1] In the present paper the results for nitrogen, carbon monoxide, oxygen, nitric oxide, hydrogen and acetylene are presented. The method used is essentially the same as that previously described although the apparatus was so modified as to permit the measurements to be extended to gases which are dissociated by the hot filament.

The essential features of the modified apparatus are shown in Fig. 1. The tube is divided into two compartments each of which is connected to a separate pump. The tantalum cylinder C is sealed into a Pyrex tube. A number of holes were drilled through the disk immediately in front of the filament F so

[1] P. T. Smith, Phys. Rev. **36**, 1293 (1930); Phys. Rev. **37**, 808 (1931).

that the region between the diaphragms S_1 and S_2 could be pumped out quickly. S_2 is about 0.035 cm in diameter and is the only opening connecting the two compartments. With this arrangement the products of the dissociation of the gas by the filament are pumped away and do not diffuse back into the main part of the tube.

Constant differences of potential are maintained between the filament and S_1 and between S_2 and S_3 while a variable accelerating potential V is applied between S_3 and S_4. With this arrangement of fields the electron current to the trap T is quite independent of V. One can conclude from this fact that any voltage correction due to space charge is not a function of V.

The electron current is confined to a fine beam by means of the magnetic field H from a solenoid surrounding the tube. With liquid oxygen on the mercury traps and with no gas in the tube a galvanometer capable of detecting a current of 10^{-11} amperes remained at zero when connected to all of the apparatus excepting the cylinder C and the electron trap T, while a current of 10^{-6} amperes was passing down the tube. With a gas in the tube at the pressures used in this work an electron current less than 0.5 percent of the total electron current was recorded by the galvanometer.

A sufficiently high field is maintained between the two parallel plates P_1 and P_2 in the ionization chamber to draw out all of the ions formed. The ions from a 4 cm length of path are measured by a galvanometer or electrometer connected with P_1. The plates P_2 and G are connected together by means of a high resistance the midpoint of which is connected to the slit S_5, so that the speed of the electrons is not appreciably altered by the transverse electric field after they enter the ionization chamber.

Procedure

The gas under consideration was allowed to leak into the tube through a small capillary and was pumped out at the other end. By using the apparatus as a pressure gauge, a constant check was kept on the pressure during a run to be sure that it was constant. Curves were obtained in this manner which showed the relative values of the efficiency of ionization as a function of the speed of the electrons. To obtain the absolute values of the ordinates the accelerating potential was set at the maximum of the curve and the flow of the gas was slowed down sufficiently so that a suitable pressure could be maintained with the pumps cut off the main compartment of the tube, the gas being pumped through the slit S_2. The pressure in the tube was then measured with a McLeod gauge. The ionization of argon and neon measured by this method differed by less than a percent from that previously determined by a static method.

The gases were prepared from chemically pure reagents and the necessary precautions observed to insure their purity. Nitrogen was obtained from the interaction of bromine, water and ammonium hydroxide, carbon monoxide from formic and sulphuric acids, oxygen from manganese dioxide, and nitric oxide from ferrous sulfate and nitric acid. The hydrogen was introduced into the tube through a heated paladium tube in an atmosphere of commercial

hydrogen. The acetylene was obtained from the Chemistry Department through the courtesy of Mr. J. L. Wilson who also purified it by repeated distillation.

Results

The results are shown in Fig. 2. The ordinate ϵ represents the number of positive charges per electron per cm path per mm pressure at 0°C. The data are also shown in tabular form in Table I. All of these gases show the same form of curve as do He, Ne, A, and Hg vapor.[1] It is of interest to note that N_2

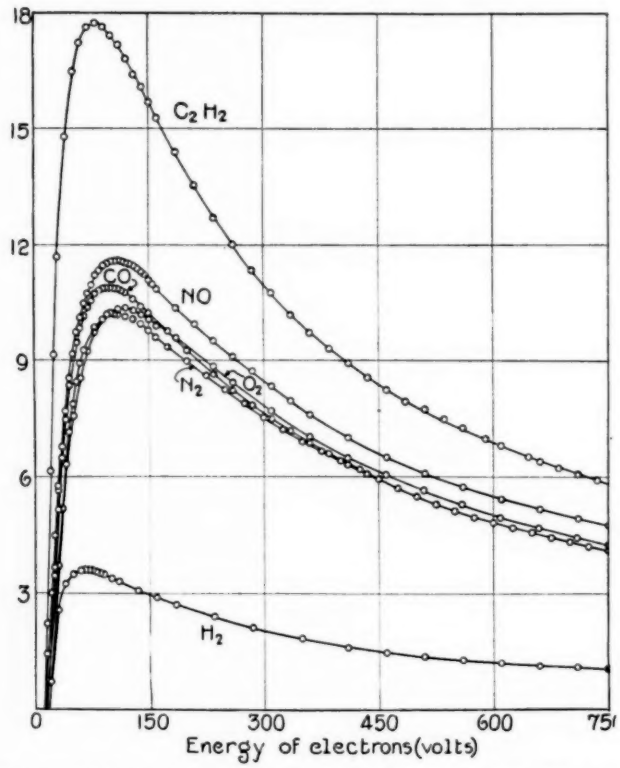

Fig. 2. The efficiency of ionization of N_2, CO, O_2, NO, H_2 and C_2H_2. The ordinate represents the number of positive charges per electron per cm path at 1 mm pressure and 0°C.

and CO share the same values for ϵ beyond about 400 volts. Bleakney[2] determined the efficiency of ionization of H_2 in arbitrary units. If the maxima of the curve shown here and his curve are made to fit, the rest of the ordinates agree almost exactly.

The ionization potentials of the gases were determined by introducing a second gas, whose ionization potential is known, into the tube for calibrating the voltage scale. A typical set of curves are shown in Fig. 3. Only the essential parts of the curves are shown. The voltages on the arrows indicate the differences between the ionization potentials of the two gases in the tube at

[2] W. Bleakney, Phys. Rev. **35**, 1180 (1930).

TABLE I. *ϵ represents the number of positive charges per electron per cm path per mm pressure at 0°C. V_a is the velocity of the impacting electron in volts and has been corrected for contact potentials and space charge.*

CO		NO		O_2		N_2		H_2		C_2H_2	
V_a	ϵ	V_a	ϵ	V_a	ϵ	V_a	ϵ	V_a	ϵ	V_a	ϵ
16	0.40	9.9	0.098	13	0.049	20	0.71	16.3	0.02	12.6	0.421
20	1.47	10.9	0.253	18	0.907	25	2.18	21.3	1.082	14.6	2.20
25	3.47	14.9	1.645	28	3.64	30	3.71	31.3	2.565	19.6	6.15
30	5.18	19.9	2.99	38	6.31	40	6.27	41.3	3.220	24.6	9.18
40	7.50	24.9	4.47	48	7.57	50	7.88	51.3	3.490	29.6	11.73
50	9.02	35	6.78	58	8.56	60	8.95	61.3	3.575	35	14.00
60	9.87	45	8.53	68	9.27	70	9.48	66.3	3.605	45	15.75
70	10.42	55	9.74	78	9.74	80	9.93	71.3	3.600	55	16.90
80	10.75	65	10.47	88	10.07	90	10.15	76.3	3.580	65	17.50
90	10.88	75	10.97	98	10.28	95	10.20	81.3	3.550	75	17.72
100	10.90	85	11.35	105	10.31	100	10.25	86.3	3.520	80	17.75
105	10.90	95	11.56	115	10.34	105	10.23	91.3	3.480	85	17.73
110	10.88	105	11.61	120	10.36	110	10.21	101.3	3.390	95	17.55
120	10.75	115	11.58	135	10.26	120	10.15	125	3.14	105	17.33
130	10.60	125	11.52	145	10.14	130	10.09	150	2.94	115	17.02
140	10.42	135	11.43	155	10.02	140	9.97	200	2.58	125	16.63
150	10.25	145	11.27	185	9.60	150	9.81	225	2.43	150	15.70
175	9.79	155	11.07	200	9.40	175	9.38	250	2.28	175	14.75
200	9.28	185	10.34	225	9.00	200	9.00	300	2.03	300	13.88
225	8.92	200	10.13	250	8.60	225	8.63	350	1.86	225	13.04
250	8.40	250	9.27	300	7.82	250	8.26	400	1.65	250	12.26
300	7.65	300	8.50	350	7.14	300	7.55	450	1.50	300	10.95
350	7.01	350	7.76	400	6.58	350	6.93	500	1.40	350	9.90
400	6.43	400	7.13	450	6.12	400	6.43	550	1.30	400	9.08
450	5.96	450	6.60	500	5.73	450	5.95	600	1.21	450	8.38
500	5.52	500	6.14	550	5.37	500	5.53	650	1.12	500	7.85
550	5.16	550	5.80	600	5.03	550	5.15	700	1.09	550	7.36
600	4.84	600	5.50	650	4.73	600	4.84	750	1.04	600	6.90
650	4.57	650	5.23	700	4.46	650	4.57			650	6.47
700	4.34	700	5.00	750	4.27	700	4.35			700	6.12
750	4.16	750	4.78			750	4.15			750	5.84

one time. The arrows also indicate how the curves were interpreted. Consistent values were obtained with other combinations of gases than those shown in Fig. 3.

Nitrogen

Both N_2+Ne and N_2+Hg show the ionization potential of N_2 to be 15.7 volts. This is somewhat lower than the generally accepted value of 16.9 volts, but it agrees with that given by Vaughan,[3] Samson and Turner,[4] Boucher,[5] and Found,[6] namely, 15.8. The data obtained by the writers indicate that 15.8 is an upper limit and that it is quite probable that the true value may be even lower than 15.7. Work is now in progress in this laboratory which will make it possible to compare the ionization potentials of argon and nitrogen.

Carbon monoxide

Combination of CO+Hg, CO+A, and CO+Ne lead to 14.1 ± 0.1 volt as the ionization potential of CO. Vaughan[3] gave 13.9 but a further consideration of his data gives 14.0, 14.1 agrees with Mackay's[7] value, while Hogness and Harkness[8] give 13.9, Foote and Mohler[9] 14.3, and Found 15.1. Birge[10] has calculated it to be 14.2 volts.

[3] A. Vaughan, Phys. Rev. **38,** 1687 (1931).
[4] L. A. Turner and E. W. Samson, Phys. Rev. **34,** 747 (1929).
[5] P. E. Boucher, Phys. Rev. **19,** 189 (1922).
[6] C. G. Found, Phys. Rev. **16,** 41 (1920).
[7] C. A. Mackay, Phys. Rev. **24,** 319 (1924).
[8] T. R. Hogness and R. W. Harkness, Phys. Rev. **32,** 936 (1928).
[9] Foote and Mohler, Phys. Rev. **17,** 394 (1921).
[10] R. T. Birge, Nature 117, 229 (1926).

Oxygen

Ionization potentials were observed at 12.5 and 16.1 volts in O_2. These agree with the values given by Mackay.[7] Smyth[11] and Foote and Mohler[12] give 15.5, while Boucher[13] gives 14.0. In the present study the work was repeated with oxygen prepared from manganese dioxide as well as from the electrolysis of dilute sulphuric acid.

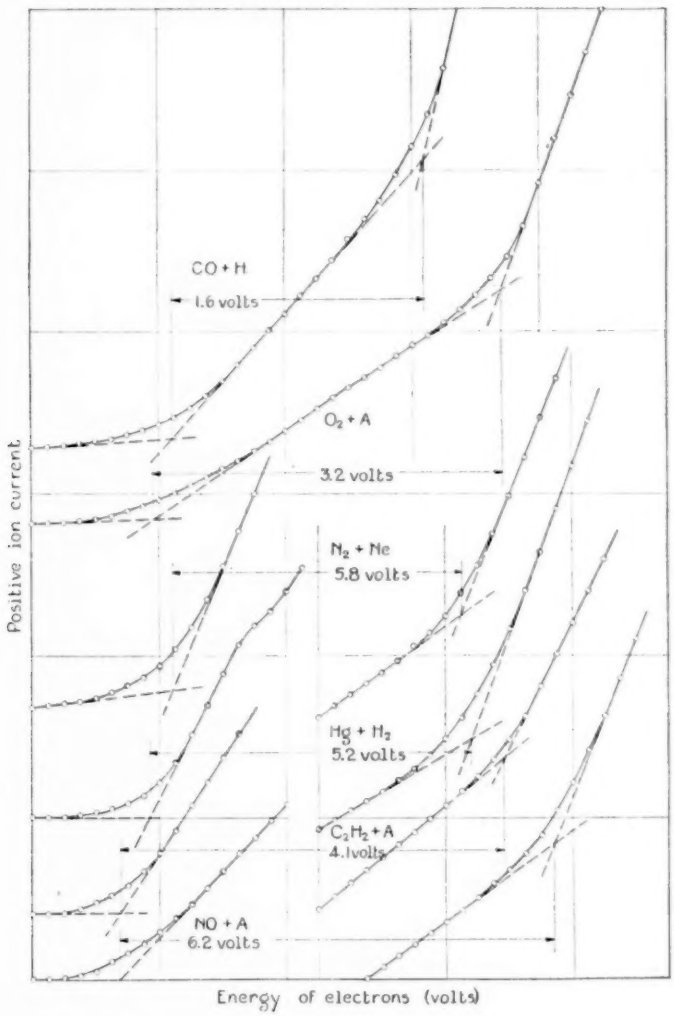

Fig. 3. Curves obtained with various mixtures of gases to ascertain the ionization potentials.

Hydrogen

H_2+Hg gave 15.6 as the ionization potential of H_2. H_2+A curves could

[11] H. D. Smyth, Proc. Roy. Soc. **A105**, 116 (1923).
[12] P. D. Foote and F. L. Mohler, Bur. Stan. Jour. Res. paper No. 400 (1920).
[13] P. E. Boucher, Phys. Rev. **19**, 189 (1922).

not be resolved. Bleakney[2] gave 15.4 whereas the previously accepted value was 15.9.

Nitric oxide

9.5 ± 0.1 is to be compared with Mackay's value of 9.4 and Hughes' and Dixon's value of 9.3.

Acetylene

Morris[14] gave 12.3 whereas the value given here is 11.6 ± 0.10 volts. C_2H_2 + Hg curves were difficult to interpret because of the point of inflexion in the Hg curve at about 11.8 volts, (see Fig. 3), but they do show that the ionization potential of acetylene is less than 12 volts.

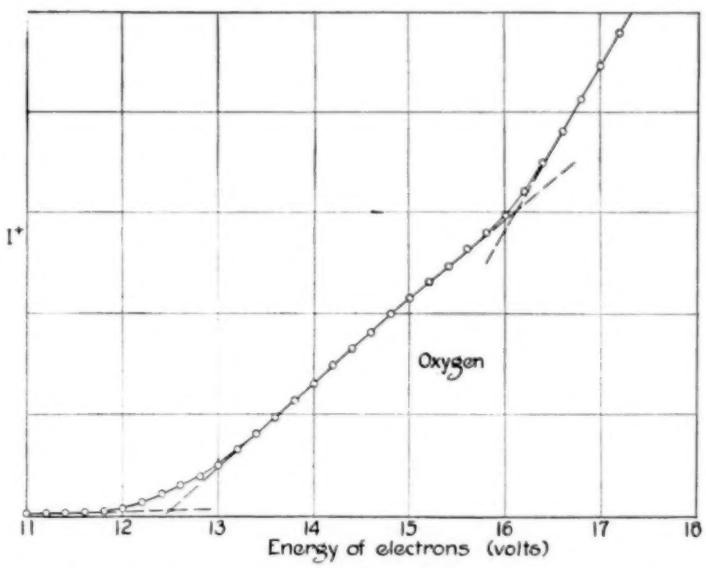

Fig. 4. Showing the second ionization potential in O_2 at 16.1 volts.

Negative ions

While working with an apparatus which contained water vapor, Lozier[15] observed two groups of negative ions which were formed only in a small range of electron velocities. Bleakney and later Mueller and Smyth[16] found them to be H^- ions. A similar group of ions was also found by Lozier[15] in CO, which Vaughan[3] showed to be O^- ions.

The writers have found that the same process exists in NO, O_2, and C_2H_2. The data are shown in Fig. 5. The ordinates are given in aribtrary units since a quantitative measure of the number of these ions found per electron was not made. In all of the gases studied the maxima of the curves represent currents

[14] J. C. Morris, Jr., Phys. Rev. **32,** 456 (1928).
[15] W. W. Lozier, Phys. Rev. **36,** 1417 (1930).
[16] H. D. Smyth, Rev. Mod. Phys. **3,** 385 (1931).

which are only a fraction of a percent of the positive ion currents at their maxima.

That these ions are atomic was indicated by the fact that they possess as much as two volts of kinetic energy which results from the dissociation of the molecule. By analogy with CO one is lead to believe that the ions in NO are O^-.

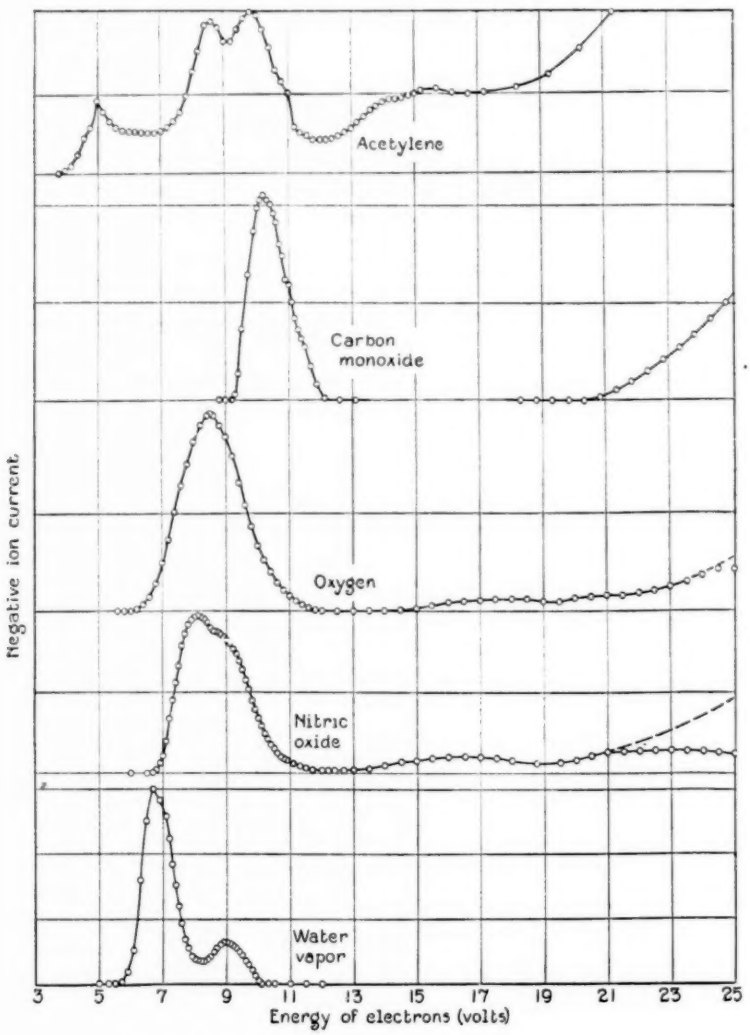

Fig. 5. Negative ions in H_2O, NO, O_2, CO and C_2H_2.

Beyond 21 volts none of the curves has the proper form since above 30 volts the electrometer in all cases showed a positive current due to the formation of positive ions having sufficient kinetic energy to be able to go through a retarding potential of several volts. A notion of the true curves is given by the broken lines.

Nothing can be said at present about the nature of the negative ions in acetylene except that they are not $C_2H_2^-$ since they possess some kinetic energy. A more detailed discussion of these ions will be given in the near future after work which is now in progress has been completed.

No negative ions could be detected in H_2[15].

The writers take this opportunity to thank the graduate school for a grant which made the continuation of this study possible.

THE ZEEMAN EFFECT AND Λ-TYPE AND SPIN DOUBLING IN THE CaH BANDS

By William W. Watson
Sloane Physics Laboratory, Yale University

(Received November 30, 1931)

Abstract

A more detailed discussion of the Zeeman effect in the 6389A $^2\Sigma$, $^2\Sigma$ band of CaH than that given previously with W. Bender is presented. General agreement with the assumption that the magnetic energy in a $^2\Sigma$ state is largely due to the interaction of the electron spin and the external field is obtained for band lines of low K value, but marked differences and asymmetries in the patterns occur for lines from the higher rotational levels. The neglected coupling between the component ρ of L along the rotational axis of the molecule and the field will account completely for these deviations, and these observations together with those on the Zeeman effect of the lines of these higher rotational levels in the $^2\Pi$, $^2\Sigma$ band of CaH are shown to be in accord with the explanation by Van Vleck and Mulliken and Christy of the large Λ-type and spin doubling in these states.

Introduction

In A recent paper the writer and W. Bender[1] reported some of the more interesting details of the Zeeman effect in the $^2\Pi$, $^2\Sigma$ band at 7000A and the $^2\Sigma$, $^2\Sigma$ band at 6389A in the spectrum of CaH. It was shown that in the case of the $^2\Pi$, $^2\Sigma$ band the observed Zeeman patterns for lines representing low rotational levels were in substantial agreement with the predictions of Hill's theoretical formulas for the Zeeman effect in $^2\Pi$ states.[2] Marked departures from the predicted patterns for the lines of high K values were noted, however, and a brief description was given of certain peculiar features of the patterns for the lines of the $^2\Sigma$, $^2\Sigma$ band. In explanation, attention was called to the fact that the very large spin and Λ-type doubling exhibited by the CaH states involved in the production of these bands indicated a relatively large component of the electronic orbital angular momentum perpendicular to the internuclear axis, the coupling of which with the external field could well account for the observed Zeeman patterns. The objects of the present paper are to present a more thorough investigation of the details of the Zeeman effect in the $^2\Sigma$, $^2\Sigma$ band in comparison with theoretical expectations, and to discuss these findings and the corresponding effect in the Π^2, $^2\Sigma$ band in relation to new conclusions of Mulliken and Christy[3] concerning the origin of the spin and Λ-type doublings in these bands.

A theoretical treatment by Hill of the action of an external magnetic field on $^2\Sigma$ states has been given by Almy.[4] This treatment considers the mag-

[1] W. W. Watson and W. Bender, Phys. Rev. **35**, 1513 (1930).
[2] E. L. Hill, Phys. Rev. **34**, 1507 (1929).
[3] R. S. Mulliken and A. Christy, Phys. Rev. **38**, 87 (1931).
[4] G. M. Almy, Phys. Rev. **35**, 1495 (1930).

netic energy to be largely due to the interaction between the spin and the field, so that if the spin doubling at the origin of the band is small, the spin is oriented either parallel or anti-parallel to the field. The coupling of the spin with the external field in the molecule is still present, however, and so each member of this twice normal doublet is split into $2J+1$ magnetic sublevels. With increase of the rotational quantum number K, the spin doubling may become much larger than $\Delta 2\nu_n$ in which case the relative orientation of S and K remains and these magnetic levels should be spaced in the interval from about $+\Delta\nu_n$ to $-\Delta\nu_n$ about the no-field position. Assuming that the perturbation energy is entirely due to the interaction of spin and field, Hill gets the following solution for the energy determinant:

$$W = \pm \tfrac{1}{2}\left\{\nu_0^2 + 4M\nu_0\Delta\nu_n/(K+\tfrac{1}{2}) + 4\Delta\nu_n^2\right\}^{1/2} \quad (1)$$

where ν_0 is the spin doublet width for the K level under consideration, the $+$ sign is for the T_1 levels ($J=K+\frac{1}{2}$), the $-$ sign for the T_2 levels ($J=K-\frac{1}{2}$), and W is measured from the center of the no-field doublet. For the two outermost sublevels $M=\pm(K+\frac{1}{2})$ of the $J=K+\frac{1}{2}$ states, the energies are given by

$$W = \nu_0/2 \pm \Delta\nu_n. \quad (2)$$

It should be emphasized that in this theory the interaction energy of S and H is just added to the experimentally known ν_0, no consideration being given to the origin of the spin doubling[5] and to the possibility of there being a sizable interaction between the component ρ of L perpendicular to the internuclear axis in the molecule and the external field. We return to this point below. In combination with Hill's formulas for the Zeeman effect in $^2\Pi$ states, however, this treatment of the effect in $^2\Sigma$ states has already been shown to supply a good agreement up to moderately large K values with the observed patterns in $^2\Pi$, $^2\Sigma$ bands of OH[4] and ZnH and CdH.[6]

The nature of the spin and Λ-type doubling in these electronic states has been made more evident by the recent work of Mulliken and Christy,[3] who use these CaH bands as one example showing the excellent agreement with Van Vleck's theoretical equations. These equations for the energy all involve terms responsible for the doubling which contain factors of the form $|BL_y(\Pi,\Sigma^+)|^2/\nu(\Pi,\Sigma)$, where the L_y is one of the components L_x and L_y of the electronic orbital angular momentum vector L perpendicular to the electric axis, and the $\nu(\Pi,\Sigma)$ is the frequency of any $\Pi\rightarrow\Sigma$ transition from the Π state in question to any Σ state and v value. From the numerical values and signs of the p_0 and q_0 for the doubling in this $^2\Pi$ state of CaH, and the equality of this p_0 with the γ_0 of the spin doubling of the upper $^2\Sigma$ state,[7] it is to be concluded that these two states stand in a relation of "pure precession" with each other. That is, these two states of the CaH molecule share the same l, and differ only in that $\Lambda=1$ for the $^2\Pi$ state and $\Lambda=0$ for the $^2\Sigma$. The calculated p_0, q_0 and γ_0, assuming pure precession, agree well with the observed constants al-

[5] J. H. Van Vleck, Phys. Rev. **33,** 467 (1929).
[6] W. W. Watson, Phys. Rev. **36,** 1134 (1930).
[7] Cf. details given in reference 3.

though the $|\nu(\Pi, \Sigma)|$ is only 1320 cm^{-1}. And since from the value of the coupling constant A, as well as from other evidence, the $^2\Pi$ state is no doubt $\cdots 4p\pi$, this upper $^2\Sigma$ must be $\cdots 4p\sigma$ and not $3d\sigma$ as earlier assumed by Mulliken.

The spin doubling $\Delta\nu_{12}(K)$ in the upper $^2\Sigma$ state becomes exceptionally large, as compared to that in most known $^2\Sigma$ states,[8] it being -22 cm^{-1} at $K=33$. For the same K in the $^2\Pi_d$ state, the spin doubling equals $+20$ cm^{-1}. Now as Mulliken and Christy point out,[9] these $\Delta\nu_{12}$ quantities may be expected to be equal to $A\rho$, where A is the same coupling constant as holds for the interaction of S and Λ in the $^2\Pi$ state. This $A=80$, and so it is to be concluded that the ρ, which is the component of l along the direction of K, is about 0.25. This represents a large uncoupling, and yet the Van Vleck formulas agree remarkably well with the data. These $^2\Sigma$, $^2\Sigma$ bands represent, then, a good opportunity for the study of the Zeeman effect for such transitions. The formulas of Hill given above serve as a guide in the measurement and interpretation of the observed patterns, and it is evident that any marked departures from the predicted patterns are to be attributed to the neglected possibility of coupling between the ρ and the field.

Experimental Procedure and Calculations

The spectrograms showing the Zeeman effect in the 6389A $^2\Sigma$, $^2\Sigma$, (0, 0) band of CaH measured in this investigation were mostly those produced with W. Bender,[1] but some more plates were also taken at several field strengths to verify the conclusions. The technique of the production of the spectrograms was the same as previously described. For the sake of brevity only measurements at two strengths of field before considered—14,000 and 24,600 gauss—will be described, with brief reference to some further changes in the patterns exhibited at the highest field strength—29,950 gauss.

Computation of the magnetic levels according to Eqs. (1) and (2) for both of the $^2\Sigma$ levels has been made for each field strength. The value of ν_0 for the ground state has been taken to be $0.045(K+\frac{1}{2})$, while for the upper state computation of the doublet interval for each value of K has been made from the original analysis of Hulthén.[10] The solid lines in Fig. 1 give the course of these levels for increasing K for $H=24{,}600$ gauss, only the extreme values of $M=\pm J$ and $M=0$ being shown. From such a diagram, giving consideration to the proper change in K for the band lines in question, and to the selection rule $\Delta M=0$ and ± 1, the predicted Zeeman patterns can be computed. Transitions from the T_1' levels to the T_1'' levels and from the T_2' levels to the T_2'' levels give the narrow "outside" blocks of Zeeman components, while the cross-over transitions for the T_1' group of levels to the T_2'' group and from the T_2' group to the T_1'' group are responsible for the broad "inside" blocks of components outlined in Fig. 2 and 3. To be noted is the predicted symmetry of the pat-

[8] The writer and W. Fredrickson have recently reported (Abstract, Chicago meeting Am. Phys. Soc., Nov. 1931) a considerably larger and similar doubling in a corresponding $^2\Sigma$ state of SrH.

[9] Reference 3, p. 118.

[10] E. Hulthén, Phys. Rev. **29**, 97 (1927).

terns of the corresponding lines in the P_1 and P_2 or R_1 and R_2 branches, because of the equality in the over-all width of the levels in the T_1 and T_2 groups.

One can get some idea of the correction that must be applied to these computed widths of the groups of levels, due to the presence of the interaction between the component ρ of l in the direction of K and the external field H, by assuming that the magnetic moment associated with ρ is that fraction of a Bohr magneton that ρ is of unit component of l.[11] Some values of ρ for this upper $^2\Sigma$ state, estimated from the spin doublet widths as indicated above for $K=32$, together with their product with $\Delta\nu_n$ for the two field strengths, are given in Table I. This additional magnetic energy for the extreme components $M=\pm J$ should be either added to or subtracted from that due to the

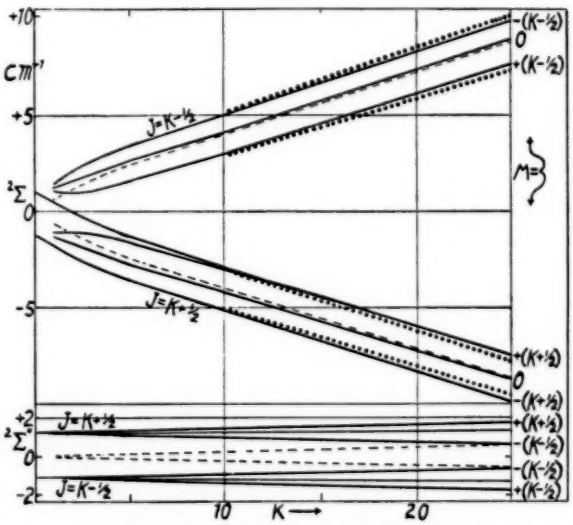

Fig. 1. Magnetic energy level diagram for 6389A $^2\Sigma$, $^2\Sigma$ band of CaH. Dashed lines give the spacing of the levels without the external field. The solid lines represent the levels for the extreme values of M and for $M=0$, the other values of M falling fairly uniformly in between. These levels are calculated with equations 1 and 2, with observed spin doubling separations, and therefore assume the magnetic energy to arise only from the interaction of electron spin and field. The dotted lines give the positions of the extreme levels when the additional energy due to the interaction of the component ρ of l along the rotational axis and the field is included.

TABLE I. *Some values of ρ for upper $^2\Sigma$ state, and corresponding magnetic energy for the two strengths of field. cm^{-1} units.*

K	$\rho(=\Delta\nu_{12}.A)$	$H=14{,}000$ gauss $\rho\times\Delta\nu_n$	$H=24{,}600$ gauss $\rho\times\Delta\nu_n$
10	0.10	0.07	0.12
15	0.14	0.09	0.16
20	0.18	0.12	0.21
25	0.22	0.15	0.26

interaction of S and H. That it should be subtracted, not added, is demonstrated by the agreement of the resulting pattern widths with the observa-

[11] I am indebted to R. S. Mulliken for this suggestion.

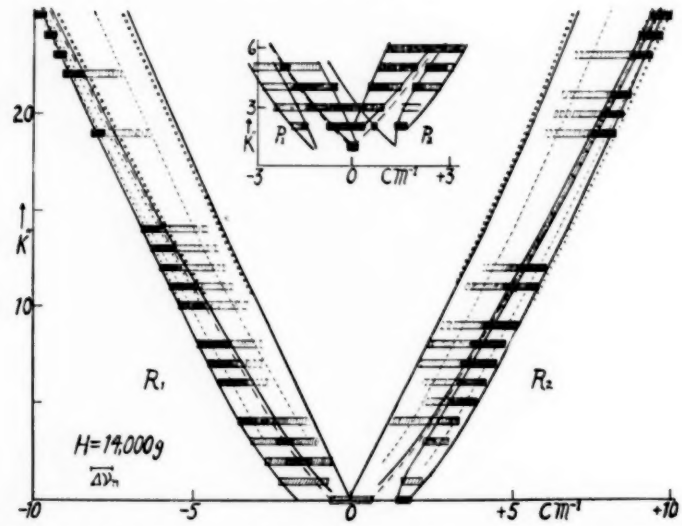

Fig. 2. Comparison of observed and calculated Zeeman patterns for $H=14{,}000$ gauss. Heavy dashed lines give no-field positions of the band lines, solid lines give the outlines of the blocks assuming the coupling of the electron spin and the field H to be the only magnetic energy, and the thin dashed lines the transitions $M'=0$ to $M''=0$. Corrected widths of pattern blocks for higher K levels upon inclusion of the energy of interaction of the component ρ of l along the rotational axis and H are indicated by the dotted lines for the narrow outside blocks and by the small crosses for the wide inside blocks. The shaded strips at each K'' level give the observed patterns, with the strength of the shading proportional roughly to the intensity. Note the general agreement with the computed patterns for the lines of low K values, and the evidence for the corrected widths at the highest K levels.

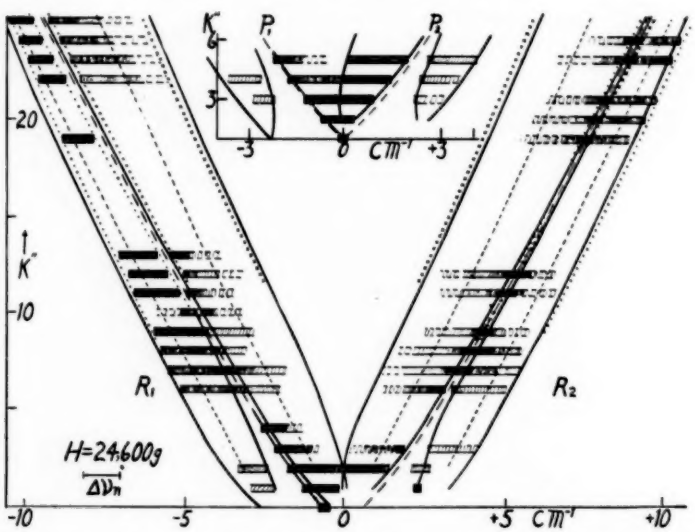

Fig. 3. Comparison of observed and calculated Zeeman patterns for $H=24{,}600$ gauss. Note the greater intensity of the inner blocks of components for lines of low K'' values, the evidence for the corrected widths of the patterns at the higher K levels (narrow R_1-blocks and intensity of R_2 patterns around no-field position), and the setting-in of these effects at lower K levels ($K''=11$) than in Fig. 2.

tions. That is, for the $J=K+\frac{1}{2}$ group of levels, the magnetic energy for $M=\pm J$ is $\pm[\Delta\nu_n$ (for the $S)-\rho\times\Delta\nu_n]$, while for the $J=K-\frac{1}{2}$ group it is $\pm[-\Delta\nu_n$ (for the $S)-\rho\times\Delta\nu_n]$. This reduces the over-all width of the magnetic levels for the T_1 group by $2\times\rho\times\Delta\nu_n$, and increases the width for the T_2 group by the same amount. And since for this $^2\Sigma$ state the l-uncoupling is very appreciable, there results the considerable correction to the widths of the groups of Zeeman levels indicated by the dotted lines in Fig. 1. The fact that this additional magnetic energy must be subtracted from that for the S and H interaction means that the ρ must be oriented anti-parallel to K along the rotational axis of the molecule. Finally, this quantity ρ is very small for the lower $^2\Sigma$ state for these bands, and should therefore have a negligible effect on the Zeeman patterns.

Details of the Zeeman Effect in the $^2\Sigma$, $^2\Sigma$ Band

The comparison of the observed pattern blocks for the two field strengths is made in Tables II and III and in Figs. 2 and 3. These graphs display the results much more vividly than do the tables, and so the attempt is made to represent as much of the information as possible in this form. Because of the fact that the P_1 and P_2 branches rather rapidly converge to form the heads of the band, the patterns of these lines overlap each other too much for $K>6$ to make measurement possible. The patterns are better resolved in the R branches, but even for these the patterns cannot be measured for quite a number of the lines due to the proximity of either another main R line or of a line of the (1, 1) band.

The positions of the no-field band lines are given by the heavy dashed curves of Figs. 2 and 3, while the outlines of the Zeeman pattern blocks of unresolved components are indicated by the solid lines for the calculations which include only the interaction of S and H. Corrected pattern widths resulting from the inclusion of the appreciable interaction energy of ρ and H for the higher K levels are indicated by the dotted lines for the outside, narrower blocks and by the lines of small crosses for the inside, broader blocks. The somewhat narrower blocks on the high frequency $(+)$ side of the R_2 and P_2 lines and on the low frequency $(-)$ side of the R_1 and P_1 lines are due respectively to the transitions from the $J=K-\frac{1}{2}$ group of levels of the $^2\Sigma'$ state to the $J=K-\frac{1}{2}$ group of levels in the $^2\Sigma''$ state in Fig. 1 and from the $J=K+\frac{1}{2}$ group of $^2\Sigma'$ to the $J=K+\frac{1}{2}$ group of $^2\Sigma''$. The rather broader "inside" blocks for these lines arise from the cross-over transitions from the $J=K-\frac{1}{2}$ group of levels of the upper state to the $J=K+\frac{1}{2}$ group of the lower state and from the $J=K+\frac{1}{2}$ group of the upper state to the $J=K-\frac{1}{2}$ group of the lower state respectively. In no instance are separate components of the Zeeman patterns resolved, although for $P_1(1\frac{1}{2})$ and $R_1(\frac{1}{2})$ a number of superposed Components of zero displacement give rise to a sharp line in the field exposure. At each K level in Figs. 2 and 3 the shaded block gives the extent of the observed pattern and the relative intensities are represented by the density of the shading. In Fig. 4 enlargements of portions of the spectrograms at the two field strengths are presented in order to give an indication of the character of the observed patterns.

TABLE II. *Comparison of some observed and predicted pattern blocks for R lines of low K values in CaH $^2\Sigma$, $^2\Sigma$ band.* Magnetic energy only that of interaction of spin and field. (+ =displacement to high frequency, − =to low frequency from no-field position. cm^{-1} units.)

	R_1	$H = 14{,}000$ gauss	R_2	
K	Calc.	Obs.	Calc.	Obs.
1	−0.41 to −1.06; 0; +0.18 to +0.64 and +0.93	−1.00 to about +0.53	+0.41 to +1.12 and −0.22 to −0.95	+0.43 to +1.02 weak
3	−1.04 to 0 and +0.10 to +1.20	−1.06 through stronger 0 to weak +edge	+0.20 to +1.06 and +0.11 to −1.24	+ edge at +0.92
4	0 to −1.03 and +0.09 to +1.35	0 to −1.02 stronger, and 0 to about +1.20 weak	+0.14 to +1.02 and −0.11 to −1.35	+ edge at +0.82, weak at 0 and weak—block to indef. edge
7	0 to −0.93 and +0.07 to +1.53	0 to −0.87 strong	+0.10 to +0.92 and −0.08 and −1.53	+ edge at +0.89, stronger at 0 and weaker to −1.54
11	0 to −0.77 and +0.06 to +1.76	−0.11 to −0.77 strong, and −0.11 to beyond +1.11 weak	+0.07 to +0.79 and −0.07 to −1.76	+edge at +0.72, stronger at 0 and weaker—to indef. edge
		$H = 24{,}600$ gauss		
1	−2.06; −1.78 to −1.02; 0; +0.24 to +0.86; +1.29	−1.00 to indef.-edge weak; 0 to about +1.00 strong	+1.04 to +2.07 and −0.28 to −1.34	+1.04 sharp; no other +; −block obscured
2	−0.73 to −2.08; 0; +0.15 to +1.69	−0.74 to −1.62 weak; + strong 0 to R_2 −block	+0.82 to +2.09 and −0.20 to −1.55	+0.38 to +0.99; − strong fusing with R_1 +block
3	−0.56 to −2.07; 0; +0.14 to +1.90	+ block strong 0 to weaker fusion with R_2 −	+0.58 to +2.03 and −0.22 to −1.87	+0.55 to ? weak; − strong but fused with other
7	0 to −1.95 and +0.19 to +2.45	stronger 0 to +1.89; +0 to (weaker) indef. edge	+0.23 to +1.91 and −0.17 to −2.43	0 strong; + to +1.89; − block same intensity
11	0 to −1.78 and +0.16 to +2.75	−0.19 to −1.64 strong; +0 stronger, gradually fading out	+0.14 to +1.79 and −0.11 to −2.71	strong center +0.04 to −0.16; + and − both gradually fade out

TABLE III. *Comparison of some observed and predicted pattern blocks for R lines of high K values in CaH $^2\Sigma$, $^2\Sigma$ band.* Magnetic interaction energy includes that of ρ (component of l along rotational axis) and field.

	R_1	$H = 14{,}000$ gauss	R_2	
K	Calc.	Obs.	Calc.	Obs.
19	−0.12 to −0.37 and +0.15 to +2.04	−0.22 to −0.63 strong; +very weak to indef. edge	−0.07 to +0.61 and +0.04 to −2.27	−0.10 to +0.68 strong; − very weak to indef. edge
22	−0.14 to −0.26 and +0.16 to +2.14	−0.12 to −0.54 strong; + block very weak	−0.08 to +0.51 and +0.06 to −2.41	
23	−0.15 to −0.26 and +0.17 to +2.18	−0.16 to −0.57 strong	−0.10 to +0.50 and +0.09 to −2.49	−0.10 to +0.58; − too weak to measure
24	−0.15 to −0.24 and +0.17 to +2.22	−0.16 to −0.52 strong	−0.10 to +0.46 and +0.09 to −2.54	−0.11 to +0.56 strong
25	−0.15 to −0.24 and +0.17 to +2.27	−0.14 to −0.53 strong	−0.11 to +0.43 and +0.11 to −2.59	−0.13 to +0.56 strong
		$H = 24{,}600$ gauss		
19	−0.21 to −1.28 and +0.31 to +2.89	−0.29 to −1.23 strong; + fused with another	−0.14 to +1.70 and +0.15 to −3.32	center very strong +0.12 to −0.32; + edge +1.35; − weaker to indef. edge
22	−0.24 to −1.11 and +0.33 to +3.21	−0.20 to −1.04 strong; + broad +0.20 to indef. edge	−0.18 to +1.60 and +0.18 to −3.49	
23	−0.25 to −1.05 and +0.33 to +3.05	−0.30 to −1.07 strong; +0.18 to indef. edge broad	−0.20 to +1.56 and +0.19 to −3.55	center stronger +0.30 to −0.38; + block strong to +1.44; − is weak
24	−0.26 to −1.00 and +0.34 to +3.08	−0.34 to −1.04 strong; +0.20 to indef. edge fairly strong	−0.21 to +1.54 and +0.32 to −3.60	center stronger +0.20 to −0.43; + strong to +1.43; −edge very weak
25	−0.27 to −0.98 and +0.34 to +3.12	−0.32 to −1.06 strong; + begins quite strong at +0.21	−0.22 to +1.50 and +0.22 to −3.67	

There is good agreement in general for the lower rotational levels up to $K'' = 14$ at $H = 14{,}000$ gauss and to $K'' = 9$ at $H = 24{,}600$ gauss between the observed Zeeman patterns and those predicted on the assumption that the

magnetic energy is very largely that of spin and field. A few points here deserve special mention. For $P_1(1\frac{1}{2})$ only a single sharp undisplaced component (six possible $M' \rightarrow M''$ transitions) is observed at all field strengths, with no

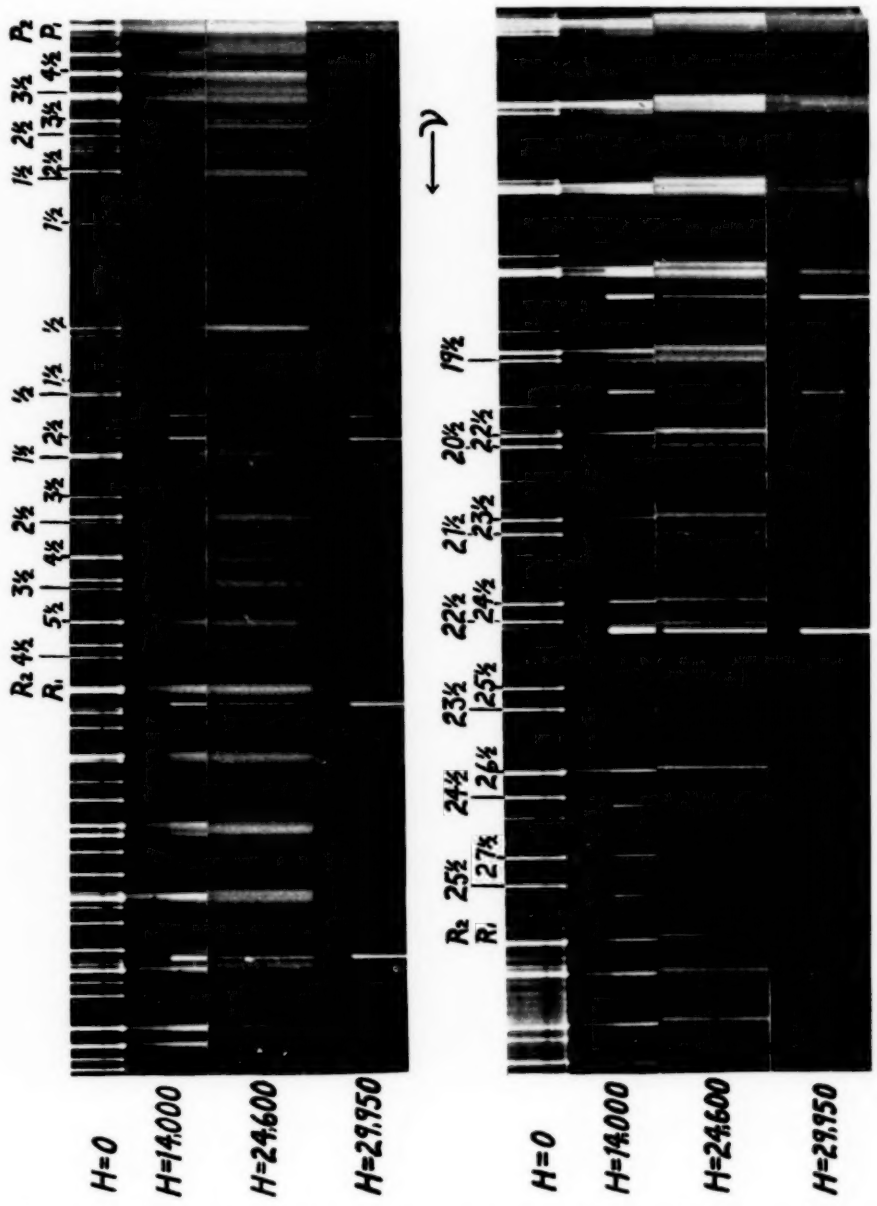

Fig. 4. Enlargements of portions of the spectrograms showing the Zeeman effect in the 6389 $^2\Sigma$, $^2\Sigma$ band of CaH. The shorter lines in the field exposures are the Fe comparison spectrum.

trace of the possible "wings" (two components each) at about $+\Delta\nu_n$ and $-\Delta\nu_n$. At the lower field strength for the lowest K values the two blocks of compo-

nents are of about equal intensity, but with increasing K the outside $(-)$ blocks of the R_1 lines become narrower and stronger, while the accompanying broader inside $(+)$ blocks become weaker and fade out to an indefinite outer edge. In the corresponding R_2 line patterns the same is true, with the greatest intensity, however, at the no-field positions. For $H = 24{,}600$ gauss the inside $(+)$ blocks for the R_1 and P_1 lines and $(-)$ blocks for the R_2 and P_2 lines with $K'' < 6$ are considerably the stronger, and for $H = 29{,}950$ gauss these are the only components visible, the patterns now filling entirely the no-field interval between the two components of the spin doublet, but with the edges of the blocks nearest the no-field positions the most intense.

This change in the patterns for the lines of low K value indicates the action of a molecular Paschen-Back effect, for with high field strength the interval between the two components of these spin doublets is of the order of $2\Delta\nu_n$. S then tends to be quantized separately in the field, and the operation of the selection rule $\Delta M_S = 0$ would cause the observed limitation of the patterns to the inside blocks with the near edges stronger. For $K'' > 6$ even the highest field is no longer "strong," so that the outer blocks appear and gain in strength as K increases.

For the R lines representing the higher rotational levels these outer blocks, the + blocks for the R_2 lines and the − blocks for the R_1 lines predominate. But, as Figs. 2 and 3 show, these blocks are neither found to be bounded by the predicted pattern outlines assuming the magnetic energy to be only that of the interaction of S and H (the solid black lines), nor do they preserve the indicated symmetry between the R_1 and R_2 patterns. Rather are these patterns found to agree very well with the predictions which also include the magnetic energy due to the coupling of ρ and the external field H, represented in Figs. 2 and 3 by the dotted lines for the more intense outside blocks and by the lines of small crosses for the broak, weak, inside blocks for both the R_1 and R_2 lines. The near edge of the narrow intense R_1 blocks for $K'' > 22$ at $H = 14{,}000$ gauss coincides nicely for each band line with the predicted interval from the no-field position. The observation that these R_1 blocks extend out farther to the low frequency side than predicted is no doubt due to the concentration of most of the components at this outer edge, owing to the fact that the $M' = M'' = 0$ line actually falls outside the limits for the extreme transitions. In the R_2 branch the corresponding pattern blocks are observed to be much broader, and coincide almost exactly with the confines set by the corrected theory.

The data for $H = 24{,}600$ gauss offer even more convincing evidence for the inclusion of the magnetic energy arising from the l-uncoupling in this $^2\Sigma$ state of CaH. For the intense − block of components for each R_1 line is observed narrowed just the calculated amount, and the inner edge of the broad + portion of the pattern falls in each case at just about the calculated separation from the no-field position. Incidentally, these + blocks, though broader, are considerably more intense than at the lower field strength. As for the R_2 line patterns, tbe corrected theory explains at once the outstanding feature, the greater intensity at and near the no-field positions of the lines. For the

two parts of the pattern are broadened to such an extent by the effect of the energy of interaction of ρ and H that they overlap considerably. And as noted in the R_1 line patterns, these broader blocks of components have their greatest intensity always adjacent to the no-field position, for which the transitions involve the magnetic levels having anti-parallel S and H. The outermost edges of these very broad blocks are of such low intensity in our spectrograms that they are just lost in the general fog on the plates.

Measurements of the spectrogram taken at $H = 29{,}950$ gauss only serve to verify the results at the other two field strengths. The differences between the patterns of the R_1 and R_2 lines are more marked, and agree closely with the calculations of the complete theory.

Zeeman Effect in the $^2\Pi \rightarrow {}^2\Sigma$ Band of CaH

Because of the pure precession relation which exists between this upper $^2\Sigma$ state and the $^2\Pi$ state of the 7000A CaH band, there should be equally prominent effects on the Zeeman patterns of the lines arising from these higher rotational levels in this $^2\Pi \rightarrow {}^2\Sigma$ band because of the l-uncoupling. But the spin doubling which originates in this way in the $^2\Pi$ state (Mulliken and Christy's $\Delta\nu_{12}(K) - [IVV, \Delta\nu_{12}(K)]$ differs for the $^2\Pi_d$ and $^2\Pi_c$ levels, being practically identical with the spin doubling in the upper $^2\Sigma$ state for the former and almost negligible for the latter. This means that for the Q branch lines, which originate in the T_c sublevels of the $^2\Pi$ state, the Zeeman patterns even for quite large values of K should be those given by Hill's treatments of the effect in $^2\Pi$ and $^2\Sigma$ states. For the P and R branch lines, however, which involve the $^2\Pi_d$ terms, the magnetic energy due to the interaction of the ρ and the field H should be considered in calculating the Zeeman patterns. It is clear that the addition of this interaction will cause one of the groups of magnetic levels in the $^2\Pi$ state to be broadened, while the other group is contracted in its over-all width. This should result in marked differences between the patterns of the P_1 and P_2 or R_1 and R_2 band lines, and a considerable discrepancy between the observations on these patterns and the predictions from Hill's formulas.

The data on the Zeeman effect in this $^2\Pi \rightarrow {}^2\Sigma$ band, though incomplete, are in accord with these considerations. The writer and W. Bender[1] have shown that for the band lines near the origin, there is general agreement with the patterns predicted from Hill's theory. Very great differences in the patterns of the P_1 and P_2 lines from the higher rotational levels were observed, however, the field radiation associated with the P_1 lines becoming very broad whereas for the P_2 lines there occurs just a rather narrow and intense inside block of components. No such differences exist between the patterns of the corresponding Q_1 and Q_2 lines, though observation is made difficult by much overlapping of patterns, but there is a considerable difference in the intensity distribution in the Q patterns as compared with the P line patterns.

One might make some rough calculations on the widths of these Zeeman levels in the $^2\Pi$ state after the fashion of our treatment above for the upper $^2\Sigma$ state, assuming case b for the higher rotational levels, but such a calculation

has not been found satisfactory. In this $^2\Pi$ state there is the usual gradual transition from case a to case b, as K increases, and the addition of the perturbing term due to the interaction of ρ and H to the rigorous treatment for the no-field situation would be a difficult task. We have shown, however, that this additional magnetic energy is present in the Zeeman effect in these states of CaH, and that with its inclusion in the theory all the details of the Zeeman effect in the $^2\Sigma$, $^2\Sigma$ band can be explained particularly well. Moreover these results are in complete agreement with our earlier conclusions, and with the interpretation by Van Vleck and Mulliken and Christy of the Λ-type and spin doubling in these states.

THE POLARIZATION OF MERCURY RESONANCE RADIATION

By L. Larrick and N. P. Heydenburg
State University of Iowa

(Received December 9, 1931)

Abstract

The polarization of the line λ2537A of mercury in resonance radiation is calculated on the assumption that isotopes 199 and 201 have nuclear moments of 1/2 and 3/2 respectively, while the even isotopes 198, 200, 202, and 204 have zero nuclear moment as Schüler and Keyston have suggested. With "broad line" and "narrow line" sources respectively, resonance radiation excited by light polarized with the electric vector parallel to the magnetic field should be 84.7 percent and 88.7 percent polarized, in fair agreement with the observations of Olson, 79 to 86 percent, and von Keussler, 79.5 percent. Relative transition probabilities within a hyperfine multiplet are calculated on the assumption of *LJS* type coupling between *J*, *F* and *I*.

ELLETT and MacNair[1] have shown that the incomplete polarization of the line λ2537A of mercury in resonance radiation is due to the peculiar behavior of the −25.6 and +22.1 mA hyperfine structure components in a magnetic field. Previously MacNair[2] had shown that the parallel Zeeman component of the −25.6 hyperfine structure line shifts toward longer wavelengths with increasing field.

Recently Schüler and Keyston[3] have proposed an explanation of the hyperfine structure of this line, assigning nuclear moments of 1/2 and 3/2 to isotopes 199 and 201 respectively, and zero nuclear moment to the even isotopes. According to this proposal the components due to the even isotopes 198, 200, 202, 204, occur at −10.3, 0.00, +11.6, +22.1 mA respectively. The stronger component of isotope 199 is located at −25.6 and the weaker at +22.6, placing the center of gravity of the 199 pattern midway between −10.3 and 0.00. Since the levels of 201 are inverted, the strongest component of 201 is assigned to +22.1, the next to −10.3, and the weakest to −25.6. This explanation gives the correct positions of all five components and gives relative intensities in fair agreement with the observations of Mrozowski,[4] but in poor agreement with Schrammen's[5] observations. This structure of λ2537 will be used in this paper to calculate the polarization of resonance radiation to be expected.

The method of calculating the polarization is that given by Ellett,[6] based on the assumption that *I* and *J* combine vectorially to a resultant *F* just as *S* and *L* combine in the alkali spectra to the resultant *J*. The selection prin-

[1] Ellett and MacNair, Phys. Rev. **31,** 180 (1928).
[2] MacNair, Proc. Nat. Acad. **13,** 430 (1927).
[3] Schüler and Keyston, Naturwiss. **31,** 676 (1931).
[4] Mrozowski, Nature **127,** 890 (1931).
[5] Schrammen, Ann. d. Physik **83,** 1161 (1927).
[6] Ellett, Phys. Rev. **35,** 588 (1930).

ciple for $F(\Delta F = \pm 1, 0)$ gives the possible hyperfine components, the intensities of which are obtained from formulas given by Hill.[7]

In order to calculate the polarization a hypothetic magnetic field is introduced parallel to the axis of symmetry, the electric vector of the incident plane polarized light in this case. This field is introduced to remove the degeneracy which exists in the absence of any field and must be considered strong enough to separate completely the magnetic energy levels, but still very weak as regards the Paschen-Back effect of the hyperfine structure. Then the principle of spectroscopic stability insures that the polarization so calculated will be the polarization in zero field. The intensities of the Zeeman components, and hence the relative transition probabilities to the various upper magnetic levels, are calculated from the usual Kronig-Hönl formulas, with the use of the quantum numbers appropriate to hyperfine structure.

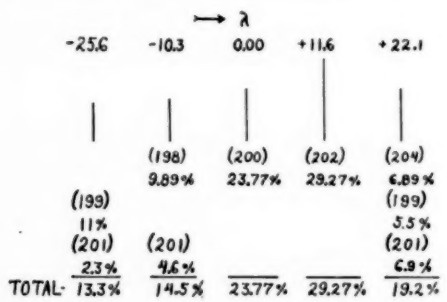

Fig. 1. The hyperfine structure of λ2537 of Hg (after Schüler and Keyston).

Since in this type of excitation only the parallel Zeeman components of the incident radiation are absorbed, the relative populations of the upper levels become equal to the transition probabilities of these parallel components. Having the relative populations we calculate the probabilities of reemission parallel and perpendicular to the magnetic field. The polarization is then given by

$$P_{0/0} = \frac{I_{\parallel} - I_{\perp}}{I_{\parallel} + I_{\perp}} 100$$

The intensity distribution in the resonance radiation depends upon the relative numbers of atoms present in the resonance lamp and upon the intensity distribution in the exciting radiation. That is, the relative intensity of each Zeeman component in the resonance radiation is proportional to the relative number of atoms of the isotope to whose hyperfine structure pattern it belongs and is also proportional to the relative intensity of that hyperfine structure component in the source which is effective in exciting the initial magnetic level on which this Zeeman component originates.

In order to have sufficient intensity in the resonance radiation, the source of excitation is usually run at such a temperature that the density of mercury vapor is high enough to cause considerable self reversal. The effect of self re-

[7] Hill, Proc. Nat. Acad. **15**, 779 (1929).

versal, being greater the more intense the line, tends to equalize the intensities in the source so that the intensity distribution is sensibly uniform across the entire hyperfine pattern. In this case, that of "broad line" excitation, the intensities in the resonance radiation will depend only on the relative abundance of isotopes in the resonance bulb.

However, if the source is run at a temperature such that the density of mercury vapor is low enough to eliminate self-reversal, then the intensity in

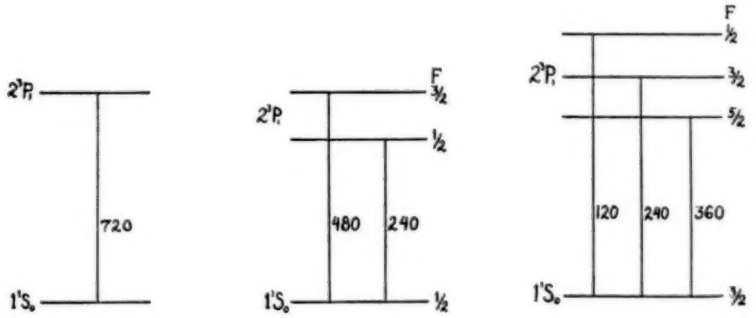

Figs. 2a, 3a, 4a. Hyperfine structure components of even isotopes, isotope 199, and isotope 201, respectively.

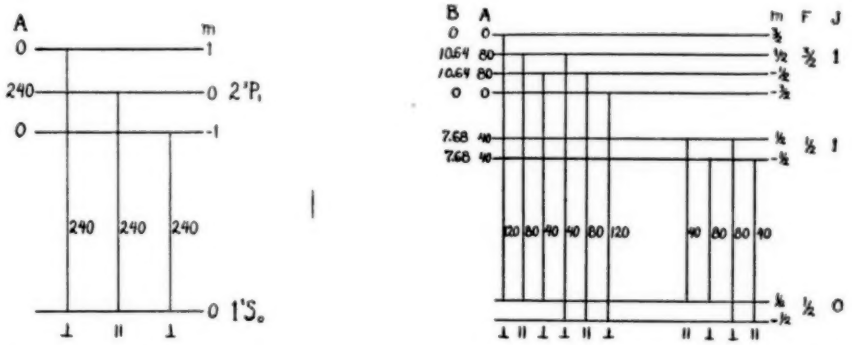

Fig. 2b. Transition probabilities and relative populations for the even isotopes, for "broad line" excitation.

Fig. 3b. Transition probabilities and relative populations for isotope 199. Column *A* gives populations for "broad line" excitation, column *B* for "narrow line" excitation.

the source is distributed across the hyperfine pattern according to the theoretical distribution and the total intensity of each Zeeman component emitted in resonance radiation will be proportional to the intensity of the hyperfine component exciting it. The theoretical intensity distribution in the source operating under these conditions is shown in Fig. 1, (after Schüler and Keyston).

The hyperfine patterns for the three types of isotopes, the even isotopes with $I=0$, the isotope 199 with $I=1/2$, and the isotope 201 with $I=3/2$, are given in Figs. 2a, 3a, and 4a, respectively, with the appropriate a priori in-

tensity written on each component. Figs. 2b, 3b, and 4b give the corresponding Zeeman patterns for the above hyperfine patterns, with the transition probability given beside each component.

At the left of the three latter diagrams, in columns A and B, are given the relative populations of the upper levels for the "broad line" and "narrow line" sources, respectively. (These populations are for equal numbers of atoms of the different isotopes in the resonance lamp and must be multiplied by the relative abundance to get the true "populations".) These populations for "narrow line" source are not tabulated for the even isotopes since the values will be different for each of these.

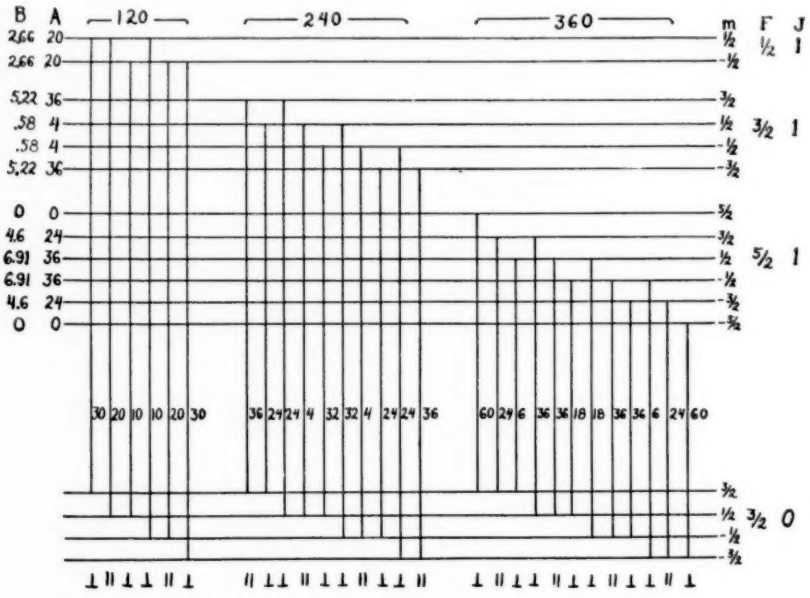

Fig. 4b. Transition probabilities and relative populations for isotope 201.

The results of the calculations are given in Table I.

TABLE I.

Excitation	Polarization ($E\|H$)
"Broad line"	84.7 percent
"Narrow line"	88.7 percent

COMPARISON WITH EXPERIMENT

Olson[8] found that the polarization of the line in zero field was dependent somewhat upon the conditions of the source. With a water-cooled quartz-mercury arc operating on 3.5 amperes, he obtained 79 percent initial polarization. The same arc operated on 1 ampere gave 84 percent, and with 0.4

[8] Olson, Phys. Rev. **32**, 443 (1928).

ampere arc current gave 86 percent polarization in zero field. Von Keussler[9] obtained 79.5 percent for the initial polarization.

These observed values for the initial polarization lie within the range from "broad line" source to "narrow line" source. The agreement between the polarizations calculated on the basis of Schüler's[3] explanation and the experimental values is fair.

[9] Von Keussler, Phys. Zeits. **27**, 313 (1926).

POLARIZATION OF RESONANCE RADIATION AND HYPERFINE STRUCTURE: THE CADMIUM RESONANCE LINES

By A. Ellett and Lewis Larrick
State University of Iowa

(Received December 9, 1931)

Abstract

The cadmium resonance lines λλ 2288 and 3261A excited by unpolarized radiation in a magnetic field parallel to the exciting light beam are found to be 76.3 percent and 86–87 percent polarized respectively. From spectroscopic evidence Schüler has assigned nuclear moments of 0 and 3/2 to the even and odd isotopes of Cd. Separations in 2288 are small compared to Doppler breadth, while in 3261 the strong component of the 3/2 isotope pattern merges with the 0 isotope line. If we suppose that the introduction of spin does not change the net transition probabilities between the gross levels concerned these polarization values both yield 2.53 for the ratio of abundance of even and odd isotopes. A recent calculation of C. G. Mitchell leads to other results, but is based on the apparently incompatible assumptions that intensities in the source are proportional to the isotope abundance but in absorption are determined by assigning equal weights to Zeeman levels making absorption by the spin isotope twice that by the non-spin isotope for equal abundance and uniform spectral distribution, conflicting with Kirchhoff's law.

THE attempt to account for hyperfine structure of spectral lines by attributing a magnetic moment to the atomic nucleus[1,2] which may have different values for the several isotopes of a single element[3,4] has been attended with a considerable measure of success at least as respects the qualitative features of such spectra.[5] As Goudsmit,[6] Breit,[7] and also Racah[8] have shown the quantitative agreement, at least with the heavy elements, is very bad. However it appears fairly certain that the introduction of a "fine" quantum number as originally suggested by Ruark and Chenault,[9] probably associated in some way with the nucleus, is necessary in order to account for the phenomena in question. Whether interval and intensity relations of the same type which prevail in gross multiplets also obtain for hyperfine multiplets is of course a question of interest.

Where hyperfine structures are on a sufficiently large scale so that the various components of a hyperfine pattern may be separately resolved intensities may be compared directly,[5] although the comparison of intensities

[1] Pauli, Naturwiss. **12,** 741 (1924).
[2] Back and Goudsmit, Zeits. f. Physik **43,** 321 (1927).
[3] Schüler and Brück, Zeits. f. Physik **56,** 291 (1929).
[4] Schüler and Keyston, Zeits. f. Physik **67,** 433 (1931).
[5] Kronig and Frisch, Phys. Zeits. **32,** 457 (1931).
[6] Goudsmit, Phys. Rev. **37,** 663 (1931).
[7] Breit, Phys. Rev. **38,** 463 (1931).
[8] Racah, Zeits. f. Physik **71,** 431 (1931).
[9] Ruark and Chenault, Phil. Mag. **50,** 937 (1925).

when resolution is effected by interference spectroscopes is not a simple matter.[10] In many cases however the separation of the hyperfine levels comprising one or both of the gross levels concerned in the emission of a given line is on a scale so small that complete resolution is impossible because of limitations imposed by the Doppler effect. Schüler has indeed succeeded in devising a source[11] which greatly reduces Doppler broadening of lines and has utilized it with noteworthy success.[12] However there is a point beyond which it is impossible to go even with Schüler's elegant technique and in such cases indirect evidence is the best that we can hope for. As one of us[13] has pointed out, the polarization of resonance radiation affords such evidence as it depends upon the intensity relations within the hyperfine multiplet.

Mitchell[14] has computed the polarization to be expected for the λ3261A cadmium line on the basis of Schüler's[15] ideas regarding the assignment of

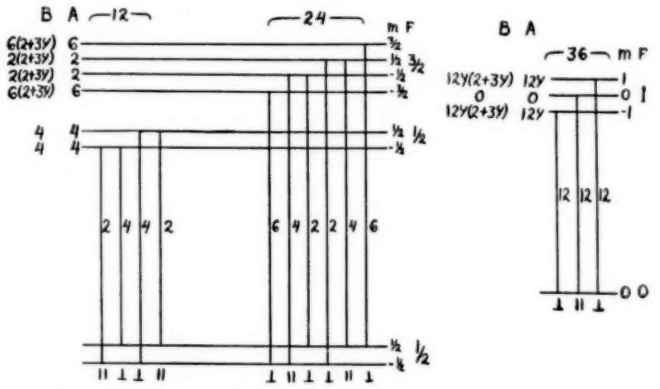

Fig. 1. Transition probabilities and relative populations for the levels 6^1P_1, 6^3P_1, and 5^1S_0 of the even and odd isotopes of Cd.

nuclear moments and using Schüler's[15] estimate of the relative abundance of odd and even isotopes, and has compared his results with Soleillet's[16] observations. However Mitchell has assumed as Schüler does that the total intensity of radiation from odd and even isotopes is proportional to their relative abundance, but has based his transition intensities governing absorption upon the assumption of equal weights of Zeeman levels, applying this assumption to both isotopes. This results in giving the assemblage of fine levels making up the 6^3P_1 gross level of the odd isotopes twice the weight of the same level of the even isotopes. This procedure is evidently not admissable, as it leads to conflict with Kirchhoff's law.

We have accordingly recalculated the results assigning to the levels such

[10] Hansen, Ann. d. Physik **78,** 558 (1925).
[11] Schüler, Zeits. f. Physik **35,** 323 (1926).
[12] Schüler and Keyston, Zeits. f. Physik **71,** 413 (1931).
[13] Ellett, Phys. Rev. **35,** 588 (1930).
[14] Mitchell, Phys. Rev. **38,** 473 (1931).
[15] Schüler and Keyston, Zeits. f. Physik **67,** 433 (1931).
[16] Soleillet, Comptes Rendus **185,** 198 (1927); **187,** 212 (1928).

weights that both emission and absorption shall be proportional to the relative abundance of the two kinds of isotopes. Fig. 1 shows the Zeeman levels involved in the emission and absorption of λ3261 for both even and odd isotopes. γ is the ratio of abundance of even to odd isotopes. The same diagram will serve for λ2288A ($6^1P_1-5^1S_0$), since the J values of the upper and lower levels are the same here as for λ3261A ($6^3P_1-5^1S_0$).

The polarization of λ2288A may be calculated on the assumption of constant intensity of exciting light across the entire pattern, as we may safely infer from the observations of Schrammen[17] and the narrowness of the cadmium red line λ6438.47A ($7^1D_2-6^1P_1$). For nonpolarized exciting radiation this gives

$$P = \frac{3 + 9\gamma}{11 + 9\gamma} 100 \tag{1}$$

a function of γ.

λ3261A is double, which is accounted for by supposing that the line due to the even (nonspin) isotopes coincides with the stronger component of the pattern due to the odd (spin) isotopes. The intensity of the two observed components will then be proportional to 1 and $2+3\gamma$. Using these as the intensities in the source we obtain, again for the case of nonpolarized existing light

$$P = \frac{27\gamma^2 + 27\gamma + 22}{27\gamma^2 + 39\gamma + 34} 100. \tag{2}$$

Experimental

Soleillet[16] has measured the polarization of λ3261 excited by nonpolarized exciting light and obtained a value of 85 percent. Using a source of the type described previously[18] we have obtained values ranging from 85 to 87 percent as long as the vapor pressure of cadmium in the source was kept fairly low, that is, low enough so that the discharge appeared a light blue in the vicinity of the side tube from which the cadmium diffused into the main discharge. Under these circumstances the cadmium red line and Hα appeared about equally intense, and the intensity of λ3261A radiation was such that it was feasible to work with a monochromator of large aperture between source and resonance bulb. However as higher values of the polarization appeared to correlate with low cadmium pressure in the source we dispensed with the monochromator in an effort to obtain sufficient intensity of resonance with the corresponding low intensities of cadmium radiation from the source. This was possible by using an absorption cell of potassium hydrogen phthalate between source and resonance lamp to cut out λ2288, the other resonance line, and a cell containing bromine vapor to eliminate the strong lines in the violet, which otherwise gave rise to troublesome scattered light. With this arrangement the source could be operated with so little cadmium that it appeared not a true blue but rather milky or almost colorless even at the

[17] Schrammen, Ann. d. Physik **83**, 1161 (1927).
[18] Ellett, J.O.S.A. and R.S.I. **10**, 427 (1925).

junction of the side tube from which the cadmium was introduced. The cadmium red line was very faint compared to $H\alpha$. Using this source we obtained a value of 86–87 percent for the polarization. We think that the effect of self reversal in this source is negligible.

During these measurements the resonance lamp was maintained at a temperature of 146°C in order to eliminate any depolarization due to secondary resonance. Upon increasing the temperature, the decrease in polarization first became perceptible at 168°C where it was 85 instead of 86–87 percent. As this increase of temperature corresponds to a fivefold[19] increase of vapor pressure it is evident that at the lower temperature the depolarizing effect of secondary resonance is negligible.

For excitation of the λ2288A line the monochromator was necessary, as there was no other way to eliminate λ3261. The polarization of this line, 76.3 ± 0.3 percent, appears not to depend upon the condition of the source, which is to be expected if the fine structure is very narrow, that is narrow enough that the lines of the hyperfine multiplet effectively coincide so that the intensity of exciting light is the same for all of them by virtue of their proximity. The resonance bulb was operated at 98–105°C, again safely below the temperature at which depolarization became apparent. That a lower temperature could be used for λ2288A is due to the fact that it is much more intense than the intercombination line λ3261A.

The observations were not made in zero magnetic field but in a field of 40 gauss parallel to the exciting light beam. Observation showed that the polarization did not depend upon the field for values from 20 gauss to 400 gauss and such an applied field reduces the chance of error due to stray magnetic fields. This is especially important in the case of λ3261A as the mean life of the upper state is about 2.5×10^{-6} seconds and the polarization consequently perceptibly reduced by a stray field of a few thousandths of a gauss along the line of observation.

Measurements of polarization were made photographically by the Cornu method, with two quartz Wollaston prisms, as in the work of Olson[20] on λ2537A of Hg.

Discussion

Inserting the observed value of the polarization of the λ2288A line, 76.3 ± 0.3 percent, in Eq. (1) above we find that γ, the ratio of abundance of even and odd isotopes, is 2.53 ± 0.05 .This value inserted in Eq. (2) gives 86.1 ± 0.2 percent for the polarization of the λ3261A line agreeing with observation. Schüler[13] from observation of relative intensities in the hyperfine structure of λ4678A ($6^3S_1 - 6^3P_0$) obtained $\gamma = 3.34$ so that the agreement of our result and his is not good. The effect of small changes in γ upon the computed polarization of λλ2288 and 3261A lines may be seen in Table I. Schüler's value of γ gives

[19] The vapor pressure was calculated from the formula given in I.C.T., for cadmium in the region of 150°C.

[20] Olson, Phys. Rev. **32**, 443 (1928).

polarizations of 80 percent and 89 percent for the λλ2288 and 3261A lines respectively, and these values are well beyond the limits of error in measurement of polarization. Our computed value depends upon the assumption of Russell-Saunders type coupling between J, F, I through the use of intensity relations appropriate to such coupling, and at the same time the strongest

TABLE I.

	P (2288)		P (3261)	
	calc.	obs.	calc.	obs.
2.40	75.5		85.6	
2.50	76.1		86.0	
2.53	76.3	76.3	86.1	86–87
2.60	76.7		86.4	
3.34	80.5		89.	

evidence for the accuracy of Schüler's intensity measurements is the fact that his results agree with the intensity scheme appropriate to this type of coupling, so that the most obvious source of the disparity, namely that the intensity relations which we have used are not appropriate, seems to be ruled out. As one of us has pointed out previously,[13,5] it is difficult to say how the polarization should be computed when the separation of levels in a hyperfine multiplet becomes less than the breadth of the line due to the finite life of stationary states, and we cannot be certain that this situation does not exist in the λ2288A hyperfine structure. This however does not affect the situation with respect to λ3261A as the levels here are widely separated.

THE RELATIVE EFFICIENCY OF SOME OF THE MERCURY ARC LINES IN EXCITING THE RAMAN SPECTRUM OF BENZOL

By Sister Magna Werth
Physical Laboratory, University of Minnesota

(Received September 8, 1931)

Abstract

A study of the Raman spectrum of benzol obtained by a modification of Wood's method was made to ascertain whether or not Raleigh's fourth power law ($I \propto \nu^4$) holds when light is scattered by a substance whose Raman spectrum, excited at ordinary temperature and pressure by a 220-volt quartz Cooper-Hewitt mercury arc, contains very few anti-Stokes lines. The Raman frequencies observed are: $\Delta\nu$ 606, 845, 992, 1175, 1585, 1603, 2947, 3060, 3185. When the patterns for the exciting lines 3650A, 3654A, 3663A; 4047A, 4078A, 4108A; 4339A, 4347A, 4358A, were mapped out from the Raman lines observed on the spectrograms many lines were missing, usually due to coincidence with other Raman lines or arc lines. This coincidence made it difficult to decide what fraction of the observed intensity should be allotted to each of the components of lines of double and triple origin; therefore only lines of single origin are considered in this investigation. *The relative intensities of the Raman patterns (different shifts for the same exciting line) have been measured.* Results show that the intensities of the Raman shifts 845 and 2947 of single origin verify Rayleigh's fourth power law in the spectrum region 3650 to 5461.

I. Introduction

ALL investigators of the Raman effect have stated that the intensity of the Raman lines increases as the wave-length of the exciting line decreases. Raman and Krishnan,[1] P. Daure,[2] Menzies,[3] Sirkar[4] report that the increase in intensity is augmented considerably as the frequency of the exciting line is increased, but does not follow the fourth power law, while Placzek[5] maintains that the intensity increases or decreases as $(\nu+\nu_{mn})^4$ according as $\nu_{jn}>\nu$ or $\nu_{jn}<\nu$; where ν_{mn} is the infrared frequency; ν_{jn} absorption frequency; ν exciting frequency. Langer and Meggers[6] state: "Relative intensity and character of different modified lines due to a given exciting line are about the same no matter which exciting line is taken. Relative intensity of a given shift increases slowly as the exciting frequency increases". Pringsheim[7] says there is apparently no relation between intensities of the same $\Delta\nu$'s from different exciting lines, but for the classical scattering of these lines, the intensity going from shorter to longer wave-lengths varies as $1/\lambda^4$. Ornstein and Rekveld[8] so

[1] Raman and Krishnan, Nature **122,** 12 (1928).
[2] P. Daure, Comptes Rendus **187,** 826 (1928) and **188,** 1605 (1929).
[3] Menzies, Nature **125,** 205 (1930).
[4] Sirkar, Ind. Jour. of Physics **5,** 159 and 593 (1930).
[5] Placzek, Zeits. f. Physik **58,** 593 (1929).
[6] Langer and Meggers, Bur. Stan. Jour. Res. **4,** 711 (1930); Phys. Rev. **33,** 115 (1929).
[7] Pringsheim, Hand. der Physik **21,** 608 (1929).
[8] Ornstein and Rekveld, Phys. Rev. **34,** 720 (1929); Zeits. f. Physik **57,** 539 (1929), **61,** 593 and **65,** 719 (1930).

far are the only ones who have reported agreement with the fourth power law for the $\Delta\nu$'s 215, 312, and 456 of carbon tetrachloride in the visible region of the spectrum.

In "Letters to the Editor"[9] the writer gave a brief account of an investigation of the intensities of the Raman lines of benzol, obtained by a modification of Wood's method. The results referred to at that time did not confirm the fourth power law. Therefore several new attempts were made with better apparatus to discover a relation between the intensities of the Raman lines per unit intensity of exciting line and the frequency of the latter; and to find an explanation, if possible, of the apparent non-agreement with Rayleigh's fourth power law. The final results and conclusions are given in the article that follows.

II. Apparatus and Procedure

1. *Making of spectrograms for wave-length determinations*

The complete apparatus used for obtaining the Raman spectrum of ben-

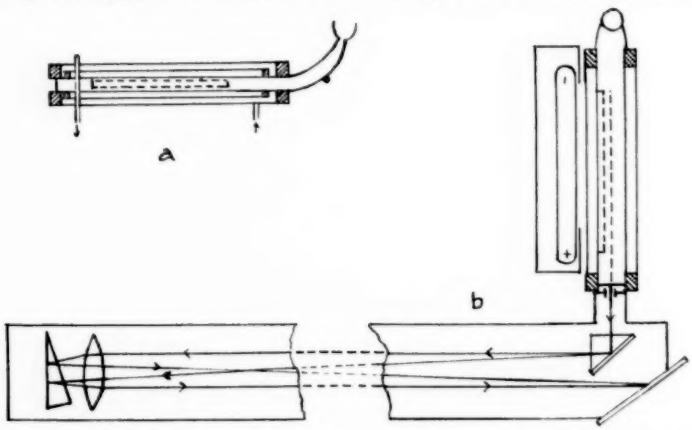

Fig. 1. Sketch of apparatus. (a), vertical section of Raman tube and jackets. (b), horizontal section of Raman tube, Hg arc and El spectrograph.

zol is shown in Fig. 1. It consists of a Wood's tube 30 cm long and 3 cm in diameter made of Pyrex glass. The cylindrical surface was silvered on the outside and protected with black Duco, except for a narrow strip about 13 cm long 2.5 cm wide along one side of the tube through which the light of the 220-volt quartz Cooper-Hewitt mercury arc irradiated the benzol. This tube was surrounded by a water jacket of Pyrex glass, 27 cm long and 6 cm in diameter. When liquid color filters were employed another Pyrex glass jacket 24 cm long and 4.5 cm in diameter was placed between the water jacket and Raman tube so that no light from the arc could enter the benzol without first passing through the color filter.

The benzol used was Baker and Adamson (C. P. quality) thiophene-free. To keep the benzol at ordinary room temperature, tap water whose temperature is very constant in this laboratory, was allowed to circulate around the Raman tube and filter jacket while exposures were being made.

[9] Werth, Phys. Rev. **36**, 1096 (1930).

At first Wood's method[10] was followed. Later it was found that better spectrograms with shorter exposure time could be obtained by discarding the screens and condensing lens[11] and bringing the window of the Raman tube close to the slit of the spectrograph. All extraneous light from the room was successfully excluded by wrapping several layers of dense black cloth around the slit-end of the spectrograph and the end of the Raman tube. The final spectrogram used for measuring the wave-lengths of the Raman lines and charting the Raman patterns of the different exciting lines was made with a Hilger E2 quartz spectrograph, dispersion 14 A/mm at 3000A, 36A/mm at 4000A, and 69A/mm at 5000A. Ilford Iso -Zenith Speed H and D 1400 photographic plates were used and an exposure time of 4 hours. The iron-arc and the mercury-arc were used as comparison spectra.

2. *Measurment of plates and Raman patterns of each exciting line*

The plates were measured with a Gaertner Comparator #103 which could be read directly to 0.001 mm and the wave-lengths of the Raman lines were computed from the average of 10 readings by a simplified Hartmann formula, $[\lambda=\lambda_0+c/(s-s_0)]$.

To determine the exciting line for each Raman line, various liquid color filters were introduced into the filter jackets and also colored glass plates bent to fit around the inner jacket were used. The filters which gave the best results were: (1) Cuproammonium sulphate, which transmitted the 4358A and 4047A and their nearest neighbors but eliminated the effect of the 3650A group and the 3341A, 4916A and 5461A lines; (2)A solution of quinine sulphate in alcohol in the filter jacket with "Blue Manhattan Lamp Coloring" painted on the outside walls of both filter and water jackets transmitted the 4358group strongly, while the 4047A and 4078A wave-lengths were so faint that they excited no Raman lines; (3) Didymium nitrate solution reduced the general background and almost eliminated the 5769A and 5790A and 3341A lines.

When the Raman pattern for the exciting lines, (3341.5A; 3650.2A, 3654.8A, 3663.3A; 4046.6A, 4077.9A, 4108.5A; 4339.5A, 4347.7A and 4358.4A;), were mapped out from the observed Raman lines on the spectrograms, it was found that a number of the members were missing. Calculation of the wave-lengths of these missing lines revealed the fact that, with few exceptions, their non-appearance could be explained by coincidence of two or more Raman lines, or Raman and arc lines. Wave-length determinations and Raman patterns of the above mentioned exciting arc lines are given in Table II. Calculated Raman wave-lengths are in italics. Anti-Stokes lines are indicated by the minus sign.

3. *Making of spectrograms for line intensity measurements*

The plates used for the measurement of the intensities of the Raman and arc lines were prepared by a method similar to that described under 1. How-

[10] Wood, Phil. Mag. **6**, 729 (1928).

[11] This method of making the spectrograms was begun early in 1930. Since then J. R. Nielsen, [J.O.S.A. **20**, 701 (1930)], has shown by elaborate computations that "if the focal length (of the collimator of a spectrograph) be *rather long* the use of a condensing lens may often be avoided." In the Hilger El quartz spectrograph, $f=155$ cm for 2537A.

ever, on account of the great number and proximity of some of the Raman and arc lines, a Hilger E1 quartz spectrograph was employed, giving a dispersion of 13A/mm at 4000A and 23A/mm at 5000A, three times as great as that of the E2. On 4×10 inch Eastman Speedway plates the following exposures were taken:

PLATE I: (*a*).

Source	Calibrated* Screens	Slit width (mm)	Time of exposure
1. Direct arc	0	0.025	1 min.
2. Carbon ribbon standard lamp (10 amp. at 40 volts)	0	0.125	45 min.
" " " " "	1	0.125	45 min.
" " " " "	2	0.125	45 "
" " " " "	3	0.125	45 "
" " " " "	4	0.125	45 "
" " " " "	5	0.125	45 "
3. Raman spectrum of benzol	0	0.125	4 hrs.
4. Direct arc	0	0.025	1 min.
5. 2-Hg-arc direct	4	0.125	45 min.

* Calibrated by means of a Macbeth illuminometer and Moll microphotometer (Kipp and Zonen).

Plates I (b) and (c) (Fig. 2) were made in a similar manner, but a tungsten ribbon standard lamp (21 amp. at 80 volts), exposure time 30 min., was substituted for the carbon ribbon lamp because the continuous spectrum of the latter did not extend far enough into the near ultraviolet to give the desired calibration and standardization graphs. On Plate I (*c*), 5 was made, with seven screens, to reduce the intensity of the direct arc still more. In addition to this, a Raman spectrum of carbon tetrachloride was made on (*c*) to get a check for the method of calculating the intensities. Since the exposure times for the calibration and Raman spectrum and arc differ by a factor less than 10, their densities are comparable because they give parallel density curves.[12]

The two one-minute exposures of the direct arc with narrow slit were used as guides in drawing lines with a sharp stylus across the six calibration spectra. The position of the lines across the spectra coincided with those arc and Raman lines whose intensities were to be measured. For groups of Raman lines that did not differ by more than 20A only one line was drawn, since a calibration curve whose wave-length is within this limit can be employed when interpolating intensities.[13]

4. *Measurement of line intensites*

The plates thus prepared were measured by a Moll microphotometer (made by Kipp and Zonen) to determine the density of Raman and arc lines, and the successive densities along each line across the six continuous spectra of the calibration exposures of the standard. Readings were also taken on each side of the Raman and arc lines to correct for the background.

To evaluate the galvanometer readings thus obtained, an inverse characteristic curve[14] was made for each line on the calibration spectra by plotting the log T (transmission of screens) as abscissas against long G (galvanometer

[12] E. F. M. van der Held and B. Baars, Zeits. f. Physik **45**, 364 (1927).

[13] Geo. R. Harrison, J.O.S.A. **19**, 279 and 286 (1929).

[14] Geo. R. Harrison, J.O.S.A. **19**, 303 and 305 (1929).

Slit with	Exposure	Time	Source	Screens
0.025	a and h	1 min.	Hg-arc	0
0.125	b . . . g	30 min.	Tungsten Stand.	0, 1, 2, 3, 4, 5, respectively
"	i and l	"	Hg-arc	7
"	j	4 hrs.	Benzol	0
"	k	"	CCl_4	0

Fig. 2.

readings) as ordinates. The intensity of the line (J_L) corresponding to its galvanometer reading was found by interpolation from the appropriate inverse characteristic curve which is also the calibration curve. The intensity of the background (J_B) was found in a similar manner from the same inverse characteristic curve. Then the intensity of the background was subtracted directly[14] from that of the line, i.e., $J_L - J_B$ gives the J_C value, intensity of line as obtained from the calibration graph. By applying Wien's law, an intensity curve for the standard sources, carbon for Plate I. (a) and tungsten for Plate I (b) and (c) was obtained by plotting wave-lengths as abscissas against J-values obtained from Wien's formula as ordinates. The I_0 (initial intensity) for each calibration curve could then be obtained from the intensity curve, and since the standard is also the calibrating source[15] we have here a more direct method of calculating intensities. Then $J_C \times I_0$ gives the absolute intensity (not corrected for sensitivity of the photographic plate and dispersion of spectrograph), in terms of the standard, where I_0 (usually designated as J_λ in tables) is the monochromatic intensity of hemispherical radiation of a perfect black body in ergs, cm^{-3} $sec.^{-1}$

The correction for the sensitivity (S) of the emulsion of the photographic plate was obtained from a graph made by plotting the sensitivity (S = reciprocal of intensity/density) as defined by Harrison[16] against wave-lengths. Another correction for the variable dispersion (D) of the quartz prism was made by first plotting the calibration curve of the spectrograph, using distances x from a fixed point on the arc spectrum against the corresponding wave-lengths. The correction graph was then made by finding $\delta\lambda$ for equal intervals, δx, and plotting these against the wave-lengths.

By applying both corrections to the calculation of the intensity of any line, we get, $J_\lambda = (J_C \times I_0)/S \times D)$ ergs, cm^{-3}, sec^{-1}. To test the validity of this method, it was applied to the three Raman shifts of carbon tetrachloride for which Ornstein and Rekveld verified Rayleigh's fourth power law. The results for this test are given in Table I:

TABLE I. (a). *Total intensities and ratio J_R/J_A of three Stokes lines of carbon tetrachloride.*

Exciting line	$J_A \times 10^8$	J_R of $\Delta\nu$ 215	J_R/J_A	J_R of $\Delta\nu$ 312	J_R/J_A	J_R of $\Delta\nu$ 458	J_R/J_A
4046.6	3930	201.9×10^6	0.0514×10^{-2}	216.8×10^6	0.0552×10^{-2}	161.0×10^6	0.0410×10^{-2}
4358.4	9630	357.08	0.0371	404.4	0.0420	280.8	0.0292
5461.0	34160	556.8	0.0163	580.8	0.0170	464.5	0.0136

(b). *Relative intensity of three $\Delta\nu$'s of carbon tetrachloride.*

Exciting line	$\Delta\nu$ 215		$\Delta\nu$ 312		$\Delta\nu$ 458	
	Ornstein and Rekveld	Author	Ornstein and Rekveld	Author	Ornstein and Rekveld	Author
4046.6A	100	100	100	100*	100	100
4358.4A	72	72	74	76	73	71.4
5461A	32	31.6	30	30.7	34	33.2

* This group was in perfect agreement with Rayleigh's fourth power law.

[15] Harrison recommends two different sources for calibration and standardization, which requires a second and more lengthy interpolation before the final results are obtained. J.O.S.A. **19,** 279 ff. (1929).

[16] George R. Harrison, J.O.S.A. **11** 342 (1925); **19,** 276 (1929).

The good agreement between the results as shown by Table I furnishes a guarantee for the correctness of the intensities of the Raman and arc lines calculated by this method. Table II gives the total intensities (numbers in parentheses) of Raman and arc lines as found on the photographic plates. The letters, T(triple), D(double), R and A(Raman and arc) below the wavelength of the Raman lines indicate the multiple origin of a line. Parent lines are given in brackets.

Of the *forty-four* observed lines recorded in Table II, it is certain that only *eighteen* are of single origin, and for these (with the exception of the $\Delta\nu$'s 992) results show that, within the limits of experimental error, Rayleigh's fourth power law holds for the spectrum region investigated. For lines of double and triple origin, as well as for Raman lines coinciding with arc lines, attempts to divide the total intensity among the components according to the relative in-

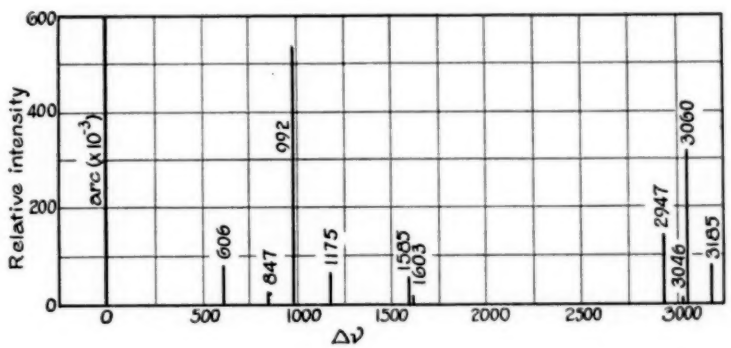

Fig. 3. Raman pattern of benzol. (Ordinates indicate average intensity of $\Delta\nu$'s.)

tensities of the exciting lines proved unsuccessful. Moreover, all attempts to find a law for the distribution of the total intensities failed. Therefore, it seemed advisable to compare the intensities of lines of single origin only. The average relative intensities of the Raman frequencies and of the exciting lines are shown in Fig. 3.

To ascertain whether or not Rayleigh's fourth power law holds for the Raman lines of single origin, the following calculations were made and recorded in Table III (a) and (b).

(1) The ratio J_R/J_A for each line (i.e., the intensity of the Raman line per unit intensity of exciting line) was found to put all lines on the same basis. This is recorded in Table III (a) for each $\Delta\nu$. To further simplify matters, the values of all $\Delta\nu$'s excited by 3650.2A were arbitrarily taken as 100 percent and all other J's found in terms of these are given in the columns marked percent. Table III (b).

(2) The theoretical values required for the verification of Rayleigh's law were found according to the following considerations: Rayleigh's fourth power law states that the intensity of the scattered radiation varies as the fourth power of the frequency (wave number). In mathematical symbols this is given by $J\alpha\nu^4$ or $J=c\cdot\nu^4$. By taking logarithms of both members of this

TABLE II. *Total intensities of Raman lines, arranged according to their frequency shifts and origin.*
J_R in ergs cm^{-3} sec$^{-1}\times 10^6$ are in ( ). J_A in ergs cm^{-3} sec$^{-1}\times 10^8$ are in ( ). (−) = Anti-Stokes, D = double, T = triple.

Exciting line	$\Delta\nu$ 606	$\Delta\nu$ 845	$\Delta\nu$ 992	$\Delta\nu$ 1175	$\Delta\nu$ 1585	$\Delta\nu$ 1603	$\Delta\nu$ 2947	$\Delta\nu$ 3060 (3046)	$\Delta\nu$ 3185
(180) 3341.5 Stokes	—	—	(74.78) 3456.2 T −3654.8 3841.5 3125.6[17]	—	—	—	—	(33.02) 3722.2	(20.33) 3737.6 D 3654.8 3341.5
(4900) 3650.2 Stokes	(56.61) 3732.6	(39.62) 3766.4	(695.0) 3787.3 R & A 3790	(72.8) 3813.7	(97.2) 3873.7	(53.0) 3878.7 D 3650.2 3654.8	(26.21) 4090.0	(1300.0) 4109.5 R & A 4108.5	(409.0) 4125.7 T 3663.3[18] 3663.3 3650.2
(1090) 3654.8 Stokes	(20.33) 3737.6 D 3654.8 3341.5	(8.76) 3771.3	(434.0) 3792.5 R & A 3790	(143.8) 3819.5 R & A 3820.3	(53.0) 3878.7 D 3654.8 3650.2	—	(5.79) 4095.9	(628.0) 4115.2 D 3654.8[18] 3654.8	(6.15) 3136.6
(997) 3663.3 Stokes	(10.17) 3746.3	(7.94) 3780.0	(206.0) 3801.2 R & A 3801.5	(39.9) 3828.0 T 3663.3 −4077.9 −4358.4	(38.9) 3889.4 T 3663.3 −4046.6 −4077.9	—	(1120.0) 4106.9 R & A 4108.5	(409.0) 4125.7 T 3663.3[18] 3663.3 3650.2	(60.0) 4148.2 D 3663.3 4046.6
(3930) 4046.6 Stokes —	(60.0) 4148.2 D 4046.6 −3663.3	(21.15) 4190.7	(717.0) 4215.7 D 4046.6 4108.5	(174.0) 4249.6 T 4046.6 4077.9 −4358.4	(52.0) 4324.5	(52.0) 4324.5 *4327.6*[18]	(151.4) 4593.9 D 4046.6 4358.4	(805.0) 4617.4 D 4046.6[18] 4046.6	—

[17] R. M. Langer, Bur. Stand. Jour. Res. **4,** 724 (1930).
[18] J. Söderquist, Zeits. f. Physik **59,** 450 (1930).

TABLE II. (*Continued*).

Exciting line	Δν 606	Δν 845	Δν 992	Δν 1175	Δν 1585	Δν 1603	Δν 2947	Δν3060 (3046)	Δν 3185
(690) 4077.9 Stokes	(7.05) 4179.9 *D* 4077.9 −4358.4	—	(174.0) 4249.6 *T* 4046.6 4077.9 −4358.4	(42.4) 4282.7 *D* 4077.9 4108.5	(?) *4359* R & A 4358.4	—	(2.4) 4634.0	(164.2) 4659.8 *T* 4077.9 4077.9 4339.5	(137.5) 4683.2[18] *2D* 4108.5 4077.9 4358.4 4358.4
(1.5) 4108.5 Stokes	(717.0) *4214.3* *D* 4046.6 4108.5	—	(42.4) 4282.7 *D* 4077.9 4108.5	(?) *4316.5* R & A 4314.0	—	—	(14.1) Cf. 4683.2 *4677.0* *2D* 4358.4 4358.4 4077.9 4108.5	—	—
(274) 4339.5 Stokes	—	—	(15.9) 4534.3	—	(164.2) 4659.8 *T* 4077.9 4077.9 4339.5	—	(?) *4976.0* R & A 4974	(?) *5004.1*	
(1190.0) 4347.7 Stokes	(70.0) *4474.8* *D* 4347.7 4358.4	—	(62.3) 4543.9	—	—	—	—	—	—
(9630) 4358.4 Stokes	(70.0) 4476.8 *D* 4347.7 4358.4	(38.2) 4525.9	(950.0) 4555.2	(151.4) 4593.9 *D* 4046.6 4358.4	(137.5) 4683.2[18] *2D* 4358.4 4358.4 4077.9 4077.9	(137.5) 4683.2[18] *2D* 4358.4 4358.4 4077.9 4077.9	(25.6) 5001.0	(455.0) 5028.9[18] *D* 4358.4 4358.4	

equation, we have $\log J = 4 \log \nu + \log c$. If we put $\log J = y$, $\log \nu = x$, $\log c = b$, and $4 = m$, this is obviously the slope intercept form of a straight line, $y = mx + b$.

(3) Construct a straight line (Fig. 4) whose slope is four and whose end-abscissas are the $\log \nu$ of 4358.4A and of 3650.2A respectively, making the ordinate corresponding to $\log \nu$ of 3650.2A equal to log 100 or 2. The ordinate for 4358.4A will then be log 49.3 or 1.692. On this straight line locate the $\log \nu$'s of the intermediate wave-lengths, 4347.7, 4339.5, 4108.5, 4077.9, 4046.6, 3663.3 and 3654.8 respectively. Read the corresponding ordinates and reduce to percents. These are the "theoretical values of J in percent" (TV) recorded in the second last column of Table III (b). The last column of this

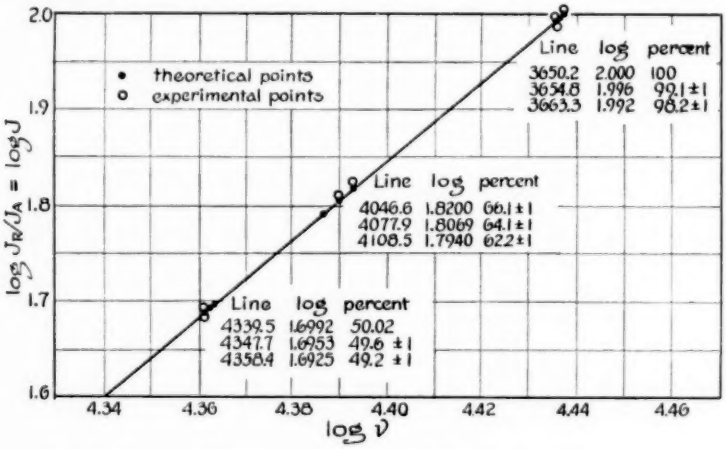

Fig. 4. Theoretical curve for Rayleigh's fourth power law. $J \propto \nu^4$.

TABLE III. (*a*). *Ratio* $J_R/J_A = J$ *for* $\Delta\nu$*'s of single origin.*

Exciting line	$\Delta\nu$ 606	$\Delta\nu$ 845	$\Delta\nu$ 992	$\Delta\nu$ 1175	$\Delta\nu$ 1585	$\Delta\nu$ 1603	$\Delta\nu$ 2947	$\Delta\nu$ (3046) 3060	$\Delta\nu$ 3185
3650.2	0.01056×10^{-2}	0.00808×10^{-2}	—	0.0148×10^{-2}	0.0199×10^{-2}	—	0.00534×10^{-2}	—	—
3654.8	—	0.00803	—	—	—	—	0.00530	—	0.00564×10^{-2}
3663.3	0.0103	0.00797	—	—	—	—	—	—	—
4046.6	—	0.00539	—	—	0.0132	—	—	—	—
4077.9	—	—	—	—	—	—	0.00343	—	—
3108.5	—	—	—	—	—	—	—	—	—
4339.5	—	—	0.0581	—	—	—	—	—	—
4347.7	—	—	0.0524	—	—	—	—	—	—
4358.4	—	0.00396	0.984	—	—	—	0.00267	—	—

(*b*). *J's of* (*a*) *referred to those of 3650.2 as 100 percent.* (*TV.=theoretical value of J in percent.*) (*AD=Average deviation.*)

Exciting line	$\Delta\nu$ 606	$\Delta\nu$ 845	$\Delta\nu$ 992	$\Delta\nu$1175	$\Delta\nu$1585	$\Delta\nu$1603	$\Delta\nu$2947	(3046) $\Delta\nu$3060	$\Delta\nu$3185	TV. percent	AD percent
3650.2	100	100	—	100	100	—	100	—	—	100	0
3654.8	—	99.3	—	—	—	—	99.2	—	99.1	99.1	0.1
3663.3	98.1	98.6	—	—	—	—	—	—	—	98.2	0.25
4046.6	—	66.7	—	—	66.3	—	—	—	—	66.1	0.6
4077.9	—	—	—	—	—	—	64.3	—	—	64.1	0.4
4108.5	—	—	—	—	—	—	—	—	—	62.2	—
4339.5	—	—	—*	—	—	—	—	—	—	50.02	—
4347.7	—	—	—*	—	—	—	—	—	—	49.6	—
4358.4	—	49.0	—*	—	—	—	50.0	—	—	49.3	1*

* $\Delta\nu$ 992 excluded. Intensity measurements of the faint $\Delta\nu$'s 992 of 4339.5 and 4347.7 probably not accurate enough to be comparable with that of the intense $\Delta\nu$ 992 of 4358.4.

table gives the average deviation (AD) of the experimental values from this theoretical value.

III. Discussion of Results

The results given in Tables II and III seem to indicate that Rayleigh's fourth power law holds for the Raman scattering and can be verified in the case of lines of single origin in the spectrum region 3650 to 5461. The only exceptions are the $\Delta\nu$'s 992 of the 4358.4 group which are very close together and of very different intensity.

Table IV. *Brief summary of results for Stokes lines.*

Raman lines	606	845	992	1175	1585	1603	2947	(3046) 3060	3185	Total
Total number excited	8	5	9	7	7	3	7	6	5	(57)**
Total number of single origin	2	5	3*	1	2	0	4	0	1	(18)

* Exception noted. ** Some lines counted more than once.

The greatest experimental difficulties in the verification of Rayleigh's fourth power law by photographic methods are due to the partial or total coincidences of lines, multiple excitation, insufficient dispersion, and resolution of spectrograph. Until the ideal condition, single excitation, is secured, no absolutely reliable results can be expected.

It may not be too presumptuous to suggest that all non-agreeing reports anent the Rayleigh's fourth power law can be traced to the above mentioned difficulties. A few illustrations may substantiate this statement. Ornstein and Rekveld[19] reported agreement for the three smallest Raman shifts of carbon tetrachloride in the visible region. These are all of single origin. Sirkar[20] claims to find small discrepancies for these same lines due to absorption corrections for the substance irradiated, (neglected by Ornstein). To this Ornstein[21] gave a satisfactory reply and confirmed his own results. Again Sirkar[22] published results for the Raman shifts 990 and 3080 of benzol, excited by the 4046 and 3132 arc lines, and reported great deviations from the fourth power law which increase as the shift increases, that for $\Delta\nu$ 3080 being about five times as great as that for $\Delta\nu$ 990. Sirkar does not mention the use of filters for separate excitation by the arc lines. In my investigation, I find that both Raman frequencies mentioned are doubly excited by the 4046 arc line, and hence are not comparable with those excited by the 3132 arc line. Moreover, Ornstein[23] points out that Sirkar's method of calculation, previously also used by P. Daure[24] is objectionable because Sirkar uses the intensity of the *unmodified scattered radiation* instead of that of the *incident radiation* to determine the

[19] Ornstein, Phys. Rev. **34,** 720 (1929); Zeits. f. Physik **61,** 593 (1930).
[20] Sirkar, Ind. Jour. Physics **5,** 159 (1930).
[21] Ornstein, Zeits. f. Physik **65,** 719 (1930).
[22] Sirkar, Ind. Jour. of Physics **5,** 593 (1930).
[23] Ornstein, Zeits. f. Physik **61,** 593 (1930).
[24] P. Daure, Comptes Rendus **187,** 826 (1928).

J_R/J_A, i.e., the intensity of the Raman line per unit intensity of exciting line. Not much importance need be attached to the visual estimates of the intensities of other observers, since corrections for dispersion of spectrograph, sensitivity of photographic plate, and similar factors change the results obtained by visual estimates appreciably. This is especially true if a large range of the spectrum is under consideration.

Therefore, it seems reasonable to conclude that Rayleigh's fourth power law holds for the Raman scattering observed in the spectrum region 3650 to 5461 and also measures the relative efficiency of the mercury-arc light in exciting the *Raman spectrum of benzol.*

In conclusion, I wish to thank Dr. Joseph Valasek, who suggested the problem and its method of attack, for his kindly interest and help during the investigation. Thanks are also due to the entire staff, especially Messrs. E. Greinke, Wm. Haliday and Charles Johnson for help with the glass work and apparatus.

ON THE ORIGIN OF THE SOLAR SYSTEM

By Ross Gunn
Naval Research Laboratory

(Received November 18, 1931)

Abstract

A new account of the formation of the solar system, based on the rotational evolution of a single star, is given which describes the system in some detail and avoids the major difficulties encountered by earlier investigators. Electromagnetic effects have been shown by the author to permit the angular velocity of a star to increase until the star breaks into two components of comparable mass. The component stars are thermally asymmetrical and momentum is radiated more rapidly from the hot face than from the cool. This important new effect, which is quantitatively satisfactory, adds kinetic energy and angular momentum to the companion stars (in a manner analogous to the mechanism of a skyrocket) and may operate to separate the stars to infinity. Applying this to the solar system, the parent semiliquid sun is supposed to have divided and lost its companion. While each companion was inside the Roche limit of the other centrifugal and tidal forces broke off the planets. These in turn immediately broke up and formed the planetary satellites. Tides and tidal couples transferred the momentum of axial spin of the two component stars to that of orbital momentum, while the planets because of their small size largely escaped the effects of this process. Planetary rotations play an important role in the theory. The account replaces the earlier improbable and "accidental" theory by a systematic evolutionary process which is probably quite common in the Universe.

IT HAS become increasingly clear during the past few years that the collision theory of the origin of the solar system, according to which the planetary system was formed by a highly improbable accidental collision of another star with our sun, faces difficulties which are perhaps nearly as serious as those which made the older nebular hypothesis untenable. The collision theory, which follows more or less closely a suggestion by the French naturalist Buffon, has been developed by Chamberlin and Moulton,[1], by Jeffries,[2] and by Jeans.[3] It takes two general forms, one in which it is considered that the close approach of a passing star to the sun raised tidal filaments and communicated sufficient angular momentum to them so that they did not fall back into the sun, but condensed and formed the planets; the other, proposed by Jeffries, considers that an actual glancing collision occurred between the visiting star and the sun. Jeffries' hypothesis, despite its assumption of a highly improbable particular glancing collision, is perhaps more satisfactory in that it at least offers the possibility of explaining the rotation of the planets, whereas the original form failed in this important respect. Calculation shows the probability of even a close approach of two stars to be so low that perhaps only one such occurs in the whole history of the Universe. There are other

[1] T. C. Chamberlin, Origin of the Earth.
[2] H. Jeffries, The Earth.
[3] J. Jeans, Astronomy and Cosmogony.

serious objections to the collision theory, as a reading of the works of the above investigators will show. Among these are the qualitative nature of the theory and hence the absence of verifiable deductions, and the inability of the theory to explain adequately some of the noteworthy characteristics of the planetary system.

Characteristics of the Solar System

The solar system is evidently not an accidental aggregation of stray bodies captured by the sun, and it seems clear that the entire system, with perhaps an occasional exception, must have had a common origin. The most noteworthy of the regularities and characteristics which must be accounted for in any complete theory of the origin of the system may be enumerated as follows:

(1) The direction of revolution of all the planets is the same.

(2) The orbits of the planets lie in nearly the same plane.

(3) The planetary system is dispersed over a region very large compared to that occupied by the sun, while the planetary satellite systems are relatively condensed.

(4) The equator of the sun lies nearly in the orbital plane of the planets.

(5) As far as is known, the axial rotations of the planets, save for one of the outermost, are in the same direction as their revolution.

(6) Except for the sun, and the two innermost planets, which have been particularly subject to tidal effect, the periods of axial rotation of all the planets are comparable.

(7) The period of axial rotation of the sun is comparatively large (31.8 days) and its angular momentum is but one thirtieth of that of the entire solar system.

(8) The massive planet Jupiter has more than half of the angular momentum of the system.

(9) Most of the planets have systems of satellites.

(10) The more massive and less dense planets have the greatest areal velocity.

(11) The orbital eccentricities of the planets are small, while those of some of the asteroids are large.

A detailed account of all the peculiarities of the solar system is manifestly impossible at the present time; for one cannot include the possibility that satellites may be transferred to other primaries or that asteroids may become satellites. Nor can one explain the peculiar numerical relations that have been found to describe the positions of the planets, satellites, etc., which relations are probably determined by conditions of stability and are believed to have no real significance in connection with the origin of the solar system. But we can, by a simple rotational theory, explain most of the above characteristics. Rotational hypotheses have been advanced by earlier investigators and we are aware that many statements are to be found in authoritative literature to the effect that "it has been proved" that the solar system could not have origi-

nated by rotational evolution. We show in the following paragraphs that these highly arbitrary opinions are based on insufficient evidence.

The present account of the genesis of the solar system depends essentially upon the rotational instability of a parent star which breaks up, forming two components of comparable mass, one of which is assumed to recede to infinity. On account of the frequent occurrence of binary stars the process of division seems quite common, and if a planetary system results each time that a star divides, many of these systems must exist within our galaxy. The solar system, therefore, instead of being a curiosity of the Universe resulting from an "accident," may well be the result of a regular and well organized plan of evolution. The following examination of events, in common with all others, is necessarily only roughly quantitative in nature and in minor details will undoubtedly need revision as more and more astrophysical data become available. Because we must necessarily neglect the density distribution functions inside the sun and planets, as well as assume that the bodies act as if they were composed of semi-liquid material, we rest content if we can show that the quantities are of roughly the right magnitude and that no inconsistencies of available energy, momentum, etc., result.

Evolution of a Rotationally Unstable Star

Under the above title the author has shown[4] that electromagnetic effects operating in the atmosphere of an energetic star permit the angular velocity of the star to increase until the star becomes rotationally unstable. A cataclysm results and the star divides into two components of nearly equal mass. Tides and tidal moments orient the two companions and cause the angular momentum of rotation to be largely transferred to that of orbital revolution. Thus the act of fission is essentially a stabilizing mechanism, because the axial rotations of the components are greatly reduced and there is no tendency for the separate components to break up again as a result of rotational instability. The two companion stars, after fission, are thermally asymmetrical, for one face of the star has just emerged from the depths of the parent star, while the other face is relatively undisturbed by the act. Radiation from the hot face is greater than from the cool one and since radiation carries off momentum there results an asymmetrical loss of momentum from the star. The reacting momentum gained by the star proper adds kinetic energy to the star and angular momentum to the pair in a manner analogous to that of a skyrocket or pinwheel. The kinetic energy added to a star by the mechanism is readily calculated; it is found that a typical energetic star will have sufficient energy added to it for the star to escape completely from the gravitational effects of a similar companion star if it radiates from one hemisphere an excess mass amounting to only 0.0003 (0.03 percent) of its total mass. This suggests that most of the single dwarf stars in the Universe have perhaps been formed by the division of more massive stars at some period in their life. In particular, our sun is well advanced in the course of stellar evolution and,

[4] R. Gunn, Phys. Rev. **39**, 130 (1932).

if the act of division is at all common to stars, our sun probably has passed through the process of division from a parent star and lost its companion.

The crucial difficulty of all rotational hypotheses concerning the solar system, first pointed out by Fouche,[5] was to account for the relatively slow rotation of the sun and at the same time account for the tremendous orbital angular momentum of Jupiter. The angular momentum of the parent star was known to be quite ample for all purposes; but by what mechanism could a large fraction of it be transferred to a satellite while the parent star retained practically none? Our present mechanism gives a definite answer to the question. When two bodies like our two companion stars separate, tidal couples convert the angular momentum of axial spin to that of orbital revolution, and the axial spin of both components decreases to small values. In an immediately preceding paper[4] we pointed out that inside the Roche limit the tides are tremendous, and this process probably takes place very rapidly. Indeed, astronomers seem generally agreed that the periods of rotation and revolution of close binaries are identical. Thus on our new hypothesis we should certainly expect the angular momentum of the sun to be small compared to the orbital momentum of the system. This agrees precisely with the observed facts.

According to Darwin's calculations the critical angular velocity ω_c of a rotationally unstable star of uniform density is specified by

$$\frac{\omega_c^2}{2\pi\gamma\rho} = 0.141 \tag{1}$$

where γ is the gravitational constant and ρ is the mean density. Moreover, the critical angular momentum Ω_c is given roughly by

$$\Omega_c = 0.4 M_s a^2 \omega_c \tag{2}$$

Substituting in these relations values appropriate to the sun, we find the critical period of rotation to be 6 hours, while the critical angular momentum approximates 11.2×10^{50} gm·cm^2 sec^{-1}. The angular momentum of the entire solar system is but 3.3×10^{50} gm·cm^2 sec^{-1} so that, even in the absence of other mechanisms, the unstable parent star had more than sufficient angular momentum to produce the solar system. It is, perhaps, significant that the angular momenta of the planetary system and that of a critically rotating parent sun should be of the same order of magnitude.

Observations show that the period of rotation of all the planets, except the two inner ones which have been particularly subject to tidal development, have effective periods of rotation systematically very close to the critical solar period of six hours. Thus the major planets, Jupiter, Saturn and Uranus all rotate about once in 10 hours. The axis of Uranus is tipped about 97° to the orbit (presumably by a resultant tidal couple acting, for a short interval of time just after birth, about an axis different from the axis of spin) and its rotation is retrograde, while Neptune, rotates once in 15 hours. The pres-

[5] Fouche, Comptes Rendus 99, 903 (1884).

ent period of rotation of the earth is 24 hours, but its initial effective value must have been only 4.1 hours; for originally the moon was at the earth's surface and the angular momentum of the earth proper must have been correspondingly much larger than its present value. In addition to the earth it is known that Eros spins with a period of 5-1/4 hours. Mars is an exception, as it should be, for there are good reasons for believing that it has lost a comparatively massive satellite, and that this possessed most of the angular momentum of the Mars-satellite system.

This bracketing of the solar critical period by the effective periods of all the planets, which we should expect to yield useful information, is perhaps the most significant of all the data we have to consider. It is a remarkably clear guide that can lead the investigator to but one conclusion. *The planetary system originated as a result of the rotational break-up of a parent star not greatly different from our present sun.* Putting the matter another way: only a most extraordinary accident would arrange the initial periods of axial spin of all the planets so that these periods were always small multiples of their critical periods of rotation.

We have, of course, neglected the effect of tidal couples and condensation on the periods of rotation of our newly formed planets; but we can advance arguments to show that these could not have greatly altered the magnitude of the rotational period from that of the parent sun. For example, we know from observed tidal data that the tidal angle of the earth is very small, and that it almost immediately accommodates its form to external systems of forces. Thus tidal couples acting on the earth during the birth process were probably not large and we infer that such will be the case for the other planets, but rough calculation show that this certainly would not be true for the massive companions. Moreover, the major planets could not have condensed greatly since the time of their formation and hence their periods cannot now be much less than their original value. The tiny satellites of Saturn, which were born simultaneously with the planet, must have cooled off almost immediately after their formation; and if Saturn has condensed appreciably from its original state, then all the satellites inside the *original* Roche limit should have disintegrated to form systems of rings. It is known that the limit between the ring system and the satellite system corresponds with really surprising accuracy to the present Roche limit of Saturn. This appears to be reliable evidence for believing the entire solar system was practically condensed when formed. We therefore need not face the very serious difficulty of earlier theories which must account for gaseous condensation onto discrete nuclei of initially very small mass.

If we are incorrect in assuming that the satellites of Saturn were formed at its birth, then we cannot insist that the parent sun was at all like the present one. Indeed, it would be quite consistent with our present account to think of the parent sun as a massive *B* type star of comparatively low density and large radius which broke up and rapidly evolved into two far denser bodies. If this type of star were the parent of our solar system and if it yielded a satellite system whose densities are comparable to that of the present sun,

then the rotational periods should correspond roughly to the sun's critical period. Thus no definite statement can be made regarding the properties of the parent star, but such evidence as is available indicates that it was not greatly different from the present sun.

Birth of the Planets

The parent sun rotated on its axis with increasing rapidity until rotational instability set in. A great cataclysm resulted and the parent star divided forming two companion stars of comparable mass. While the two companion stars were each well within the Roche limit of the other, tidal, gravitational, and

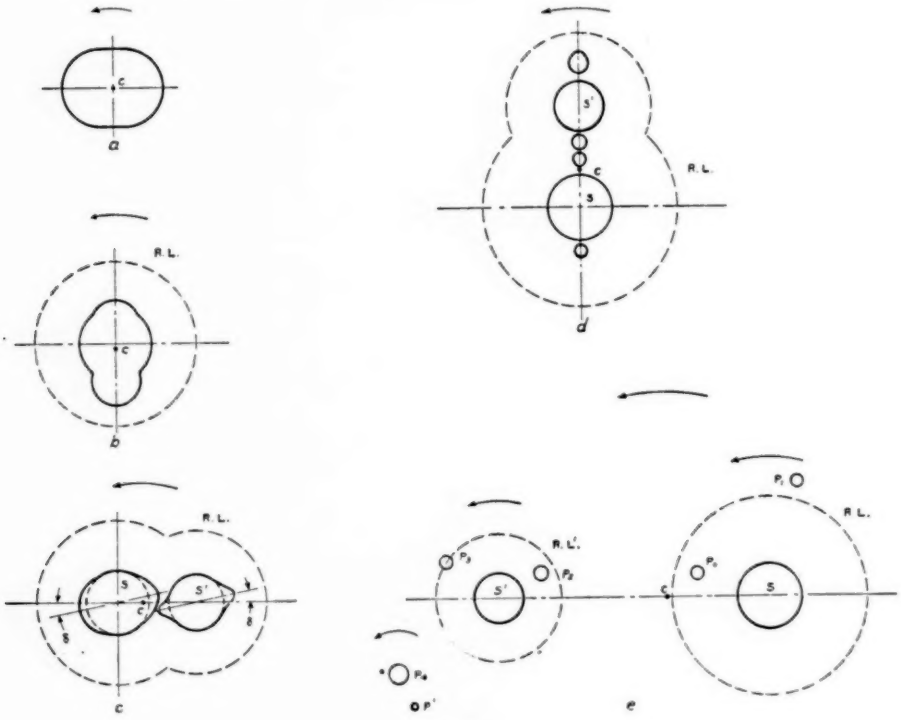

Fig. 1.

centrifugal forces were unbalanced in the regions of the inside and outside surfaces of the pair, so that the companions disintegrated in these special regions and produced the planets. These, in turn, while still inside the Roche limit of the parent star, broke up and formed the planetary satellite systems.

The history of each mass after it had been detached cannot be given in detail because its motion depended in a complicated manner on the mass ratio of the component stars, on the instantaneous positions of the planet relative to them both, and on the rate at which both stars lost their mass by radiation from the newly exposed hot face.

An idealized diagram of the process of formation is shown in Fig. 1. In this figure *a* represents the approximate configuration of the star just before

rotational instability sets in. In ***b*** the process is well under way and in **c** the star has divided, tides are raised on each component, and tidal couples are transferring the angular momentum of axial spin of both components to that of orbital revolution. The approximate Roche limit for a non-rotating star is indicated by dashed circles in each case. In ***d*** parts of the tidal bulge indicated in **c** have broken off as a result of tidal and centrifugal forces and formed the planets. By this time the center of gravity of the system **c** has moved outside the sun S, and the path of the planets (assumed to have uniform surface temperatures) becomes complicated. The satellite systems of the planets are immediately formed and sometime later the system approximates that indicated in **e**. Some of the planetary masses have fallen back into the sun; some, such as P_0, deficient in angular momentum, cannot get outside the Roche limit and are broken up and eventually dispersed, while others, like P_1, might develop into one of the innermost planets. Both companions have kinetic energy and angular momentum added to them by radiation reaction forces. The exposed areas and effective surface temperatures of both hot faces initially are the same so that the rate of loss of momentum by radiation is the same for each. Thus, at first, the accelerations of the stars are nearly inversely proportional to their respective masses and the stars separate from each other with constantly increasing velocity. The companion sun S^1 starts out with its family of satellites, P_2, P_3, etc., in an orbit about the sun, but it is constantly accelerated by non-central forces and calculations show that this acceleration may quite reasonably exceed the gravitational acceleration of the planets. In favorable parts of the planetary orbits the companion star, due to its constantly increasing velocity, loses gravitational control of the planet while the sun proper, due to its smaller non-central acceleration and greater mass, retains control and the planet finally revolves about it. The net result of the process is that a number of planets are strung out through space, perhaps to infinity; these have considerable angular momentum about the sun and they are necessarily many solar radii distant from the sun. By quite reasonable special hypotheses, additional details of the solar system, such as the comets, can be accounted for.

We may therefore think of the solar system as being almost completely formed when it was still condensed into a relatively small space where tidal forces were important, and may attribute its present open structure to the asymmetric loss of mass by radiation. Thus the net result of our rotational cataclysm is a very disperse system of two slowly spinning stars and a system of planets and planetary satellites. All bodies of the system revolve in the same direction and in the same plane and spin on their axes with an angular velocity comparable to that of the parent star. One star is eventually lost to infinity and the solar system, as we know it, results. Our planets, therefore, are simply the disintegration products of a great cataclysm.

The Satellite Systems

During the time that the planets were still inside the Roche limit of their respective primaries, tidal and centrifugal forces broke off the planetary

satellites. The planets were probably largely liquid when formed, and because of the relatively small size and high density of the minor planets, they largely escaped during the birth process the loss of angular momentum of spin due to tidal couples. For example, the rotational period of the earth before it lost the moon was 4.1 hours, while its critical period according to Eq. (1) was very close to this, or 3.3 hours. Thus when the earth was inside the Roche limit of the companion stars we might well expect a breakup which shared some of the characteristics of both rotational instability and tidal instability. If the break-up were purely rotational, the component masses would be comparable in size; if tidal, the masses would differ greatly in size. A break-up due to both causes might be expected to produce satellites of intermediate size. Qualitatively this agrees with the observed Earth-Moon mass ratio, and we may hope to obtain in the future more useful information by considering the mechanism in greater detail.

After the moon was actually detached from the earth, tidal couples rapidly transferred the moon's angular momentum of spin to that of orbital momentum and the earth is still losing and transferring its angular momentum by the same means. This process adequately accounts for the present position of the moon and the fact that its period of axial rotation corresponds to its revolution.

It seems possible that a similar division of the other minor planets took place. Mars is deficient in angular momentum according to our present account, and it seems quite probable that it has lost a fairly massive satellite which perhaps broke up and formed the asteroids.

Because of the small size of the planets, the surface temperatures were probably nearly uniform so that radiation reaction forces were comparatively small. Hence the positions of the satellites were largely determined by their initial momenta and therefore the planetary satellite systems are quite compact. Satellites which have transferred to other primaries will revolve in remote orbits and we should expect that retrograde satellites would be so placed. Tidal couples acting on the major planets produced angular accelerations which were probably greater than those of the minor planets so that they were rotationally stable after birth and produced only small tidal satellites which necessarily revolved only in the forward direction.

Remarks

We do not attempt to discuss here various earlier theories of the origin of the solar system, the earth-moon system, etc., because these are all adequately discussed in available texts. The problem of the eccentricity of the orbits in the new theory cannot be definitely solved without greater attention to detail. It seems quite possible that the initial eccentricities were nearly as low as that of the present orbits since our special mechanism after break-up adds angular momentum to the system. In any case, the present account is superior in this respect to any of the older ones; for it too can assume a resisting medium even though this seems a most unsatisfactory artifice. We can account for the observed differences in the density of the major and minor

planets by suggesting that the major planets were born from the outer layers of the parent star while the minor planets were born from the hotter inner regions; however, the evidence for such an explanation is not clear cut and the suggestion is only tentative.

Many features of the solar system remain to be examined; but the foregoing account describes our system in some detail and definitely removes the objections of earlier investigators to a theory postulating evolution from a single rotationally unstable parent star. The entire account could be given equally well without the introduction of radiation reaction forces if we were to assume that the companion star was captured and carried away by another star. This event, although relatively improbable, is far *more* probable than an actual close collision of two stars; for, the collision would be a three-body collision of an open pair and the momentum conditions could be readily satisfied.

In an immediately preceding paper which should be read in connection with the present one, the author discussed the fission theory of binary star systems and showed that the theory was entirely consistent with observation if the stars' electric and magnetic fields and the effects of radiation reaction forces were considered. Binary stars are very common in the Universe, and the process of fission probably takes place at least once in the history of each star. Thus it seems probable that many planetary systems exist, some with one sun, some with two, and occasionally one with several close stars of the same system. Whether life as we know it exists on these planets must long remain unanswered; but conditions on many of them must be comparable to those existing on the earth. It seems clear that the solar system was not the result of a highly improbable accident and the presence of man upon the earth a still greater one, but the complete organization was brought about as the result of a definite orderly and evolutionary plan. According to our series of investigations the course of evolution was largely guided by the electric and magnetic forces that act on the ions of a star's atmosphere.

POSSIBILITIES IN RELATIVISTIC THERMODYNAMICS FOR IRREVERSIBLE PROCESSES WITHOUT EXHAUSTION OF FREE ENERGY

By Richard C. Tolman
California Institute of Technology, Pasadena, California

(Received November 13, 1931)

Abstract

Previous applications of relativistic thermodynamics have been either to systems in *static thermodynamic equilibrium* or to non-static systems in which *reversible processes* are taking place. The present article deals with non-static systems in which *irreversible processes* take place. It is shown that the failure of the principle of energy conservation to hold in relativistic mechanics in its older simple form removes a classical limitation on the irreversible increases in entropy which can take place in an isolated system. The removal of this limitation provides possibilities in relativistic thermodynamics for irreversible processes to take place in an isolated system without ever reaching an unsurpassable state of maximum entropy and minimum free energy where further change would be impossible. Such possibilities are found to be illustrated by non-static models of the universe which could undergo a continued series of irreversible expansions and contractions without ever arriving at a state of rest. Special attention is given to a non-static model of the universe in which the irreversible annihilation of matter would take place in the later stages of expansion and the irreversible formation of matter out of radiation in the later stages of contraction. Finally, remarks are made concerning the bearing of the findings on the interpretation of phenomena in the actual universe.

§1. Introduction

IN PREVIOUS articles the principles for an extension of thermodynamics to general relativity have been presented,[1] and applications of the principles to several different problems have also been given.[2]

The new principles were first applied to problems in *static equilibrium*. For example in the case of a static gravitational field it was shown that the conditions for thermal equilibrium would necessitate a definite temperature gradient in order to prevent the flow of heat from regions of higher to those of lower gravitational potential.[3] And in the case of a static Einstein universe, it was shown that the concentration of matter in equilibrium with radiation, assuming their interconvertibility, would be the same as in flat space-time.[4]

The principles were then applied to non-static systems in which *reversible processes* take place. In contradiction to a familiar conclusion of classical thermodynamics, the possibility was found in relativistic thermodynamics for such processes to take place both at a finite rate and nevertheless re-

[1] Tolman, Proc. Nat. Acad. Sci. **14,** 268 (1928); ibid. **14,** 701 (1928); Phys. Rev. **35,** 875 (1930); ibid. **35,** 896 (1930).

[2] See references 3 to 8.

[3] Tolman, Phys. Rev. **35,** 904 (1930); Tolman and Ehrenfest, Phys. Rev. **36,** 1791 (1930).

[4] Tolman, Proc. Nat. Acad. Sci. **14,** 348, 353 (1928); ibid. **17,** 153 (1931).

versibly without increase in entropy, owing to an opportunity for correlated changes in entropy density and gravitational field not contemplated in the older thermodynamics. This possibility for reversible changes at a finite rate was illustrated by studies of three different systems,—a non-static universe filled solely with black-body radiation,[5]—a non-static universe filled with incoherent matter exerting no pressure,[6]—and a non-static universe filled with a mixture of monatomic gas in equilibrium with black-body radiation.[7] In all three cases it was shown that the systems could expand or contract at a finite rate and nevertheless reversibly without increase in entropy, the latter of the three, however, only under the special assumption that the gas remain in equilibrium with the radiation. It was also shown that the entirely reversible expansion of such universes would be accompanied by a number of phenomena, such as the outward flow of radiation, which are similar to processes that have ordinarily been interpreted as irreversible. Finally, the possibility for the periodic expansion and contraction of these systems was investigated, since any thermodynamic obstacles to such behaviour are evidently eliminated by the demonstrated reversibility.[8] It was found that no strictly periodic solutions for the equations of motion of such systems could exist, but that nevertheless quasi-periodic solutions would be possible such that the system would expand from zero proper volume to a maximum and return once more to the starting point without increase in entropy, the solution failing however at this exceptional point. It was emphasized, moreover, in view of the physics of the situation, that the return of such a system to zero volume without increase in entropy could be followed by a duplicate repetition of the expansion even though the over-idealized analysis fails to carry through the exceptional point of zero volume.

In contrast to these previous applications to systems which are in static equilibrium, and to non-static systems in which reversible processes are taking place, it is the purpose of the present article to apply the principles of relativistic thermodynamics to non-static systems in which *irreversible processes* take place. Such an extension in the range of application may have considerable interest for the interpretation of cosmological phenomena, since, even though it has been shown that reversible changes can take place at a finite rate in such a way as to give some phenomena which are similar to important ones in the actual universe, it is evident that reversible changes form only a limited class of the totality of conceivable thermodynamic processes.

The special task of this article will be to examine an essential change in point of view which becomes necessary when the effects of irreversible processes in isolated systems are to be studied by the new methods of relativistic thermodynamics. The necessity for the change arises primarily because of the well-known conclusion that the principle of the conservation of energy cannot hold in the mechanics of general relativity in the same simple form as in

[5] Tolman, Phys. Rev. **37,** 1639 (1931).
[6] This was discussed in connection with the work on periodicity; see reference 8.
[7] Tolman, Phys. Rev. **38,** 797 (1931).
[8] Tolman, Phys. Rev. **38,** 1758 (1931).

the classical mechanics. On account of this difference, we shall find in relativistic thermodynamics, that the possible increases in entropy which accompany the occurrence of irreversible processes in an isolated system are not subject to a limitation such as is imposed in the classical thermodynamics by a fixed constant value for the energy of the system. Indeed we shall find in relativistic thermodynamics a possibility for irreversible processes to take place in an isolated system without ever reaching a condition of maximum entropy and minimum free energy where further change would be impossible.

We may now proceed to the detailed examination of our problem. In the next section, §2, we shall first obtain some expressions, giving the dependence of entropy on the variables which determine the state of a system, in a form which will be suitable for our further work. These expressions will be derived by the methods of classical thermodynamics, but, in accordance with the principle of equivalence, will also be valid in relativistic thermodynamics when applied to an infinitesimal region using proper coordinates. With the help of these expressions, we can then explain in detail in §§3, 4 the reason why the failure of the principle of energy conservation in its old simple form does provide hitherto unsuspected possibilities for a continuous increase in the entropy of an isolated system without ever reaching an unsurpassable maximum. In §5 we shall then show that such possibilities could actually be realized in the case of a considerable class of non-static models of the universe. And in §6 we shall consider in more detail a particular one of these models which contains a mixture of monatomic gas and black-body radiation which do *not* remain in equilibrium, in other words a non-static model of the universe with possibilities for irreversible annihilation of matter instead of the reversible annihilation previously discussed. Finally in §7 we shall make a few remarks concerning the possible bearing of our findings on the phenomena of the actual universe.

§2. Dependence of Entropy on the State of a System

In the present section we shall obtain some expressions for the dependence of entropy on the state of a system which will be needed for our further work. The expressions will be obtained by the methods of the classical thermodynamics, which tacitly assumes flat space-time, and will be found to be valid in the curved space-time of general relativity only when applied to an infinitesimal region using proper coordinates.

We shall limit our consideration to simple systems, having uniform temperature, pressure and composition throughout, so that the state of the system can be completely specified by a statement of the energy E, volume v, and number of molecules $N_1 \cdots N_n$, of the different substances which the system contains. Since the entropy S of the system is a function of its state we can then evidently write in accordance with the principles of the differential calculus

$$dS = \frac{\partial S}{\partial E} dE + \frac{\partial S}{\partial v} dv + \frac{\partial S}{\partial N_1} dN_1 + \cdots + \frac{\partial S}{\partial N_n} dN_n. \tag{1}$$

For an infinitesimal change in energy and volume, however, keeping the composition constant, we have for the change in entropy the familiar expression

$$dS = \frac{1}{T}\,dE + \frac{p}{T}\,dv \tag{2}$$

which gives us for the partial differenials of entropy with respect to energy and volume the well-known values

$$\frac{\partial S}{\partial E} = \frac{1}{T} \quad \text{and} \quad \frac{\partial S}{\partial v} = \frac{p}{T} \tag{3}$$

where T and p are temperature and pressure, and substituting above can write our first equation in the more useful form[9]

$$dS = \frac{1}{T}\,dE + \frac{p}{T}\,dv + \frac{\partial S}{\partial N_1}\,dN_1 + \cdots + \frac{\partial S}{\partial N_n}\,dN_n. \tag{4}$$

Two other forms of this equation will also be useful. As an expression for the entropy of the system in terms of the Helmholtz free energy A we have by the equation of definition

$$S = \frac{E - A}{T} \tag{5a}$$

and in terms of the thermodynamic potential, or free energy F as used by chemists, we have

$$S = \frac{E + pv - F}{T} \tag{5b}$$

and by differentiation can write

$$dS = \frac{1}{T}\,dE - \frac{1}{T}\,dA - \frac{S}{T}\,dT \tag{6a}$$

and

$$dS = \frac{1}{T}\,dE + \frac{p}{T}\,dv + \frac{v}{T}\,dp - \frac{1}{T}\,dF - \frac{S}{T}\,dT \tag{6b}$$

Equating the expression for dS given by (4) with those given by (6a) and (6b), and solving for dA and dF, we then easily obtain

$$dA = -SdT - pdv - T\frac{\partial S}{\partial N_1}\,dN_1 - \cdots - T\frac{\partial S}{\partial N_n}\,dN_n \tag{7a}$$

and

$$dF = -SdT + vdp - T\frac{\partial S}{\partial N_1}\,dN_1 - \cdots - T\frac{\partial S}{\partial N_n}\,dN_n. \tag{7b}$$

[9] Allowing for the difference in notation this equation is entirely equivalent to a fundamental equation upon which Gibbs based his work on the equilibrium of heterogeneous substances. See his "Collected Works" Longmans, Green and Company (1928) Vol. I, Eq. (12), page 63.

Examining these equations, it is evident that if we regard the Helmholtz free energy A as a function of temperature, volume and composition, and the thermodynamic potential F as a function of temperature, pressure and composition we can write

$$\left(\frac{\partial A}{\partial N_i}\right)_{T,v} = \left(\frac{\partial F}{\partial N_i}\right)_{T,p} = -T\left(\frac{\partial S}{\partial N_i}\right)_{E,v}. \tag{8}$$

Where the subscripts indicate the independent variables, in addition to those giving the composition $N_1 \cdots N_n$, which are regarded as determining the quantities A, F, and S.

With the help of (8) we can now re-express our fundamental Eq. (4) in two further useful forms, giving us altogether the three expressions

$$dS = \frac{1}{T}dE + \frac{p}{T}dv + \left(\frac{\partial S}{\partial N_1}\right)_{E,v} dN_1 + \cdots + \left(\frac{\partial S}{\partial N_n}\right)_{E,v} dN_n \tag{9a}$$

$$dS = \frac{1}{T}dE + \frac{p}{T}dv - \frac{1}{T}\left(\frac{\partial A}{\partial N_1}\right)_{T,v} dN_1 - \cdots - \frac{1}{T}\left(\frac{\partial A}{\partial N_n}\right)_{T,v} dN_n \tag{9b}$$

$$dS = \frac{1}{T}dE + \frac{p}{T}dv - \frac{1}{T}\left(\frac{\partial F}{\partial N_1}\right)_{T,p} dN_1 - \cdots - \frac{1}{T}\left(\frac{\partial F}{\partial N_n}\right)_{T,p} dN_n \tag{9c}$$

§3. Limitation on Entropy Increase Imposed in Classical Thermodynamics by Conservation of Energy

With the help of these equations we can now see clearly the reasons why the classical thermodynamics has accustomed us to expect that the occurrence of irreversible processes in an isolated system would ultimately lead to a condition of maximum entropy and minimum free energy such that no further change would be possible.

For example, we could consider our isolated system either to be a coherent mass of solid or liquid situated somewhere in free space, or to be a mass of gas situated in free space and prevented from escaping by enclosure in an idealized container, having constant volume but otherwise adding nothing to the thermodynamic properties of the system of actual interest. We could then apply Eq. (9a) to analyze the increase in entropy which must accompany the occurrence of irreversible processes in such systems.

Considering the variables E, v, $N_1 \cdots N_n$, to be changed one at a time from their initial to their final values in order to calculate the increase in entropy ΔS which accompanies the change in state of the system, we should conclude that the first term on the right hand side of Eq. (9a) could contribute nothing to the increase in entropy, since we should have

$$\int \frac{dE}{T} = 0 \tag{10}$$

owing to the constant value of E for an isolated system prescribed by the classical principle of the conservation of energy; and we should also conclude that the second term could contribute nothing, since we should have

$$\int \frac{pdv}{T} = 0 \tag{11}$$

owing to the value of the pressure $p=0$ in the case of the coherent mass, and owing to the constant volume of the idealized container in the case of the gas. Hence we should be forced to the conclusion that the actual increase in entropy accompanying irreversible processes in our system could be calculated solely from the last terms in Eq. (9a) in accordance with the expression

$$\Delta S = \int \left[\left(\frac{\partial S}{\partial N_1} \right)_{E,v} dN_1 + \cdots + \left(\frac{\partial S}{\partial N_n} \right)_{E,v} dN_n \right]. \tag{12}$$

The possibilities for increase in entropy, however, provided by this last equation are limited, since for our isolated systems of constant energy it is evident that there is only a restricted range of possible adjustment for the variables N_1 to N_n which determine the composition. Hence when the most favorable adjustment has been reached the entropy will be at a maximum and further change cannot take place. In addition it is to be noted by comparing the equivalent forms (9a), (9b) and (9c), that in this final state of the system not only will the entropy be a maximum, but the Helmholtz free energy A will be a minimum for adjustments in composition at constant temperature and volume, and the thermodynamic potential or chemists' free energy F will be a minimum for adjustments in composition at constant temperature and pressure. It is by considerations such as these that the classical thermodynamics has led to the belief that the ultimate state of an isolated system would be a condition of maximum entropy and minimum free energy, where possibilities for further change or for the performance of useful work would no longer exist.

§4. Possibility Provided in Relativistic Thermodynamics for Removal of Limitation on Entropy Increase Imposed by the Conservation of Energy

We may now turn to an analysis of this same problem using the methods of relativistic thermodynamics. To carry this out, we cannot forthwith apply Eqs. (9) to our isolated system as a whole to calculate the entropy increases which accompany the irreversible processes that take place in it, since our reason for resorting at all to a relativistic treatment lies in the consideration that gravitational action in producing a deviation from the flat space-time of the classical theory may have an important effect on our results; and in the curved space-time of general relativity such quantities as the entropy, energy, and volume of a system need special interpretation.

In accordance with the principles of relativistic thermodynamics, however, which I have previously developed,[10] we can define the entropy of a finite system by the expression

[10] See reference 1, last article §3.

$$S = \iiint \phi_0 \sqrt{-g} \frac{dx_4}{ds} dx_1 dx_2 dx_3 \tag{13}$$

and by applying the second law of thermodynamics in its relativistic form obtain as a necessary condition for thermodynamic change in an isolated system

$$\frac{\partial S}{\partial x_4} = \iiint \frac{\partial}{\partial x_4} \left(\phi_0 \sqrt{-g} \frac{dx_4}{ds} \right) dx_1 dx_2 dx_3 \geqq 0 \tag{14}$$

where x_1, x_2 and x_3 are the spatial coordinates, x_4 is the time coordinate, ϕ_0 is the proper density of entropy as measured by a local observer, g is the determinant formed from the gravitational potentials, dx_4/ds is the ratio of increase in coordinate time to increase in proper time at the point in question, and the integration is to be taken over the whole range of spatial coordinates necessary to include the system.

The two signs of inequality and equality in the above expression refer respectively to the case of irreversible and reversible processes, and we may now limit ourselves to the former since our present interest lies in irreversible processes. Furthermore, for our present purposes it will be sufficient to consider cases where the general inequality given by (14) is satisfied by having the inequality

$$\frac{\partial}{\partial x_4} \left(\phi_0 \sqrt{-g} \frac{dx_4}{ds} \right) > 0 \tag{15}$$

itself hold at each point in our thermodynamic fluid.[11]

The physical interpretation of this expression can be made more evident, however, if we choose our coordinate system so that the thermodynamic fluid under consideration is everywhere at rest in the spatial coordinates x_1, x_2 and x_3. Since the macroscopic velocities dx_1/ds, dx_2/ds and dx_3/ds will then everywhere be zero, it is evident that the amount of fluid in any given coordinate range $\delta x_1\ \delta x_2\ \delta x_3$ will not be changing with the time; and in accordance with the principles of relativity we can write for the proper volume δv_0 of the small element of fluid in such a range the well known equation

$$\delta v_0 = \sqrt{-g} \frac{dx_4}{ds} \delta x_1 \delta x_2 \delta x_3 \tag{16}$$

and, by substituting above, rewrite expression (15) in the form

$$\frac{d}{dx_4} \left(\phi_0 \sqrt{-g} \frac{dx_4}{ds} \delta x_1 \delta x_2 \delta x_3 \right) = \frac{d}{dx_4} (\phi_0 \delta v_0) = \frac{dS_0}{dx_4} > 0 \tag{17}$$

[11] This has the effect of limiting our present considerations to cases where the proper entropy of each element of the fluid will be found increasing with the time when measured by a local observer, without reference to the flow of heat in or out of that element. (See expression 17). If flow of heat were taking place out of an element, we could have irreversibility even without an increase in the proper entropy of the element, but this will not be of interest for our present purposes since the later work of this paper will deal only with systems where there is no flow of heat. In any case there is of course no loss in rigour in using (15) since we are only interested now in having a *sufficient* condition for irreversibility.

We thus obtain as a sufficient condition for the occurrence of irreversible processes in our isolated system the very satisfactory result that the proper entropy, $S_0 = \phi_0\ \delta v_0$, of each element of fluid as measured by a local observer shall increase with the time.[12]

This simple condition, moreover, is now in a very satisfactory form for purposes of calculation since the proper entropy of a small element of the fluid will depend on its proper energy, $E_0 = \rho_{00}\delta v_0$, proper pressure p_0, proper temperature T_0, and number of molecules in the element $N_1 \cdots N_n$, in the same way as in the classical thermodynamics. Hence, by analogy with Eq. (4), we can now write

$$dS_0 = \frac{1}{T_0}\,dE_0 + \frac{p_0}{T_0}\,d(\delta v_0) + \frac{\partial S_0}{\partial N_1}dN_1 + \cdots + \frac{\partial S_0}{\partial N_n}\,dN_n \tag{18}$$

as an expression which gives the dependence of the proper entropy of our small element of fluid on the variables which determine its state. And our sufficient condition for irreversible processes will be met if the proper entropy of each small element of the fluid, as calculated with the help of Eq. (18), increases with the time.

At first sight it might appear as though Eq. (18) provided no more opportunity than our former classical Eq. (4) for a continuous increase in entropy without reaching an unsurpassible maximum corresponding to the most favorable values for the variables $N_1 \cdots N_n$. And from the classical point of view this would seem to be the case, since attempts to adjust the other variables E_0 and δv_0 so as to obtain a greater increase in entropy would appear to be of no avail, as the energy and volume of one element of the fluid would have to be increased at the expense of other elements.

In relativistic mechanics, however, it is well known that the principle of the conservation of energy does not hold in the simple form which would require a constant value for the total proper energy of an isolated system. The quantity analogous to energy which is actually conserved in relativistic mechanics is[13]

$$\int\int\int (\mathfrak{T}_4^4 + \mathfrak{t}_4^4)\,dx_1 dx_2 dx_3 = \text{const.} \tag{19}$$

where $\mathfrak{T}_4^4$ is the energy-momentum tensor-density and $\mathfrak{t}_4^4$ is the pseudo tensor-density of potential energy and momentum. In proper coordinates the first term of this expression reduces to proper energy

$$\mathfrak{T}_4^4 dx_1 dx_2 dx_3 = \rho_{00}\delta v_0 = E_0 \tag{20}$$

and the second term reduces to zero, but in general proper coordinates cannot be used throughout the whole system, and in general the total proper energy of an isolated system is not a constant in relativistic mechanics.

[12] Since an increment in proper time dt_0 and the corresponding increment in coordinate time dx_4 are both to be taken as having the same sign, the inequality (17) is also true for a local observer.

[13] See for example, Tolman, the third article in reference 1.

Hence in relativistic thermodynamics we must investigate the possibility that a continuous increase in the proper entropy of each element of an isolated system could be brought about by increases in the proper energy of the elements, without every reaching an unsurpassable maximum. In the next section it will be shown by an illustrative example, that this new possibility for the continuous occurrence of irreversible processes without reaching a final state of quiescence, might actually be realized in a way which is not trivial.

§5. Possibility for Continuous Increase in Entropy in a Non-Static Universe if the Cosmological Constant is Zero or Negative

a. The mechanics of the model.

As an isolated system to illustrate the possibility for the continuous occurrence of irreversible processes, we shall choose a non-static model of the universe filled with a homogeneous distribution of matter and energy.[14] The line element for such a non-static universe can be derived[15] by treating the contents of the model for purposes of large scale considerations as a perfect fluid, and written in the form

$$ds^2 = -\frac{e^{g(t)}}{[1 + r^2/4R^2]^2}(dr^2 + r^2d\theta^2 + r^2 \sin^2\theta d\phi^2) + dt^2 \qquad (21)$$

where r, θ and ϕ are the spatial coordinates, t is the time coordinate, R is a constant, and the dependence of the line element on the time is given by the exponent $g(t)$.

With this choice of coordinates, particles at rest in the coordinate system will not be subject to acceleration but will remain permanently without spatial velocity. Hence the choice of coordinate system is such that we may regard the thermodynamic fluid filling the model as macroscopically at rest with respect to the spatial coordinates, and can apply expressions (17) and (18) of the preceding section to the entropy of any small element of this fluid. For the proper volume of a small element of the fluid contained in the coordinate range $\delta r\ \delta\theta\ \delta\phi$, we may evidently write

$$\delta v_0 = \frac{e^{3g/2}}{[1 + r^2/4R^2]^3} r^2 \sin\theta \delta r \delta\theta \delta\phi \qquad (22)$$

and this in general will be changing with the time, if $g(t)$ is not a constant. In accordance with the above, however, the contents of the element will not be affected by any net flow of particles across its boundaries.

Of the possible non-static models which could agree with the line element (21), the special class which will illustrate our considerations will be obtained if the constant R occurring in the line element is real, and the cosmological constant Λ occurring in Einstein's relation between the energy-momentum

[14] For a partial historical account of various treatments which have been given to the non-static line element for the universe, see Tolman, Proc. Nat. Acad. **16,** 582 (1930).

[15] See Tolman, Proc. Nat. Acad. Sci. **16,** 320 (1930).

tensor and the curvature of space-time is not a positive quantity. If R is real the "radius" of the model $Re^{g/2}$ will be real and the universe closed. As to the cosmological constant Λ, our only experimental evidence is that it must be small enough not to affect phenomena in the solar system. If we take it zero the equations of relativistic mechanics are somewhat simplified, but there is one point in our later development where a small negative value might seem preferable. These restrictions, R real and $\Lambda = 0$ or $\Lambda < 0$, will be adopted in what follows.

We are now ready to consider the behaviour of this class of non-static models. Taking the material filling the model as a perfect fluid of proper macroscopic density ρ_{00} and proper pressure p_0, the components of the energy-momentum tensor corresponding to the line element (21) have been worked out,[16] and with $\Lambda = 0$ give for the pressure and density the values

$$8\pi p_0 = (-8\pi T_i^i) = -\frac{1}{R^2}e^{-g} - \ddot{g} - \tfrac{3}{4}\dot{g}^2 \qquad i = (1, 2, 3)$$

$$8\pi\rho_{00} = (8\pi T_4^4) = \frac{3}{R^2}e^{-g} + \tfrac{3}{4}\dot{g}^2 \tag{23}$$

together with

$$T_\mu^\nu = 0 \qquad (\mu \neq \nu)$$

where the dependence of the pressure and density on the time is given through their dependence on the exponent $g(t)$ and its first and second time derivatives $\dot{g}$ and $\ddot{g}$. Furthermore, substituting the expressions for T_μ^ν in the fundamental equation of relativistic mechanics, which for this purpose can be expressed most conveniently in the form

$$\frac{\partial \mathfrak{T}_\mu^\nu}{\partial x_\nu} - \tfrac{1}{2}\mathfrak{T}^{\alpha\beta}\frac{\partial g_{\alpha\beta}}{\partial x_\mu} = 0 \tag{24}$$

we obtain[17] for the case $\mu = 4$

$$\frac{d}{dt}\left[\frac{\rho_{00}e^{3g/2}}{(1 + r^2/4R^2)^3}\right] + p_0\frac{d}{dt}\left[\frac{e^{3g/2}}{(1 + r^2/4R^2)^3}\right] = 0 \tag{25}$$

which, since r and R are independent of t, can also be written in the simple form,

$$\frac{d}{dt}(\rho_{00}e^{3g/2}) + p_0\frac{d}{dt}(e^{3g/2}) = 0 \tag{26}$$

and in addition by noting the expression for proper volume given by (22), can be written in the specially illuminating form

$$\frac{d}{dt}(\rho_{00}\delta v_0) + p_0\frac{d}{dt}(\delta v_0) = 0. \tag{27}$$

[16] See reference 15, Eqs. (34).

[17] See Tolman, Proc. Nat. Acad. Sci. **16**, 409 (1930), Eq. (4).

This last form shows that, as the exponent g changes with the time, the behaviour of each element of the fluid is such that its increase in proper energy can be regarded as the work done on it by its surroundings. In other words as time proceeds each element of the fluid may be regarded as subjected to an adiabatic[18] expansion or compression, according as g is increasing or decreasing with the time.

We can also obtain information as to the behaviour of the model as a whole over long periods of time. Solving for $\ddot{g}$ the equation for pressure given by (23), we obtain

$$\ddot{g} = -\frac{1}{R^2}e^{-g} - \tfrac{3}{4}\dot{g}^2 - 8\pi p_0. \tag{28}$$

Since R is real by hypothesis and the pressure p_0 could not be negative for the kinds of fluid with which we shall wish to regard the universe as filled, we see that the acceleration $\ddot{g}$ would always be negative, and hence, if the model were expanding, that g and the "radius" $Re^{g/2}$ would ultimately reach maximum values and the model would start contracting. The only possible exception to such behaviour would perhaps be a special case in which g would become infinite and g and p_0 zero at the upper limit.[19] Even this possibility, however, could be ruled out, by ascribing a small negative value to the cosmological constant Λ, since the equation corresponding to (28) when Λ is not omitted reads[20]

$$\ddot{g} = -\frac{1}{R^2}e^{-g} - \tfrac{3}{4}\dot{g}^2 - 8\pi p_0 + \Lambda \tag{28a}$$

and with Λ a negative constant, the acceleration would always be negative even if g went to infinity and g and p_0 to zero.

After the model has passed its point of maximum expansion, then in accordance with (28) the negative acceleration would get greater and greater and the contraction would continue at an increasing rate to zero proper volume with $g = -\infty$ and the "radius" $Re^{g/2} = 0$. The equations of motion fail to carry us through this exceptional point, perhaps because of an over idealization of the model.[21] From a physical point of view it is evident, however, that this contraction to the lower limit could only be followed by renewed expansion.[22]

We thus see that relativistic mechanics appears to provide within its framework conceivable models of non-static universes which would undergo a continued succession of expansions and contractions. In any case we shall assume this possibility in what follows.

[18] Note that in English usage the word "adiabatic" applies to a change in state with no flow of heat into the system, without reference to whether the change is a reversible or irreversible one.

[19] In a later paper my colleague Professor Morgan Ward and I hope to show that this exceptional case would not occur even with the cosmological constant Λ exactly equal to zero.

[20] See reference 15, Eqs. (34).

[21] Compare, Einstein, Berl. Ber., 1931, p. 235.

[22] Compare, Tolman, reference 8.

b. The thermodynamics of the model.

We must now inquire into the thermodynamics of such models, since from the classical point of view we have become accustomed to the idea that there must be some thermodynamic hindrance to such a continued succession of expansions and contractions in an isolated system. From the relativistic point of view, however, it appears that no such hindrance could exist, since we were led to the conclusion that the series of expansions and contractions would take place solely from the fact that the expressions (28) – (28a) prescribe a negative value for the acceleration $\ddot{g}$ so that expansion will always be followed by contraction. And, if we fill our model by hypothesis with a material that cannot exert a negative pressure,[23] it is evident that this negative value of $\ddot{g}$ would obtain without reference to the thermodynamic nature of the reversible or irreversible processes taking place inside the model.

It hence appears in general that relativistic thermodynamics could not impose restrictions which would prevent such a series of expansions and contractions. It will also be of interest, however, to analyze the thermodynamics of our model in somewhat more detail.

In the first place, it is of course immediately evident that there would be no restriction imposed on the succession of expansions and contractions provided they took place reversibly without increase in entropy, since the model would then arrive at the lower limit of contraction with unchanged entropy, and a renewed expansion identical with the previous one could be initiated. Such behaviour, which becomes of interest since relativistic thermodynamics provides new possibilities for reversible changes at a finite rate,[24] has already been discussed in a previous article.[25]

In the present article, however, we are primarily interested in any thermodynamic hindrance to the succession of expansions and contractions which might arise because of irreversible processes. To analyze this point we may best consider the behaviour of a small element of the fluid which we take as filling our model. In accordance with Eq. (27) as $g(t)$ increases and decreases with the time, such an element would be subjected to a series of adiabatic expansions and compressions without flow of heat from the outside and with perfect balance between internal and external pressure, because of the uniformity of p_0 throughout the model. Irreversibility with its accompanying increase in entropy could arise, however, on account of internal changes within the element, and in general this would presumably occur since the expansions and contractions would take place at a finite rate, and the internal variables, in our case the quantities $N_1 \cdots N_n$ which determine the composition of the fluid, would adjust themselves to the changing volume with a certain lag behind the condition of equilibrium, thus leading to an increase in the entropy of the element.

It is evident, however, that such behaviour would provide nothing which

[23] Note that the non-negative pressure would be necessary only in the last stages of expansion.

[24] Reference 5.

[25] Reference 8.

would make the continued expansion and contraction impossible. Except for the absence of friction and the balance between internal and external pressure, the behaviour of the fluid in the element is similar to the classical behaviour of a fluid placed in a cylinder with non-conducting walls and subjected to a series of compressions and expansions with the help of a movable piston. Classically the entropy of the fluid would increase because of the lag in the adjustment of the internal variables determining the state of the system behind their equilibrium values. And this increase in entropy would continue as long as the expansions and contractions were continued, without of itself preventing us from subjecting the fluid to further expansions and contractions, provided we have the desire to do so and the mechanical energy which may be needed to move the piston. Similarly in the relativistic case, if the equations of relativistic mechanics do inevitably prescribe a continued succession of expansions and contractions for a particular class of non-static models of the universe, it is evident that the occurrence of irreversible processes inside the model furnishes no thermodynamic preventive to such behaviour.

Before turning from this general discussion of the thermodynamic behaviour of the class of models under consideration to the discussion of any special model, it will also be of interest to analyze somewhat more in detail the mechanism by which entropy increases occur in the elements of our fluid, and show a general type of relation which exists between the entropy content and energy content of an element. In accordance with Eq. (18) we can write for the rate with which the entropy of any given element is increasing with the time

$$\frac{dS_0}{dt} = \frac{1}{T_0}\frac{dE_0}{dt} + \frac{p_0}{T_0}\frac{d(\delta v_0)}{dt} + \left(\frac{\partial S_0}{\partial N_1}\right)\frac{dN_1}{dt} + \cdots + \left(\frac{\partial S_0}{\partial N_n}\right)\frac{dN_n}{dt}. \tag{29}$$

It is evident from this that the immediate occasion for the entropy increase taking place at any given time in an element must lie in the changes taking place in the variables $N_1 \cdots N_n$, which determine the composition, since for the first two terms above we can write

$$\frac{1}{T_0}\frac{dE_0}{dt} + \frac{p_0}{T_0}\frac{d(\delta v_0)}{dt} = 0 \tag{30}$$

owing to the adiabatic character of the change given by Eq. (27). The changes in the variables $N_1 \cdots N_n$, however, can contribute to a positive rate of entropy increase since they will occur in the direction towards equilibrium under conditions where the partial differentials $((\partial S_0/\partial N_1 \cdots \partial S_0/\partial N_n)$ do not have their equilibrium values. For example if the fluid were a mixture of diatomic gas and the elements, into which it dissociates in accordance with the reaction

$$A_2 = 2A \tag{31}$$

and the rate of expansion were too great for the dissociation to keep pace, we should have A_2 breaking up into $2A$ under non-equilibrium conditions and

this would lead to an increase in entropy. We thus see that the immediate mechanism by which the entropy increase actually takes place is through the adjustment of the internal variables $N_1 \cdots N_n$ which determine the composition.

On account of this fact that the actual mechanism of entropy increase lies in the adjustment of composition, it might at first sight be supposed that the continuous increase in entropy would require no change in the energy of the element. In the long run, however, this is not the case. Let us consider the condition of an element of the fluid at two different instants t_1 and t_2 which are a long time apart so that there has been a very great increase in its entropy, and for simplicity let us pick t_2 such that $g(t)$ for the universe and δv_0 for the element have their earlier values. We could then use Eq. (18)

$$dS_0 = \frac{1}{T_0} dE_0 + \frac{p_0}{T_0} d(\delta v_0) + \frac{\partial S_0}{\partial N_1} dN_1 + \cdots + \frac{\partial S_0}{\partial N_n} dN_n \tag{32}$$

to calculate the difference in entropy of the two states, by considering the effect of changing the variables one at a time from their initial to their final values. If the increase in entropy has been large it is then evident that the proper energy E_0 will have to be greater in the final state than in the initial state, since δv_0 is taken the same in the two states, and the adjustment of the composition at constant E_0 and δv_0 could only lead, as already discussed in §3, to a limited increase in entropy.

We hence conclude that in the long run we must expect the proper energy of each element of the fluid filling the model to increase with the time. The mechanism by which this occurs will of course have to lie in a general tendency for the pressure p_0 to be on the average greater during a compression than it was during the preceding expansion. This, however, is in qualitative accord with the behaviour that we should expect if the composition lags in adjusting itself to equilibrium. We thus see that although the actual mechanism of entropy increase lies in the adjustment of composition, which sometimes takes place in one direction and sometimes in the other according as conditions are changed, nevertheless in the long run the continued increase in entropy involves and is made possible by an increase in proper energy.

The possibility for such an increase in proper energy is, as discussed in §4, a characteristic feature of relativistic as distinguished from classical mechanics. For example let us return once more to our comparison between the classical behaviour of a fluid placed in a cylinder with non-conducting walls and subjected to a series of expansions and contractions, and the relativistic behaviour of an element of the fluid in our expanding and contracting universe. From the classical point of view, it would not be the increase in the entropy of the fluid in the cylinder *per se*, which would prevent us from subjecting it to further expansions and compressions, but the fact that ultimately we should expect to have no further external mechanical energy available for completing another compression. In the relativistic case, however, the laws of mechanics do not require any constancy in the total supply of proper energy. Indeed in accordance with Eq. (27),

$$\frac{d}{dt}(\rho_{00}\delta v_0) + p_0 \frac{d}{dt}(\delta v_0) = 0 \tag{33}$$

if p_0 is positive, the proper energies of *all* elements of the fluid are decreasing when the model is expanding and increasing when it is contracting, and hence in the long run there can be a tendency for the total proper energy to increase, if the pressure on compression tends to be higher than on expansion.

Noting the expressions for proper volume and proper density of energy given by (22) and (23), it is evident that the proper energy of each element of the fluid and the total proper energy of the model will be proportional to

$$8\pi\rho_{00}e^{3g/2} = \frac{3}{R^2}e^{g/2} + \tfrac{3}{4}e^{3g/2}\dot{g}^2. \tag{34}$$

Hence in a long series of expansions and contractions we must expect $g(t)$ and the "radius" of the model $Re^{g/2}$ to become greater and greater at succeeding times when the velocity g has the same values, for example at succeeding points of maximum expansion. Similarly for succeeding points where $g(t)$ and the "radius" $Re^{g/2}$ have their earlier values we must expect the velocities $\dot{g}$ to get greater. This permits a rough plot of the "radius" $Re^{g/2}$ against the time for any model of the class under consideration—the upper limit of the "radius" to which the model expands gradually getting greater and greater, and its rate of change at a given value also getting greater.

§6. Model of Non-Static Universe with Irreversible Annihilation of Matter

In a previous paper[26] I have treated a non-static model of the universe, containing a mixture of perfect monatomic gas and black-body radiation, which were taken to be capable of conversion one into the other. Making the hypothesis that equilibrium was maintained between the matter and radiation, it was shown that such a model could expand or contract reversibly at a finite rate, with a reversible annihilation of matter (i.e., conversion into radiation) during expansion and a reversible formation of matter during compression. With the help of our present considerations, we may now treat such a non-static model, on the perhaps more probable hypothesis that the interconversion does not have a high enough rate to maintain equilibrium—in other words, a non-static model of the universe with the possibility for *irreversible* annihilation of matter.

In such a model if we start expanding from a point at which the matter and radiation are at their equilibrium concentrations, or better pass through such a point in the course of an expansion, then as the expansion continues matter will tend to go over into radiation,[27] and, if this cannot take place rapidly enough to maintain equilibrium concentrations, irreversibility will re-

[26] Reference 7.

[27] See Eqs. (36) and (38), reference 7. We pick for our illustration a case where the temperature does not have the extremely high values where formation of matter accompanies expansion.

sult and the changes of matter into radiation that do occur will be accompanied by an increase in entropy. In accordance with our general treatment of the mechanics of this class of models, the expansion will continue to a maximum point where contraction will set in. As the contraction proceeds, the matter will still be for a time in excess of its equilibrium concentration and will continue to change into radiation, thus making the pressure higher on the return path than at the same volume during the expansion. As the contraction proceeds still further, however, a point will be reached where we again pass through new equilibrium values for the concentrations, immediately followed by conditions such that radiation will now be going over into matter irreversibly with increase in entropy, the actual pressure of the radiation being now higher than would correspond to equilibrium. We thus see in a general way the mechanism by which increase in entropy and increase in proper energy would take place in such a model.

We may also draw certain conclusions as to the long range behaviour of the model. For the proper entropy S_0 of an element δv_0 of the fluid filling the model, we may evidently write the sum of the entropies of the gas and radiation in the element

$$S_0 = \frac{3}{2} Nk \log T_0 + Nk \log \frac{\delta v_0}{N} + Nk \log be^{5/2} + \frac{4}{3} aT_0^3 \delta v_0 \tag{35}$$

where N is the number of atoms in the element, k is Boltzmann's constant, a is Stefan's constant, and b is a constant of the right magnitude to assure the same starting point for the entropy of the gas and the radiation when their interconversion is to be considered, the form of the term containing b being chosen in such a way as to give a simple form to the expression for the equilibrium concentration of gas, which can be shown to be[28]

$$\frac{N}{\delta v_0} = bT_0^{3/2} e^{-mc^2/kT_0} \tag{36}$$

where m is the mass per atom and c is the velocity of light.

By using the ordinary methods for determining a maximum, it can easily be shown from Eq. (35) that at a given temperature T_0 and a given volume δv_0, the proper entropy S would have its maximum possible value with the composition

$$N = be^{3/2} T^{3/2} \delta v_0 \tag{37}$$

And substituting this value into (35) we obtain in general for the proper entropy of an element

$$S_0 \leqq \left(bke^{3/2} T_0^{3/2} + \frac{4}{3} aT_0^3 \right) \delta v_0 . \tag{38}$$

In accordance with our hypothesis of irreversibility, however, we must expect

[28] See Eqs. (12) and (13), reference 7.

the entropy of any given element of the fluid to increase ultimately without limit. Hence we can conclude from (38) that in a long series of expansions and contractions, the proper temperature and thus also the proper energy of any given element will be greater and greater at times when the volume of the element and "radius" of the model return to their earlier values; and *vice versa* that the volume and "radius" will become greater when the temperature returns to its earlier value. This is in agreement with our more general considerations in the preceding section.

§7. Conclusion

The main purpose of this article has been a further examination of the bearings of relativistic thermodynamics on the well known problem of the entropy of the universe as a whole. The work has again illustrated the necessity of using relativistic rather than classical thermodynamics in treating this problem, and has demonstrated that the framework of general relativity at least provides a class of conceivable models of the universe which would undergo a continued series of expansions and contractions without being brought to rest by the irreversible processes which accompany these changes. The findings of relativistic thermodynamics thus stand in sharp contrast to the familiar conclusion of the classical thermodynamics that the continued occurrence of irreversible processes would lead to an ultimate condition of maximum entropy and minimum free energy where change would cease.

Attention has also been given to a somewhat special non-static model of the universe containing a uniform distribution of matter and radiation which by hypothesis could be converted one into the other. Such a model would undergo a succession of expansions and contractions and would provide possibilities in the later stages of expansion for the irreversible transformation of matter into radiation, and in the later stages of contraction for the irreversible transformation of radiation back into matter, without ever being brought to rest by thermodynamic obstacles. The result is of interest in connection with the annihilation or transformation of matter into radiation which the astrophysicists believe to be taking place in the actual universe.

It should perhaps be emphasized again, however, as I have previously done, that at present we discuss only very highly idealized models of the universe, partly on account of mathematical difficulties, and partly on account of the limited range of our observational knowledge which at best extends to some 10^8 light-years. For example the hypothesis of roughly uniform conditions throughout the whole universe at a given time, which is assumed in the derivation of the non-static line element for the universe, can be justified only on the grounds that it introduces simplification into the mathematics, and that we have at present no observational knowledge to the contrary. For reasons such as these we must not be too dogmatic in our assertions as to the actual universe. The important thing at the present time is to investigate the properties of the highly simple and abstract models that we can treat, in order to gain ideas as to the general kind of phenomena that could conceivably be present in the actual universe.

THE FERROMAGNETIC SYMPOSIUM AND CONFERENCE AT THE SUMMER MEETING OF THE AMERICAN PHYSICAL SOCIETY AT SCHENECTADY, SEPTEMBER 12, 1931

APROPOS of the Faraday-Henry centenary celebration of the Society at Schenectady, the program committee appointed a sub-committee to arrange for a Magnetic Symposium. The interaction of ideas resulted in the plan for a symposium in the morning to be followed by a conference lasting through the afternoon for those more directly and intimately interested in ferromagnetics. The sub-committee has drawn up a detailed report covering its experience and the new ideas gained, and has sent copies to various officers of the Society. Here the sub-committee is submitting the two papers presented at the Symposium followed by abstracts of the conference papers, together with the discussion on them. The sub-committee feels that the space required for this will have been well used if, as a result, there is an increased use of the conference method at American Physical Society Meetings.

The sub-committee

F. BITTER
R. M. BOZORTH
L. W. MCKEEHAN
L. TONKS, *chairman*

ON THE INTERPRETATION OF SOME FERROMAGNETIC PHENOMENA

An Address presented before the Symposium on Ferromagnetism at the Meeting of the American Physical Society, Schenectady, New York, September 12, 1931

BY FRANCIS BITTER

WESTINGHOUSE RESEARCH LABORATORIES, EAST PITTSBURGH, PENNSYLVANIA

DURING these first years of the twentieth century our knowledge of ferromagnetism has made great progress. In the first place we have learned empirically how to make those magnetic materials which are the foundation of the countless electrical circuits woven around the earth. Instruments have been built to work equally well under most varied conditions—at the equator and near the poles, in damp cellars and on the desert. Materials are available that will respond to the enormous forces produced by generators in power stations, and to the faint current signal produced by sounds thousands of miles away. And in the second place we are beginning to learn something of the mechanisms which are responsible for the existence of ferromagnetism and for the various phenomena associated with it. It remains one of the important tasks of the future to link together these two avenues of progress so that we may not only produce, but also understand how we produce the materials which we use, and so that we may have an intimate knowledge of the actual complex physical world around us and use it to check and clarify the fundamental laws of science. In the following I shall outline some of our present knowledge of ferromagnetism, and indicate a few places where progress along the above lines is to be expected.

Starting from the conception that magnetic materials are made up of elementary atomic magnets in thermal interaction, and that magnetization results from their reorientation, the

classical theory, with modifications introduced by quantum considerations, leads to an expression relating the magnetization, the absolute temperature, and the field of the form

$$\frac{I_w}{I_0} = \tanh \frac{\mu_B}{KT}(H + N_w I_w) \tag{1}$$

I_w is the Weiss magnetization, or that value which satisfies Eq. (1). The subscript is used to differentiate it from the observed magnetization I of actual samples. I_0 is the absolute saturation, K is the Boltzmann constant, μ_B is a Bohr magneton, and N_w is a proportionality factor called the Weiss molecular field constant. The above equation states that I_w even for $H=0$ is different from zero up to a critical temperature $T=\theta$, or the Curie point. I_w for $T<\theta$ and $H=0$ is called the spontaneous magnetization. The dependence of I_w on H for temperatures below and not too near θ is slight because the term $N_w I_w$ is large compared to those values of H which can be obtained in the laboratory. If an entire sample is uniformly magnetized in one direction, then $I_w=I$. If, on the other hand, spontaneous magnetization occurs in regions, and I_w has different orientations in different parts of a sample, it will be found that $I<I_w$. A study of the constant N_w in the light of recent developments in atomic theory has led to the following conclusions: that the magnetic moments associated with electron spins are almost exclusively responsible for the magnetization of ferromagnetic bodies, (this has been substantiated by the Barnett and Einstein-de Haas effects, and by x-ray investigations) and that the spin interactions are responsible for the Weiss molecular field, or in other words, for spontaneous magnetization. Obviously the model on which Eq. (1) is based is much too crude. The only disposable constants are I_0 and N_w, and it is hardly to be expected that by varying these alone all the complexity of ferromagnetic phenomena can be reproduced. It is, nevertheless, surprising how far we can go. For numerical comparisons it is convenient to rewrite Eq. (1) with $H=0$ in the form

$$\frac{I_w}{I_0} = \tanh\left(\frac{I_w}{I_0}\,\frac{\theta}{T}\right) \tag{2}$$

$$\theta = \frac{\mu_B N_w I_0}{K}$$

and to deduce for the initial susceptibility in the paramagnetic state, $T>\theta$

$$K_0 = \left(\frac{\partial I_w}{\partial H}\right)_{H=0}$$

$$\frac{1}{N_w K_0} = \frac{T}{\theta} - 1. \tag{3}$$

A peculiar difficulty arises from the fact that experimentally the conditions at the critical point are found to be rather involved, and it is consequently difficult to decide on any one temperature as the one which is meant by θ in Eqs. (2) and (3). A plausible procedure is to use Eq. (3) to find θ, and use this same θ, called the paramagnetic Curie point, or θ_p, to check Eq. (2). The first part of this program has been carried out in Fig. 1 for nickel and cobalt. The theoretical curve is the heavy line having unit slope. The experimental data contain a certain amount of contradictory evidence. A fairly thorough review, however, indicates that the most probably correct results are those plotted. For a reasonable range of temperatures not too close to the Curie point the observations do lie along a straight line which has, however, a smaller slope than is to be expected on the basis of Eq. (3). The dotted lines indicate the deviations that are usually observed near the critical temperature. As a rule the paramagnetic susceptibility is independent of the field strength, but near the Curie temperature this is no longer true, and observations in small fields should be instructive. In plotting Fig. 1, the value of θ_p used for cobalt was 1413° and is between the values found by Bloch and Preuss, namely 1411°K and 1415°K respectively. For Ni the value 650°K was used.

The experimental points for iron, shown in Fig. 2, reveal much the same conditions as those found in nickel and cobalt. The occurrence of the γ-phase makes the determination of the relationship between K_0 and T rather difficult, especially since it appears that the true con-

dition is perhaps not represented by a straight line. This point is of especial interest in connection with an article by Dehlinger[1] on the transformation points, A_3 and A_4, of iron to which the reader is referred for further discussion. The values of θ_p used in plotting Fig. 2 were those used by the authors; Terry, 1043°K; Weiss and Foex, 1043°K; and Ishiwara 1048°K. This is done because it is not easy to see from the above data how a revision had best be made. Ishiwara's points might be taken to lie on a straight line having an intercept slightly above $T/\theta=1$, but the other results do not support the correctness of drawing a straight line from the γ through the α range. Further experimental work is needed to clear up the situation.

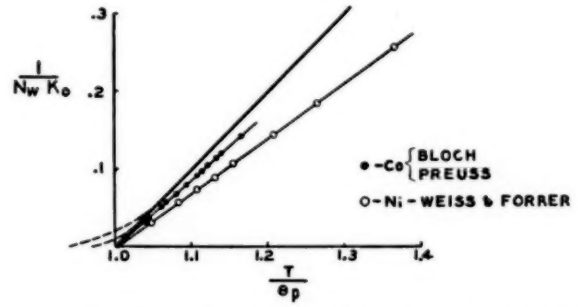

Fig. 1. The reciprocal of the initial susceptibility times the Weiss molecular field constant is plotted as a function of the reduced temperature. The heavy line is the theoretical curve expressed in Eq. (3). The experimental points are taken from O. Bloch, Thesis, Zürich, 1912; A. Preuss, Thesis, Zürich, 1912; P. Weiss and R. Forrer, Ann. de Physique **5**, 153 (1926).

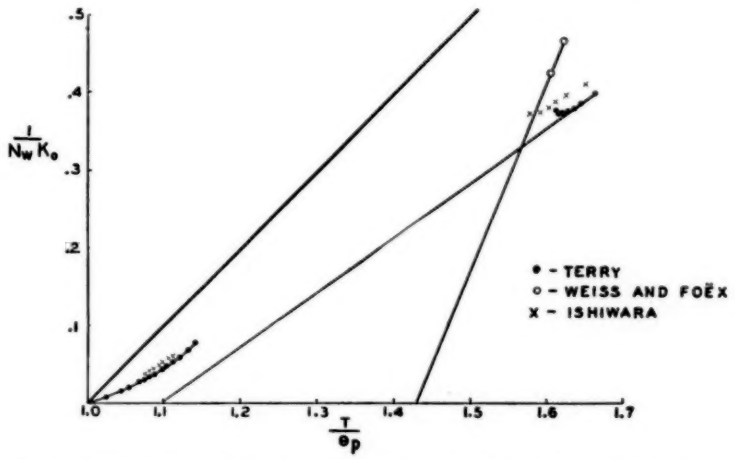

Fig. 2. The experimental points are for iron and are taken from E. M. Terry, Phys. Rev. **9**, 255, 394 (1917); T. Ishiwara, Sci. Rep. **6**, 133 (1917); P. Weiss and G. Foëx, Jour. de Physique **40**, 744 (1911). See Fig. 1 for an explanation of the symbols used.

With critical temperatures determined as above, observational data bearing on Eq. (2) have been plotted in Fig. 3. Near the critical temperature all the points lie below the theoretical curve. This is most probably due to the fact that in the fields used $I<I_s$. In the intermediate temperature range pyrrhotite and magnetite seem definitely to follow some other law; nickel and cobalt (the latter has a face-centered cubic lattice in this region) follow the curve very well indeed; iron shows a distinct departure from the theoretical curve which may be partly due to a too low estimate of θ. Most probably, however, the discrepancy is real, and has its roots some-

[1] U. Dehlinger, Zeits. f. Physik **65**, 535 (1931).

where in the statistics of atomic interactions. At low temperatures none of the observed points lie on the theoretical curve. In Fig. 4 the results have been replotted on a larger scale in which the square of the reduced temperature is used to bring out the linear relationship between T^2 and I_w at low temperatures. Curve 1 represents the classical equation in which the Langevin function $L(x)$ appears, and curve 2 represents Eq. (1). Weiss and Forrer, whose data are plotted in Fig. 4, emphasized the linear relationship here indicated. In addition it should be noticed that when plotted in this way the results for the cubic lattices fall together into one

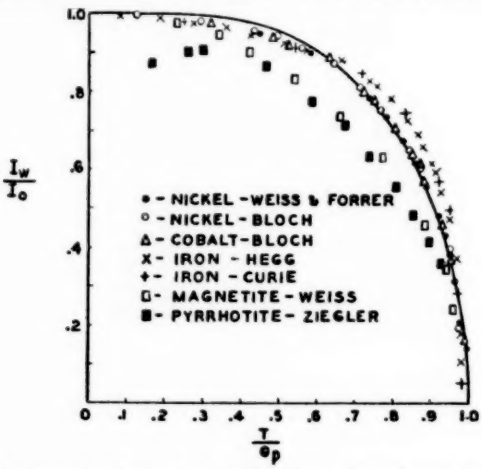

Fig. 3. The reduced saturation intensity is plotted as a function of the reduced temperature. The experimental results are taken from the papers referred to in Figs. 1 and 2, and from F. Hegg, Thesis, Zürich, 1910; P. Curie, Ann. de Chim. et de Phys. **5,** 289 (1895), P. Weiss, Jour. de Physique **6,** 661 (1907); and Zeigler, Thesis, Zürich, 1915.

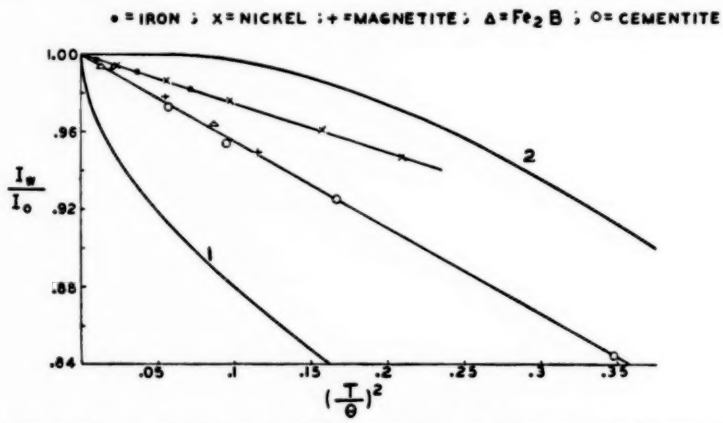

Fig. 4. The reduced saturation intensity is plotted as a function of the square of the reduced temperature. The experimental points are taken from P. Weiss and R. Forrer, Ann. de Physique **12,** 279 (1929).

group, and those for the non-cubic orthorhombic lattices into another. As for cobalt and pyrrhotite at low temperatures, in which range both have hexagonal lattices, the comments made below will make clear that saturation is difficult to obtain except in the direction of easy magnetization. It would be of great interest to make observations on single crystals in this direction and determine whether the dependence on crystal form indicated above may be extended. A difficulty that would be encountered in plotting the data is that the Curie temperature of hexagonal cobalt is not known.

One of the outstanding problems connected with the part of the theory outlined above is that of determining the magnetic moment of the ferromagnetic atoms. Two methods have been used, the first being based on measurements of I_0, the absolute saturation, the second being based on observations of the slope of the susceptibility curves above the Curie point. These methods were found to give different results, and led to the adoption of the Weiss magneton as an experimental unit of magnetic moment. Recently Wolf[2] has shown that by assuming several states to exist simultaneously within a ferromagnetic crystal the experimental results can be satisfactorily accounted for without making use of other magneton numbers than those indicated by spectral analysis. The arrangement of atoms in different excited states in a solid is most probably influenced by impurities and strains, which may account for the discrepancies which exist between various observations of the quantities discussed above. Now that delicate methods are available for controlling and observing the condition of a piece of metal it should be possible to delve further into the questions raised by Wolf's paper by studying those factors which influence I_w and K_0.

While the above model is in many ways adequate and promising, it absolutely fails in one important respect. The presence of the applied magnetic field H next to the "molecular field" $N_w I_w$, which is of a much larger order of magnitude, makes Eq. (1) effectively independent of the applied field. In other words, there exists only spontaneous magnetization, and no magnetization as a function of H. The way around this difficulty, as has already been suggested, is to assume that Eq. (1) applies to small regions only. What the size and shape of these regions are to be, need for the present not be specified. Each one is to be capable of orienting its magnetization independently. The energy as a function of orientation depends on the crystal structure and the strains, and in the absence of strains assumes the following especially simple forms for single crystals[3]

$$E_{\theta,H} = K(I_{wx}^2 I_{wy}^2 + I_{wy}^2 I_{wz}^2 + I_{wz}^2 I_{wx}^2) - (\vec{I}_w \cdot \vec{H}) \tag{4}$$

$$= K_1 I_{wx}^2 + K_2 I_{wy}^2 + K_3 I_{wz}^2 - (\vec{I}_w \cdot \vec{H}). \tag{5}$$

Eq. (4) applies to cubic crystals, and Eq. (5) to hexagonal crystals. The direction in which the regions are magnetized is given by the absolute minima of $E_{\theta,H}$. If two or more equal minima exist it is convenient to assume that they are equally occupied. These statements form a perfectly definite set of rules for constructing magnetization curves, and even if they are somewhat over-simplified, it will be found useful to apply them as suggested. The chief difficulties will appear whenever $E_{\theta,H}$ has two or more minima of almost equal depth. The above rules say that only the lowest is occupied, whereas in truth this is the case only after the difference exceeds a certain value, and even then only if the intervening maxima are not too high. This is, then, a theory of magnetization in the absence of hysteresis, and as we shall apply it to single crystals, in which hysteresis effects are known to be slight, we may expect fair agreement.[4]

It is convenient, in plotting the magnetization curves derived from Eqs. (4) and (5), to introduce a reduced field, h, given by

$$\frac{H}{h} = \frac{K I_w^3}{8} \tag{6}$$

for cubic crystals, and

$$\frac{H}{h} = 2I_w(K_2 - K_1) \tag{7}$$

for hexagonal crystals, two of the three coefficients K_x being chosen equal, corresponding to the fact that hexagonal crystals are found to be magnetically isotropic in an (0001) plane. In

[2] A. Wolf, Zeits. f. Physik **70,** 519 (1931).

[3] These considerations are based on the work of: G. S. Mahajani, Roy. Soc. Proc. **228,** 63 (1929); W. L. Webster, Proc. Phys. Soc. **42,** 431 (1930); N. S. Akulov, Zeits. f. Physik **67,** 794 (1931); F. C. Powell and R. H. Fowler, Proc. Cam. Phys. Soc. **27,** 280 (1931); F. Bloch and G. Gentile, Zeits. f. Physik **70,** 395 (1931); F. Bitter, Phys. Rev. **38,** 528 (1931).

[4] The magnetization of distorted lattices has recently been investigated by R. Becker, Zeits. f. Physik **62,** 253 (1930) and R. Becker and M. Kersten, Zeits. f. Physik **64,** 661 (1930).

Fig. 5 are plotted the results of Honda, Masumoto, and Kaya[5] for iron. The solid curves are those deduced from Eq. (4). The bend in the curve for the (111) axis near $h=12$ has no particular significance as the minimum of $E_{\theta,H}$ is very flat in this region, and allows of a considerable range of orientations without the expenditure of any appreciable amount of energy. The

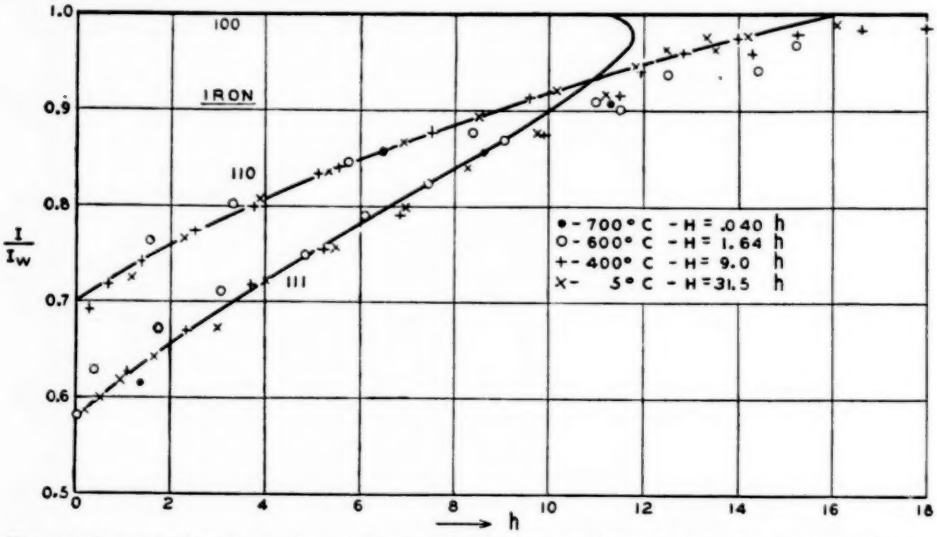

Fig. 5. Theoretical and experimental magnetization curves for single crystals of iron. Experimental points are by Honda, Masumoto, and Kaya.[5]

experimental points are fitted to the theoretical curves at one point which determines the ratio H/h. This ratio, which measures the difference in energy for various directions of magnetization, varies with the temperature as shown in Fig. 6. There is as yet no theoretical interpretation of

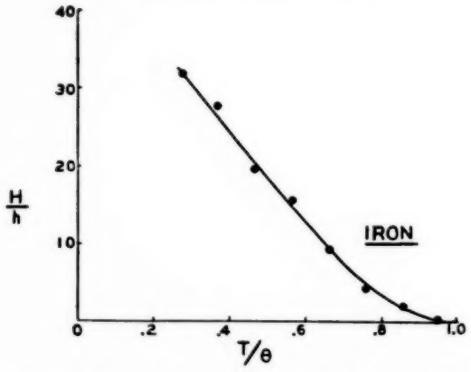

Fig. 6. The ratio H/h is plotted as a function of the reduced temperature for iron. H/h measures the magnetic anisotropy of a crystal.

this curve. The magnetization curves for hexagonal crystals at room temperature are shown in Fig. 7. In Co the direction of easy magnetization is (0001), the plane perpendicular to this axis being magnetically isotropic. In pyrrhotite the situation is reversed. The (0001) axis is the direction of difficult magnetization. The plane perpendicular to this axis is isotropic, and is sometimes referred to as the magnetic plane. While the agreement shown in the figure is fair, the discrepancy for cobalt in the direction of difficult magnetization is considerable. Further

[5] K. Honda, H. Masumoto, and S. Kaya, Sci. Rep. **17**, 111 (1928).

experimental work should be undertaken to check the shape of this curve, especial care being taken to aline the crystal in the field. The above considerations make certain predictions concerning the thermal behavior of hexagonal crystals possible. There is no reason for supposing that the coefficients K_2 and K_1 have identical temperature coefficients, and if they have not, a temperature T' may be reached for which $K_2=K_1$. At this temperature every direction will be one of easy magnetization. If below this temperature the (0001) axis is easily magnetizable, it will not be so above T', and vice versa. This is the behavior that Honda and Masumoto[6] have recently observed in cobalt. They found T' at approximately 250°C. Above this temperature the magnetic behavior of cobalt is similar to that of pyrrhotite at room temperature. It is quite

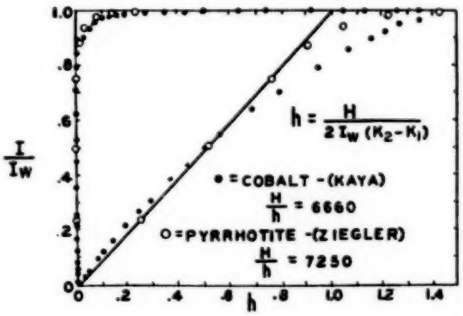

Fig. 7. Theoretical and experimental magnetization curves of nickel and pyrrhotite crystals at room temperature. Experimental points are by S. Kaya, Sci. Rep. **17**, 1157 (1928), and Ziegler, Thesis, Zürich, 1915, or Int. Crit. Tables **6**, 413 (1929).

possible that a similar phenomenon takes place in pyrrhotite at low temperatures, and is responsible for the anomalous behavior shown in Fig. 3. That is, if for temperatures below $T/\theta_p=0.35$ there were only a magnetic axis, and *two* directions of difficult magnetization instead of one, the material would be magnetically harder, and would consequently be difficult to magnetize to saturation. An investigation of crystalline pyrrhotite at low temperatures could settle the point.

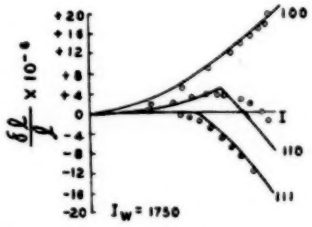

Fig. 8. Magnetostriction as a function of magnetization in iron crystals. Theoretical curves are by Heisenberg,[8] experimental points by Webster.[3]

Any quantity that depends on the direction of magnetization of the elementary regions can be calculated in a manner similar to the above. One of these is magnetostriction. The elementary regions do not possess perfect cubic lattices, but are distorted by their magnetization, and the shape of a macroscopic sample will evidently depend on the direction of magnetization of these regions. Calculations of the magnetostriction of single crystals have been made by Akulov[7] and Heisenberg.[8] In Fig. 8 the result is plotted as found by Heisenberg, with observations on iron by Webster. The assumptions made are somewhat different from those used in this paper, but

[6] K. Honda and H. Masumoto, Sci. Rep. **20**, 323 (1931).
[7] N. S. Akulov, Zeits. f. Physik **69**, 78 (1931).
[8] W. Heisenberg, Zeits. f. Physik **69**, 287 (1931).

the curves obtained are not greatly affected by this difference. In both cases the derivations are of a preliminary character, and the agreement shown in Fig. 8 may be taken as satisfactory. For further detail the reader is referred to the above papers.

These and related problems which concern the structure-insensitive properties of ferromagnetic substances are at least on the road to being solved. The structure-sensitive properties, on the other hand, are not at all understood, and require further knowledge of the detail of the structure of solids. Before it is possible to apply the ideas which have been advanced, especially those of Zwicky on block structure, it will be necessary to have more definite observations to work on. Two promising directions are illustrated in Figs. 9 and 10. In the first of these the ini-

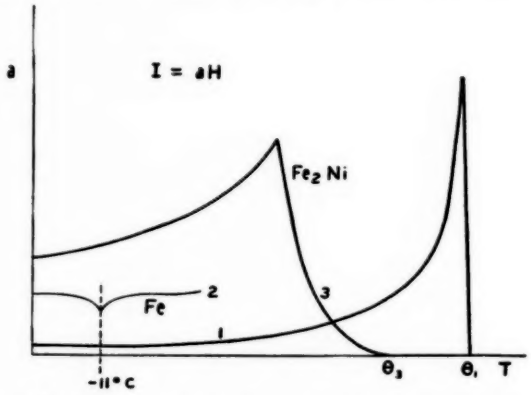

Fig. 9. Initial susceptibility as a function of temperature.[9,10]

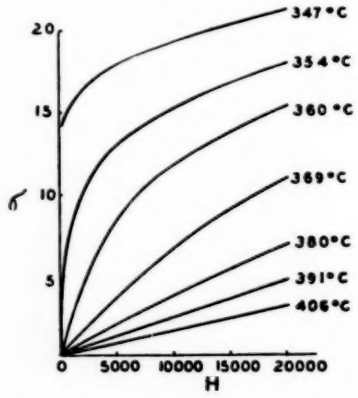

Fig. 10. Magnetization curves of polycrystalline nickel near the Curie point after Weiss and Forrer.[11] σ is the specific intensity of magnetization.

tial susceptibility of various substances is plotted as a function of temperature. The data are taken from Renger[9] and Weiss and de Freudenreich.[10] Curve 1 represents qualitatively the behavior of iron and nickel. In iron an anomaly is reported at $-11°C$ which is plotted on a larger scale in curve 2. This peculiar behavior is related to a time lag and to a magnetic aging. That is, at $-11°C$ the time required for a steady value of I to set in after a change in H, is much greater than either above or below this temperature. Further, the exact shape of the kink depends on how long the material was kept at a temperature near 120°C during its previous heating. It should be useful for our understanding of the subject to investigate such critical temperature ranges in some detail. In curve 3 the peculiar behavior of an iron-nickel alloy is

[9] K. Renger, Thesis, Zürich, 1913.

[10] P. Weiss and J. de Freudenreich, Arch. des Sci. **42**, 449 (1916).

shown. Another set of phenomena that requires further experimental investigation is that accompanying the transition from the ferromagnetic to the paramagnetic state. For some purposes it is sufficient to speak of a single critical temperature, but a closer inspection shows that in some substances, at any rate, the various properties change more or less continuously over a range of temperatures, and that there may even be two or three distinct critical temperatures quite close to each other. In Fig. 10 are plotted magnetization curves of nickel taken by Weiss and Forrer[11] near the Curie point. It would be of great interest to study these curves in relationship to the constant K of Eq. (4), whose behavior for iron is plotted in Fig. 6, and so to separate these effects which are due to the orientation of the regions as discussed above from those which are due to other mechanisms.

[11] P. Weiss and R. Forrer, Ann. de Physique **5,** 153 (1926).

SOME NEW EXPERIMENTAL METHODS IN FERROMAGNETISM

An address presented before the Symposium on Ferromagnetism at the meeting of the American Physical Society, Schenectady, New York, September 12, 1931

By S. L. Quimby

Physics Laboratories, Columbia University

WHEN your Committee honored me with an invitation to address this body on the subject "New Experimental Methods in Ferromagnetism," I accepted on condition that I be permitted to prefix this title with the adjective "Some." Taking advantage of this bit of forethought, I propose this morning to limit my remarks to a brief description of certain methods which have been devised for observing the magneto-elastic, mechanical and thermal properties of single crystals of nickel, as well as of polycrystalline specimens of the same substance.[1]

Attention should first be directed to the process used in refining the nickel.[2] The initial stage in this process is the preparation of a nickel chloride bath by dissolving Mond nickel in hot hydrochloric acid. Iron is then removed from the bath by precipitation of the hydroxide, and copper by electrolytic deposition on a rotating platinum cathode. Finally the pure nickel is deposited electrolytically on a stationary carbon cathode. This nickel is spectroscopically free from iron, cobalt and all other metallic impurities except a trace of copper too small to be detected by chemical means.

I shall now describe the apparatus used for the manufacture of single crystals of nickel. The specimens are desired in the form of rods 4 to 6 mm in diameter and 5 to 10 cm long.

The crystals are grown in a molybdenum-wire-wound vacuum electric furnace, following the method developed by Bridgman for the production of single metallic crystals. The novelty of the present arrangement consists in those features of design which permit the use of this method at a temperature of 1500°C.

Fig. 1 is a cross section silhouette of the furnace. On the outside is a fused quartz tube $5\frac{1}{2}$ inches in diameter and 28 inches high. A clear quartz window is fused in at the top to permit the use of an optical pyrometer. The bottom is ground flat and makes a vacuum tight seal with the flat iron plate which forms the base of the furnace. Next is a radiation trap consisting of a tubular alundum furnace core 3 inches in diameter. Next is an alundum tube 2 inches in diameter and 24 inches long on the upper 9 inches of which are wound 80 turns of molybdenum wire. The diameter of the wire is 0.036 inches. Next is an alundum tube 1 inch in diameter and 10 inches long upon which are wound 90 turns of molybdenum wire. The space between these

[1] These methods have been developed through the cooperative activity of the following group working in the Physics Laboratories at Columbia University: Lewis Balamuth, W. T. Cooke, Fred Rose, Sidney Siegel, Clarke Williams, and Jerrold Zacharias. Detailed descriptions thereof will appear in due course in separate papers under appropriate authorship.

[2] F. A. Rohrman, Transactions of the Electrochemical Society **57,** 325 (1930); **58,** 403 (1930); **59,** 359 (1931).

two tubes is filled with alundum powder to prevent arcing between neighboring turns of the inner heating coil. Last is the crucible, which is molded of a mixture of refractory cement and alundum grain. The crucible is mounted on an alundum rod, which in turn is mounted on an iron tube of $\frac{3}{4}$ inch outside diameter closed at the lower end. This tube floats in mercury contained in a surrounding iron tube of 1 inch inside diameter. The mercury chamber is connected through a rubber hose with a reservoir for adjusting the initial height of the crucible, and through a glass tube with a stopcock. The aperture in this stopcock is plugged in such a manner as to form two small buckets of about 5 cubic mm capacity. When it is desired to lower the crucible out of the furnace the stopcock is rotated continuously by an electric motor acting

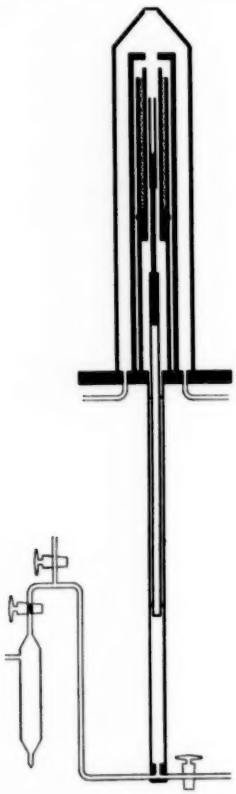

Fig. 1.

through a gear train. Each half revolution spills 5 cubic mm of mercury from the system into an evacuated chamber and lowers the crucible 0.01 mm. The crucible is lowered about 4 cm per hour. The nickel is premelted in a hydrogen furnace and cast into rods whose diameter is slightly less than that of the crucible. With this furnace single crystals of nickel are secured in the form of rods 4 to 6 mm in diameter and 6 cm long.

A Laue photograph yields the orientation of the cylinder axis in the crystal lattice by interpolation in the series of fifty face centered lattice patterns published by Majima.[3] In this manner the orientation can be determined with an accuracy of about one degree.

The first measurement which is taken upon the crystal is the variation of the coefficient of thermal expansion with temperature through the Curie point. As long ago as 1910 observations made upon specimens of very impure polycrystalline nickel showed that in the neighborhood of the Curie point the coefficient of thermal expansion varies with temperature in the

[3] Majima, Tokyo Institute of Physical and Chemical Research, Scientific Paper No. 111.

manner shown in Fig. 2.[4] The elegant method used by Colby cannot readily be adapted to a long cylindrical specimen. The present apparatus for the investigation of this phenomenon is mentioned here chiefly because it is an excellent example of the use which may be made of recent developments in the art of making and handling clear fused quartz. The apparatus sketched in Fig. 3 is composed entirely of clear fused quartz. One end of the specimen is fixed relative to the apparatus by virtue of its resting on a knife edge which engages with a tiny scratch in the specimen. The other end rests on a quartz roller 1 mm in diameter which in turn rests on a flat plane. Sputtered gold mirrors reflect into a telescope images of two scales placed five meters distant. These mirrors are rotated slightly with respect to each other about the roller axis to increase the range of the instrument. A third scale is reflected from a mirror on the front face of the mount and a fourth from a mirror under the knife edge. Observations on these scales

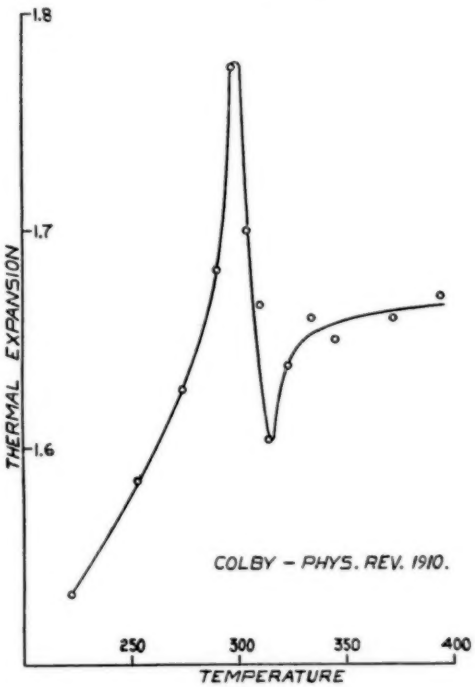

Fig. 2.

permit the evaulation of any shift of the apparatus or its mounting in the furnace. The apparatus is mounted on one end of a quartz tube 2 inches in diameter which is fastened at the other end and projects into the furnace.

Initial observations on the variation of the coefficient of thermal expansion with temperature in single crystals of pure nickel indicate that this quantity behaves near the Curie point in a manner similar to that previously reported for impure polycrystalline nickel.

The ordinary magnetostrictive change in length has been measured with this apparatus by using the central cylindrical portion of a long thin ellipsiod of revolution. When it is desired to make observations on short ellipsoids, a length of about 2 mm on each end is ground into a cylinder, and these cylinders rested on the knife edge and roller respectively.

The behavior of these quartz rollers is surprisingly good. Fig. 4 shows the design of a much more elaborate system constructed for the purpose of studying the variation of Young's modulus with stress, temperature, and magnetic field intensity in specimens whose form is a long thin cylinder or wire a mm or so in diameter. In specimens of this sort both the temperature and

[4] Colby, Phys. Rev. **30,** 506 (1910).

the magnetic field are uniform only over a region some 10 cm in length near the center of the wire, and the problem is that of measuring the change in length under the applied stress of this portion alone. Two parallel rollers 2 mm in diameter and 10 cm apart rest upon a flat quartz plate and upon them bears the specimen under longitudinal stress. On the first roller there rests in addition a small triangular shaped quartz plate which has its upper surface ground flat. A third idling roller supports the rear end of this plate. The bearing surfaces of the plate on the rollers are two parallel polished quartz rods 1 mm in diameter fused to the plate. On top of the

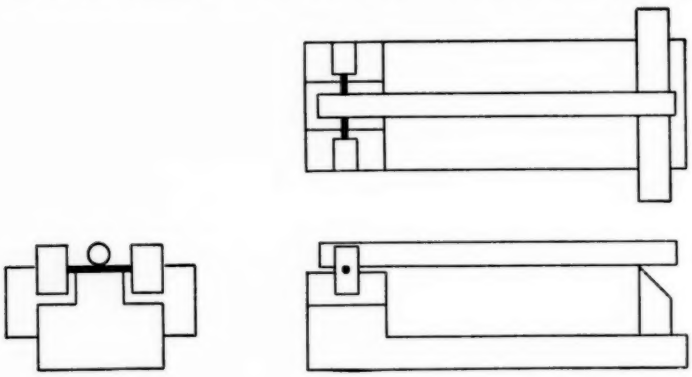

Fig. 3.

plate rests the roller carrying the mirrors. On the rear roller rests a block of roughly the same material as that under examination having quartz bearing surfaces as before. A metal rod of the same material screwed to this block leads forward and rests upon the mirror roller. If now the entire specimen be stretched by making one end fast and pulling on the other, then the rotation of the mirrors will be determined solely by the change in length of that portion of the specimen which lies between the rollers. Auxiliary mirrors as before permit the evaluation of any shift of the apparatus as a whole. The effect of thermal expansion is compensated sufficiently to keep

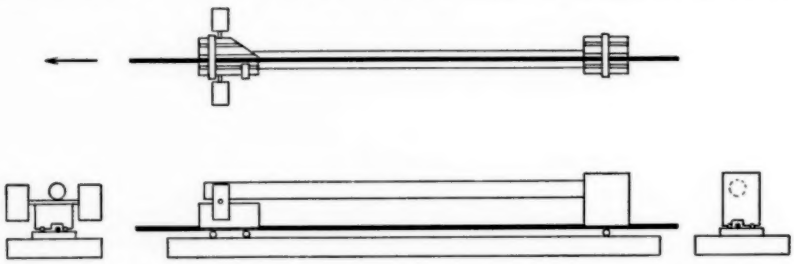

Fig. 4.

the scale images in view throughout a run by the device of making the upper bar of nearly the same material as that under examination. Fig. 5 gives an idea of the behavior of this rather complicated system. It shows the stress-strain relation for 8.6 cm of a nickel wire 1 mm in diameter when the applied load is altered between 1 kg and 3.5 kg. The lines are drawn straight The lower line gives the effect of increasing load and the upper line the effect of decreasing load. The cause of the relative shift, which represents a linear displacement of about 1000 atomic layers, has not yet been determined. The obvious explanation, that of elastic fatigue, is not the correct one as the shift varies erratically from run to run.

I now return to a description of further experiments upon single crystals of nickel. It is desired to measure the variation with temperature through the Curie point of Young's modulus in the direction parallel to the axis of the cylindrical specimen. The method about to be de-

scribed requires the experimental determination of the frequency of free longitudinal elastic vibration of the cylinder. This being known, the velocity of sound in the direction of the cylinder axis is given by the relation

$V = f_N \times \lambda$, where $\lambda = 2 \times$ length of cylinder, and Young's modulus for this direction by the relation $V = (E/\rho)^{1/2}$, where $\rho =$ density of specimen. The crystal is sawed in half, the ends ground flat, and the two halves cemented to a plate of piezoelectric quartz 0.4 mm thick. An electric axis of the quartz is parallel to the cylinder axis. The specimen is then suspended by and in electrical contact with two very thin wires, and these wires are connected to an oscillating electric circuit which establishes across the quartz an alternating potential difference of variable frequency. Accordingly the quartz, which is thus situated in a sinusoidally varying electric field, suffers a sinusoidally varying piezoelectric strain which is transmitted to the nickel rods. The result is that the entire system is set into forced longitudinal elastic vibration. Under these circumstances the electric current which flows into the little condenser with quartz for dielectric is determined in part by the ordinary electric polarization associated with the field and in part by the polarization associated with the stress in the quartz due to the

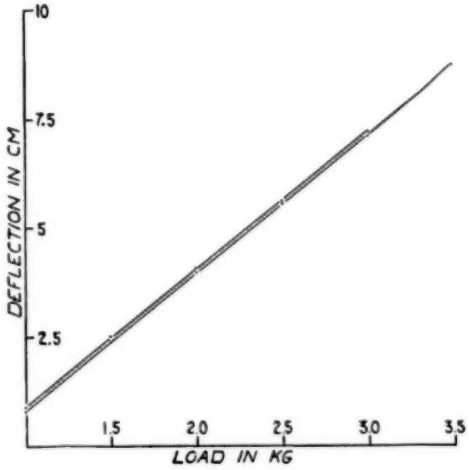

Fig. 5.

mechanical vibration. At a certain value of the impressed frequency the amplitude of vibration attains a maximum value, that is, the quartz-nickel system resonates. In the neighborhood of this frequency the current passes in succession through a maximum and a minimum value.[5] The resonance frequency of the system may be calculated from the observed values of current and frequency corresponding to these maximum and minimum currents. With this quantity and the known elastic data for the quartz plate, the desired free period of the specimen alone can readily be computed.

The foregoing considerations apply with only numerical modification to a nickel-quartz oscillator constructed by cementing a rod of quartz of rectangular cross section to one end of a single rod of nickel. In this case the quartz is so cut that the optic axis and an electric axis both lie in a plane perpendicular to the cylinder axis. The electric axis is perpendicular to a pair of opposite faces of the crystal and the electrodes are made by coating these faces with gold leaf.[6]

These composite piezoelectric oscillators can also be used to measure the coefficient of rigidity. For the system may be excited to torsional vibration by using a quartz rod of circular cross section and four quadrantal electrodes, or by using a quartz rod of different cut.[7] A knowledge of Young's modulus and the coefficient of rigidity affords a complete description of the

[5] Cf. Van Dyke, Proc. Inst. Radio Eng. **16,** 742 (1928).
[6] Quimby, Phys. Rev. **25,** 558 (1925).
[7] Giebe and Scheibe, Zeits. f. Physik **46,** 607 (1926).

elastic properties of an isotropic medium. It is not as yet possible to measure in this manner the rigidity modulus for single crystals of nickel. It can be shown that the free period of torsional vibration of crystalline rods depends upon the rigidity modulus alone only if the cylinder axis is oriented in certain directions in the crystal lattice. So far in the case of nickel no way has been discovered for controlling the orientation of the crystal axes when the crystal is grown.

Two experimental details of these methods require special mention. One is the nature of the cement which will cause nickel to adhere to crystalline quartz at a temperature of 400°C. The ends of the nickel rods are first thinly copper plated. The stick is then made under pressure, in a vacuum at a temperature of 600°C with copper borate as the adhesive.

The other detail is concerned with the way in which the frequency-current curves are obtained. The frequency difference between the maximum and minimum currents may be 100 cycles or less for an oscillator whose resonance frequency is 50,000 cycles. In order therefore properly to use this method a means must be provided for measuring easily and quickly the frequency of the oscillating electric circuit with an accuracy of 1 or 2 cycles in 50,000. For this purpose use is made of a piezoelectric clock and its auxiliary apparatus. A schematic of the method is given in Fig. 6. The frequency of an oscillating circuit is controlled by a piezoelectric quartz crystal mounted in a thermostat which assures a temperature constant to a hundredth

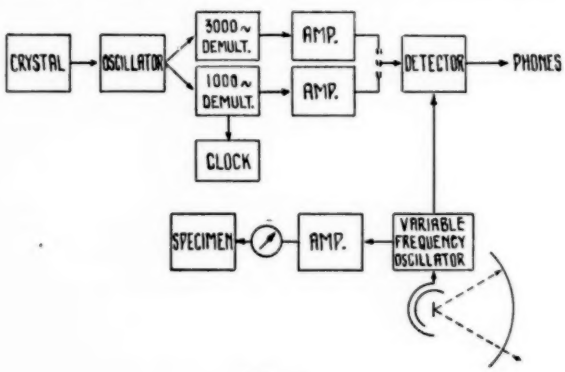

Fig. 6.

of a degree. Under these circumstances the frequency remains constant to a few parts in a million over a period of days and to a few parts in a hundred thousand over a period of years. The output of this circuit is used to control the frequencies of two demultiplying circuits. The latter are push-pull oscillators in which the natural frequency is determined by a resistance and a capacity. These circuits possess the peculiar property that if a high frequency alternating potential difference of a few volts be superimposed on the plate voltage then over a wide range of variation of their circuit constants they are constrained to oscillate at a frequency which is an integral sub-multiple of the superimposed frequency. In the system here depicted the piezoelectric oscillator frequency is approximately 51 kilocycles. One of the demultipliers is adjusted to oscillate at the 17th subharmonic and the other at the 51st subharmonic of this frequency, The latter drives a synchronous clock which is compared from time to time with the radio time signals from Arlington. Since the wave form of the demultipliers is extremely rich in harmonics. this arrangement affords standard frequencies good to one part in a million at intervals of 1000 cycles up to several hundred kilocycles.[8]

The variable frequency oscillator driving the specimen is coupled electrically to the output of the 1000 cycle demultiplier from which the audible harmonics have been filtered out, and the resultant beat note rectified and rendered audible in a pair of head phones. The frequency of this oscillator is controlled both by a tuning condenser and by a vernier condenser whose full scale value alters the frequency about 500 cycles. This vernier has a scale with 500 one millimeter divisions. Let us assume that the resonance curve which it is desired to obtain lies be-

[8] Hull and Clapp, Proc. Inst. Radio Eng., Feb. 1929, p. 267.

tween the frequencies 53,000 cycles and 53,500 cycles. The clock supplies the frequencies 52,000, 53,000 and 54,000. Thus the detector tube receives these frequencies together with the oscillator frequency, and its output contains the beat notes between the two. The frequency of the oscillator having been adjusted approximately to 53,000 by means of its rough calibration, the vernier is set at zero and the tuning condenser varied slightly until consonance is heard between two 1000 cycle notes. These are the beat notes between the oscillator frequency, 53,000, and the clock frequencies 52,000 and 54,000. The condition of consonance implies that the zero of the vernier corresponds to a frequency of exactly 53,000 cycles. Leaving the tuning condenser alone, the vernier is now altered until consonance is heard between two 500 cycle notes. These are the beat notes between the oscillator frequency of 53,500 and the clock frequencies of 53,000 and 54,000. Accordingly this position of the vernier corresponds to a frequency of exactly 53,500 cycles. Since, as was remarked, the size of the vernier and the distance of its scale are adjusted to give about 500 mm for 500 cycles, it follows that the frequency of the exciting oscillator may be determined over the range of the resonance curve to one cycle in 50,000.

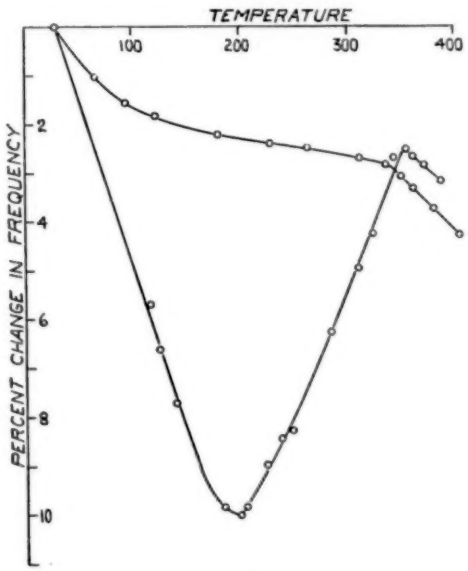

Fig. 7.

Fig. 7 shows the change in resonance frequency of two nickel rods as the temperature is raised from 23°C to 400°C. The lower curve is for a single crystal and the upper curve for a polycrystalline specimen. Attention is directed to the precision of measurement indicated by these curves. The resonance frequency may be measured with a precision of one tenth of one percent or better. Since Young's modulus varies as the square of the resonance frequency, this quantity may be measured with a precision of two tenths of a percent or better.

Unfortunately it is not possible to calculate Young's modulus from the observations on the lower portion of the single crystal curve with the aid of the simple formulae heretofore given. The reason for this is the fact that over this range of temperatures the internal friction of single crystal nickel increases to a point where it appreciably affects the resonance frequency of the specimen, i.e., the velocity of sound in the material. While this complicates the present investigation it is of considerable interest otherwise for the reason that there is a very intimate connection between magnetism and internal friction in ferromagnetic materials. It follows that the present method for studying Young's modulus demands a concurrent investigation of the variation with temperature of the internal friction in the material.

Fig. 8 is a schematic of an apparatus designed to measure the coefficient of internal friction of solids by direct determination of the decrement of longitudinal vibration in freely suspended

rods. The rod is excited to resonance at one of its harmonics piezoelectrically as before. The exciting crystal is then switched rapidly from the driving oscillator to an amplifier. The potential difference across the crystal produced by the piezoelectric charge, which is proportional in magnitude to the stress in the quartz and hence to the amplitude of vibration in the rod, is amplified and rectified. As the vibrations in the rod die out one obtains from the detector tube a logarithmically diminishing direct current whose decrement is twice that of the vibrations in the rod. This current is passed through a resistance and the consequent potential difference is impressed on the grids of two vacuum tube relays. The circuit of one of these relays appears

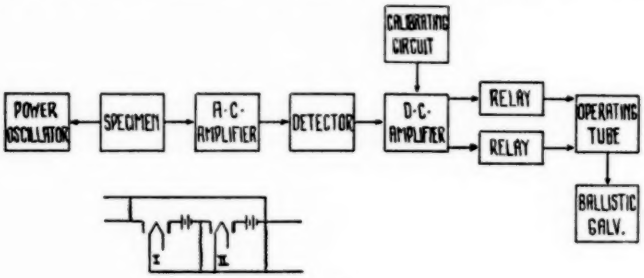

Fig. 8.

in the figure. This circuit possesses two stable states of current distribution. In state one current is flowing only in tube I and there is no measurable plate current in tube II: in state two current is flowing in tube II and there is no current in tube I. The system may be caused to pass from the first state to the second by applying a critical negative potential to the grid of tube I. The magnitude of this critical potential is subject to control. In the present apparatus one of these relays is set to operate at a voltage whose magnitude lies near the top of the decay curve just described, and the other relay to operate at a voltage which is $1/e$ of this value. These relays control the grid potential of an operating tube in the plate circuit of which is a ballistic gal-

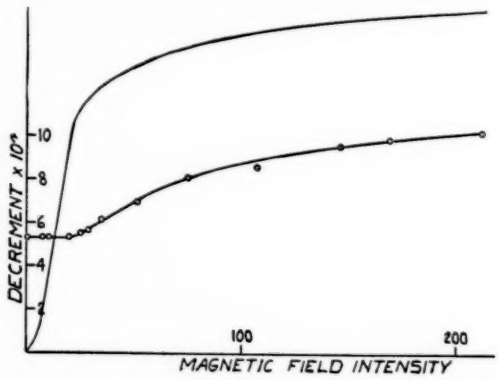

Fig. 9.

vanometer. Normally the plate current of this tube is made zero by a high negative grid bias. The operation of the first relay elevates the grid potential and allows current to flow through the galvanometer; the operation of the second relay restores the negative grid potential and stops the flow of current through the galvanometer. Thus current flows through the galvanometer; the operation of the second relay restores the negative grid potential and stops the flow of current through the galvaometer. Thus current flows through the galvanometer only during the time interval required for the detector plate current to diminish in the ratio 1 to $1/e$. Accordingly the ballistic galvanometer deflections are directly proportional to the time constant of the vibrating rod. The relay-galvanometer system is calibrated directly by replacing the

detector plate current by a logarithmically diminishing current in an electric circuit containing a standard resistance and a standard condenser.

Fig. 9 shows the variation with magnetic field intensity of the decrement of longitudinal vibration in a soft iron rod magnetized parallel to its axis. The curve upon which no points appear is the so-called "reversible" magnetization curve for the iron. It will be noticed that the internal friction remains constant over the entire steep portion of the magnetization curve and then increases to twice its initial value as the magnetization approaches saturation.

The magnitude of the coefficient of internal friction may also be obtained by measuring the electrical resistance of the piezoelectrically excited oscillator at resonance with an ordinary a.c. bridge. The bridge method, while more difficult to handle, has a wider range of application than the decremeter. The two methods supplement one another in a study of the behavior of these composite piezoelectric oscillators.

Abstracts and Discussion of Papers presented at the Conference on Ferromagnetism at the meeting of the American Physical Society, Schenectady, New York, September 12, 1931

BARKHAUSEN EFFECT: ORIENTATION OF MAGNETIZATION IN ELEMENTARY DOMAINS

By Richard M. Bozorth

Bell Telephone Laboratories, New York

SINCE the postulate of the elementary domain by Weiss,[1] and the discovery of the discontinuous nature of the magnetization process by Barkhausen,[2] there have been many investigations attempting to throw more light on the nature of the elementary regions in each of which the magnetization changes as a unit. On the experimental side we are interested in knowing the sizes of the domains, the extent to which the domain is localized in space, the extent to which it is "saturated" in one direction, and the orientation of its magnetization vector before and after the change.

It has been found that all, or nearly all of the change in magnetization takes place in jumps, at least on the steeper portions of the hysteresis loop;[3] and that the volume of a domain varies but little with the condition of the iron, being sometimes thousands of times smaller, and sometimes thousands of times larger than a crystal.[4]

Mr. Dillinger and the writer have obtained some evidence that the elementary domain is a region well localized in space, within the whole of which the elementary magnets reverse. The following experiment is to the point. Two search coils are connected in series opposing to the amplifier. They are placed coaxially with the sample, equidistant from its middle. The distance between them is varied and the intensity of the Barkhausen effect is measured as a function of this distance. The differential effect increases rapidly with the distance between the coils until the distance is greater than about 3 cm. But the attainment of maximum at this distance is not due to the permanent change in magnetization over the 3 cm, but rather to the spread of eddy-currents for about that distance along the wire. This is proved by placing a small coil of wire carrying a small alternating current, around the middle of the specimen and making measurements similar to those of the Barkhausen effect just mentioned. The results,[5] plotted in Fig. 1, show that the measured spreading of a single disturbance due to an alternating field will account for the observed spreading of the Barkhausen discontinuities. As far as the data go they are consistent with a point source of the Barkhausen disturbance, but the accuracy

[1] P. Weiss, Jour. de physique [3] **8,** 542 (1899); Phys. Zeits. **9,** 358 (1908); P. Weiss and G. Foex, Le Magnétisme, Paris, 162 (1926).

[2] H. Barkhausen, Phys. Zeits. **20,** 401 (1919).

[3] R. M. Bozorth, Phys. Rev. **34,** 772 (1922). A similar result has also been obtained by F. Preisach, Ann. d. Physik (5) **3,** 737 (1929) with a different method.

[4] R. M. Bozorth and J. Dillinger, Phys. Rev. **35,** 733 (1930).

[5] Calculated from data already published (reference 4).

merely fixes the length of the domain as less than a few mm. The best assumption now is the simplest, that the group is as compact as possible.

Closely related to the spatial extent of a domain is the question as to its degree of saturation. Is the magnetization always at saturation in some direction, only the orientation changing? Mr. Dillinger and the writer have answered this question to some extent by a study of what may be called the *transverse* Barkhausen effect.[6] The experimental arrangement is shown in Fig. 2. The specimen is in the form of a tube about 2 feet long. Along its axis is a heavy cop-

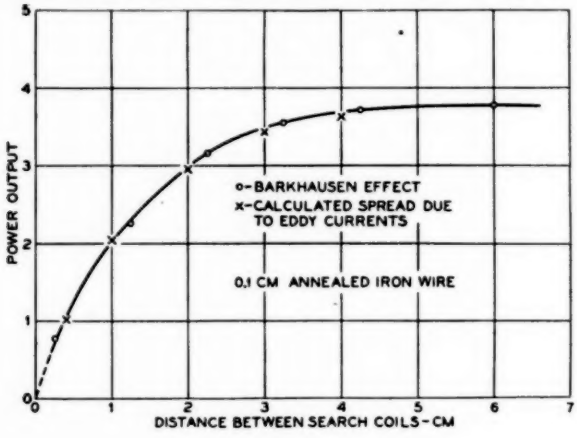

Fig. 1.

per wire carrying a current, effecting circular magnetization of the tube. Changes in magnetization perpendicular to the direction of gross circumferential magnetization are picked up by the search coils shown. The longitudinal or ordinary Barkhausen effect is determined in the usual way by magnetizing the tube lengthwise in a long solenoid, with the same search coils.

The ratios of the average transverse to the average longitudinal change in magnetization for various parts of the magnetization curves[7] are shown in Fig. 3. It is better to plot this ratio as a function of B-H as shown in Fig. 4; here the hysteresis is much less pronounced, and it is

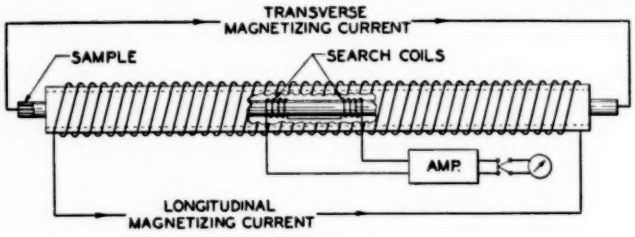

Fig. 2.

seen that the transverse effect becomes relatively much more important at higher inductions. The minimum ratio is 0.05 corresponding to the complete reversal of magnetization in a domain with the direction of magnetization inclined 5° to the direction of the field. At higher magnetizations the ratio increases until it is almost equal to unity when $B-H=15{,}000$ and rises quickly to six when $B-H=16{,}000$.

These data can be interpreted best in connection with the diagrams of Fig. 5. Some possible modes of change are shown consistent with Akulov's recent theoretical investigations[8] which,

[6] Preliminary note by R. M. Bozorth and J. F. Dillinger, Phys. Rev. [2] 38, 192 (1931).

[7] Magnetization curves were determined for both longitudinal and transverse magnetization and were found to be almost identical.

[8] N. S. Akulov, Zeits. f. Physik **67**, 794 (1931).

in connection with experimental data[9] on single crystals, indicate that the magnetization is directed very closely along one of the six <100> directions in the crystal (parallel to the edges of the crystallographic unit cube), at least until the material is about three-quarters saturated.

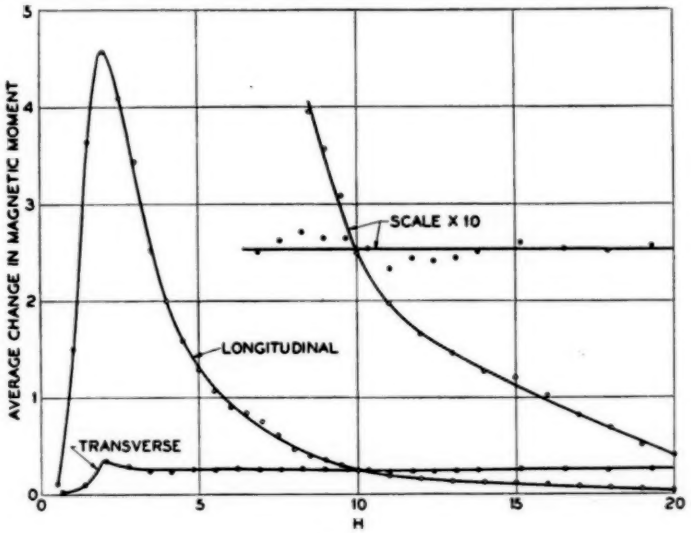

Fig. 3.

In the figure the solid arrow indicates the direction of magnetization before the change, and the dotted arrow the direction after the change. In (a) the direction of magnetization of the crystal which constitutes the greater part of the domain coincides as always with the direction of the

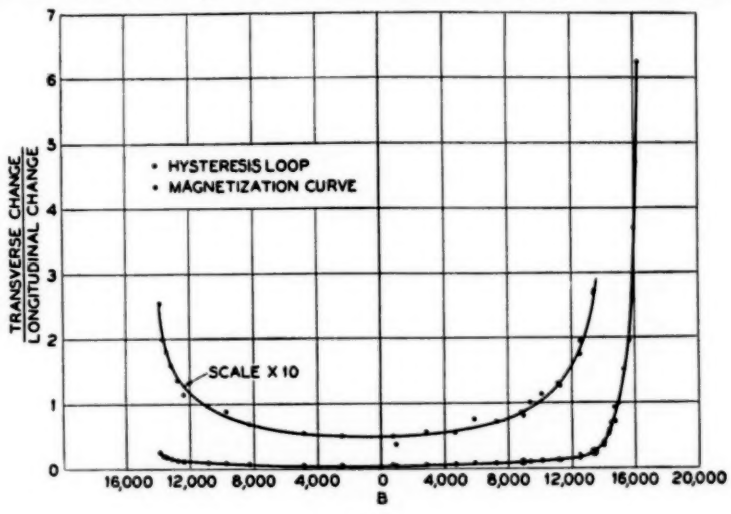

Fig. 4.

cube edge and makes an angle of more than 135° with the direction of the applied field, *H*. By assuming in accordance with Akulov's theory that the magnetization takes up the position of minimum potential energy, the most stable position after the change is that shown, again coincident with a cube edge. If the direction of magnetization, however, happens to lie initially

[9] W. L. Webster, Proc. Roy. Soc. Lond. **107A**, 496 (1925). K. Honda and S. Kaya, Sci. Rep. Tohoku Univ. **15**, 721 (1926).

between 135° and 90° to the direction of H, as shown in (b), the change in its direction will be 90° and not 180° as before. In this case the ratio of the transverse component (T) to the longitudinal component (L) of the change will be much greater than before. This ratio will be still greater as the initial direction of magnetization approaches nearer to that of H, as shown in (c), until the angle between the magnetization and field is 45°. When the direction of magnetization coincides with a cube edge and makes an angle of less than 45° with the direction of the applied field, there will be no other direction of less potential energy to which the magnetization can change and therefore there will be no Barkhausen effect. When the field-strength becomes high enough, of the order of 100 gauss, the direction of magnetization will depart from the <100> direction nearest to that of the applied field, and saturation will be approached. In a more quantitative treatment the two-dimensional diagram must, of course, be abandoned and three dimensions taken into account

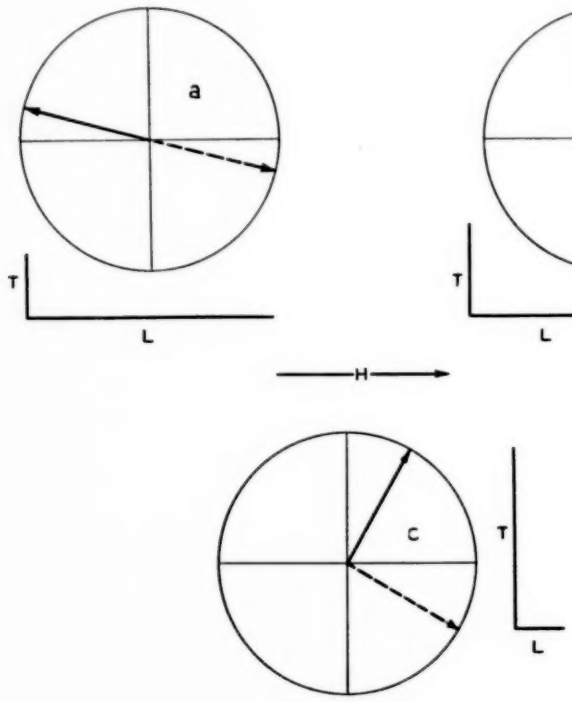

Fig. 5.

In a demagnetized specimen the directions of magnetization in the various domains will be oriented at random. As the field-strength is slowly increased from zero those domains will be first affected in which the direction of magnetization makes the greatest angle with the direction of the field, because the potential energy of those domains will be greatest. The diagram illustrates how the ratio T/L changes as the magnetization of the whole specimen increases according to this scheme; the ratio is small when the magnetization is small, and continually increases as magnetization proceeds, finally becoming much larger than one. Qualitatively, the data support this theory, the ratio of transverse to longitudinal change becoming greater as domains with less potential energy are turned by the field. As $B-H$ increases, the transverse change tends to become constant and the longitudinal change smaller according to both theory and experiment. We should expect the ratio to increase as $B-H$ increases up to that value of $B-H$ beyond which changes from one <100> direction to another cannot increase the magnetization parallel to the applied field. We should expect also that the Barkhausen effect should vanish when the individual magnetization vectors are within 45° of the field vector, that is at about 85 percent saturation, a magnetization attained in ordinary iron at about $H=100$ gauss. It is hoped that more quantitative tests of these ideas can soon be made.

FURTHER EXPERIMENTS ON THE PROPAGATION OF LARGE BARKHAUSEN DISCONTINUITIES

By K. J. Sixtus and L. Tonks

Research Laboratory, General Electric Company, Schenectady, New York

THE formula[1] for the time of penetration for a large travelling Barkhausen discontinuity has been recalculated on the assumption that at each point on the discontinuity in the wire the resultant of the impressed field H and the eddy current field is the critical field H_0. This results in doubling the numerical coefficient so that the formula now reads

$$\delta t = 3.94 \times 10^{-8}\ a^2 \Delta I/\rho(H - H_0) \qquad (8A)$$

where a is the radius of the wire, ΔI the change in induction, and ρ the specific resistance. This alteration halves the ratio of $\delta t_{exp.}/\delta t_{calc.}$ as given in Table I[1] to the value 2. The corresponding formula for a strip of thickness $2a$ has the coefficient 7.88×10^{-8}. Oscillograms taken, however

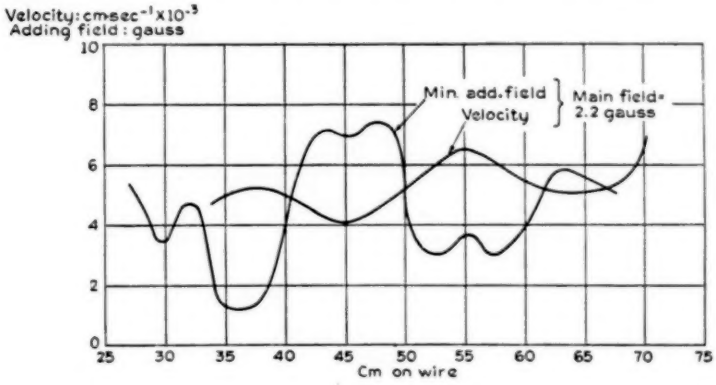

Fig. 1.

to check the validity of these formulas for different size wire fail to verify them, in that t was proportional to a rather than to a^2. Empirical substitution in the formula of $0.031a$ for a^2 reproduce the experimental values reasonably well. Probably the assumption regarding the magnetic field balance at the discontinuity in the wire needs revision. Perhaps the existence of a field arising from the distribution of magnetic pole strength along the wire should be taken into consideration.

Introduction into the formula of either the velocity of propagation v, or the spatial length λ of the discontinuity naturally involves the other of these two quantities through the relationship $\delta t = \lambda/v$. Thus the slope A of the $v - H$ characteristic can be expressed by the formula

$$A = \frac{v}{H - H_0} = 0.26 \times \frac{10^8 \rho \lambda}{0.031 a \Delta I}.$$

This shows that over the considerable ranges of magnetic field, tension and wire radius where ΔI and A change only slightly, λ/a should also be constant to the same degree. This has been verified experimentally.

In the propagation of large discontinuities, two parameters were found to be of particular significance, H_0, the critical field below which no propagation could be obtained, and the constant A, giving the slope of the velocity-field curve. In the wires investigated the change in H_0 with tension, heat treatment, etching, etc., is very similar to the change in coercive force in ferromagnetic wires which have small discontinuities. The slope, however, varied in ways not at all suggestive of other known properties of the material.

[1] K. J. Sixtus and L. Tonks, Phys. Rev. **37**, 930 (1931), Eq. (8).

The first series of experiments bearing on slope variation were conducted with etched wires. Since the front edge of the discontinuity lies on the surface of the wire, it was of interest to observe what effect changes in the surface, such as caused by etching, would have. For wires which were etched from 15 mil down to anywhere between 14.8 and 5 mil, the slope A increased about 50 to 100 percent. It could be shown that neither the reduction in diameter itself, nor absorption of hydrogen was the cause. It may be that the cracks which developed in the surface during the etching were responsible for this effect.

In other experiments a circular field was applied by sending a current through the wire which was under tension and torsion or under torsion alone. In this case also variations in slope of 60 percent were observed.

A plausible explanation for this behavior in the last experiments was finally found as a result of investigating the possible connection between critical adding field and $v-H$ slope at different places along the wire. In places where only a small adding field was necessary to start the discontinuity with a given main field, the velocity and also the $v-H$ slope were higher than in places where a higher adding field was needed. (Fig. 1.) A small critical adding field evidently indicates that the alignment of the magnetic axis of the elementary regions is imperfect, and we may conclude that in regions with imperfect alignment the velocity and slope is high and vice versa.

Thus we arrive at the view, that in the experiments with etched wires the applied tension cannot produce a perfect alignment in the surface of the wire on account of the irregular cracks present. In the other set of experiments, too, the circular field presumably produces a deviation from perfect alignment resulting in an increase in slope.

EFFECT OF IMPURITIES ON FERROMAGNETISM*

By T. D. Yensen

Research Laboratories, Westinghouse Electric and Manufacturing Company, East Pittsburgh

ELEMENTS present in, or added to iron may generally be divided into two classes depending on the position they occupy in the iron space lattice. The first class includes the elements that take the place of the iron atoms and for this reason are called *substitution elements.* Even in large percentages they remain as a part of the iron lattice. Some of them, like Ni and Co, are soluble in all proportions. Others, like Si and Al, have an unlimited solubility in the liquid state and a limited solubility in the solid state due to their tendency to form compounds with iron that are precipitated and can be identified as distinct phases under the microscope. The other class of elements are sufficiently different from iron to prevent their atoms from falling into the ranks of the iron atoms, and yet there are definite indications that to a small extent they become entangled in the iron lattice. Such elements are sometimes called *interstitial elements*, because the only way in which the experimental results can be accounted for is by assuming that their atoms, within the slight solubility range, occupy the position *between* the iron atoms. To this class belong C, O, N and S. If the solubility range (less than 0.01 percent) is exceeded, they are precipitated from solution as compounds of iron, Fe_3C, FeS, FeO, etc. as the temperature drops towards room temperature.

The term "impurities" will be applied to the elements of the second class, because they are usually found in the iron whether they are wanted or not and are very difficult to remove quantitatively. What applies to iron in this respect applies in general to nickel and cobalt and to alloys of these three elements with each other and with other substitution elements.

The effect of impurities on the magnetic properties of iron has been studied very extensively in an attempt to determine the magnetic properties of actually pure iron. While the effect of small amounts of impurities on the saturation value is very small, their effect on the initia- and maximum permeabilities and on the coercive force and hysteresis loss is very great. An

* Scientific Paper #544.

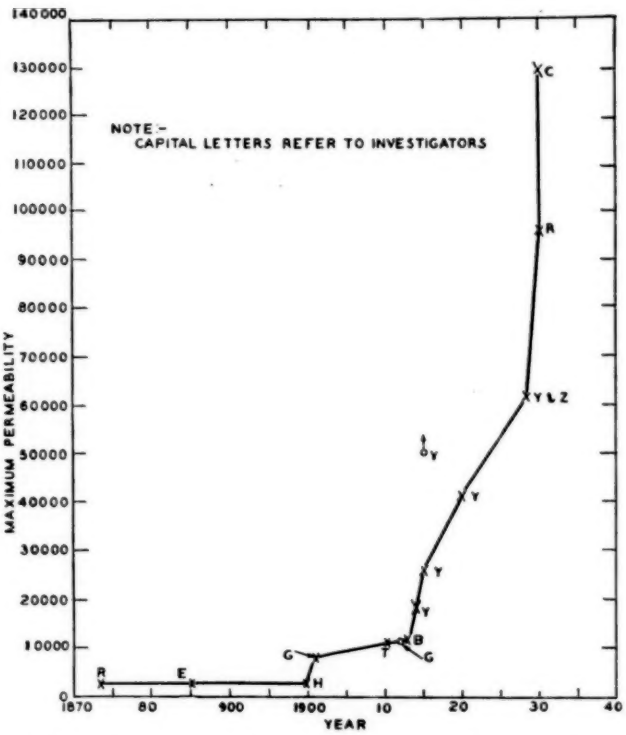

Fig. 1. Improvement in maximum permeability of iron.

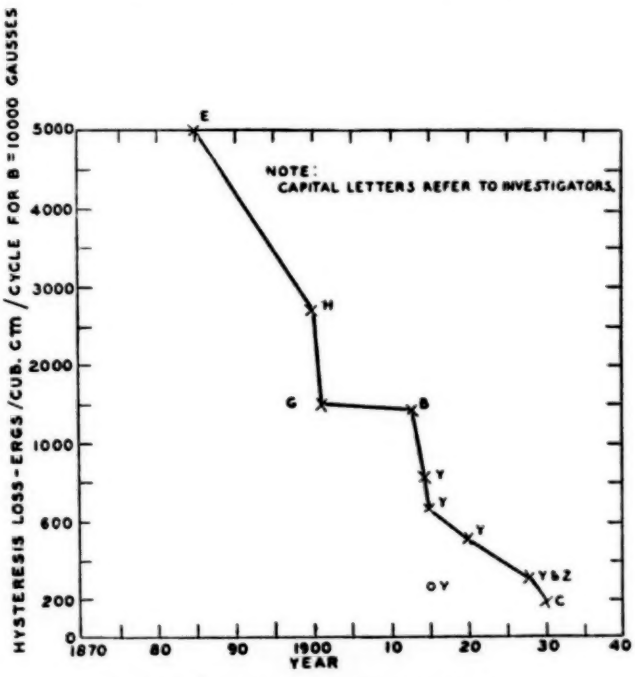

Fig. 2. Decrease in hysteresis loss of iron.

idea of the magnitude of this effect is shown in Figs. 1 and 2 which show the increase in maximum permeability and decrease in hysteresis loss of the purest iron available at the time between 1870 and 1930. This improvement has been found to be associated with minute amounts of impurities as illustrated in Fig. 3 for carbon. In order to obtain the first part of the curve (for C less than 0.01 percent) it was necessary to develop methods of determining carbon with an accuracy of ± 0.0001 percent. Under the microscope no separate phase of Fe_3C is visible below 0.006–0.008 percent C at magnifications of 500 diameters, and it was consequently at first assumed that this was the solubility limit for carbon in iron at room temperature. Further considerations, however, has led to the conclusion that this is not necessarily correct, as Fe_3C is precipitated during the cooling from 700°C as shown in Fig. 4. At the lower temperatures there would be little chance for these precipitated particles to diffuse and coagulate into particles

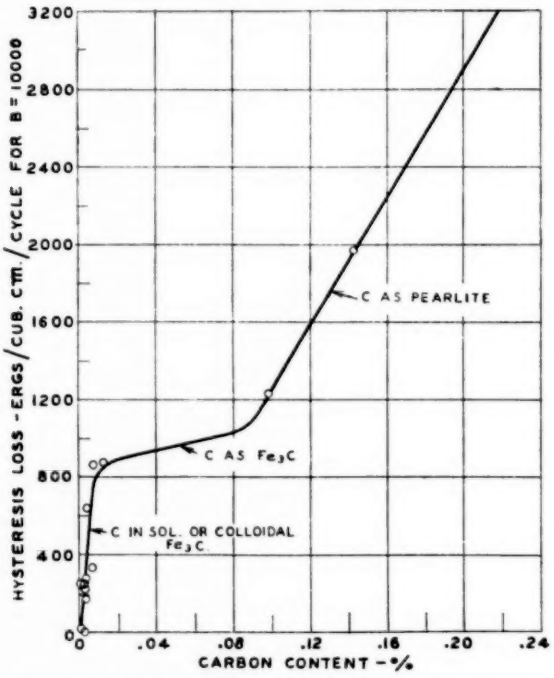

Fig. 3. Effect of carbon on the hysteresis loss of iron.

large enough to be seen even at a magnification of 5000 diameters, so that we must assume that for concentrations less than 0.008 percent carbon is *either* in solution *or* occurs as colloidal Fe_3C particles within the iron crystal, i.e., in a very diffuse state intimately connected with the iron lattice.

In order to account for the large effect on the magnetic properties of these minute amounts of carbon particles it was assumed that the carbon atom occupying the interstitial spaces in the iron lattice exerts a distorting effect on the lattice and that the magnetic properties depend in some way on the regularity of the lattice. Now, carbon being precipitated as Fe_3C and remaining in the lattice may conceivably have an even greater distorting effect on the lattice than the single carbon atoms, but if given a chance to coagulate into larger particles would have a smaller effect as indicated in Fig. 3 due to the smaller aggregate surface. In pearlite, a lammelar structure of Fe and Fe_3C, carbon is associated with an even larger amount of iron than in free Fe_3C and accounts for the greater slope of the curve in Fig. 3 for carbon above 0.08 percent.

What has been stated above in regard to carbon applies in general to the other impurities N, O, and S, except that the available data are still very meager. In regard to nitrogen, the equilibrium diagram is very similar to that for Fe-C, showing precipitation of Fe_4N as the iron

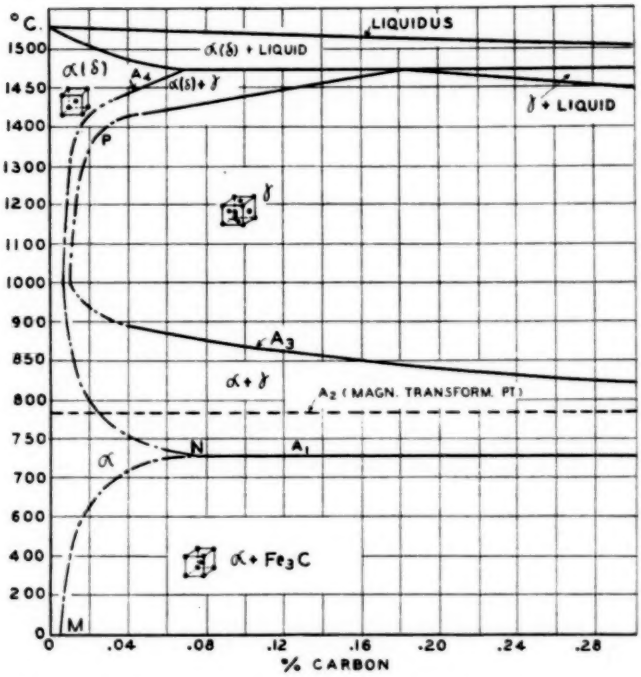

Fig. 4. Proposed constitutional diagram of the Fe-C system.

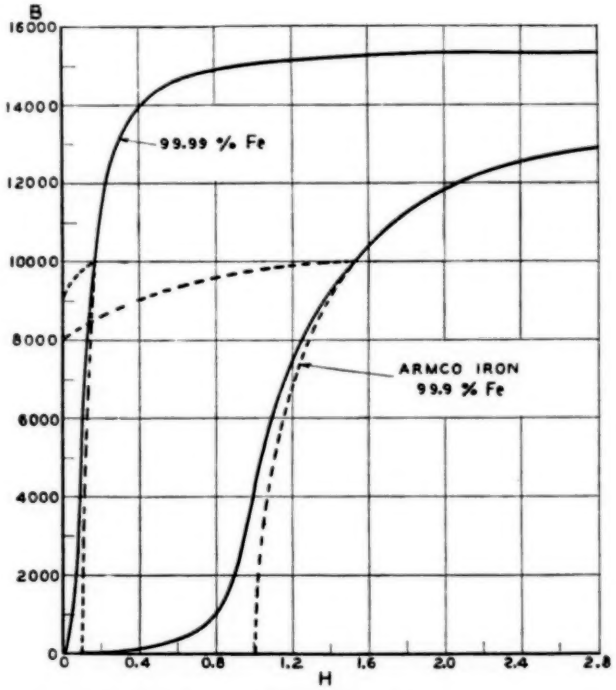

Fig. 5. Hysteresis loops and B-H curves for nearly pure iron.

cools from 580°C at which temperature the solubility is 0.5 percent according to Fry and Hägg. The solubility of oxygen in iron according to Ziegler is about 0.1 percent at 1000°C but decreases very rapidly with the temperature and is of the order of 0.01 percent at 900°C the excess precipitating as FeO. Sulphur precipitates as FeS.

At the relatively low temperatures at which the precipitation of Fe_3C, Fe_4N, FeO and FeS occur on account of the solubility decreasing gradually even down to room temperature, the attainment of equilibrium is a very slow process requiring days or weeks for completion. This gives rise to the phenomenon called "aging," a gradual change in the physical properties of most annealed materials at temperatures at which they are generally operated, ranging from 20° to 150°C. Low carbon iron, for example, will show a decrease in maximum permeability and an increase in hysteresis loss amounting to as much as 10 percent merely by being kept at room temperature for several weeks, the rate of change accelerating with the temperature.

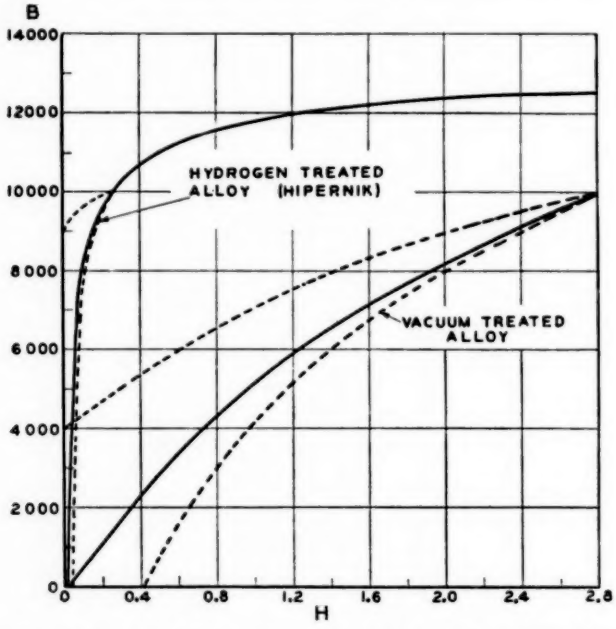

Fig. 6. Hysteresis loops and B-H curves for nearly pure 50 percent Fe-Ni alloys.

Köster has shown similar effects for nitrided steel, and precipitation hardening is a well-known phenomenon in connection with light alloys.

It is interesting to note that the new theories of ferromagnetism require a regular crystal lattice for the occurrence of ferromagnetic properties and consequently that any factor distorting the symmetry of the lattice will greatly affect these properties. In 1924 the writer predicted on extrapolating experimental data that the pure iron single crystal should show zero hysteresis and very high maximum permeability. Experimental evidence is confirmatory of this prediction as we have already approached very closely to the goal. Of course we can not hope ever to reach it absolutely.

In conclusion let us glance at the B-H curves and hysteresis loops of some of these high permeability materials and compare them with the curves for more ordinary materials differing from them in composition only by what an analytical chemist would term traces of impurities. Fig. 5 shows the difference between the purest commercial iron made, namely, Armco iron, containing less than 0.1 percent of impurities, and a sample of iron from which the carbon and oxygen have been eliminated down to a few thousandths of a percent by melting and annealing in vacuum. The maximum permeabilities and hysteresis losses are in the ratio of 10 to 1.

Similarly Fig. 6 shows the difference between a 50 percent Fe-Ni alloy prepared in the lab-

oratory by melting electrolytic iron and nickel in a vacuum furnace and annealing in vacuum at 900°C and a similar alloy after hydrogen annealing to reduce the oxygen content from a few hundredths to a few thousandths of a per cent. The latter has received the name "Hipernik." Here the maximum permeabilities and hysteresis losses are in the ratio of 20 to 1, the former having recently reached a value of 167,000.

July 14, 1931

HYDROGENIZED IRON

By P. P. Cioffi

Bell Telephone Laboratories, New York

SINGLE crystals of iron grown by a new method[1] with high temperature heat treatments in hydrogen were found to have better magnetic characteristics than single crystals grown at lower temperatures in hydrogen[2,3] or in vacuum.[4] Experiments showed that the improved

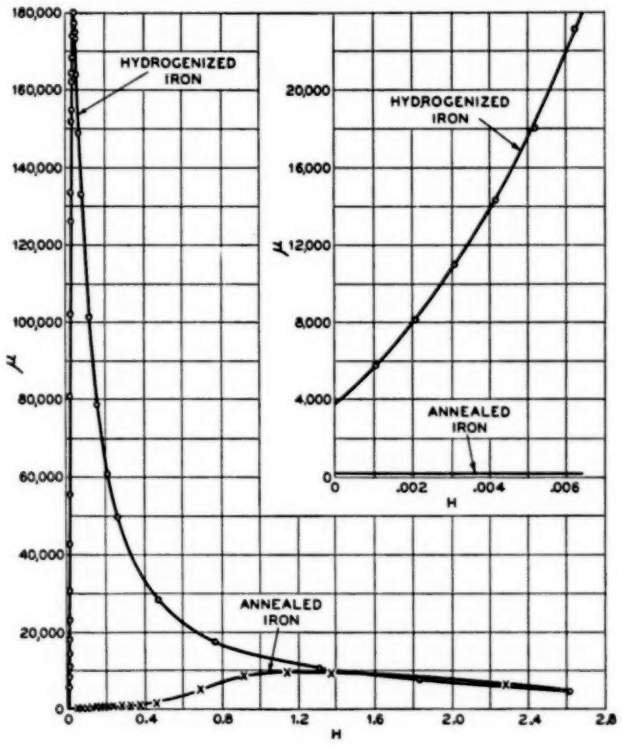

Fig. 1.

characteristics were not due to the large grain size but rather to the high temperature hydrogen treatment. It is now possible to produce iron having very high initial and maximum permeability regardless of grain size and orientation. The most recent results are shown in Figs. 1 and 2 for a ring of Armco iron 1-7/8″ outside diameter, 1-9/16″ inside diameter and ¼″ high, heat treated in moist hydrogen at 1475°C for 18 hrs., cooled to 880°C in one hr., then annealed at 880°C for 12 hrs., followed by slow cooling to room temperature. The initial and maximum per-

[1] L. W. McKeehan, Nature **119**, 705–706 (1927).
[2] W. Gerlach, Zeits. f. Physik **38**, 828–840 (1926).
[3] K. Honda and S. Kaya, Tohoku Imp. Univ. Sc. Rep., **15**, 721–753 (1926).
[4] D. D. Foster, Phys. Rev. **33**, 1071 (1929).

meabilities for this specimen are 4,000 and 180,000 respectively. The coercive force is 0.025 gauss and the hysteresis loss for $B_m = 14{,}000$ is 190 ergs/cm³/cycle. These results can be readily reproduced.

Early experiments with wires of one mm diameter showed that heat treatments at 1500°C for 30 min. give high initial and maximum permeabilities when the rate of cooling through the

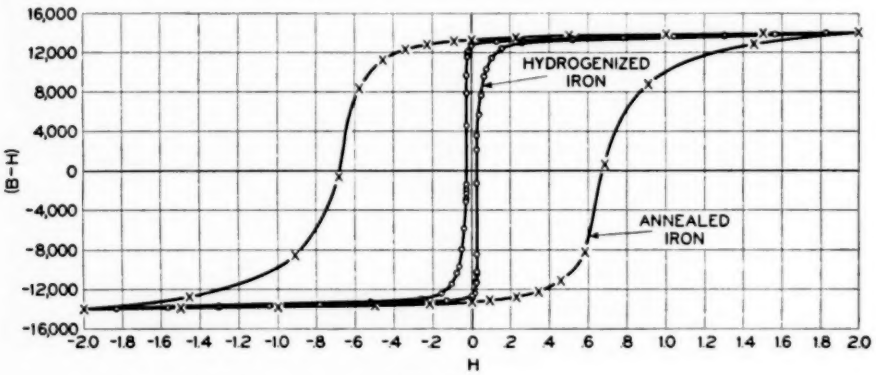

Fig. 2.

alpha-gamma transformation point is slow. By giving the hydrogen treatment in two steps: a high temperature treatment followed by rapid cooling, and a low temperature anneal below the alpha-gamma transformation point, a further improvement in magnetic characteristics is obtained. These results are shown in Fig. 3. It has been found that considerable overstrain may be applied between the high temperature treatment and the low temperature anneal without preventing good results.

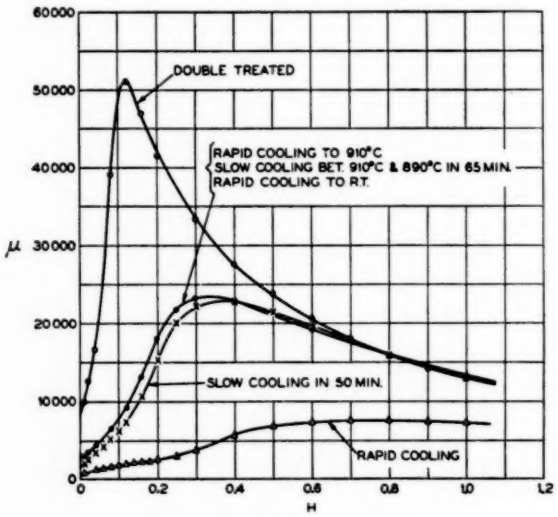

Fig. 3.

The magnetic characteristics of hydrogenized iron are dependent upon the cross-section of the metal, the maximum permeability rising rather rapidly with thickness as shown in Fig. 4. On the other hand, the required time of high temperature treatment increases with thickness of the metal, 5/32″ thick specimens requiring as long as 18 hours.

Good results have been obtained by heat treatments at 1500°C in hydrogen at pressures as low as 45 mm and as high as 760 mm of mercury, but for pressures of 1 mm or 1520 mm the

results have been less satisfactory. There is reason to believe that there is an optimum pressure of hydrogen for every temperature of treatment.

High temperature heat treatments have been carried on in other atmospheres and in hydrogen containing various gaseous impurities. The most satisfactory results are obtained when the hydrogen is saturated with water vapor at room temperature.

Ordinary amounts of carbon, sulphur, phosphorus, oxygen and nitrogen, which are known to have harmful effects on the magnetic characteristics of iron, are reduced to very small quantities by prolonged hydrogen treatment. The large improvement obtained when water vapor is introduced in hydrogen is believed to be due to its increased effectiveness in decarburizing. E. D. Campbell[5] pointed out that moist hydrogen is most effective between 950° and

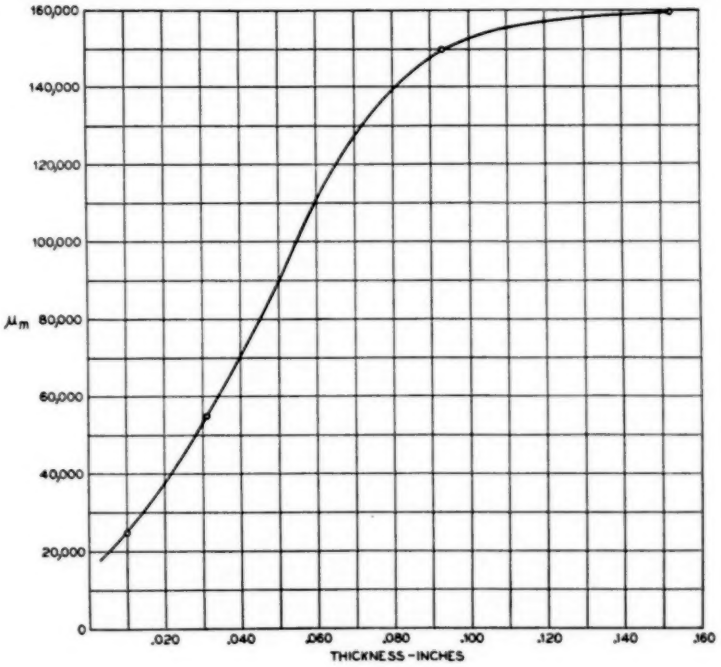

Fig. 4.

1000°C and since 1924 numerous experimenters, particularly those concerned with growing large single crystals of iron have treated their specimens at 950°C in moist hydrogen to remove the carbon which was supposed to inhibit grain growth. If decarburization plays an important part in these results, it appears as though temperatures higher than 950°C are much more effective. Ordinary impurities of silicon, manganese, copper and aluminum neither change in amount nor prevent good results. Vacuum treatments of hydrogenized iron cause a liberation of about ½ volume of gas, consisting of approximately 21 percent hydrogen, 33 percent CO_2, 34 percent CO, 2 percent N_2 and 10 percent H_2O. The quantity of carbon evolved as CO and CO_2 represents less than 0.002 percent.

Hydrogenized iron is nearly as soft as annealed copper. Its tensile strength is 14,000 lbs./in.,[2] its yield point is 7,000 lbs./in.[2] and its Rockwell *B* hardness lies between +10 and −10. Another characteristic is that grain growth in hydrogenized iron is more pronounced than in ordinary iron, ranging from about 0.04″ to 0.2″. Some grains are more than 0.5″ in length, occupying the full cross-section of the specimen. Toroidal specimens of 2″ diameter have been obtained consisting of 5 or 6 single grains. There is evidence that the large grains grow at the high temperature and that under certain conditions retain their identity even after cooling

[5] E. D. Campbell, J. F. Ross and W. L. Fink, Jour. Iron and Steel Inst. **108,** 179–185 (1923).

through two transformation points. In many respects, however, hydrogenized iron is no different from ordinary iron. For instance, the high temperature hydrogen treatment produces no appreciable change in resistivity, temperature coefficient of resistance, density and lattice parameter.

We do not know yet in what manner the high temperature hydrogen treatment produces the remarkable results described. It is well known that the magnetic characteristics of iron are improved by purification.[6] Chemical analyses show that the high temperature treatment does purify, and further evidences of this purification are large grain growth and mechanical softness. It is plausible therefore to suggest that purification plays a considerable part in these results. On the other hand the dependence of the magnetic characteristics of hydrogenized iron on the pressure of hydrogen, rate of cooling and time of anneal at 880°C are consistent with the view that absorbed hydrogen also plays an important part in these results.

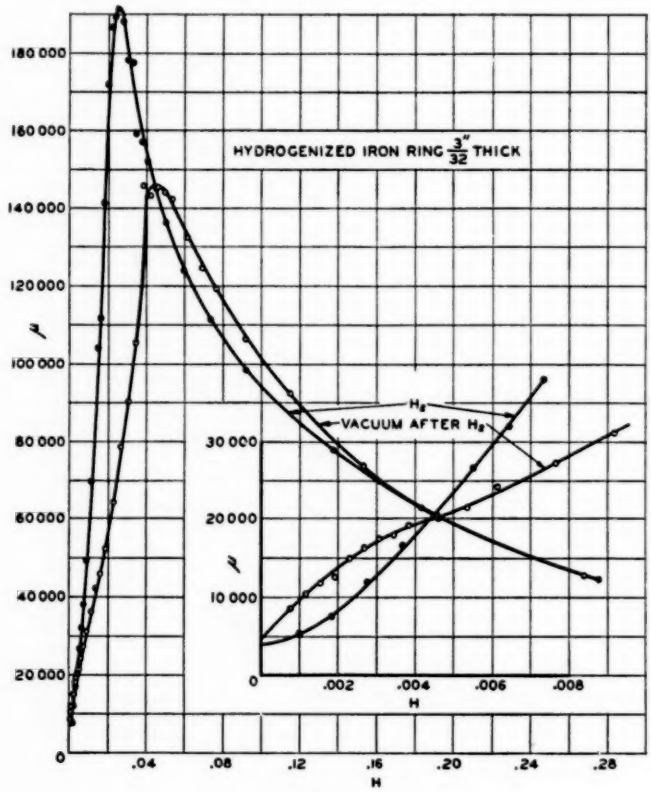

Fig. 5.

It was reported in a previous note[7] that further purification of hydrogenized iron by heat treatment in a high vacuum causes a diminution in permeability. This diminution was believed to be due to the pumping out of absorbed hydrogen. Since then, it has been found that the magnetic characteristics are dependent upon thickness, the permeability diminishing with decrease in thickness, and the previously reported diminution in permeability can now be largely accounted for by the decrease in thickness of the specimen produced by excessive evaporation during the vacuum treatment. In a more recent experiment, a specimen 3/32″ thick having a maximum permeability of 190,000 was heat treated in vacuum at 1200°C for 100 hours and at 880°C for 24 hours. The decrease in maximum permeability to 145,000 as shown in Fig. 5, can

[6] T. D. Yensen, Jour. Franklin Inst. **206,** 503–510 (1928).

[7] P. P. Cioffi, Nature **126,** 200–201 (1930).

also be largely accounted for by the decrease in thickness produced by evaporation. It now appears as though what previously seemed to be an effect ascribed to the pumping off of absorbed hydrogen may have been an effect due to decrease in thickness. It is just possible, however, that for this thickness of metal the 100 hours treatment in vacuum may have been insufficient to cause all of the absorbed hydrogen to diffuse out. The change in shape of the initial part of the permeability curve suggests inhomogeneity possibly due to a concentration gradient of absorbed hydrogen. In any case, a high vacuum treatment, supposedly producing further purification of hydrogenized iron has not been found to produce a further increase in permeability.

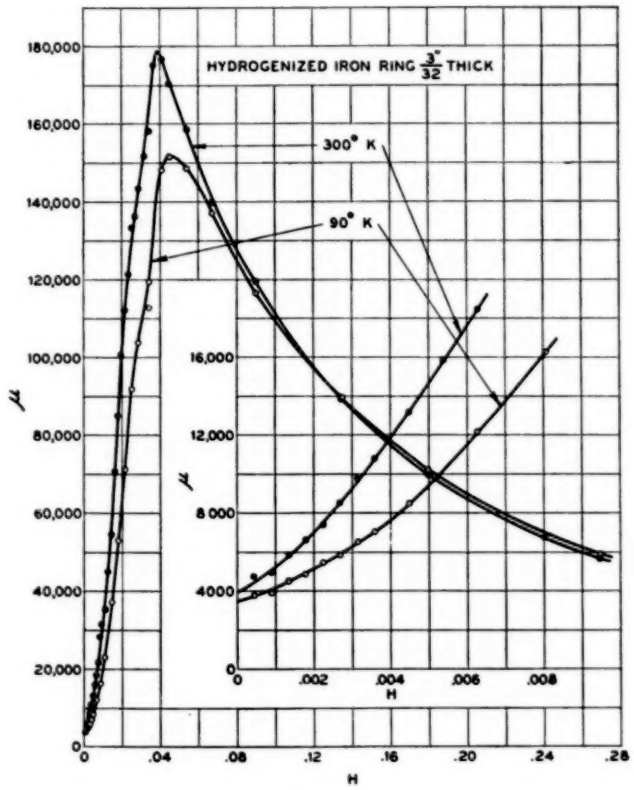

Fig. 6.

Grain size and thickness of specimen affect the magnetic characteristics as soon as the grains become so large or the specimen so thin that only a few grains occupy a cross-section perpendicular to the applied magnetic field. This has been checked in several ways. Under these conditions the flux distribution becomes non-uniform and the average permeability of the specimen drops.

The effect of lowering the temperature of hydrogenized iron to that of liquid air is shown in Fig. 6. The relatively small diminution in permeability accompanying a large decrease in temperature makes it appear unlikely that the characteristics of hydrogenized iron are due to thermal impacts between the absorbed hydrogen and iron atoms.[8,9]

October 15, 1931.

[8] L. W. McKeehan, Nature **126,** 952–953 (1930).

[9] K. Honda, Zeits. f. Physik **67,** 808–811 (1931).

MAGNETIZATION AND THERMAL E.M.F's*

By S. R. Williams
Amherst College

THE thermal e.m.f. developed between transversely and longitudinally magnetized wires is shown in Fig. 1 for the case of iron and nickel. The experimental arrangement has been given in Fig. 1 of Seass' paper. This effect was predicted by Sir William Thomson.[1] A related phenomenon is the von Ettingshausen-Nernst effect in which a heat flow perpendicular to a

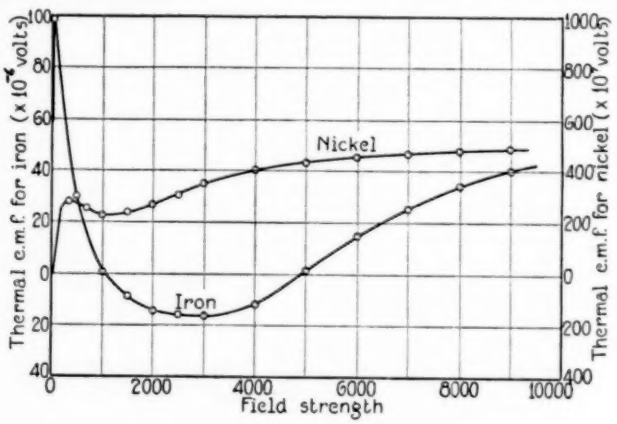

Fig. 1.

magnetic field is the conductor causes a potential gradient parallel to the heat flow. A correlation of the two effects for various conductors is of great interest, particularly for bismuth, antimony, and carbon, since these three have some interesting properties in connection with their conductivites.[2]

The present experiments show that temperatures determined by thermocouples in magnetic fields are not reliable unless the elements of the couple are unaffected by the field. A number of elements are displaced in the thermo-electric series by being in a magnetic field. Naturally, relations with magneto-striction[3] and magneto-resistance[4] will be sought.

* Some of the material of this presentation has since been published by S. Seass; Thermocouples whose elements are longitudinally and transversely magnetized ferromagnetic substances, Phys. Rev. **38,** 1254 (1931). Accordingly the present résumé has been shortened in such a way as to avoid unnecessary duplication.

[1] W. Thomson, Math. and Phys. Papers **2,** p. 286.

[2] Raman, Nature **124,** 412 and 762 (1929).

In addition, the e.m.f. in iron and nickel throughout complete hysteresis loops is to be studied.

[3] L. W. McKeehan, Phys. Rev. **36,** 498 (1930) and **28,** 146 (1926); Williams and Sanderson, Phys. Rev. **307,** 39 (1931).

[4] Rhoads, Phys. Rev. **15,** 321 (1902); Bidwell, Proc. Roy. Soc. London **73,** 413 (1904).

MAGNETOSTRAIN AND MAGNETORESISTANCE

By L. W. McKeehan
Yale University

THE dimensions and electrical conductivities of a ferromagnetic body are affected in two ways by its magnetization.

The conspicuous effects at temperatures far below the Curie points are anisotropic. With reference to the direction along which the magnetization increases the longitudinal and transverse effects are opposite in sign. The longitudinal magnetostrain may be positive or negative depending upon the nature of the material. The longitudinal magnetoresistance is always positive.

The anisotropic magnetostrains are most apparent in monocrystal specimens. Their signs and magnitudes depend upon the orientation of the magnetization vector with respect to the crystallographic axes. It is not yet known whether the anisotropic magnetoresistances differ for different orientations of magnetization, but variations in magnitude, at least, are very probable.

The anisotropic effects of magnetization reach limiting values—become saturated—for magnetizations easily attainable in the softer magnetic materials. The magnitude of each effect is not, however, directly proportional to the change in net magnetization over any wide range. A given magnetostrain or magnetoresistance increases at low magnetizations more slowly than the magnetization. At higher magnetizations the order of variability reverses, and at still higher magnetizations it reverses again so that the magnetostrains and resistances saturate more sharply than does the magnetization.

In poly-crystal specimens anisotropic elastic strains affect the anisotropic magnetostrains and magnetoresistances. Such elastic strains also affect the magnetic permeability. These two effects are so closely related that we may always predict the nature of one from the nature of the other. In one set of experiments—where, however, the strains were not wholly elastic—a quantitative prediction has been verified. The same reciprocity doubtless exists in monocrystals, but data are lacking. The anisotropic effects are conspicuously structure-sensitive.

Another fact which points to an intimate relation between the anisotropic effects and the process of magnetization is found in studying ferromagnetic alloys. Other things being equal an alloy with vanishing magnetostrains will be found very easy to magnetize and little energy will be required for traversing its hysteresis loop.

A consideration of all this leads us to the conclusion that the anisotropic effects must be due to the reorientation within the material of some structural element which differs from a sphere. As we know that the atom-centers do not move more than is made necessary by the gross shearing strains we are forced to suppose that the structural element concerned is of atomic or sub-atomic dimensions. This is a restatement of my former conclusion that what I then called "atomic magnetostriction" was important in controlling the process of magnetization. It does not deny the hypothesis that many adjacent atoms change their orientations in the same manner at once or nearly at once, as the Barkhausen effect so clearly suggests.

The equivalence of magnetic (vectorial) control and elastic (tensorial) control in effecting reorientations is so complete that we must suppose the ferromagnetic atom symmetrical with respect to a diametral plane perpendicular to its magnetic axis.

We must now consider the second way in which magnetization affects dimensions and electrical conductivities. The conspicuous magnetostrains and magnetoresistances in the neighborhood of the Curie points are, at least in cubic crystals, apparently isotropic. The so-called Curie point anomalies in thermal dilatation and in the temperature coefficient of resistance must really accumulate over the whole range in temperature within which a material is ferromagnetic, but the rates of accumulation at temperatures far from the Curie points are negligible.

The isotropic magnetostrain may be of either sign. The isotropic magnetoresistance is negative, that is, the resistance increases as the magnetization diminishes with rise in temperature.

The Curie point anomaly in the specific heat of a ferromagnetic is intimately related with the isotropic effects on atomic volume and electrical resistivity and all three depend upon the intrinsic magnetization rather than upon the apparent (or resultant) magnetization in any particular direction.

In looking for an explanation of the isotropic effects we have to remember that the difference between the ferromagnetic and nonferromagnetic conditions of a single material lies in the relative fixity of atomic orientations in the former condition. The magnetic axes of the atoms remain nearly unaltered in direction as time passes at temperatures below the Curie points. It is also now customary to suppose that at least in soft magnetic materials large numbers of neighboring atoms have their magnetic axes parallel and that their common direction is one of

the so-called "easy" directions of magnetization. A direction of easy magnetization is a direction of low crystallographic indices which is in no known case the direction along which the atoms are most closely packed.

The process of magnetizing at temperatures within the ferromagnetic range consists then primarily in redistributing the directions of the atomic axes, singly or in groups, so that they lie along those directions of easy magnetization which lie at small angles from the applied magnetic field. At all stages the atoms, at least, and probably regions containing many atoms, remain magnetized to saturation.

The suggestion now advanced is an extension of the notion of atomic magnetostriction by which we may account for the isotropic magnetostrains and magnetoresistances by the mere existence of such preferred orientations of atoms as have just been mentioned, without regard

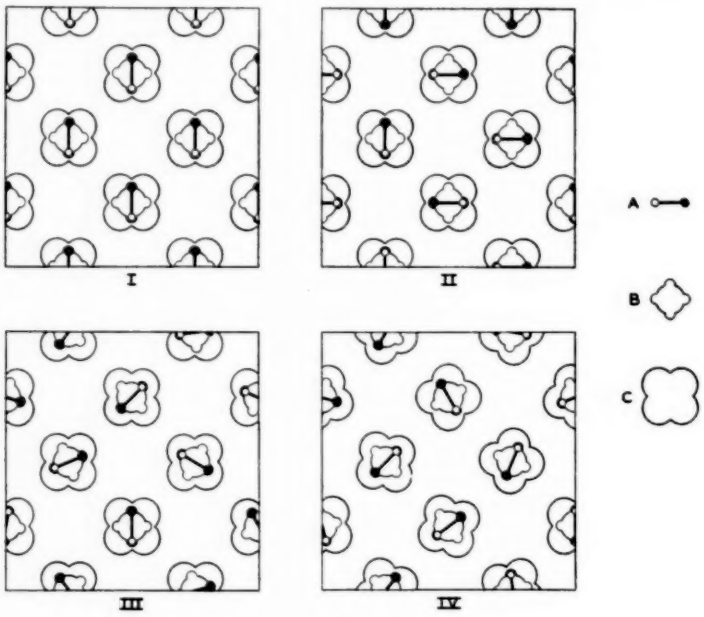

Fig. 1.

to which of the several possible orientations is preferred. The intrinsic magnetization, which measures the degree of preference is therefore here important, but the magnetization vector, which registers the particular orientations preferred as a result of previous magnetic and mechanical history, is not.

We need only to suppose that the atoms of the ferromagnetic metal have as nearly as possible the symmetry of their crystals. In iron and nickel they must have nearly cubic symmetry, the slight defect being due to their possessing a magnetic moment which conditions what we have previously termed their atomic magnetostriction. In hexagonal cobalt the atomic symmetry may be strictly hexagonal.

An atom of cubic symmetry need not, of course, resemble a cube any more exactly than a starfish resembles a regular pentagon. If such spiny atoms have preferred orientations the interatomic forces and the atomic volume may depend much more upon the fact that all (or many) of them present certain non-magnetic structural features to their neighbors than upon the particular direction of the magnetic axis in each. The existence of low resistance paths for electrical conduction may equally well depend upon the regular repetition along a row of atoms of the same non-magnetic structures in each.

In the case of iron, at least, some further complexity of the atomic structure appears necessary. The nearly cubic "habit" of the atom of iron must, in fact, be retained above the Curie points at least up to the α-γ transition temperature, for the α-iron crystal structure in this tem-

perature range is incompatible with sphericity of the component atoms. The simplest hypothesis seems to be that there are here two nearly cubic parts of the atomic structure, one controlling the crystal structure, the other controlling the orientation of the atomic magnetic moment. The Curie point would then be interpreted as the temperature at which these two structural elements —or group of eleme :ts —uncouple so that above this temperature the atomic magnet is no longer constrained to lie in particular crystallographic directions. Fig. 1 illustrates schematically—in two dimensions—how a dipole A may be contrained by a structure B with the symmetry of a square, while a second structure C, also having the symmetry of a square, determines the structure of the crystallographic net. In (I) the dipole axes are parallel, corresponding to magnetic saturation in an "easy" direction at low temperature. In (II) the dipole axes are dispersed among the several "easy" directions, corresponding to a demagnetized state, still at low temperature. In (III), at a higher temperature, the dipole control has been lost, so that ferromagnetism has vanished, but the crystal structure is still stable. In (IV) at a still higher temperature the crystal structure has become unstable and an allotropic transformation is imminent. The transition from (III) to (II) involves the isotropic magnetostrains and magnetoresistances. The transition from (II) to (I) involves the anisotropic effects.

Non-sphericity need not at all be confined to ferromagnetic atoms. There is plenty of evidence in the mechanical properties of non-ferromagnetic metals that many atoms are but poorly represented by spheres. The mere existence of crystal structures less symmetrical than the face-centered cubic arrangement is good evidence for the non-sphericity of atomic fields.

The mathematical formulation of the problems of ferromagnetism is up to the present so beset with difficulties that the solutions under any but ideal conditions may be long in appearing. In these circumstances we are still justified in picturing a mechanism capable of explaining the exchange interaction integral of Heisenberg's theory by the mutual potential energy of non-spherical atomic fields in special orientations. We may by such an artifice foresee more clearly the effects of agencies which it may be very troublesome to include in any rigorous analysis.

ON THE VERIFICATION OF THE THEORY OF MAGNETIZATION OF SINGLE CRYSTALS

By Francis Bitter

Westinghouse Research Laboratories
East Pittsburgh, Pennsylvania

THE theory of magnetization outlined elsewhere in this issue[1] makes it possible not only to construct the magnetization curves of single crystals in their principal crystallographic directions, as has been done, but also to predict the magnetization produced by any field acting on a crystal in any direction. The procedure is briefly the following: assume the material to be made up of small regions magnetized to an intensity I_w, but free to orient their magnetization independently of their neighbors. The potential energy per unit volume of such a region as a function of its direction of magnetization within an unstrained crystal is then given by expression of the form[2]

$$E_{\theta,H} = K(I_{wx}^2 I_{wy}^2 + I_{wy}^2 I_{wz}^2 + I_{wz}^2 I_{wx}^2) - (\vec{I}_w \cdot \vec{H}) \tag{1}$$

for cubic crystals, or

$$E_{\theta,H} = K_1 I_{wz}^2 + K_2 I_{wy}^2 + K_3 I_{wz}^2 - (\vec{I}_w \cdot \vec{H}) \tag{2}$$

for hexagonal crystals. For every value of H, the function $E_{\theta,H}$ has a set of minima and maxima. It is assumed that I_w will orient itself in those directions in which $E_{\theta,H}$ has an absolute minimum, and that if there are two or more equal minima, equal numbers of regions will be found in each. The assumptions are probably correct only if the absolute minima are considerably be-

[1] In the symposium paper; "On the Interpretation of Some Ferromagnetic Phenomena."

[2] For illustrations of typical curves see F. Bitter, Phys. Rev. **38**, 534 (1931).

low the next lowest ones, and if the potential barrier separating them is not too high. The above assumptions will certainly not cover any phenomena involving hysteresis. It is found convenient to use a reduced field strength h, which is given by

$$h = \frac{8H}{KI_w^3} \tag{3}$$

for cubic crystals, and

$$h = \frac{H}{2I_w(K_2 - K_1)} \tag{4}$$

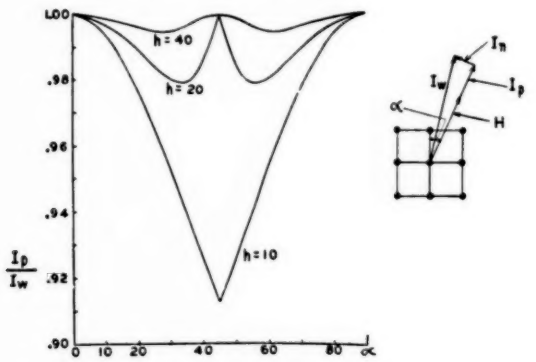

Fig. 1 Theoretical curves for the component of I parallel to H as H takes on various orientations in a (100) plane in iron. $\alpha=0$ corresponds to H in a (100) direction.

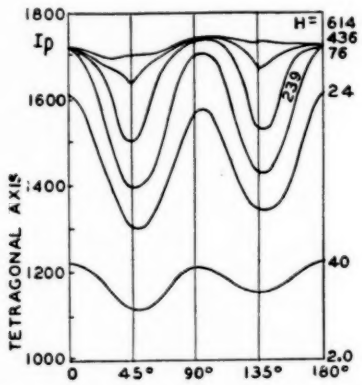

Fig. 2. The experimental data checking the curves in Fig. 1. H/h is approximately 30. The observations are by K. Honda and S. Kaya, Sci. Rep. **15,** 721 (1926).

for hexagonal crystals, in which two of the three coefficients K_x are chosen equal, corresponding to the fact that the (0001) plane is magnetically isotropic.

The symbols used are illustrated in Fig. 1. The angle between some fixed crystallographic direction and the applied fields is called α. I_p is the component of I_w parallel to H, and I_n is the component normal to H. The theory is applied to iron crystals, in which K is positive. In nickel K is negative, and as a consequence I_n is in general not confined to either a (100) or a (110) plane, even if H is in this plane, which renders the conditions difficult to portray graphically, or to observe experimentally in disk-shaped samples. In Figs. 1 and 2 the theoretical and experimental results are recorded for the parallel component in a (100) plane in iron. At room temperature H/h is approximately 30. The dissymmetry of the experimental curves indicates that the sample was probably somewhat distorted. Further experimental work should indicate what

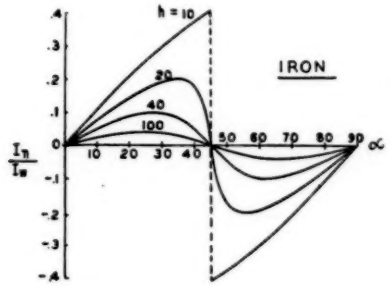

Fig. 3. Theoretical curves for the component of I normal to H as H takes on various orientations in a (100) plane in iron.

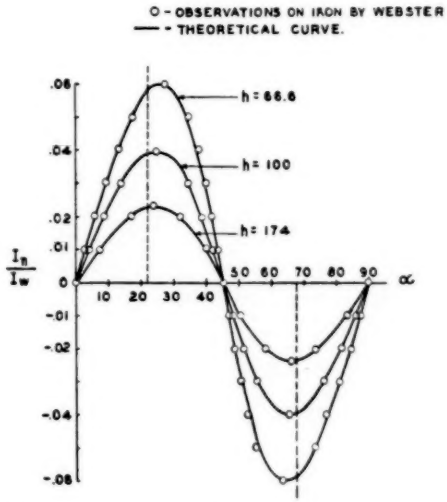

Fig. 4. The experimental data checking the theoretical curves of Fig. 3. The observations ar by W. L. Webster, Roy. Soc. Proc. **107**, 496 (1925).

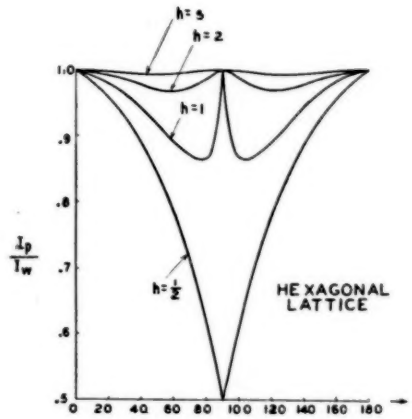

Fig. 5. Theoretical curves for the component of I parallel to H as H takes on various orientations in a plane containing the axes of difficult and easy magnetization in a hexagonal lattice.

distortions influence the observations. They may be of a more subtle kind than macroscopic strains.[3] Certain similarities between the curves in Figs. 1 and 2 are to be observed.

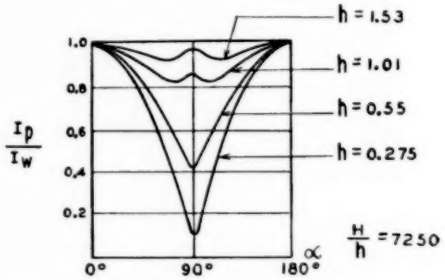

Fig. 6. The experimental data on pyrrhotite checking the curves in Fig. 5. The observations are by Weiss, and are taken from Int. Crit. Tables **6,** 413 (1929).

Figs. 3 and 4 show the corresponding curves for the normal component of I. The agreement is excellent, but a discrepancy should be pointed out. In order to secure coincidence be-

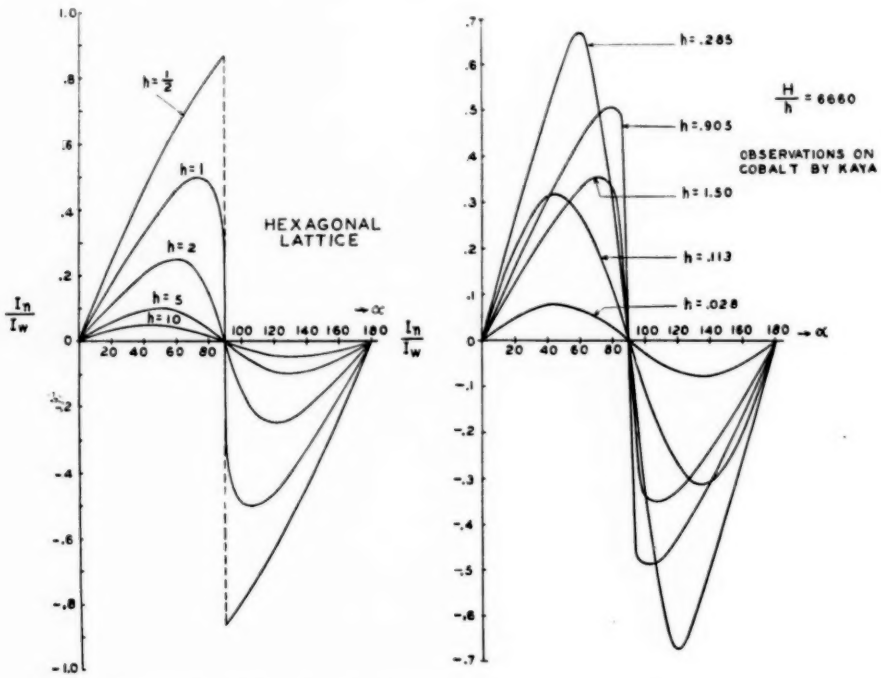

Fig. 7. Theoretical curves for the component of I normal to H as H takes on various orientations in a plane containing the axes of difficult and easy magnetization in a hexagonal lattice.

Fig. 8. The experimental data checking the curves in Fig. 7. The observations are by S. Kaya, Sci. Rep. **17,** 1157 (1928).

tween the theoretical and experimental curves the values of H/h were chosen for each curve so that the maximum values of I_n agreed. But these ratios had not the same value for each curve.

[3] Concerning the magnetic symmetry of crystals, see J. Kunz, Bull. Nat. Res. Council **3,** 165 (1922).

$$H/h = \frac{7620}{174} = 43.4$$

$$H/h = \frac{3500}{100} = 35$$

$$H/h = \frac{2030}{66.6} = 30.5.$$

Webster's measurements were, however, made on disks having a comparatively small axial ratio, and it is conceivable that the above discrepancy is due to an error in determining the true effective field.

In Figs. 5 and 6 are shown the theoretical and experimental results for the parallel component of hexagonal lattices. $\alpha=0$ represents a direction of easy magnetization, which is the (0001) axis for cobalt at room temperatures and any direction in an (0001) plane for pyrrhotite. $\alpha=90$ is then a direction of difficult magnetization. The agreement shown is good.

Figs. 7 and 8 show the corresponding curves for the normal component. The experimental curves for $h=0.028$ and 0.113 have no theoretical counterpart, in accordance with the fact that we do not have a theory of magnetization for small fields, in which only slight differences in the depths of the minima of $E_{\theta,H}$ occur, and where there is hysteresis. The curves for $h=0.285$, 0.905, and 1.50 resemble the theoretical curves except for values of α near 90°, where again two minima of $E_{\theta,H}$ differing only slightly in depth are to be found.

From the above discussion the following inferences may be drawn: that the above scheme is capable of representing the main features of the deviation effect in crystals; that certain departures from symmetry which require further investigation are found in some substances; and that studies of the magnetization of single crystals in large fields in the neighborhood of the axes of difficult magnetization should supplement studies of the initial susceptibility, as both quantities depend on the distribution of magnetized regions among minima of $E_{\theta,H}$ differing only slightly in depth. It may further be concluded that I_n for fields nearly parallel to a direction of difficult magnetization will probably be found structure-sensitive.

October 6, 1931.

Discussion of Papers by Messrs. Bozorth and Sixtus

Mr. Tonks asked what the significance was of discontinuities in magnetization that cover more than one crystal grain.

Mr. Bitter replied that the important point to be decided is whether the magnetized regions cover more than a single grain. It is, of course, quite possible that they do not, and that large discontinuities are due to the interaction of neighboring regions. Beyond this it is important to discover whether all the spins contributing to the magnetization of such a region are coupled together by the exchange interaction forces, or whether only smaller groups of spins are so coupled, these smaller groups being held together by other, say magnetic forces. It may be possible to answer the first part of the question quite definitely, depending on whether one can produce small-grained material in which the internal strains may be neglected. The direction of magnetization of a region is determined by the minima of the function representing its potential energy in terms of the crystal structure and of the orientation of the lattice in the applied field. If each region is confined to a single grain the usual expression for the potential energy is applicable and the magnetization curve can be calculated from a knowledge of the distribution of grain orientations. If, on the other hand, a magnetized region covers more than one grain, its potential energy will consist of the sum of the energies of the individual grains and will in general have minima that lead to different magnetization curves.

Mr. Bozorth remarked that no reason had been suggested for believing that a single domain may not include crystal boundaries. If we regard the change in magnetization within a domain from the point of view of the interchange interaction theory, the atoms near the crystal boundary will be different from the others in that they will be at somewhat different distances from each other and surrounded less symmetrically. But this means only that the interaction will be generally less intense and not that it will prohibit the progress of

magnetization. In fact Slater's calculations (Phys. Rev. [2] **36,** 57–64 (1930)) indicate that the interaction does not fall off very fast as the distance between atoms increases.

Mr. Dillinger remarked that in measurements that he and Mr. Bozorth had made on unstrained annealed samples of several permalloys they had found that the velocity of propagation of the large groups of Barkhausen impulses was dependent upon the electrical resistance in the magnetizing coil circuit. This indicated that the velocity was at least partially controlled by the voltage induced in the magnetizing coil by the sudden change in flux. He asked if Mr. Sixtus had found this to be true in his experiments.

Mr. Sixtus replied that he had tried varying the resistance in the circuit by a factor of two or three and in that case the velocity of the impulse was unaffected.

Discussion of Papers by Messrs. Yensen and Cioffi

Mr. Elmen inquired why, if the best magnetic condition was obtained when the material had reached equilibrium, did iron with low carbon content become poorer after aging.

Mr. Yensen answered: The original hypothesis (1923) was that carbon has the greatest effect when in solution, i.e., when the carbon atoms occupy the interstitial spaces, and that about 0.006–0.008 percent C is in solution at room temperature. This was based on microanalysis in combination with analysis for total carbon. As stated in the paper, further considerations have led to the conclusion that what we earlier regarded as carbon in solution is largely carbon in the form of colloidal particles of Fe_3C, invisible under the most powerful microscope, but probably having a greater distorting effect on the lattice than single atoms of carbon. Aging, on this basis, is due to carbon in solution, exceeding the solubility limit and consequently precipitating as colloidal Fe_3C at room temperature or at slightly elevated temperatures.

In order that a particle shall be visible at a magnification of 5000, it must contain at least 10^6 atoms, and particles of this size and larger will have a relatively smaller effect than the same amount of material in the form of colloidal particles, containing between 10 and 10^6 atoms, dispersed throughout the iron grains.

Mr. Ruder confirmed Mr. Yensen's statements concerning aging from his experience with silicon steel. With this substance too rapid cooling results in aging, whereas rapid cooling followed by re-heating with slow cooling causes the precipitation of foreign particles, presumably as larger aggregates, and aging is prevented.

In answers to questions by F. J. Norton Mr. Yensen stated that zircon was used for the crucible and that the treatment was carried out in vacuum.

Mr. McKeehan pointed out that high initial permeability is dependent upon atomic disorder which may sometimes be produced by rapid cooling and by small quantities of impurities. Hydrogen in the iron lattice may produce such disorder and so cause high initial permeability. This view is consistent with Sixtus' observation in his experiments on the Barkhausen effect that a disturbance of alignment, as by twisting, favors reversal of domains both to form nuclei and to increase propagation velocity.

Mr. Tonks asked whether a second hydrogen treatment produced further improvement in the magnetic characteristics of a vacuum-treated specimen of hydrogenized iron, in view of the fact that gaseous impurities are given off during the vacuum heat treatment. Mr. Cioffi replied that this experiment had not yet been done with specimens of the high permeability now obtainable, but expressed the opinion that the second hydrogen treatment would produce results comparable with the first hydrogen treatment.

Mr. Sixtus pointed out that iron permeated with hydrogen, from use as a cathode in an electrolytic cell, is brittle and has high coercive force and hysteresis loss. He asked whether such cathodically pickeled iron should not also be expected to have characteristics similar to hydrogenized iron, if the characteristics of the latter are attributable to absorbed hydrogen. Mr. Cioffi replied that the absorption of hydrogen by the two methods and its distribution are sufficiently different to give different results. By the high temperature treatment the iron is left soft, free from strain, while by the electrolytic method hydrogen is absorbed under high pressures (Anson Hayes: Trans. A.S.S.T. **17,** 527–537 (1930)) which weakens the metal and renders it brittle. It is well known also, that iron which is quenched after a high temperature treatment in hydro-

gen has characteristics similar to cathodically pickeled iron.

Mr. W. E. Ruder expressed the opinion that iron becomes saturated with molecular hydrogen in much less time than it takes for a hydrogen treatment. The long period of treatment necessary indicates that the process is one of purification. Furthermore, the absorbed hydrogen would be given up very quickly during the vacuum treatment. Experiments with silicon steel show that improvements in magnetic characteristics by hydrogen treatment are obtained in a relatively short time. Mr. Cioffi maintained that hydrogen is absorbed in the atomic state, evidence of which is found in the observations of numerous experimenters that absorption and diffusion are proportional to the square root of the pressure. While absorption of hydrogen by iron is nearly proportional to temperature (A. Sieverts, Zeits. f. phys. Chem. 591–613 (1911)), the rate of diffusion is an exponential function of the temperature (O. W. Richardson, J. Nicol, T. Parnell; Phil. Mag. **8,** 1–29 (1904)). Early experiments by Sieverts (loc. cit.) and more recently by Martin (Metals and Alloys **2,** 831–835 (1930)), indicate that hydrogen-metal equilibria are established in a few minutes. On the other hand, Steacie and Johnson (Roy. Soc. Lond. Proc. **117,** 662–679 (1928)) have shown that the silver-hydrogen system takes several hours to come to equilibrium even when the metal is only 0.006″ thick. In view of this it is not at all certain that a vacuum treatment at 1200°C for 100 hours is sufficient to drive all of the hydrogen out of a specimen of hydrogenized iron. By hydrogen treating silicon steel near its melting point, a temperature very much higher than that used by Mr. Ruder, it has been possible to obtain initial permeabilities of nearly 4000.

Mr. Yensen expressed satisfaction over the fact that the vacuum treated specimen of hydrogenized iron suffered no large decrease in permeability, indicating that the effect of hydrogen is only one of purification. Mr. Cioffi replied that if this were true, there should have been a further increase in permeability as a result of further purification by the vacuum treatment during which gaseous impurities are given off.

Mr. O. E. Buckley asked how long it takes for the flux to build up in a high permeability specimen. Mr. Cioffi stated that it takes about one minute. At liquid air temperatures, however, it takes as long as four minutes for the flux to build up to a steady state in a specimen having a section $5/32'' \times \frac{1}{4}''$.

Discussion of Paper by Williams

Mr. Tonks inquired as to the essential difference in set-up between having the short length of wire longitudinally magnetized with the leads in a transverse field and vice-versa.

Mr. Williams replied that in all three set-ups were used, each yielding different results.

Mr. Tonks stated that theoretically it could not make any difference how the lead-in wires were carried through the magnetic field provided that they were kept at constant temperature.

Mr. Williams pointed out in reply that the e.m.f. of a cell was affected by orientation in a magnetic field irrespective of temperature.

The possibility of a correlation by means of thermodynamic relations between the effects Mr. Williams is investigating and the calorific investigations of Mr. Quimby was suggested by Mr. Tonks. Mr. Williams remarked that the thermoelectric relations were far from simple in that cooling the wire between hot and cold junctions changed the e.m.f.

LETTERS TO THE EDITOR

Prompt publication of brief reports of important discoveries in physics may be secured by addressing them to this department. Closing dates for this department are, for the first issue of the month, the twenty-eighth of the preceding month; for the second issue, the thirteenth of the month. The Board of Editors does not hold itself responsible for the opinions expressed by the correspondents.

Absorption of γ-Rays

The Klein-Nishina formula based on scattering by extranuclear electrons gives a value of the coefficient of absorption per electron which is independent of the atomic number and equal to 1.235×10^{-25}. However, the experimental values all show an increase with atomic number of the quantity σ_e obtained by dividing the coefficient of absorption per atom σ_A by the number of extranuclear electrons, as Beck[1] has shown.

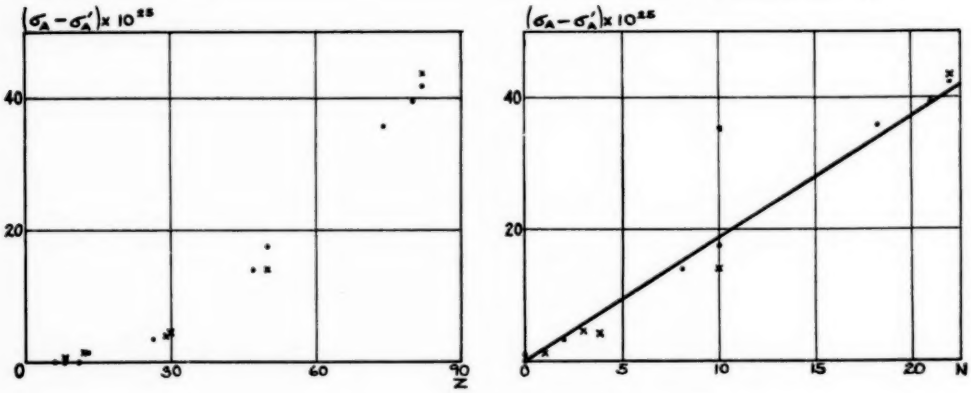

Fig. 1.

Converting back the experimental data to expression in terms of σ_A we obtain Fig. 1A. The points marked with crosses are taken from the data of Meitner and those with dots from the data of Chao. The ordinates $\sigma_A-\sigma_A'$ represent the value of σ_A less the contribution to the atomic absorption coefficient from the Klein-Nishina formula. They are plotted against the atomic number. The discrepancy in the figure are regarded as real by Meitner and were investigated with special care for Mg 12 and Al 13. However their existence seems to the writer to imply that the quantity fundamental to the nuclear scattering is not the atomic number but some quantity varying discontinuously with it. Such a quantity is n, the number of nuclear electrons unassociated with α particles. It can be obtained if we assume that the protons in the nucleus are collected into α-particles to the fullest extent possible leaving residues of one, two or three protons as the case may be. Fig. 1B, shows $\sigma_A-\sigma_A'$ plotted against n. It will be seen that the discontinuities specially investigated by Meitner have disappeared. Other discontinuities remain but they are for points less carefully investigated and for which the discontinuities lie within the experimental error. The linearity of the curve suggests independence of the scattering centers. If we work out the expression for $\sigma_A-\sigma_A'$ from wave mechanics we find for scattering by n' electrons the result

$$\sigma_A-\sigma_A'=\frac{8\pi}{3}n'\left\{\frac{2\omega^2e^2}{c^2}\sum_n\frac{(E_n-E_0)}{(E_n-E_0)^2-(2\pi\hbar\omega)^2}|r_{n0}|^2\right\}^2 \quad (1)$$

where ω is the frequency of the γ radiation and r_{n0} the moment of the transition between

[1] Beck, Naturwiss **18**, 896 (1930).

the two energy states E_n and E_0 of the nucleus. Eq. (1) is similar in form to the Klein-Nishina formula, except that on account of our lack of knowledge of the precise form of the ψ equation for the nuclear electrons the form of the ψ function which determines r_{n0} cannot be stated. The formula depends upon the assumption of the absence of coherence in phase between the energy scattered by the individual electrons. With wide generality we can make use of the general wave-mechanical relation

$$\sum_n (E_n - E_0)\left| r_{n0}\right|^2 = \frac{4\pi^2\hbar^2}{2m} \qquad (2)$$

to eliminate $|r_{n0}|$ on the basis of the assumption that the scattering by the electrons in α-particles is negligible compared with that of the other nuclear electrons. This assumption is justified by the fact that $E_n - E_0 \gg 2\pi\hbar\omega$ for the electrons in α-particles whereas $E_n - E_0 < 2\pi\hbar\omega$ for the other nuclear electrons, so that only the latter contribute appreciably to (1). Thus there results

$$\left[\frac{E_n - E_0}{(E_n - E_0)^2 - 4\pi^2\hbar^2\omega^2}\right]^2 = \left[\frac{E_n - E_0}{4\pi^2\hbar^2\omega^2}\right]^2$$

so that, in virtue of (2) Eq. (1) becomes

$$\sigma_A - \sigma_A' = \frac{8\pi}{3}\frac{e^4}{m^2c^4}n$$

where we have now replaced n' by n.

On inserting numerical values we find $8\pi e^4/3m^2c^4 = 6.63\times10^{-25}$ while the slope of Fig. 1B gives $1.89\cdot10^{-25}$, which verifies as regards order of magnitude at any rate, the numerical agreement between theory and experiment.

The consequence of attributing the nuclear scattering to α-particles has been worked out by Gamow (Constitution of Atomic Nuclei and Radioactivity) on the basis of coherence in phase between the scattering centers; but, here, the amount of the scattering comes out 1600 times too small.

ARTHUR BRAMLEY

Bartol Research Foundation,
Swarthmore, Pennsylvania,
December 18, 1931.

Superconductivity with Respect to Alternating Currents

In a recent paper Professor J. C. McLennan and Messrs A. C. Burton, A. Pitt, and J. O. Wilhelm[1] described experiments at low temperatures with a lead helix and capacitor, which led them to conclude that lead does not become superconducting to alternating currents of a frequency of 10^7 cycles per second. In view of this announcement experiments were made on two samples of tin at frequencies intermediate between this value and zero frequency, or direct current, at which both tin and lead are superconducting. The frequencies used were 60, 2640 and 1,410,000 cycles per second.

The two test resistors were formed of strips of tin foil 0.02×0.0025 cm wound bifilarly with paper insulation into small coils, and had resistances at room temperature of 13 and 2.3 ohms respectively. They were mounted below the expansion valve of the helium liquefier within a cylindrical copper chamber 2.5 cm long and 1.5 cm in diameter. Each specimen was provided with current and potential leads of No. 38 copper wire brought out of the liquefier through a copper-nickel alloy tube 0.12 cm in diameter. The liquefier used is similar to the one designed by Ruhemann.[2]

At 0, 60 and 2640 cycles per second, the resistances of the specimens were compared, using potentiometer methods, with the resistance of a 0.05 ohm non-inductive standard connected in series with them. For direct currents the potential drops across the specimen and resistance standard were measured with a Wenner potentiometer. For 60 and 2640 cycles, the impedance drops were opposed to that in an adjustable portion of a calibrated slide wire, the specimen and slide wire being supplied with current through suitable rheostats from two duplicate windings on a step-down supply transformer. Any slight difference in phase of the impedance drops was balanced by the secondary voltage of an adjustable mutual inductor, the primary winding of which was inserted in series with the current leads while the secondary was in series with the potential leads of the specimen. The equality of the opposed potential drops was indicated by a separately excited electrodynamometer. At 2640 cycles per second, a special 10 ohm telephone head set was used also as the detector.

It was found on the three different days that liquid helium was made, that whenever

[1] McLennan, Burton, Pitt and Wilhelm, Phil. Mag. **12**, 707 (1931).

[2] Ruhemann, Zeits. f. Physik **65**, 67, (1930).

the specimens were superconducting to the direct current, the resistances to the 60 and 2640 cycle currents were less than could be detected experimentally. Under the best experimental conditions the upper limits of the resistance of the 13-ohm specimen in the superconducting state are 3×10^{-4} and 2×10^{-3} times the resistance just above the threshold temperature for 60 and 2640 cycles respectively.

A current of radio frequency (1,410 kilocycles) was passed through the 13 ohm specimen connected in a tuned circuit loosely coupled to an oscillator. Observation of an electrothermic milliammeter in series with the specimen showed an abrupt increase or decrease in the current as the temperature of the specimen was lowered or raised gradually through the critical or threshold value. The magnitude of the corresponding change in resistance, as inferred from the changes in current produced by resistance changes of known value in the external part of the tuned circuit, was found to be 0.72 ± 0.03 ohm. The excess of this value over the resistance change, 0.13 ohm, observed with direct current is presumably due in part to skin-effect and in part to disturbing effects of the capacitance between the specimen with its leads and the inclosing metal container and conduit. No observable discontinuity in current occurred when the experiment was repeated in an identical way except that the radio-frequency current flowed only in the two leads running to one end of the specimen.

When one of the two specimens carried direct current and the other radio-frequency current, and the temperature in the liquefier was allowed to drift gradually through the critical value, the discontinuity in resistance appeared first in the specimen of low resistance, supplied with direct current, and was followed a few seconds later by the change in the other specimen. As the "breaks" occurred in the same order for these two specimens on both rising and falling temperature, the lag was presumably, merely the result of the greater thermal insulation of the higher resistance specimen.

In another experiment, a direct current of 6 m.a. was superposed on the radio-frequency current of 36 m.a., and the d.c. potential drop was measured by one observer on the Wenner potentiometer while another watched the electrothermic milliammeter, through which only the radio-frequency current flowed. As the temperature gradually drifted through the critical value, the discontinuity in resistance appeared simultaneously on both instruments.

In a brief note[3] which appeared after these experiments had been carried out, Professor McLennan reports that his earlier experiments had not been crucial and that later work had shown a definite discontinuity in resistance at 10^7 cycles per second. He also states that he observed the "break" at a slightly lower temperature for the high frequency current than he did for the direct current. The results reported above may be considered as confirming the first conclusion of Professor McLennan's second article, and as not necessarily conflicting with his second conclusion.

F. B. Silsbee
R. B. Scott
J. W. Cook
F. G. Brickwedde

Bureau of Standards,
Washington, D. C.,
December 21, 1931.

[3] McLennan, Trans. Roy. Soc. of Canada (3rd Series) **25,** 191 (1931).

The Spectrum of Carbon Dioxide. II. Electron Levels

In a recent paper in the Physical Review I discussed at length the emission spectrum of carbon dioxide in the region between 2800 and 4500A. It now appears probable that this spectrum comes from a neutral CO_2 molecule excited to a state about a volt above its ionization potential. This conclusion is based on some very simple experiments of my own and on some new measurements of the absorption spectrum of CO_2 to be published by Henning in the Zeits. f. Physik in the near future.

I have been studying the spectrum emitted by the positive column of a Geissler tube discharge in flowing CO_2, taking simultaneous plates with a fluorite vacuum spectrograph and a medium sized (E2) quartz Hilger spectrograph. My primary object was to complete the search for the Leifson absorption bands in emission. I found no trace of them, thus confirming the results previously obtained with electron beam excitation.

[1] Smyth, Phys. Rev. **38,** 2000 (1931).

As so often happens the chief interest of these experiments proved to be in entirely unforeseen results. The plates obtained showed the CO_2 system mentioned above, the fourth positive, third positive, 3A, 5B, Angstrom and probably comet tail systems of CO and a trace of the second positive bands of nitrogen. The first negative bands of CO were certainly not present. The relative intensities of these systems might be expected to depend on the relative concentrations of CO_2 and CO and on the strength of the electrical excitation. These in turn will depend experimentally in a complicated way on the pressure and rate of flow of the gas and on the current in the discharge.

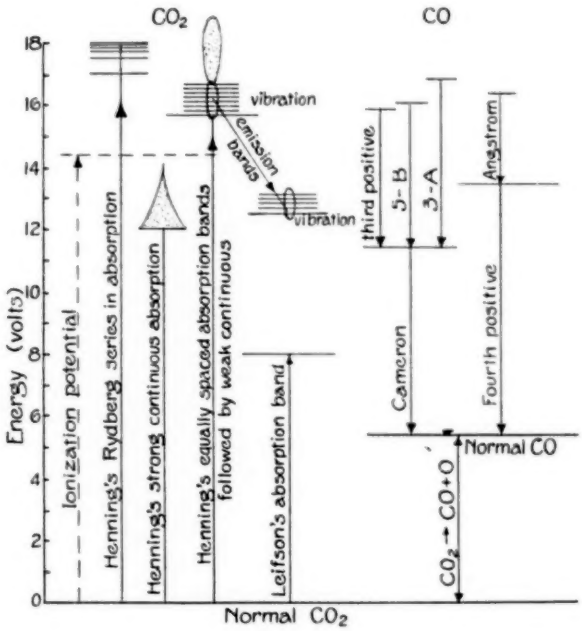

Fig. 1.

Actually I have obtained some twenty-five different exposures under a wide variety of conditions and have observed such variations. The results are only qualitative and an attempt to explain them in detail would be premature. Suffice it to say that they indicate a close relation between the CO systems mentioned above and the CO_2 system, small changes in conditions causing considerable changes in relative intensity. Now the energies required to excite the CO systems from normal CO are from 10.4 to 11.4 volts for the positive systems and 16.6 for the comet-tail bands. If the CO systems can also be excited directly from CO_2, 5.5 volts, the energy required for the dissociation $CO_2 \rightarrow CO+O$, must be added giving 15.9 to 16.9 for the positive systems. Duffendack and Smith[2] found that the CO_2 system was excited in mixtures of CO and O_2 with He or Ne but not with A. They explained this in terms of ionic collisions of the second kind but it may be equally well explained in terms of collisions with excited atoms or limited electron velocity and suggests that the excitation potential is between that of argon and neon. A value just below the neon potential (16.6 volts) would be in excellent accord with my results if the CO systems are excited in part or wholly from CO_2. Such a value would be above the I.P. of CO_2 (14.4 volts) but this is the only reason for attributing this spectrum to CO_2^+ since it can be excited directly from neutral CO_2 either in the positive column or by an electron beam at low pressures. But if the excitation potential is below 16.6 volts and the electron transition is of the order of three volts the lower state of these bands is below the I.P. of CO_2. An attractive way out of this dilemma is revealed by Henning's results.

[2] Duffendack and Smith, Phys. Rev. **34**, 68 (1929).

Studying the region below 900A Henning has found three types of absorption in CO_2, continuous, a Rydberg series of bands and a series of bands equally spaced at intervals of 1120 ± 50 cm^{-1}. These last bands are eight in number with wave-lengths corresponding to from 15.7 to 16.7 volts. Excepting the one of longest wave-length each band is double with a doublet separation of about 350 cm^{-1}. Now the upper levels of the CO_2 emission bands have separations given by $1135 - 3.7v'$, ($v' = 1 \cdots 9$), are eight to ten in number and have an excitation potential probably a little below 16.7 as we have seen. There is therefore good reason to identify them with the upper levels of Henning's absorption bands. It is true that the scheme of vibration levels I gave in my earlier paper would give triplet levels with a total spread of only 166 cm^{-1} but that scheme was admittedly subject to correction (see below). I think that we can conclude with assurance that the two sets of upper levels belong to the same electronic state and are probably identical and that consequently the CO_2 emission bands come from a neutral molecule excited above its I.P.

Proceeding on this assumption it is possible to construct an electron level diagram for CO_2 and compare it with the similar scheme for CO. I have included in the figure below the upper level of Leifson's bands[3] though its location can only be guessed.

With reference to the discrepancy between Henning's doublet separation and the narrower triplet predicted by my analysis I may say that the relative intensities of certain bands within the CO_2 system are not the same in my recent plates as in those taken with electron beam excitation last year and that it seems possible that some rearrangement of the levels may be necessary to explain these variations. But as I have not been able to find any equally simple scheme which fits the wave numbers equally well I prefer not to present a different scheme until further data are available. I feel this the more strongly because the proof that this spectrum comes from the neutral molecule makes the application of Dennison's theory more plausible. Attempts to rearrange the levels along the lines of Fermi's recent discussion[4] of the Raman effect have not been successful.

I need hardly say that I am continuing the study of this spectrum. Thanks to the support of the Guggenheim Foundation I am doing so in Professor Franck's Institute where my sojourn has already been profitable as well as pleasant. I am indebted to him, to Dr. Sponer, Mr. Henning and others for making it so.

H. D. SMYTH

Zweites Physikalisches Inst. d. Univ.
Göttingen,
December 22, 1931.

[3] Leifson, Astrophys. J. **63,** 73 (1926).
[4] Fermi, Zeits. f. Physik **71,** 250 (1931).

Some Studies of Negative Point Discharges at Low Pressures

Only a few spectrographic investigations of point discharges at low pressures have been published.[1] Therefore, the results of some experiments may be of interest which were undertaken to find the lowest pressures at which negative point discharges may be maintained and to study their spectrum emitted in the vacuum.

The main difficulty encountered with point discharges is that a discharge from a pointed conductor is well defined for a very short time only as then the shape of the point will change and accordingly the characteristics of the discharge. For this reason, a wire was taken as cathode; the discharge takes place then only from distinct points which are assumed to be caused by submicroscopic summits on the surface of the wire. The tube used for the investigations was evacuated to a pressure of about 10^{-3} mm Hg. If now a rectified voltage was applied, from one to three bright *light brushes of blue color* appeared starting near the cathode wire. With the pressure decreasing to about 10^{-4} mm Hg the brushes became shorter and finally only bright *blue points* were observed on the wire. The voltage necessary to excite now the point discharges was 78 kv_{max}, the current passing through the tube being 10^{-4} amp. If the pressure was lowered to $< 10^{-5}$ mm Hg it was not possible to excite the appearance of the blue points with voltages up to 95 kv_{max}.

The point discharges were not affected if the cathode wire was slowly *heated*, at a high temperature, however, the points could visually not be detected. Together with the excitation of the point discharges a considerable *sputtering* from the cathode wire took place.

The light emitted by the point discharges in a high vacuum showed *no polarization.*

Spectrographic investigations were carried by means of a Fuess quartz spectrograph with a dispersion of 17A per millimeter at 2500A. The spectra were examined with a Goos-Koch registering microphotometer[2] with two photocells. Fig. 1 shows some microphotometer curves of spectra from point discharges taken at a pressure of 10^{-4} mm Hg; the abscissas being wave-lengths, the ordinates, intensities in an arbitrary scale.

It is to be seen that *point discharges at a high vacuum emit mainly a continuous spectrum,* some bands and lines from the gas and vapor content of the tube are merely indicated. If the pressure is raised inside the tube, the bands and lines appear with increasing intensity in comparison to the continuous spectrum. The maximum of intensity of the continuous spectrum (photographically determined from many exposures) is found at 4600 ± 50A, the spectrum could be traced from 6200 to 2150A. From these results follows:

(1) The pressure necessary to excite bands and lines with negative point discharges is to be $\geqq 10^{-4}$ mm Hg. According to different investigators—cf. Mierdel[3]—negative point discharges will lead by means of ionization by impact to both negative and positive ions near the cathode; beyond a thin layer, only negative ions are considered to be present. In this way, the excitation of the bands and lines from the gases and vapors contained in the tube may readily be explained.

(2) To excite the continuous spectrum of negative point discharges only a very small amount of gases and vapors is to be present in the tube, the pressure being of the order of 10^{-4} mm Hg. The distribution of intensity in the continuous spectrum received from the discharges at a low pressure recalls the observations of the author on exciting continuous spectra by means of electron bombardment of solid bodies, gases and vapors,[4] and we may assume that the continuous spectrum of point discharges is generated by means of an action of electrons emitted from the cathode points on ions present in the tube in a corresponding way as with electron bombardment of solid bodies, gases and vapors as outlined in detail in my former papers. Thus is to be concluded that the emission of band and line spectra and the emission of the continuous spectrum connected with negative point discharges are to be considered as resulting from two different processes of excitation.

It seems to be likely that also in other types of discharges which usually show lines, bands and a "continuous background" the discontinuous and continuous parts of the spectrum are excited by such different processes of excitation as found with negative point discharges.

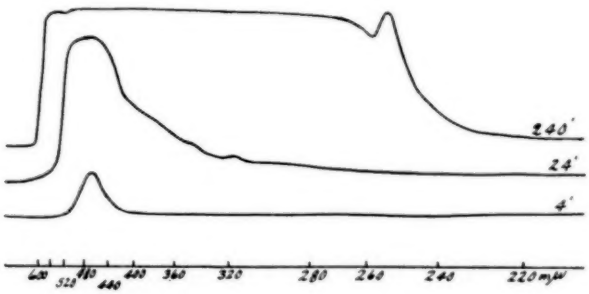

Fig. 1

[1] M. Weth, Ann. d. Physik. **62,** 589–602 (1920); A. Schultz, d. Ann. Physik **64,** 367–376 (1921); H. Oyama, Technol. Reports Tôhoku Imp. Univ. **10,** 1–10 (1931).

[2] F. Goos and P. P. Koch, Zeits. f. Physik **44,** 855–859 (1927).

[3] G. Mierdel, Townsendentladungen. Handb. d. Exp.-Phys. **13,** III, 93–310 (1929).

[4] W. M. Cohn, I. Zeits. f. Physik **70,** 662–666 (1931); II. ibid. **70,** 667–678 (1931); III. ibid. **70,** 679–694 (1931); IV. ibid. **72,** 392–422 (1931); V. ibid. In press; VI. ibid. In press.

WILLI M. COHN

Cambridge, Mass.

December 29, 1931.

High-Speed Protons

We have recently succeeded in obtaining and photographing the tracks produced in a Wilson cloud-chamber by high-speed protons from a high-voltage tube used with a Tesla coil,[1] and have made a preliminary measurement of the range in air of 1000-kilovolt protons.

Measurements on the high-speed protons from a "flashing" tube were reported at the June meeting in Pasadena. Visual observations of the Thomson parabolas produced by electric and magnetic deflection of a narrow pencil of rays identified without ambiguity the H^+, H_2^+, and heavier high-speed ions accelerated by voltages of the order of one million volts, and thus verified the production of high-speed protons by a "flashing" tube as observed using magnetic deflection alone throughout the previous year. Photographic recording of these parabolas was not seriously attempted due to the fogging of the plates by scattered electrons and light. The protons presumably arise from occluded hydrogen on the electrodes, and from residual gas in the tube.

A Wilson chamber[2] separated from such a "flashing" tube by a thin mica window was operated last spring without definite results. Even when the electrons were deflected away from the window, any proton-tracks which were present were masked by the ultraviolet light and x-rays which entered the chamber through the window and produced very dense fogging. The rather strict requirements for proper synchronization of the high-voltage impulse and the "sensitive time" of the chamber (0.012 to 0.035 second after the piston drop) were also emphasized by these preliminary experiments.

Accordingly during the past summer and early fall efforts were made to obtain proton-tracks using a Dempster-Ramsauer proton-source (lithium bombarded by 50-volt electrons) in conjunction with a dark tube (flashing prevented by the equalization of voltage-distribution among the tube-sections by their capacity to a "ring-shield" connected to the high-voltage corona-cap). This experiment failed by reason of too low a proton-intensity. The proton-current was of the order 10^{-10} ampere, and the on-time of the peak-voltage of the order 10^{-6} second. With these factors and the small fraction of the initial proton-current which goes through all sections of the tube (solid angle and probable de-focussing effects), apparently from electron-measurements of the order of 10^{-4} or less when focussing is not attempted, there were too few full-speed protons reaching the mica window to detect reliably even with the Wilson chamber. The sensitivity of the latter to single high-speed protons from the tube has since been demonstrated very clearly.

We consequently returned to the use of the flashing tube, utilizing magnetic analysis and obtaining x-ray shielding by means of thick slits which are considerably out of line with the window. Unambiguous results were obtained as soon as this set-up was operated. For the first observations a wide band of proton-velocities was admitted to the chamber and tracks of a great variety of lengths (ranges up to 4 cm) were obtained. Heavier and hence slower ions deflected to the same point by the magnetic analysis (electric deflection omitted) cannot pass through the mica window, which has a stopping power of 1.8 cm of air for α-particles. The number of proton-tracks observed varied from one to more than 200 (unresolvable). The tube was operated to moderate voltages only, spark-gap measurements indicating somewhat above one million volts.

Although we have had ample experience of the fact that the Tesla coil and particularly the flashing tube are far from ideal for quantitative work, we have used this set-up with increased magnetic resolution to obtain at least a rough measurement of the range of 1000-kilovolt protons. Since protons of any speed down to zero can arise from intermediate electrodes, it is necessary to compare the maximum range observed with the maximum $H\rho$ which any proton can have and still enter the mica window of the Wilson chamber. The result of the measurements was a maximum total range of 2.8 cm in air reduced to stand-

[1] G. Breit and M. A. Tuve, Nature **121,** 535 (1928); G. Breit, M. A. Tuve, and O. Dahl, Phys. Rev. **35,** 51 (1930); M. A. Tuve, G. Breit, and L. R. Hafstad, Phys. Rev. **35,** 66 (1930); M. A. Tuve, L. R. Hafstad, and O. Dahl, Phys. Rev. **35,** 1406 (1930) and **36,** 1261 (1930).

[2] We are indebted to Dr. L. F. Curtiss, of the Bureau of Standards, for the loan of parts and for assistance with the design and technique of the automatic Wilson-chamber apparatus.

ard conditions (1.0 cm in chamber), for a given setting of the magnetic field and a fixed position of the window. This figure was obtained from three separate runs, each involving approximately 50 pictures of proton-tracks (from 10 to several hundred protons per picture) with major changes of voltage-distribution, with and without carbon point-flasher, and with greatly altered vacuum-conditions and electrode-contamination at the high-voltage end of the tube between the different runs. The separate films gave results for the maximum range agreeing within about 6 percent.

The assignment of the proper maximum value of $H\rho$ to be associated with this maximum measured range requires an assumption as to the precise direction of motion of these protons in the tube. If the proton-beam is parallel to the axis of the tube, the magnetic field measurements yield the result that 1035-kilovolt protons will be deflected 6.2 cm to the center of the 3 mm window, and 1100-kilovolt protons can just enter the window on the side of least deflection. The assumption that the protons move very nearly parallel to the axis of the tube appears to us the most reasonable one to make in view of the tendency of the electric fields between successive electrodes to make parallel to the axis the motion of particles which are moving near the axis and at a small angle to it, and to remove from the beam particles which move at a considerable angle with the axis. This effect has been shown in the work of Sloan and Lawrence.[3] However, if the proton-beam is assumed to have the solid angle (0.02 radian) determined by the entire area of the high-voltage end of the tube which is visible from the slit-system through the holes in the electrodes (3 mm slits, 25 cm apart), the spread in values of $H\rho$ is considerably increased, and the maximum value then corresponds to nearly 1300 kilovolts. This possibility appears to us as highly improbable on the basis of our previous experience, particularly with the Thomson parabolas.

Assuming from the literature that the range of a proton struck head-on by a Ra-C α-particle, and therefore given a velocity of 3.08×10^9 cm per second, is 32 cm in air at 15°C and 760 mm, the range of a 1000-kilovolt proton is 2.92 cm on the assumption of the α-particle law of range proportional to the cube of the velocity. Assuming the β-particle law of range proportional to the fourth power of the velocity, this figure becomes 1.32 cm. The corresponding figures for 1100 kilovolts are 3.32 cm and 1.60 cm. The voltages corresponding to a 2.8-cm range are respectively 960 and 1460 kilovolts on the two laws. It appears to us that our measurements exclude the β-particle law and suggest that the law governing the range of protons is nearer to the velocity-cubed law which holds for α-particle ranges.[4]

The difficulties of doing quantitative work with a Tesla coil, due to the short on-time and fluctuating value of the peak-voltage, are obvious, and we hope in the near future to undertake a program of quantitative measurements using the newly developed Van de Graaff electrostatic generator[5] as the source of high voltage for the tubes.

M. A. Tuve
L. R. Hafstad
O. Dahl

Department of Terrestrial Magnetism,
Carnegie Institution of Washington,
Washington, D. C.,
December 29, 1931.

[3] D H. Sloan and E. O. Lawrence, Phys. Rev. **38,** 2021 (1932).

[4] See Chadwick, Constable, and Pollard, Proc. Roy. Soc. **A130,** 477 (1931) and Blackett, Proc. Roy. Soc. **A103,** 65 (1923).

[5] R. J. Van de Graaff, Phys. Rev. **38,** 1919-A (1931).

On the Classification of Certain Lines of Radium

The radium spark lines of wave-length 6446.1, 5823.7, 2836.5, 2813.7, and 2708.9A can be accounted for by assuming a set of doublet levels at 73,820; 72,162 cm^{-1} and at 36,917; 36,632 cm^{-1}. The lower levels are analogous to the $^2D_{5/2,3/2}$ levels of Ba II at 75,781; 74,980 cm^{-1}, while the upper levels are analogous to the $^2F_{7/2,5/2}$ Ba II levels at 32,397; 32,172 cm^{-1}.

The positions of the levels are fixed by the combination of the two lower levels with the known $7^2P_{3/2}$ level. The $7^2P_{1/2}$ combination should give a line at 8121A, which is beyond the region investigated by various workers (6642–2709A).[1] The estimated intensities are in the correct order for each line of the multiplet.

[1] Kayser, Handbuch der Spectroscopie, B6.

Two weak lines at 4927.7 and 4859.5A have the same frequency separation as the ^2F terms and may possibly represent the ^2FG combinations with 5^2G at 16,444 cm^{-1}.

By analogy with the other alkali earths no other unclassified Ra II lines would be expected in the region thus far photographed, with the possible exceptions of the second members of the sharp and diffuse series (around 2800–2600A). The remaining lines are probably mostly arc lines resulting from transitions between normal type electron configurations and configurations of type $(d)^2$, $(d\text{-}p)$, etc.

The six lines of wave-length 6200.4-($I=10$), 6337.0-(6), 6438.9-(4), 5406.6-(8), 5481.9-(6), and 5097.3-(6)A form a multiplet in the region where ^3PD of Ra I is expected. Further, the intervals 348:252 cm^{-1} for upper levels, and 2715:1376 cm^{-1} for lower levels indicate ^3D type and ^3P type levels. The total spread of the levels compares well with the corresponding ^2D and ^2P separations of Ra II.

WALTER ALBERTSON

Department of Physics,
Massachusetts Institute of Technology,
January 1, 1932.

Molecular Beams of Salt Vapors

Molecular beams are easily formed from vapors of the alkali halides. Sufficient vapor pressure is obtained to form a beam by heating the salt to the neighborhood of the melting point. The method of detection developed by J. B. Taylor (Zeits. f. Physik **57**, 242 (1929)) for beams of alkali vapors is found to work apparently quite as well for alkali halides. This method depends upon the formation and emission of positive ions from a positively charged, hot, tungsten filament. Presumably the salt molecules are dissociated by the filament and the action is then precisely as with the alkali vapor.

The beam of salt molecules has been tested for ions by passing it between parallel plates, on which a difference of potential was maintained. If ions are present, the number is too small to produce an observable deflection on a high sensitivity galvanometer.

When the beam is passed through an inhomogeneous magnetic field a considerable broadening is observed due to the magnetic moment of the rotating dipoles. It is hoped that by making certain assumptions, the dipole moment may be calculated.

W. H. RODEBUSH
W. F. HENRY

University of Illinois,
January 1, 1932.

BOOK REVIEWS

Physical Theory. VICTOR F. LENZEN. Pp. 301, xii, figs. 8. John Wiley & Sons, Inc., New York, and Chapman and Hall, Limited, London, 1931. Price $3.50.

It frequently happens that one who is a professional philosopher is not also a mathematician, and vice versa. However, in "Physical Theory" the reader has the advantage of a book written by one who has made a study of philosophy and of mathematical physics, each from its own standpoint. The physicist, therefore, profits by the viewpoint of the philosopher in so far as it can be crystallized into his own language, and the philosopher profits by the viewpoint of the mathematical physicist, expressed in a form as simple mathematically as is possible and consistent with anything like an adequate presentation.

Professor Lenzen has attempted a very ambitious program in covering in a book of some 300 pages such a wide system of topics as fundamental concepts, Euclidean geometry, the fundamentals of dynamics, electrodynamics, and thermodynamics, relativity, non-Euclidean geometry, and quantum theory, together with a discussion of all of the allied topics of a philosophical nature which fall in the category of these fields. It is probable that no two persons interested in such domain would agree, word for word and page for page, upon the relative importance or significance of the various maters treated. It would, therefore, be quite impossible to discuss in a brief space the complete contents of Professor Lenzen's work. It may suffice, however, to say that the book is one which will be found of great value to the physicist, particularly to one who wishes to widen his horizon as to the philosophic bearing of his subjects, and is not acquainted extensively with the mathematical technique of the more difficult parts. Moreover, Professor Lenzen does not adopt a dogmatic point of view, but presents different possibilities of viewpoint and methods of approach. The book is one which can serve the purpose of giving to many a physicist a clear vision of what he is actually doing in the mathematical manipulation of his science. As already implied, moreover, the book is written in relatively simple form and so should be intelligible to a wide range of readers both in philosophy and in mathematical physics.

W. F. G. SWANN
Bartol Research Foundation

Johann Kepler, A Tercentenary Commemoration of His Life and His Work. Special Publication No. 2 of the History of Science Society. Williams and Wilkins Co. Baltimore, $2.50.

The book contains three separate articles; one, Kepler as an astronomer, a mathematician and a mystic by W. Carl Rufus, D. J. Struik, and E. H. Johnson respectively, to which are added a brief introduction by Sir Arthur Eddington, and a bibliography by F. E. Brasch. Rufus's article consists of a charmingly written account, very evidently authoritative, of Kepler's life, paying special attention to Kepler the astronomer, though it must needs deal largely with the mystic also. Interspersed with delightful bits of humor, which make it even more readable this article seems to be as objective a biography as it is humanly possible to write; out of it emerges a Kepler almost greater than Newton. In the second article D. J. Struik writes his appreciation of Kepler as a mathematician; considering that such an article affords so little opportunity for biographical sketching, and is by nature somewhat "cataloguey," it is interestingly written, though the ending is rather abrupt. The third article by E. H. Johnson takes up first the intellectual and cultural background of Kepler's times, so essential in understanding the work of any man, and discusses with much needed detail Kepler's dealings with and dabblings in astrology—a subject to which so often loose references are made.

As is commonly the case with a collection of articles by different authors, opinions as to the "real" Kepler vary somewhat. Eddington, in his introduction makes us see Kepler as differing from his contemporaries in that he broke away from mechanistic models. Johnson's description of Kepler the mystic shows him to us essentially as a child of his time, full of whims and fancies, and what we now would call superstitions.

Not the least valuable part of the book is the extensive bibliography compiled by F. E. Brasch, and containing not only a list of Kepler's own works, but one of the principal commentaries as well.

The work is unusually, though not entirely free from misprints, as one should expect considering the elaborateness of the publishers' description of its typographical excellence, but even so, the price seems a trifle high, since it is only 5 by 8 inches in size, and contains no more than 85 pages of text and 48 of bibliography. It is just this small size, and the brief but comprehensive way in which Kepler's life and work have been treated which render the book so useful to those who have no time or inclination to consult the more voluminous tomes on the subject, but this usefulness is seriously hampered by its high price.

W. J. LUYTEN
University of Minnesota

Fortschritte der Roentgenforschung in Methode und Anwendung. Ergebnisse der Technischen Roentgenkunde II. Edited by J. EGGERT AND E. SCHIEBOLD. Pp. 332+viii, Figs 145. Akademische Verlagsgesellschaft. Leipzig. 1931.

This volume is a collection of lectures on some of the technical applications of x-rays given at Heidelberg in 1930, by various specialists. There is a miscellaneous assortment of subjects such as:—molecular arrangements; liquid crystals; fats, oils, and lubricants; molecular structure of organic substances; electron diffraction; new methods of crystal analysis; size and form of submicroscopic crystals; deformed crystals; crystal chemistry; new results on organic crystals; modern metallography; iron alloys; changes in state of alloys; quantitative chemical analysis; effects of chemical combination on spectra; fundamentals of industrial radiography; and densographic evaluation of Roentgenograms. The list of authors contains such authorities as:—Debye, Mark, Schiebold, Goldschmidt, Bernal, Hevesy, and others. As a rule, each lecture contains a good bibliography.

JOSEPH VALASEK
University of Minnesota

Wilhelm Conrad Roentgen und die Geschichte der Roentgenstrahlen. OTTO GLASSER. Pp. 337, figs. 96. Verlag von Julius Springer, Berlin, 1931. Price. RM 29.60.

The author has combined biography and history in a very interesting manner. The personality of Roentgen is vividly brought out with the aid of excerpts from his correspondence and by accounts of his recreation. In this connection, the book is considerably enhanced through a chapter by Margret Boveri, Roentgen's niece.

Although Roentgen's scientific activity is recounted to the date of his death, the history of x-rays and their manifold applications is only carried through the first year. This greatly restricted history is treated with extreme thoroughness as may be inferred from the 1044 references to magazine articles, all from the year 1896. Many Roentgen photographs of the year 1896 are reproduced. That the discovery made an immediate impression on the popular mind is reflected in the popular writings and cartoons, especially in the humoristic journals, excerpts from which are reprinted.

The author has done an excellent piece of work. It is to be hoped that more books of this character will be written and that they will have the effect of making scientists more interested in history, and historians more interested in the history of science.

JOSEPH VALASEK
University of Minnesota

Spektroskopie der Roentgenstrahlen. Second edition. Manne Siegbahn. Pp. 575+vi, figs. 255, tables 224. Verlag von Julius Springer, Berlin, 1931. Price, RM 49.60.

This classic has been thoroughly rewritten and a large amount of new material has been added. Included in the new material is a chapter entitled the "Optics of Roentgen rays" which deals with the interference, refraction, dispersion, and diffraction of x-rays. Herein is contained the beautiful experimental work of Larsson on "anomalous" dispersion by many of the crystals

used in x-ray spectroscopy together with the corrections to be applied in the calculation of wave-lengths from data obtained with these crystals.

As in the older edition, the chapter on technique is a rich source of information for the experimental worker. The well known excellence of the work done at Upsala depends in no little measure on the ingenuity of conception of the spectroscopic apparatus, on its precise construction, and the carefully planned methods of adjustment and measurement. These points are fully discussed in this chapter.

The spectroscopic tables have been completely brought up to data. One set of tables contains just about all the wave-length measurements ever made in the characteristic radiation, tabulated for each series and for each element. Following these tables, the most probable wave-lengths for each series and each element are presented. Then the corresponding values of the Rydberg frequencies are given. A similar procedure is followed in the case of the absorption edges.

In the discussion of the systemization and theory of x-ray spectra, the results of the newer theory are outlined. Graphical methods enhance the discussion. Following this, a complete tabulation of all the known energy levels is given. The results on intensity measurements in the line spectra are summarized and discussed with reference to theory. However, a similar treatment of the absorption spectra is not presented. The variation of absorption with wave-length and the magnitudes of the various absorption discontinuities should certainly have been included in a work of this type, all the more so, perhaps, because the new theory is having difficulty with the complete and quantitative elucidation of the absorption phenomenon.

The influence of chemical combination on absorption edges is summarized and the results as to secondary absorption are reviewed. In the discussion of the spectra of multiply-ionized atoms, it is pleasing to see that Langer's recent suggestion as to the origin of the lines has been included.

The extension of the x-ray region toward longer wave-lengths is treated very fully. This is another field in which remarkable advances have resulted as a consequence of improvements in apparatus and technique largely originating in Siegbahn's laboratory. There is a chapter on the secondary beta rays and one on the continuous spectrum. The appendix contains many useful tables for the laboratory worker. The literature is listed year by year up into 1931. The index, by subject and by author, refers to the literature as well as to the text.

This encyclopedic work, containing as it does, complete and up to date numerical tables, literature references, and valuable suggestions as to technique, will be indispensible for reference wherever x-ray spectra are being investigated.

JOSEPH VALASEK
University of Minnesota

Signals from the Stars. George Ellery Hale. Pp. 138+xx, figs. 56. Charles Scribner's Sons, New York, 1931. Price $2.00.

When Dr. Hale writes about the progress of astronomy, professionals and amateurs alike find his narrative absorbingly interesting. It is not only his felicitous selection of facts but the gradual development of his line of thought, intelligible to everyone, and so suggestive of new ideas that make each of these little books a gem, well worthy of possession.

The present volume deals largely with problems of and for large telescopes, but the often important part that can be played by small instruments is not overlooked. A brief historical survey of the observational equipment and methods in vogue from the dawn of civilization down to the present era of a 100 inch telescope precedes the prediction of some of the difficulties to be encountered in the making of large mirrors for telescopes—and ways to overcome them. The second and third chapter are devoted to a description of problems of the solar atmosphere, and the way in which prominences and solar cycles—sun-spots—could be effectively observed with a small spectrohelioscope, and stresses the need for more international cooperation on this front. The fourth and final chapter considers in much greater detail than Chapter I the more recent advances made toward the goal of a 200 inch mirror, and the important part played in this by the General Electric Company. It describes the final plans for the design and the

mounting of the proposed 200-inch as well as the preparations made in selecting the all-important site, and deals with an enumeration of the various auxiliary apparatus which now forms the astronomer's indispensable tools. The chapter closes with an eloquent appeal to recognize the great debt of human civilization to astronomy.

The book is richly illustrated and this reviewer was especially struck with the last plate, which exhibits in so admirable a fashion the "redshift" of the spiral nebulae as dependent upon their apparent size and distance.

W. J. LUYTEN
University of Minnesota

CURRENT LITERATURE OF PHYSICS

Extracts from the Tables of Contents of Some of our Contemporaries

PROCEEDINGS OF THE ROYAL SOCIETY

SERIES A. VOL. 134, No. A824 — DECEMBER 2, 1931

Optically Active spiro-5:5-Dihydantoins. By **Sir William Jackson Pope and J. B. Whitworth** 357

Condensation of Chloral with Urea and Phenyl Urea. By **F. D. Chattaway, and E. J. F. James** 372

Investigation of the Attack of Platinum and Tungsten by Iodine. By **G. Van Praagh and E. K. Rideal** 385

On the Contact of Smooth Surfaces. By **S. H. Bastow and F. P. Bowden** 404

Viscosity of Dilute Solutions of Strong Electrolytes. By **W. E. Joy and J. H. Wolfenden** 413

Photoelectrons and Negative Ions. By **E. M. Wellish** 427

On the Circulation Caused by the Vibration of Air in a Tube. By **E. N. Da C. Andrade** 445

Commutative Ordinary Differential Operators. II. The Identity $P^n = Q^m$. By **J. L. Burchnall and T. W. Chaundy** 471

On Finite Sequences of Real Numbers. By **H. B. Heywood** 486

Isotherms of Hydrogen, Carbon Monoxide, and their Mixtures. By **D. T. A. Townsend and L. A. Bhatt** 502

Kinetics of Adsorption Processes. By **A. R. Ubbelohde and A. Egerton** 512

On the Mass of the Proton. By **Sir Arthur Eddington** 524

PHILOSOPHICAL MAGAZINE

SEVENTH SERIES, VOL. 12, No. 81 — DECEMBER, 1931

Thermionic Emission and Electrical Conductivity of Oxide Cathodes. By **A. L. Reimann and L. R. G. Treloar** 1073

Structure of Ferromagnetic Ferric Oxide. By **J. Thewlis** 1089

Hyperfine Structure of Spectrum Lines of Lead Arc in the Visible and the Ultraviolet Regions. By **Wali Mohammad and Prem Nath Sharma** 1106

Observations on the Paper by Messrs. Seth, Gulati, and Singh on the E. M. F. between Metals. By **P. E. Shaw** 1110

Influence of Electrolytes on Dielectric Constant of Water.—Part I (Experimental Method) and Part II. (Uni-univalent Salts) By **R. T. Lattey and W. G. Davies** 1111

Aluminum-Manganese System of Alloys. By **A. J. Bradley and Phyllis Jones** 1137

Note on Heat-flow through a Granulated Material. By **J. H. Awbery** 1152

Investigation into some of the Properties of Porous Building Materials.—Part I. The Absolute Porosity and Saturation Coefficient. By **E. Madgwick** 1155

Some Properties of Porous Building Materials.—Part II. The Flow of Air through Porous Bodies. By **E. Madgwick** 1160

Colour of the Light from High-Frequency Discharges in Helium. By **J. S. Townsend and S. P. McCallum** 1168

Theory of the Electrification of Aerosols. By **H. S. Patterson** 1175

Elastic Ring. Comparison of Strains Determined Experimentally with the Strains calculated from the Elastic Ring Theory. By **C. E. Larard** 1183

Vibrations of Revolving Shafts. By **D. M. Smith and R. C. J. Howland** 1189

Oberbeck's Vortices. By **D. E. Rutherford and J. Caldwell** 1190

Significance of the Compton Effect in Absolute Gamma-Ray Absorption Measurements. By **L. H. Clark** 1191

NATURE

VOL. 128, NO. 3241 — DECEMBER 12, 1931

Letters to the Editor:

Specific Heat of Ferromagnetics and Ewing's Model of the Magnetic Atom. By **J. R. Ashworth** 1003
Rotatory Magnetic Polarization. By **Edm. van Auble** 1004
Superconductivity at High Frequencies. By **J. C. McLennan, A. C. Burton, A. Pitt, and J. O. Wilhelm** 1004

NATURE

VOL. 128, NO. 3242 — DECEMBER 19, 1931

Letters to the Editor:

Polarization of Downcoming Wireless Waves in the Southern Hemisphere. By **E. V. Appleton** 1037
Bands in the Spectrum of Barium Hydride. By **A. Schaafsma** 1042

ZEITSCHRIFT FÜR PHYSIK

VOL. 73, NOS. 5 AND 6 — DECEMBER 10, 1931

Further Investigations of the *D* Line Fluorescence of Sodium at High Vapor Pressures. By **A. Jablonski and Peter Pringsheim** 281
Determination of the Atomic Form Factor in the Management of Anomalous Dispersion. By **R. Glocker and K. Schäfer** 289
New Electrodeless Method for the Measurement of Conductivity. By **Werner Braunbeck** 312
On the Change of Electric Conductivity of Molten Bismuth on Solution of Bismuth Chloride. By **Werner Braunbeck** 335
Monochromatization of de Broglie Waves of Molecular Rays. By **I. Estermann, R. Frisch and O. Stern** 348
Investigations of the Hyperfine Structure of Spectral Lights. II. By **K. Murakawa** 366
Graphic Representation of Some Results of Band Spectroscopy. By **Ragnar Rydberg** 376
Wave Mechanical Theory of the Kerr Effect. By **Th. Neugebauer** 386
Contributions to the Analysis of the First Spark Spectrum of Mercury. By **B. Venkatesachar and T. S. Subbaraya** 412

DIE NATURWISSENSCHAFTEN

VOL. 19, NO. 51 — DECEMBER 18, 1931

New Investigations of the Three-Body Problem. By **V. A. Wintner** 1010
Nuclear Moment of Rhenium. By **L. A. Sommer and P. Karlson** 1021

DIE NATURWISSENSCHAFTEN

VOL. 19, NO. 52 — DECEMBER 25, 1931

Technology of Glass in the Light of Scientific Investigation. By **Hans Jebsen-Marwedel** 1033
On the Hyperfine Structure of 4916A (Hg I). By **B. Venkatesachar and L. Sibaiya** 1038
On the Striking Potential of Helium Discharge for Small Values of pd (p = pressure; d = electrode separation). By **F. M. Penning** 1042
On the Explanation of the Destruction of Photo-Luminescence of Fluorescing Systems by Oxygen: the Formation of Active Diffusing Oxygen Molecules by Sensitization. by **H. Kautsky and H. De Brujin** 1043
On the Question of Resonance in the Artificial Disintegration of Atoms. By **E. Steudel** 1044

PHYSIKALISCHE ZEITSCHRIFT

VOL. 32, NO. 23 — DECEMBER 1, 1931

Addresses and Discussions at the Seventh Physical Society's Meeting September, 1931.
New Observations on the Field of Photoelectric Effect on External Surfaces. By **R. Suhrmann** 929

Direct Crystal Amplification of Ultra Short Waves. By **H. Straubel** 937
On the Theory of the Collision of Alpha Particles with Light Nuclei. By **E. Guth and Th. Sexl** 941
On Gas Concentration in Electron Beams. By **W. Ende** 942
Saturation Current and Processes at the Electrodes of Liquid Dielectrics. By **A. Nikuradse** 945
Observations on the Emission of Light by Metal Vapors Excited in the Positive System. By **H. Krefft** 948
Original Contributions:
Contributions to the Physics of the Nitro-Benzene Kerr Cell. By **F. Hehlgans** 951
On the Electrolytic Solution Potential and the Necessity of the Consideration of the Galvanic Potential Metal/Metal in Galvanic Circles. By **H. Hammerschmid and E. Lange** 958

ANNALEN DER PHYSIK

VOL. 12, NO. 2 DECEMBER, 1931

On the Emission of Phraseodymium in the Alkali Earth Phosphates. By **Herman Evert-Marburg** 137
On the Law of Electrolytic Resistance at Low Temperatures. By **R. Peierls** 154
Magnetic Saturation Phenomena at Low Temperatures. By **Otto Halpern** 169
Note on the Rotational Polarization Phenomena of Ferromagnetic Substances. By **Otto Halpern** 181
On the Deflection of Slow Electrons by Ionic Crystals with Special Attention to the Internal Potential of Calcite and Aragonite. By **W. Dames** 185
On the Analysis of the Band Spectrum of the Lenard Phosphates. By **Ferdinand Schmidt** 211
Photographic Action of Slow Cathode Rays. By **Valentin Weidner** 239

COMPTES RENDUS

VOL. 193, NO. 23 DECEMBER 7, 1931

On the Gravitational Equation of Einstein. By **Charles Racine** 1167
Photography of the Solar Corona With no Eclipse. By **B. Lyot** 1169
Remarks on Preceding Note by **Ernst Eschlangon** 1172
Remarks on Note by B. Lyot. By **Charles Fabry** 1172
On the General Equation of Brownian Movement. By **Jacques Metadier** 1173
On the Construction of Electrostatic Machines. By **Henri Chaumet and Edouard Lefrand** 1176
Discontinuous Variation of the Electromotive Force of Photo-Voltaic Cells Having Colored Liquids. By **A. Grumbach and F. Taboury** 1178
Magnetic Properties in Crystal Structure in the Different Varieties of Anhydrous Cobalt Sulfate. By **R. Hocart and Mlle. A. Serres** 1180
Action of Boric Acid and of the Borates on the Rotating Power of Glucose, of Galactose and of Fructose. By **E. Dormois and Mlle. Peyroux** 1182
On the Action of Hydrogenated Substances as Stabilizers. By **M. L. Jaques** 1185
Study of Infrared Radiation Emitted from the Terrestrial Atmosphere. By **J. Devaux** ... 1207

LE JOURNAL DE PHYSIQUE

VOL. 2, NO. 12, SERIES VII DECEMBER, 1931

Theoretical Considerations on the Circular Polarization of Light in the Raman Effect. By **J. Cabannes** 381
Conductivity of Rare Gases. By **M. Curie and A. Lepape** 392
On the Red Fluorescence of Glass. By **L. Brüninghaus** 398
On the Use of High Dispersion in the Study of the Raman Effect. By **P. L. Mesnage** 403

PHYSICA

VOL. 11, NO. 10 — DECEMBER, 1931

Diffusion of Small Particles with Taking into Account Losses by Collision. By **W. De Groot** 337
On the Properties of the Gravitational Field in a Rotating Space with an Attracting Centre. By **M. G. L. Lely** 343
Isochronous Conical Pendulum of Christian Huyghens. By **C. A. Crommelin** 359

PHYSICA

VOL. 12, NO. 1 — JANUARY, 1932

Absolute Wave-Length Measurements of X-Rays. I. By **J. A. Prins and J. D. Hanawalt** 1
Absolute Wave-Length Measurements of X-Rays. II. By **J. S. Prins** 15
Remarks on Variations in the Electrical Behavior of Various Substances. By **L. Hamburger** 19

BUREAU OF STANDARDS JOURNAL OF RESEARCH

VOL. 8, NO. 2 — FEBRUARY, 1932

Deteriorative Effect of Sulphur Dioxide upon Paper in an Atmosphere of Constant Humidity and Temperature. By **Arthur E. Kimberley** 407
Tensile Properties of Rail Steels at Elevated Temperatures. By **G. Willard Quick** 408
The Resistance to Impact of Rail Steels at Elevated Temperatures. By **G. Willard Quick** 409
Kaolins: Effect of Firing Temperature on Some of Their Physical Properties. By **R. A. Heindl, W. L. Pendergast, and L. E. Mong** 410
Composite-coil Electrodynamic Instruments. By **F. B. Silsbee** 411
Some Studies of Radio Transmission over Long Paths Made on the Byrd Antarctic Expedition. By **L. V. Berkner** 412
Phase Equilibra in the System SiO_2-ZnO-Al_2O_3. By **E. N. Bunting** 413
System CaO-Na_2O-Al_2O_3. By **L. T. Brownmiller and R. H. Bogue** 414
Determination of Tin in Iron and Steels. By **J. A. Scherrer** 415

JOURNAL OF THE OPTICAL SOCIETY OF AMERICA

VOL. 22, NO. 1 — JANUARY, 1932

Proceedings of the Sixteenth Annual Meeting 1
Interferometer Method of Studying the Vibrations of an Oscillating Quartz Plate. By **Harold Osterberg** 19

THE REVIEW OF SCIENTIFIC INSTRUMENTS

VOL. 3, NO. 1, NEW SERIES — JANUARY, 1932

Generating Voltmeter for the Measurement of High Potentials. By **Paul Kirkpatrick and Iwao Miyake** 1
Exhibit of Testing Apparatus and Machines Held in Connection with the 34th Annual Meeting of the A.S.T.M. 8
Thyraton Voltage Regulator for an Alternator. By **Clarence E. Weinland** 9
Voltage-Regulating Auto-Transformer. By **Frederick Bedell and Jackson Kuhn** 20
Device to Measure the Amount of Plane Polarized Light in Low Intensity Radiations and to Measure Small Rotations of the Plane of Polarization. By **D. R. Morey** 24
Wedge Spectrograms Without an Absorbing Wedge. By **Oran E. Miller** 30
Convenient Design of Photoelectric Photometer and Its Use in Comparing X-ray Intensities. By **Elmer Dershem** 43
Penta Comparison Prism for Spectroscopes. By **Samuel D. Bryden, Jr.** 51
Compound Compass for Drawing Arcs of Great Radius. By **L. W. McKeehan** 52
Carborundum Tool for Cutting Fine Surfaces. By **Roland Schaffert** 55

PHYSICS

VOL. 2, NO. 1 JANUARY, 1932

Impedance Characteristics of Loaded Lecher Systems. By **Lewi Tonks** 1
Photoelectric Properties of Thin Films of Alkali Metals. By **S. Asao** 12
Electrokinetic Potentials. XI. Effect of Sodium Soaps on the Electric Moment of the Double Layer at an Aqueous-Cellulose Interface. By **Henry B. Bull and Ross Aiken Gortner** 21
Magnetic Susceptibility of Some Binary Alloys. By **Francis L. Meara** 33
Thermionic Frequency Doubler. By **C. K. Stedman** 42
Electron Diffraction for Classroom Demonstration. By **C. J. Phillips** 48
Unpolarized Resistivity of Glass. By **Denis M. Robinson** 52